SHTARWaRS

Final Report

Design Synthesis Exercise - Group 1

M. Albu	5717582	A. Bilbao Pardo	5792347
S. Cox	5792770	S. de Boo van Uijen	5048796
I. Hendrickx	5693586	P. Huciu	5323169
Z. Księżak	5757770	A. Moëc	5684382
M. Murcia Fernandez	5696380	Á. Valderrabano Megias	5467772

Delft University of Technology

TU Delft

This page is intentionally left blank.

SHTARWaRS

Final Report

by

Design Synthesis Exercise - Group 1

M. Albu	5717582	A. Bilbao Pardo	5792347
S. Cox	5792770	S. de Boo van Uijen	5048796
I. Hendrickx	5693586	P. Huciu	5323169
Z. Księżak	5757770	A. Moëc	5684382
M. Murcia Fernandez	5696380	Á. Valderrabano Megias	5467772

Tutors: Dr Ivan Langella, Prof Dr Arvind Gangoli Rao
Coaches: Jakob Smretschnig, Dante Raso
Faculty: Faculty of Aerospace Engineering

Delft, 24 June 2025

This page is intentionally left blank.

Executive Overview

Project Background & Objective

As European Union (EU) policy[1] and environmental pressures begin to steer industrial trends towards strict sustainability targets, the aviation sector is no different in its need to respond and adapt. Despite recent developments regarding emission reduction, the aviation industry remains a significant contributor to the anthropogenic climate impact, responsible for 3.5% thereof between 2000 and 2018, and is projected to contribute more over the next decade [1]. For this reason, the EU Green Deal[2] and the International Air Transport Association (IATA) [2] have dictated the goal that the aviation industry shall produce net-zero carbon emissions by 2050. Technological and operational efficiency improvements are expected to contribute to around 30% of the reduction of emissions in 2050, whereas Sustainable Aviation Fuels (SAF) will be responsible for 24-70% of such reduction towards net-zero CO_2 [3]. Although the aviation industry relies on both developments for decarbonization, but the production of SAF requires either large amounts of energy or land use [4]. Implementing new Powertrain (PT) powered by hydrogen eliminates this effect, as they operate without producing notable carbon emissions, while operating with a higher energy density than batteries. This gives hydrogen technologies the potential to be a part of the key to carbon-free aviation. Analyzing this opportunity further is critical in meeting this need indicated by global aviation regulators, as outlined by the following need statement:

Mission Needs Statement

The aviation sector needs to demonstrate a hydrogen-electric PT in short-to-medium haul aircraft by 2035, as part of the EU Clean Aviation program.

With the goal of meeting the above industry need, the Scaled-up Hybrid-Electric Turboprop AiRcraft with Water Recovery System (SHTARWaRS) project aims to create a preliminary design of a hydrogen fueled, hybrid-electric, megawatt-class PT to retrofit the Beechcraft 1900D aircraft design by 2035 without significantly changing its mission profile, while minimizing the design's impact on the climate and air quality. The retrofitted Beechcraft 1900D will be named H_2D_2 for its double use and double distribution of hydrogen. With this goal defined, the project objective statement may be outlined:

Project Objective Statement

To adapt the design of the Beechcraft 1900D into a robust, low-maintenance, low NO_x emission hybrid hydrogen-electric powered aircraft with 10 students in 10 weeks time.

Design Concept

The project objective statement outlines the scope of the SHTARWaRS project, but requires supplementation with a description of the general design concept: the H_2D_2 will integrate hydrogen storage and Fuel Cell (FC)s into its structure, and an Electric Motor (ELMO) will supply additional inline power to the turboprop shaft (making the PT hybrid hydrogen-electric). Hydrogen will be supplied by the storage to the FCs and the turboprop motor. The FC system generates electricity for the ELMO and produces water as a byproduct that is injected into the Combustion Chamber (CC) to reduce NO_x emissions by decreasing its temperature. The original fuel storage will be removed, but the space gained from this will not suffice for the new components to fit, thus requiring alterations to the internal configuration of the aircraft. These interactions can be seen in Figure 1.

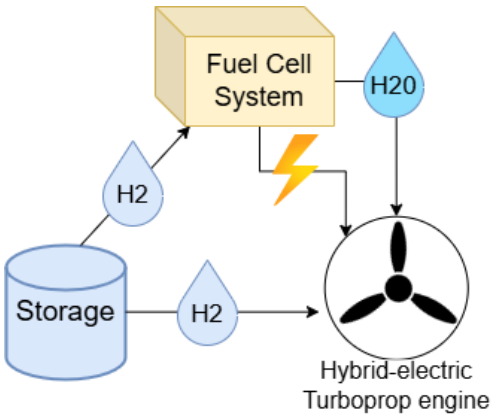

Figure 1: *Interaction between main systems*

[1] URL https://commission.europa.eu/strategy-and-policy/priorities-2019-2024/european-green-deal_en
[2] URL https://commission.europa.eu/strategy-and-policy/priorities-2019-2024/european-green-deal_en [Cited 25 April 2025]

H_2D_2 Design

The H_2D_2 design is able to transport **15 passengers (PAX)** a distance of **707 km**, while having a **four times lower climate impact** than the Beechcraft 1900D, as detailed in Chapter 8. This performance is achieved at a cost of **€221 per seat** per flight to account for an **14% ROI** over 20 years of operation for a fleet of 500 aircraft, as outlined in Chapter 21. Comparatively, airlines in Canada flying the Beechcraft 1900D today charge €200-250 for a similar flight [3]. Figure 2 shows the layout of the aircraft and its most important systems.

Figure 2: *Design layout of H_2D_2 [Computer-Aided Design (CAD) software used: CATIA v5©, NX© and Blender©]*

The modified design provides power by operating the CC and FC in conjunction during take-off and climb, but reverting to full FC usage during cruise, taxi and other flight stages to operate more efficiently. Additionally, a comprehensive Thermal Management System (TMS) is created to cool the FC and other systems. Table 1 describes the key system sizes of H_2D_2.

Table 1: *Key system sizes of H_2D_2*

Design Point	MTOW	Fuel Cell Mass	Hydrogen Mass	TMS Mass	Storage Mass	Storage Volume
H_2D_2	7911 kg	563 kg	160 kg + 64 kg reserve	275 kg	252 kg	4.49 m3

Liquid Hydrogen (LH_2) is stored in the rear of the aircraft, which is pumped to the FCs and CCs on both wings, providing the necessary thrust for operation. On a typical flight, 160 kg of hydrogen is used. During use, minimal emissions are produced, instead, the climate impact is driven by the production of hydrogen to be used as fuel.

Flight Performance

In order to properly analyze the aircraft's performance, a flight performance model was created, analyzing the state of the PT and the fuel use over the entire flight profile. Figure 3 displays the power produced by the FC and CC over the flight profile.

[3] URL: `https://www.flycma.com/` cited June 17th, 2025

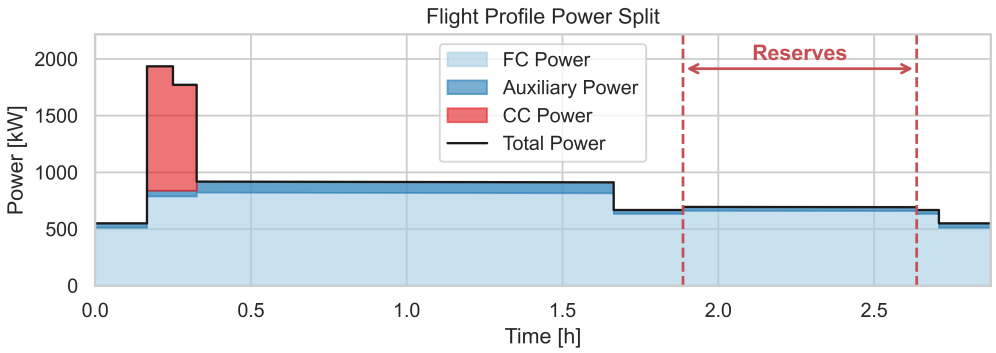

Figure 3: *Power provided over flight profile from FC and CC*

Choice of Design

The optimal design was selected by comparing various FC vs CC usage rates in order to balance the cost and climate impact (measured in terms of Global Warming Potential (GWP) over a 100 year time horizon) of the design over its lifetime. This was performed by varying the FC size and its usage over the flight profile. This resulted in many possible design points, whose performances are shown in Figure 4 below. Note that although the ideal design goal was to transport 19 PAX, the size of the hydrogen storage tank requires the removal of some seats in the aircraft. This modification was taken into account in the design analysis, as each Key Performance Indicator (KPI) was divided by the amount of PAX. If there were to be two designs with different capacities, but otherwise equal scores, the higher-capacity aircraft thus performs significantly better. It was quickly learned that it was required to remove two rows of PAX to accommodate the storage tank in all feasible designs, so a capacity of 15 was selected.

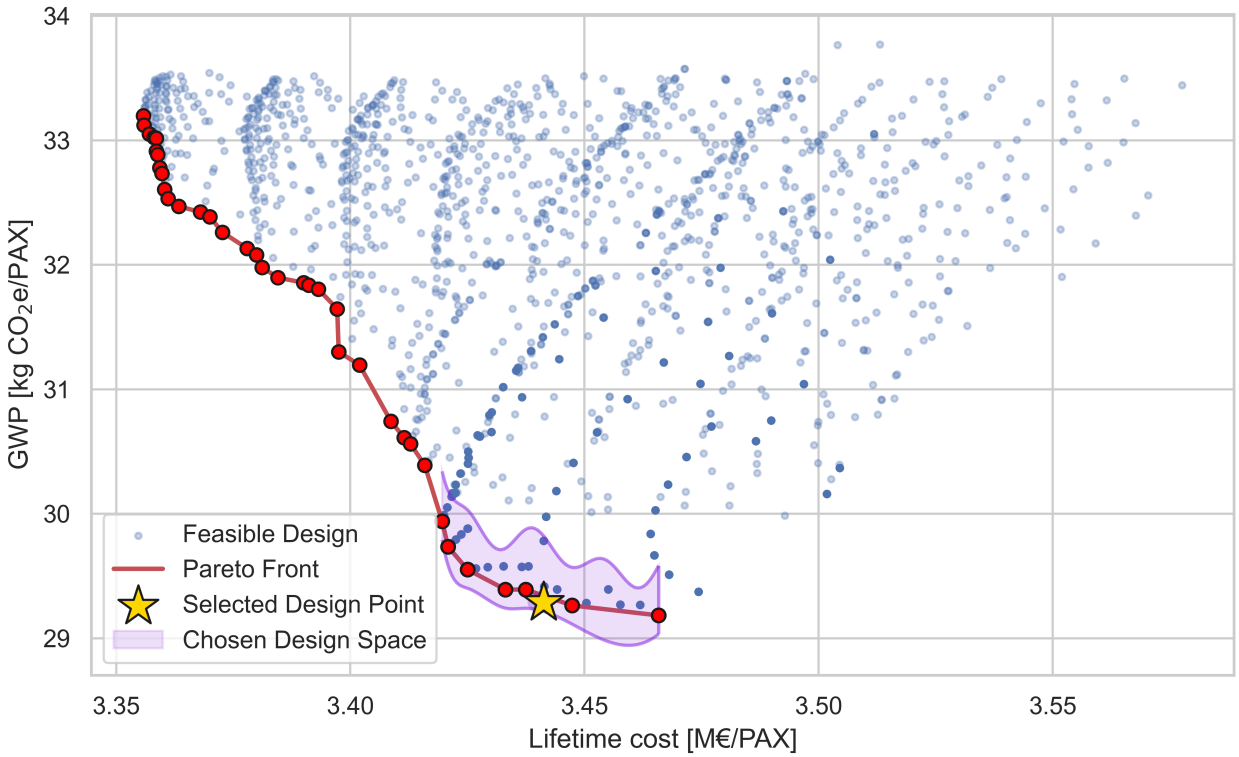

Figure 4: *Performance of possible H_2D_2 design points*

The red Pareto front highlights the most optimal designs for lifetime cost and sustainability. H_2D_2 aims to have a sustainable, cost-effective design, which is the bottom-left section of Figure 4. All points on this front

are viable, but one must be selected to balance the two KPIs. At a lifetime cost of €3.42 million per PAX and sustainability of 23.7 $kgCO_{2,eq}$ per PAX per flight, there is a clear point of diminishing returns where the increase in sustainability no longer matches the increase in cost. This point is selected as the optimal design. If it becomes clear that sustainability or cost become more relevant for the stakeholders, this design point may be shifted to prefer one over the other.

Stakeholder Requirements

The stakeholder requirements define the critical objectives which must be met in order to produce a feasible, marketable design. The requirements, given in Table 2, outline the high-level requirements, from which requirements of each system and subsystem can be extrapolated.

Table 2: *Stakeholder requirements*

ID	Requirement	Type
REQ-TE-STK-A	The aircraft shall contain a hybrid-electric PT	**DRIVING**
REQ-TE-STK-B	Limiting emissions shall be a key performance metric in design	**DRIVING**
REQ-TE-STK-C	The aircraft shall have a minimum range of 700 km	**KEY**
REQ-TE-STK-E	The aircraft shall be of megawatt class	-
REQ-CO-STK-F	The aircraft shall produce less emissions than aircraft of the same caliber	-
REQ-CO-STK-G	The aircraft should be able to transport at least 15 people	**KEY**
REQ-CO-STK-H	The aircraft should be financially desirable for consumers	-
REQ-CO-STK-I	The system shall be safe and reliable	-
REQ-CO-STK-J	The Beechcraft 1900D shall be the baseline for the design	-
REQ-CO-STK-L	The PT should not exceed a mass of 2541.9[kg] (3 times the original PT)	**DRIVING**

Requirements have been labeled according to their role in guiding the design team: those marked **driving** represent essential design drivers, and **key** requirements are critical to stakeholder objectives or carry heightened risk. The H_2D_2 design complies with all stakeholder requirements, and is competitive with competitors while being much more sustainable.

Powertrain Components & Systems

The primary PT components and systems are outlined in order to define the primary design considerations for each system and the key interactions between the systems:

- Hydrogen storage, conditioning, and distribution
- FCs and their oxygen supply
- Cooling and water recovery
- Emissions minimization in the CC
- Electrical Power System (EPS)

For each of these concepts, a Design Option Tree (DOT) was made to examine all possible configurations. Some concepts were pruned as they were deemed infeasible. Initial design concepts were developed for the most leading design options. The ones that have the most influence are the state of the hydrogen, and the type of FC used.

Selection of Design Options

A trade-off was performed for all important design options, outlined in Chapter 7. The resulting options were the High-Temperature Proton-Exchange Membrane Fuel Cell (HT-PEMFC) for the FCs, LH_2 for the state of the stored hydrogen, and an inner and outer layer of the storage tank made from S-Glass Fibre UD (Prepreg).

The HT-PEMFC was chosen due to its high specific power for the total weight of the FC system, and easier integration into the aircraft compared to other FCs. Other options were the Solid-Oxide Fuel Cell (SOFC), which was expensive and difficult to integrate, and the Low-Temperature Proton-Exchange Membrane Fuel

Cell (LT-PEMFC), which is more difficult to integrate into the aircraft than the HT-PEMFC, but otherwise will have very similar performance compared to the HT-PEMFC in 2035. The latter was chosen because by 2050, the HT-PEMFC will outperform the LT-PEMFC significantly in specific power. While both options are viable for 2035, the HT-PEMFC slightly outperforms the LT-PEMFC, and future projections put the HT-PEMFC high above the others. The FC efficiency varies with the throttle level as displayed in Figure 5. With increasing power, the FC efficiency reduces drastically. This explains the low chosen throttle values for the FCs operation, as it reduces the hydrogen needed and the heat produced by the FC.

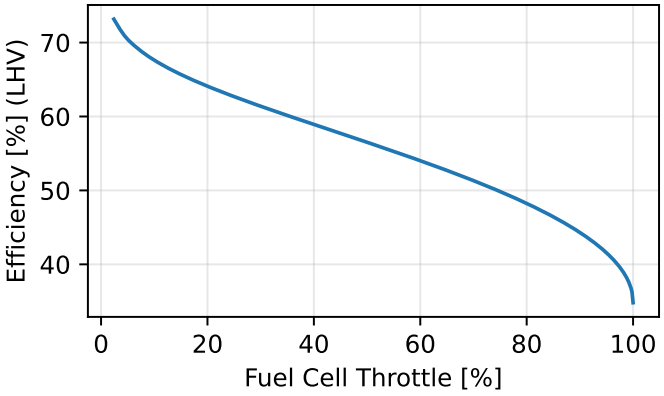

Figure 5: *FC efficiency with changing throttle*

The state of the hydrogen was chosen to be LH_2. This was decided because it has smaller mass needed for the storage system, and it does not need as much space as other options. Two other options were considered for the hydrogen state trade-off: Gaseous Hydrogen (GH_2), and Cryo-Compressed Gaseous Hydrogen (CcH_2). GH_2 required far too much space, and CcH_2 had many risks associated with it, and had low operational flexibility.

With the fuel state defined, the attention could be switched to the hydrogen tank material trade-off, and its sizing, from which S-Glass Fibre UD (Prepreg) was the best option. A tool was created that sized four defined layers from the inside to the outside:

- **Layer 1:** Inner layer that is in contact with the LH_2.
- **MLI:** Multi layer insulation in vacuum.
- **Vacuum:** Pure vacuum insulation layer.
- **Layer 2:** Outer layer that is in contact with the ambient.

Using this tool, the gravimetric and volumetric efficiencies were found for the different material combinations to be used as criteria for the trade-off. Using these efficiencies and other criteria such as its life cycle and maintenance cost, an inner and outer tank of S-Glass Fibre UD (Prepreg) would be the best option for the SHTARWaRS fuel tank. The other combinations of materials came up short compared to this one.

Powerplant Redesign & Emissions Analysis

It was chosen to not redesign the complete Powerplant (PP), as this would take much more time than is available for this project. Only the design of the CC was manipulated to tap into the power of hydrogen. The main challenges that are caused by using hydrogen are the instabilities of the flame and the risk of flashback. The high stoichiometric temperature of hydrogen can also cause very high NO_x emissions. Despite that, hydrogen does also have positives. It can burn in ultra rich or -lean conditions. It is also a great heat sink, and most importantly: it does not create direct carbon emissions.

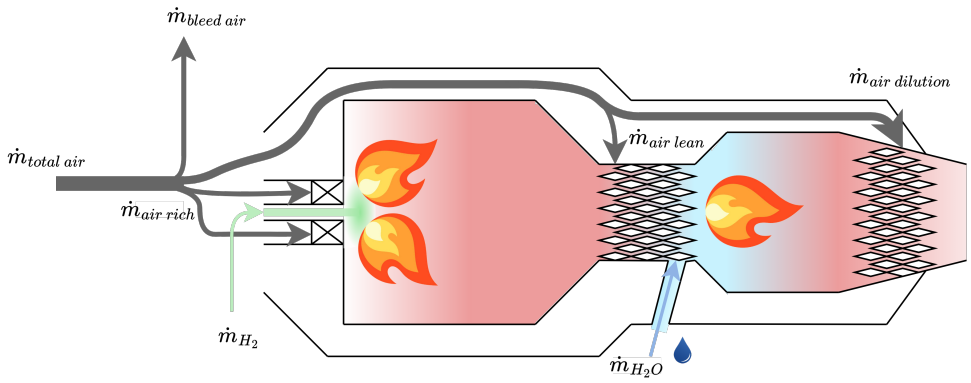

Figure 6: *Rich-burn, quick-mix, lean-burn (RQL) combustor*

Rich burn, Quick Mix, Lean burn (RQL) was selected as the architectural solution for the combustion system, as it allows for the introduction of large amounts of heat into the flow while avoiding zones of high NO_x formation. An RQL combustor is shown in Figure 6. It is also resistant to flashback phenomena and thermo-diffusive instabilities due to the rich burn stage. Other types of combustion system that were researched, but were not selected are lean-burn, micro-mix and reheat combustion.

Another way to reduce the formation of NO_x studied is by injecting third bodies, usually water, into the CC. This will decrease the temperature of combustion, decreasing NO_x emissions. Liquid water was chosen because it removes more heat from the CC, and it requires orders of magnitude less specific work to be compressed.

Risk Analysis, Verification & Validation

Both system technical risks and Regulator/User technical risks were analyzed, and a mitigation plan was developed to prevent them from affecting the project negatively. System technical risks are risks which may impact the PP during operation. Regulatory and user technical risks refer to risks which affect the compliance of SHTARWaRS with its user requirements during design. Each identified risk was analyzed for its likelihood, impact and failure condition, and assigned a risk factor score. The most consequential risks were identified, and mitigation & contingency strategies were drafted to reduce their likelihood and/or impact.

To ensure the functioning and compliance of the product, a Verification and Validation (V&V) procedure which was proposed in the Midterm Report was put into action. V&V were applied to both the design tools and the final product using a bottom-up approach, starting with unit tests and progressing to full system validation. Each requirement was assigned a specific V&V method - Inspection, Analysis, Demonstration, or Test - to ensure it was properly addressed.

Subsequent Design

After this 10-week long project stage is completed, the PT architecture shall be defined, but many aspects of the aircraft design will not be finalized. As this project is designed for implementation as of 2035, the development of FC and hydrogen technologies must be monitored, and the design updated accordingly. Additionally, many aspects of integrating this PT in the aircraft will not be analyzed. It is recommended to perform structural and stability analysis with the new PT, possibly adapting the aircraft design to account for these aspects. The turbomachinery of the current engine will also not be radically redesigned with hydrogen in mind. It is recommended to redevelop or update the current engines to adapt to the use of hydrogen to maximize their efficiency and reliability. Once these adaptations have been adopted, further development can be made to ensure compliance with Certification Specifications on Normal-Category Aeroplanes (CS-23) regulations so that an airworthy model can be built, and large-scale production can be planned and then ultimately conducted.

Operations would also change due to the introduction of the hydrogen systems. People trained in handling

and maintenance are required for operation, and logistic networks need to be established to transfer the hydrogen to the aircraft.

In conclusion, the H_2D_2 supports the short-haul aviation sector to reach net-zero carbon emissions through the integration of a HT-PEMFC, and a CC capable of using hydrogen, into the Beechcraft 1900D. Liquid water will be injected in this CC to reduce NO_x emissions, and LH_2 will be used in a storage tank made from S-Glass Fibre UD (Prepreg). The integration of these components does lower the PAX to 15, but this does not stop the H_2D_2 from being competitive in the aviation market. The SHTARWaRS PT will be a critical stepping stone to the aviation industry's sustainability goals. Lastly, the characteristics of H_2D_2 are summarized in Table 3.

Table 3: *Characteristics of the design*

Characteristics of the Design	**Value**
Number of PAX	15
Range	707 km
Cost per seat per flight	€221
Lifetime cost per PAX	€3.42 million
Return On Investment (ROI) (over 20 years of operation for a fleet of 500 aircraft)	14 %
Sustainability	23.7 $kgCO_{2,eq}$
MTOW	7911 kg

Contents

Glossary

a/c aircraft 9, 115–118, 120, 121
AIT Assembly, Integration & Testing 103
AP Auxiliary Power 53, 69, 91
ASK Available Seat Kilometer 93, 94

BoP Balance of Plant 1, 48, 49, 52

CAD Computer-Aided Design iv, 82, 83, 122
CBS Cost Breakdown Structure 111
CC Combustion Chamber iii–ix, 1, 8, 16, 17, 24, 27, 31, 34–36, 38, 40–43, 45, 47, 48, 50, 52, 54–57, 64, 71, 72, 81, 82, 84, 87, 89, 92, 102, 108, 110, 118, 119, 121, 122
CcH$_2$ Cryo-Compressed Gaseous Hydrogen vii, 32
CDHS Control & Data Handling System 13, 27, 88–90, 107, 117, 119, 120
CDT Concurrent Design Tool 68, 71–73, 91
CG Centre of Gravity 74–76, 82, 92
CommFD Communication Flow Diagram 87, 88, 117, 119–121
Cp Specific Heat Capacity 55
CS-23 Certification Specifications on Normal-Category Aeroplanes viii, 6, 9, 24, 102, 116

DLR the German Aerospace Center 49
DOT Design Option Tree vi
DSE Design Synthesis Exercise xiii, 13, 102, 105

EASA European Union Aviation Safety Agency 6, 12, 75
EG Ethylene Glycol 60, 67
EIS Entry-in-Service 36, 38–41, 45, 46
ELMO Electric Motor iii, 8, 19, 24, 53, 69, 73, 82, 84, 86–89, 91, 100, 108, 111, 116, 118, 119, 123
EOL End Of Life 99, 103
EP Electric Power 87
EPS Electrical Power System vi, 13, 27, 29, 53, 68, 69, 73, 81, 84, 86, 87, 89, 105, 107, 108, 111, 118, 119
ESA European Space Agency 18
ESHP Equivalent Shaft Horse Power 16
EU European Union iii, 1, 24, 29, 79, 80

FADEC Full Authority Digital Engine Control 11, 38, 89
FBS Functional Breakdown Structure 19
FC Fuel Cell iii–viii, 1, 8, 13, 19, 24, 27, 29, 31, 32, 45–50, 52–56, 60, 62, 66–69, 71–73, 81, 82, 84, 87–89, 91–100, 102, 105, 108, 111, 112, 115–123
FEM Finite Elements Method 92, 117
FFBD Functional Flow Block Diagram 19
FFD Functional Flow Diagram 1, 116
FPP Flight Performance & Propulsion 69, 71, 82

GH$_2$ Gaseous Hydrogen vii, 32, 57
GHG Greenhouse Gas 28, 30, 117
GO Ground Operations 19, 99, 116, 119–121
GWP Global Warming Potential v, 27, 28, 30, 52, 78–80, 93, 95–98, 123

H$_2$D$_2$ iii–vi, ix, 1–7, 13, 31, 33, 47, 48, 52, 54, 73–76, 81–83, 92–103, 105, 107–109, 111–115, 122, 123
HEX Heat Exchanger 56, 62–66, 84, 85, 87, 91, 105, 107, 108
HSP Heat Sink Potential 32, 55
HT-PEMFC High-Temperature Proton-Exchange Membrane Fuel Cell vi, vii, ix, 31, 32, 48, 49, 84, 95, 96, 99, 108, 123

IATA International Air Transport Association iii
ICAO International Civil Aviation Organization 17, 75
ISA International Standard Atmosphere 56
ISO International Organization for Standardization 7, 9, 24, 27, 116
ITT Inter Turbine Temperature 16

KDE Kernel Density Estimate 78, 79
KPI Key Performance Indicator v, vi, 28, 29

LCA Life Cycle Assessment 19, 23, 28–30, 32, 52, 93, 123
LH$_2$ Liquid Hydrogen iv, vi, vii, ix, 32, 57, 61, 81, 84, 92, 99, 116, 123
LHV Lower Heating Value 49, 71
LT-PEMFC Low-Temperature Proton-Exchange Membrane Fuel Cell vi, vii, 31, 32, 48

MAWP Maximum Allowable Working Pressure 57
MC Maintenance Cost 32, 33
ME Mass Efficiency 32
MLI Multilayer Insulation 57, 86, 123
MTOW Maximum Take-off Weight 10, 13, 14, 18, 69, 73, 75, 76, 81, 82, 84, 91

NDT Non-Destructive Testing 106
NRM Need for Risk Mitigation 32

OEW Operating Empty Weight 10, 69, 75
OF Operational Flexibility 32

P&W Pratt & Whitney 1, 11, 12, 17, 18, 71
PAX passengers iv–vi, ix, 3, 4, 9, 10, 13, 17, 19, 24, 29, 74–76, 79–82, 86, 92, 94, 95, 112, 115, 117, 122
PP Powerplant vii, viii, 1, 10, 11, 13, 19, 24, 28, 34, 87–89, 99, 101, 105, 108, 109, 115, 117–121

PT Powertrain iii, iv, vi, viii, ix, 1, 4, 5, 8, 9, 11, 13, 14, 16, 18, 19, 24, 27, 29–31, 33, 54, 60, 68, 73, 74, 76, 79–82, 86, 88, 90–92, 99, 100, 102, 105, 115–123

RAMS Reliability, Availability, Maintainability & Safety 99, 100, 123
ROC Rate of Climb 71, 72
ROD Rate of Descent 71, 72
ROI Return On Investment ix, 111, 112, 114
RQL Rich burn, Quick Mix, Lean burn viii, 35, 36, 41, 44, 47, 108, 123
rwy runway 117

SAF Sustainable Aviation Fuels iii, 93, 94
SFC Specific Fuel Consumption 12
SHP Shaft Horse Power 12, 16, 17, 87
SHTARWaRS Scaled-up Hybrid-Electric Turboprop AiRcraft with Water Recovery System iii, vii–ix, 1–3, 5, 6, 8, 13, 14, 23, 27–29, 31, 57, 66, 80, 81, 87, 88, 90–92, 99, 102, 105
SHX Skin Heat Exchanger 66, 84, 85
SOA State-of-the-Art 36, 38, 39
SOFC Solid-Oxide Fuel Cell vi, 31, 32
SSS Specific System Size 32
SWOT Strengths, Weaknesses, Opportunities, Threats x, 3, 5

TIT Turbine Inlet Temperature 35, 36, 45, 71
TMS Thermal Management System iv, 1, 8, 9, 24, 27, 48–50, 52, 54, 55, 60–62, 64, 66–69, 71, 73–75, 81, 82, 84, 85, 87, 89, 91, 94, 97, 98, 102, 111, 115, 116, 118, 120, 121, 123
TOGA Take-Off/Go-Around 12, 14, 16, 18, 36, 37, 45, 46, 68, 73, 78, 81, 82, 84, 96–99
TR Thrust Ratio 64
TRA Technical Risk Assessment 101, 116
TRL Technology Readiness Level 6, 48

V&V Verification and Validation viii, 1, 9, 23, 27, 28, 105, 115, 122, 123

WBS Work Breakdown Structure 12
WRS Water Recovery System 13, 24, 89, 117–119, 123

1

Introduction

As EU policy[1] and environmental pressures begin to steer industrial trends towards strict sustainability targets, the aviation sector is no different in its need to respond and adapt. The development of novel solutions to lower industrial and operational environmental footprints has accelerated over the past decades with the aviation sector specifically looking to minimize it current share of around 13.9% of global transport emissions[2]. Engine redesigns to improve efficiency and lower fuel consumption can only go so far, opening the door for the use of alternative fuels. The gravimetric energy capacity of hydrogen has therefore drawn much attention in this developing area of transportation, while offering zero-CO_2 emissions either through its combustion or use in FCs.

The market need for hydrogen-powered aircraft is driven by the demand for more sustainable air travel solutions. The Beechcraft 1900D, commonly used for frequent routes to less popular destinations from hub airports, offers a competitive advantage in terms of cost and accessibility. In lower-demand routes with no high speed rail connections and no market for large capacity aircraft due to high operational costs, small commuter aircraft such as the Beechcraft 1900D provide superior travel times than other methods, opening a market segment especially in high-wealth, high-relief countries and regions such as Norway and Scotland [5]. Hydrogen-powered aircraft have the opportunity to disrupt this market by offering cleaner alternatives in the face of rising carbon regulations, while the use of a hybrid – FCs and hydrogen combustion – PT offers advantages in nitrous oxide compounds (NO_x) mitigation. The economic viability of such designs will be influenced by new policies, technological advancements, and the general shift toward cleaner aviation practices.

This technical report aims to present a preliminary design of a hybrid, hydrogen-electric FC and CC PT to be integrated within the Beechcraft 1900D aircraft, including selecting FC types, hydrogen storage solutions, and the power split. In order to maintain its flying characteristics and market competitiveness, it is engineered to be robust, low-maintenance, low-emission, and highly responsive, while splitting the power delivered by the FC and CC in order to minimize in-flight NO_x emissions.

Beginning with the identification of a market need through analysis, requirements are drawn in strict accordance to the project objective so as to promote a market-competitive design for the SHTARWaRS PT. The original Beechcraft 1900D is also analyzed and various budgets are documented, with particular emphasis on the Pratt & Whitney (P&W) PT6A-67 engine. The general architecture of the project is described along with the Functional Flow Diagram (FFD), leading to the project development protocol. This includes a risk assessment and mitigation strategy, as well as the V&V plan for both requirements and product, and a sustainable development strategy.

Trade-offs are performed for the FC, the hydrogen state, and the storage tank, followed by a detailed insight into the new CC design and emission estimations. This chapter includes the PP redesign reasoning, the CC model simulation, and the emission quantification, along with effects of water injection. The FC is subsequently analyzed on the basis of performance, cost and sustainability, including the Balance of Plant (BoP). The hydrogen system used to provide and store the hydrogen used by both the FC and CC is then sized, along with the piping required for efficient delivery. The TMS is also sized; detailing various options to dispose of unwanted heat, and its impact on the sustainability of the H_2D_2.

[1] URL `https://commission.europa.eu/strategy-and-policy/priorities-2019-2024/european-green-deal_en` [Cited 20 April 2025]

[2] URL `https://climate.ec.europa.eu/eu-action/transport-decarbonisation/reducing-emissions-aviation_en` [Cited 28 May 2025]

Following all of the main systems' chapters, the design is synthesized and the result is described. H_2D_2's characteristics are reported and the impact of retrofitting is analyzed. Additionally, a view into the sustainability of the final design is provided. Next, the operations and logistics concept is presented, together with the future project design and development logic. A production plan and Gantt chart are included. Lastly, the economic feasibility of SHTARWaRS is thoroughly inspected, along with the compliance with initial requirements.

2

Market Analysis

This chapter discusses the analysis of a potential market for the SHTARWaRS project. Subsection 2.1.1 identifies a market possibility stemming from the user requirements, current competitor trends, and the performance of a SWOT analysis that helps narrow down the scope. Section 2.2 delves into the stakeholder map, analyzing interest and influence on the project, and how these might shape the development.

2.1. Competition Analysis

This section provides the potential location of the H_2D_2 aircraft within the market by analyzing the current market and competitors, as well as current and future Hydrogen-Electric Aircraft projects. A SWOT analysis complements this analysis by locating possible gaps in the market and threats to beware of.

2.1.1. Broad Market Definition & Competition Analysis

The broadest definition of the market for this aircraft can be derived from its highest-level performance requirements. These requirements dictate the ability to carry at least 15 PAX over a minimum mission range of 700 km, with a minimum cruise velocity of Mach 0.4. With these, the general market can be defined as travel between destinations which have enough demand for the transport of 10-20 PAX and are less than 700 km apart.

For popular routes of this distance, travelers are often confronted with a multitude of possible methods of travel, including driving, busses, trains, ships, and aircraft. An analysis of each of these methods' advantages and disadvantages will allow a more precise definition of the market where this aircraft is economically feasible.

To compete with other methods of transportation, this aircraft must either be cheaper, faster or offer a unique benefit that other methods do not (e.g., practicality, luxury, or sustainability). The speed of aircraft enables them to compete with cars, busses, regional trains and ships, where the demand is large enough to justify an airport near the destination. Along high-demand routes, high-speed rail and larger capacity aircraft provide faster service at a higher volume, reducing the practicality of regional aircraft [6, 7]. In lower-demand routes with no high-speed rail connections and no market for large capacity aircraft due to high operational expenses, small-to-medium aircraft provide superior travel times than other methods, opening a market segment. Since H_2D_2 provides a unique selling point through its superior sustainability to current aircraft, this market may be viable for this project, even with a potentially higher cost.

The hub and spoke network philosophy creates the largest market for this project's aircraft type: short-haul flights from larger airports to smaller destinations [7]. Adding small-capacity, high-frequency flights to less-demanded destinations enables airlines to provide service to a high number of destinations while reducing layover times. Thus, the main market for this aircraft type is between hub airports and low-population cities and towns, especially to those with limited infrastructure for other transportation methods, e.g., due to geographical conditions.

2.1.2. Existing Flying Aircraft & Current Cost of Competition

The 19 PAX aircraft is an established segment of short/commute aviation, even though our aircraft will carry 15 PAX, market analysis has been performed on this segment as it is where the original Beechcraft 1900D operated in. Assessing the cost of competing aircraft will enable the creation of basic market expectations for the cost of operating H_2D_2. There are multiple comparable scope and specifications of aircraft, which have to be included in the competitor analysis. The competitors that will be looked at are shown in Table 2.1.

Table 2.1: *Aircraft with similar PAX capacity*

Aircraft	Power per Engine (kW)
Dornier 228NG[1]	579
Let L410 Turbolet[2]	597
Fairchild Metro III[3]	701
BAe Jetstream 31[4]	700
Antonov 28[5] (17 PAX capacity)	720
Beechcraft 1900D[6]	955

Except for the Dornier 228, all other direct competitors' aircraft have a range surpassing 1000 km, while loaded with all 19 PAX, so this may not be the leading marketing aspect. Since such aircraft are our main competitors, and they provide a near-identical product to ours, the product developed during this exercise should provide a separate unique benefit, such as low operating cost or low NO_x emissions.

Since the Beechcraft 1900D is no longer in production, its production and operating costs may vary too much regarding modern aircraft which have newer technology and have costs which mirror the current market. One of the latest 19-PAX aircraft to enter the market is the Cessna 408 SkyCourier, which was introduced to the market in 2022 [8], and has readily available information on its purchase and operating costs. The base price of a new PAX-configured Cessna 408 SkyCourier was $8.35 million in 2024 [9]. Additionally, annual fixed costs are estimated to be $397,466, with variable costs of $3,415 per flight hour[7].

These costs can be used as an ideal target purchase and operational cost for H_2D_2 to be competitive in today's market. Of course, the price of ownership and operation will change by the target year of operation of H_2D_2, which should be considered in further financial analyses. Additionally, this price does not reflect the cost of the negative environmental externalities produced by the Cessna 408 SkyCourier, or the possible economic incentives which may impact the cost of operating H_2D_2.

2.1.3. Hydrogen-Electric Aircraft Projects

Due to the new technology of hybrid hydrogen-electric engine integration to aircraft, the direct competition within this niche is very aggressive, although compressed into a few but strong players in the aviation industry. One of the most ambitious and probably the most popular project is the Airbus ZEROe initiative. Although Airbus has not officially declared any operating cost data, since their first and primary goal is to fly with zero emissions, cost should not be a major limiting factor in this design [10]. Therefore, proving this technology may have a significant impact on the legislative side, considering authorities to be more strict regarding emissions, a fact that could possibly affect the whole industry.

From a more specific perspective, and technologically more applicable to this project, the competitors are comprised of companies that retrofit existing aircraft, integrating a hydrogen-electric PT. Two of the main direct competitors for this project are ZeroAvia and Stralis.

ZeroAvia is an important player within this market niche of implementing hydrogen-electric PT to aircraft. They have already retrofitted two Dornier 228 aircraft to this kind of PT. As stated in Subsection 2.1.2, the original Dornier 228 has similar capabilities and applications as the original Beechcraft 1900D, therefore making ZeroAvia's project a very close one to the Beechcraft's retrofitting. The greatest strength that ZeroAvia possesses currently is the head start they have, as ten flight tests have been performed by the company by July 2023 [11]. In addition to that, in collaboration with other companies, ZeroAvia is starting a pilot training program [12], showing a primary demand of the company for a rapid process of certifica-

[1] URL https://www.ga-ats.com/en/do228 [Cited 2 May 2025]
[2] URL https://www.let.cz/en/press [Cited 8 May 2025]
[3] URL https://www.flugzeuginfo.net/acdata_php/acdata_metro_en.php [Cited 2 May 2025]
[4] URL https://www.airliners.net/aircraft-data/british-aerospace-jetstream-31super-31/55 [Cited 2 May 2025]
[5] URL https://www.airliners.net/aircraft-data/antonovpzl-mielec-an-28/38 [Cited 2 May 2025]
[6] URL https://www.airliners.net/aircraft-data/raytheon-beechcraft-1900/329 [Cited 2 May 2025]
[7] URL https://jetadvisors.com/jet/skycourier-passenger-ce-408/operating_costs/ [cited 30 April 2025]

tion. Technology-wise, ZeroAvia states that their PT implies 90% less life cycle emissions, 40% less fuel and maintenance costs and 75% less hourly maintenance costs[8].

On the other hand, an ongoing project, exactly on the Beechcraft 1900D is run by Stralis. They claim to keep the retrofitted aircraft within the same weight and balance envelope of the original one, with the same engine characteristics as the original Pratt&Whitney PT6A-67D[9]. Moreover, they claim their PT to lower the overall operation costs by 50%[10]. Moreover, their time projection includes test certification by 2026, and an ambitious program of using the Beechcraft as mean of transport for athletes participating in the Olympic and Paralympic Games in Queensland, Australia, in 2032[11].

Therefore, to obtain a feasible position in the restrained range of the market, this exercise shall have an outcome at least as effective as the competitors mentioned within this subsection. The other options would include trading performance, for lower operating costs and/or NO_x emissions, although, remaining comparable to the competition is necessary.

2.1.4. SWOT Analysis

To match an organization's goals, programs, and capacities with the environment where it is active, a SWOT analysis should be performed. The acronym stands for Strengths, Weaknesses, Opportunities and Threats, and it is one of the most efficient decision-making techniques to identify competitive advantages. The SWOT analysis is a crucial part of the market analysis since it underlines the key aspects that may be included in the marketing strategy, as well as areas that must be avoided during the development of a product.

The SWOT analysis for the H_2D_2 can help to identify the key factors which may enable it to become competitive, and define the key market segments which may benefit from the project.

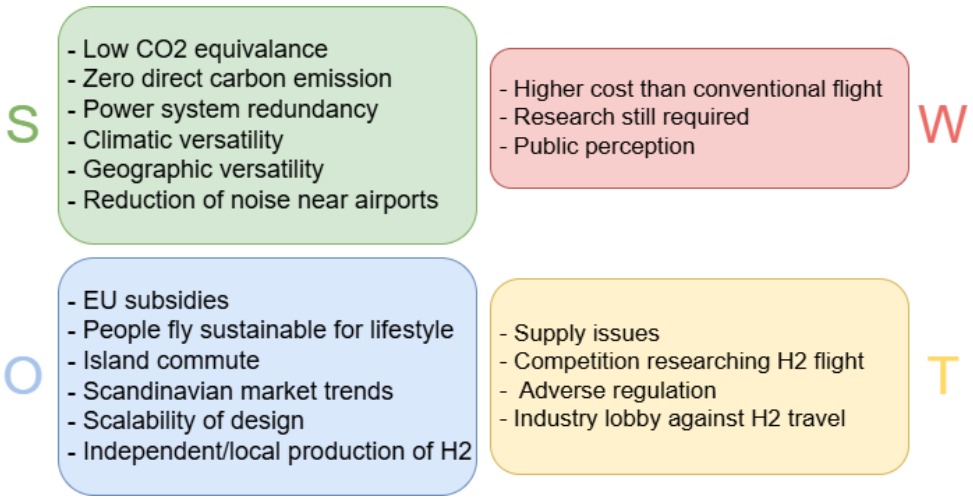

Figure 2.1: *SWOT matrix*

The main strength of the H_2D_2 is its low emissions (with zero operational CO_2 emissions) compared to competitors. This comes with expected weaknesses in high R&D, production, maintenance and operational costs. The opportunities which may improve the economic viability of SHTARWaRS are related to the public sentiment on sustainability. Policies driven by governments which enable and encourage sustainable technologies provide direct economic help, while individuals who boycott traditional flights due to their carbon emissions may choose hybrid-electric aircraft as well. Opportunities in expansion of (local) hydrogen production would also increase the feasibility and versatility of the operations of such aircraft. Despite these opportunities, current technologies limit the opportunity to expand this market. Hydrogen

[8] URL https://zeroavia.com/PTs/ [Cited 2 May 2025]
[9] URL https://smartaviation-apac.com/australias-stralis-aircraft-using-retrofit-program-to-aid-clean-sheet-aircraft-design/ [Cited 2 May 2025]
[10] URL https://www.stralis.aero/why [Cited 2 May 2025]
[11] `https://www.autoevolution.com/news/a-modified-beechcraft-1900d-to-become-australias-first-hydrogen-powered-airplane-216272.html` [Cited 2 May 2025]

supply limits and low Technology Readiness Level (TRL) of hydrogen technologies reduce the feasibility of wide-spread production in the short term. Competing hydrogen aircraft companies and lobbying against hydrogen technologies also pose direct threats to the H_2D_2.

2.2. Consumer & Stakeholder Analysis

The H_2D_2 aircraft is part of the market of turboprop aircraft. This market has a compound annual grow rate of 5.47% from 2025 to 2030, and the market has a total value of $ 8.47 billion in 2025 [13]. This shows that - however, not declining - the market, as it is now, has reached its maturity stage [14]. For aircraft designed to enter this market, something different needs to be done to appeal to the consumers. This design seeks to do this by using no fossil fuels and as little NO_x emissions as possible. This will appeal to consumers wanting to increase their sustainability, making this aircraft design a viable option.

Different customers/stakeholders can be determined for an aircraft of this type. They are shown in 2.2. This is a stakeholder map that shows the different stakeholders and their interest/influence.

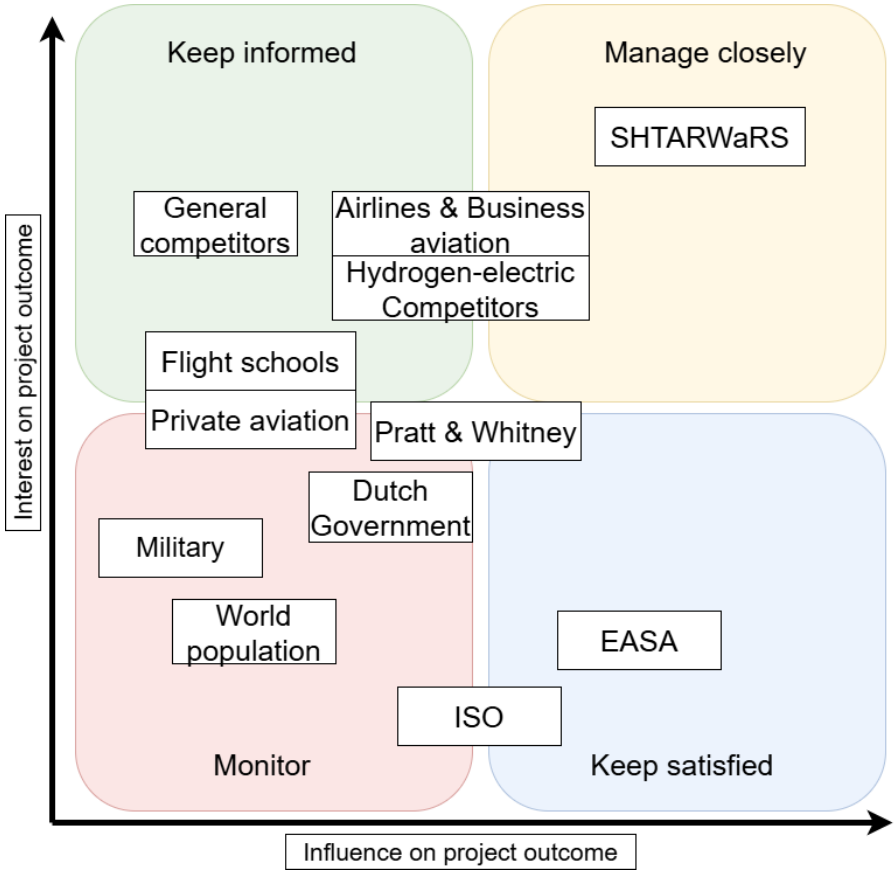

Figure 2.2: *Stakeholder map*

The figure shows that the most important stakeholder is SHTARWaRS itself. The developers and funding bodies of the project exert the most amount of influence on the design as they decide the driving requirements, and are the most interested in the outcome because they commissioned this design. Other stakeholders that are in Figure 2.2 are airlines & business aviation, general competitors, and hydrogen-electric competitors. The airlines & business aviation have a lot of interest due to the need to go green for many companies. Their influence will be less, but still enough that they shape the design. Competitors are also interested in the project and, of the two, hydrogen-electric competitors have more influence because they compete with this project. To the left are the flight schools and private aviation, which are interested in the project, but do not have a large amount of influence due to their smaller market share of the turboprop market. The government is also interested because of the reduction of emissions and exerts influence due to laws and regulations. Another regulatory stakeholder is the European Union Aviation Safety Agency (EASA), whose influence is large compared to its interest. The EASA provides the CS-23 [15] standard to determine

an aircraft's airworthiness in Europe. This will have a large influence on the design due to having to meet these regulations. Regulations for hydrogen aircraft are not yet defined. The International Organization for Standardization (ISO) standards [16] will be used as a stakeholder due to this. It will provide safe practices for the hydrogen storage, conditioning, and distribution. As this aircraft will only be the preliminary design, only the more general requirements from these agencies will be considered during the design process, as trying to fulfill all regulations for a concept is too time-intensive. The stakeholders that are last are the military and the world population. The military has a smaller incentive for sustainability and is not a large part of the intended market; thus it has low influence. The world population is also a stakeholder, since everyone will benefit from less pollution.

There are three key factors influencing the purchase process of a consumer: the cost of ownership, the aircraft utility and the product support. The cost of ownership consists of fixed and variable costs. The fixed costs are the depreciation (excluding engine), insurance, and storage. The variable costs are the depreciation of the engine, fuel, airport taxes, and maintenance cost. As of now, these are more costly for a hydrogen plane, but future innovations will decrease these. The costs associated with the H_2D_2 aircraft are explored more in Chapter 21. The user requirements compromise of the aircraft utility. If a company needs an aircraft that ferries 15 people across a maximum distance of 700 km, this design will meet it, and the consumer will consider purchasing this aircraft. The low emissions also contribute to customers' desire to use this design.

3

Project Objective & Requirements

This chapter uses the objectives of project SHTARWaRS, which are achieved by adhering to the stakeholder requirements. The mission need and project objective statements are presented in Section 3.1 and a summary of these requirements is provided in Section 3.2.

3.1. Project Objective

Hydrogen technologies are particularly interesting as a potential aircraft power source, since hydrogen production and use can be carbon-free through electrolysis employing renewable energy. This gives hydrogen technologies the potential to be a part of the final solution to carbon-free aviation. Analyzing this opportunity further is critical in meeting this need indicated by global aviation regulators, as outlined by the following need statement:

Mission Needs Statement

The aviation sector needs to demonstrate a hydrogen-electric PT in short-to-medium haul aircraft by 2035, as part of the EU Clean Aviation program.

Developing a Hydrogen-powered propulsion system for an aircraft poses many challenges, including lightweight tanks and FCs, and developing CCs that are safe, reliable, efficient, and climate-friendly. The aim of this project is to determine the feasibility, and to produce a system that may facilitate the aviation industry's fulfillment of global climate goals. To narrow the scope of this project, the following project objective statement is presented:

Project Objective Statement

To adapt the design of the Beechcraft 1900D into a robust, low-maintenance, low NO_x emission hybrid hydrogen-electric powered aircraft with 10 students in 10 weeks time.

This project strives to produce a hybrid hydrogen-electric-powered aircraft with minimal NO_x emissions. This will be achieved through the parallel use of hydrogen FCs and turboprop engines to produce engine power. Low emissions are to be achieved through water recovery for injection into the CC to reduce the production and emission of nitrogen oxides.

The power plant consists of a turboprop engine using hydrogen as fuel operating in parallel with an ELMO. A hydrogen FC supplies power to the ELMO and produces water. The water produced is injected into the engine to reduce the production of NO_x. To support this, a hydrogen storage and distribution system and a TMS must be designed.

3.2. Requirements Definition

Stakeholder requirements are presented in Table 3.1, and the compliance of the requirements will be discussed again in Chapter 22. The table contains the V&V procedures to be followed, where I stands for inspection, A for analysis, D for demonstration, and T for test. These will be explored in more detail in Section 6.2.

Table 3.1: *Stakeholder requirements*

ID	Requirement	M	Verification Method
REQ-TE-STK-A	The aircraft (a/c) shall contain a hybrid-electric PT	I	Check if the PT is hybrid-electric
REQ-TE-STK-B	Limiting emissions shall be a performance metric.	A	Confirm this performance metric was taken into account for the design of the system
REQ-TE-STK-C	The a/c shall have a minimum range of 700 km	D	The a/c shall be flown under nominal conditions and operations to determine the maximum range
REQ-TE-STK-D	The PT shall include a TMS	I	Check if there is a TMS in the design
REQ-TE-STK-E	The a/c shall provide a minimum 1 [MW] propulsive power during cruise	A	Compute if the PT is able to provide a MW of power
REQ-CO-STK-F	The a/c shall produce less emissions than a/c of the same caliber	T*	The emissions will be measured of the PT and compared to similar a/c
REQ-CO-STK-G	The a/c shall be able to transport at least 15 people	I	Check if there are 15 usable seats for PAX on the a/c
REQ-CO-STK-H	The a/c shall be financially desirable for consumers	A	Determine the total cost per available seat kilometer (CASK) to compare against competitors'
REQ-CO-STK-L	The PT shall not exceed a weight of 2541.9[kg] (3 times the original PT)	I	weigh the PT and compare to 3x the original
REQ-CO-STK-M	The system shall be completed and feasible by the expected time	A	Make a schedule of when what stage of the design is achieved
REQ-CO-STK-N	The PT shall comply with CS-23	A	The retrofitted Beechcraft design shall be checked against relevant CS-23 regulations
REQ-CO-STK-O	The a/c shall comply with H2 safety ISO standards	A	The hydrogen storage, conditioning, and distribution shall be checked against the relevant ISO standards

4

Original Aircraft Review & Budget Breakdown

This chapter discusses the original aircraft review and budget breakdown. Section 4.1 outlines the relevant parameters of the current design of the Beechcraft 1900D. Section 4.2 discusses the PP configuration of the Beechcraft 1900D. Section 4.3 explains the time, mass, power, volumetric, cost and emissions budget of the Beechcraft 1900D.

4.1. Current Aircraft Configuration

This section discusses the aircraft configuration of the Beechcraft 1900D[1]. The general characteristics and performance data are shown in Table 4.1.

Table 4.1: *Current configuration of the Beechcraft 1900D*

General characteristics		
Parameter	**Value**	**Unit**
PAX	19	-
Crew	2	-
Fuselage length	17.62	m
Wing span	17.64	m
Wing area	28.79	m^2
Aspect ratio	10.81	–
Operating Empty Weight (OEW)	4932	kg
Maximum Take-off Weight (MTOW)	7765	kg
Maximum fuel weight	2022	kg
Performance		
Parameter	**Value**	**Unit**
Cruise speed (TAS)	144	m/s
Range	707	km
Service ceiling	7.62	km

The limits of the center of gravity are given in Table 4.2. These values are with respect to the datum located 2.121 [m] forward of the center of the front jack point of the aircraft [17]. This jack point was estimated from a technical drawing, placing it at 11% of the fuselage length. Given that this is an approximation, the center of gravity range was cross-referenced with that of the Embraer 120, due to similarity in the characteristics. The estimated range aligned with the same relative position along the fuselage length [18].

Table 4.2: *Center of gravity limits of the Beechcraft 1900D*

Aft limit			
Operational mode	**Value**	**Unit**	**At specific weight**
Take-off	7.618	m	All weights
Cruise	7.696	m	From MTOW to 5585 [kg]
Forward limit			
Operational mode	**Value**	**Unit**	**At specific weight**
Take-off, cruise	7.188	m	MTOW

[1] URL https://customer.janes.com/display/JAU_9418-JAU_ [Cited 2 May 2025]

4.2. Current Powertrain Configuration

The Beechcraft 1900D is the only aircraft which flies the PT6A-67D engine, produced by P&W. This model stems from the more general PT6A, a legacy model from 1960 widely used in the turboprop industry. It specifically hails from the PT6A-60 family, which are the heavy-duty models. The model produced for the Beechcraft is further differentiated from the standard family through renovations introduced to increase performance (redesign of turbomachinery components, lightening, and strengthening the gearbox). All of these iterations have made this PP very resilient, which has enabled it to become one of the most dominant models of its class[2].

However, having a design based on one produced in the 1960s comes with its shortcomings. All internal controls are analog. This means they are operated by series of gauges and spring mechanisms that add weight. In contrast, modern aero-engines come with Full Authority Digital Engine Control (FADEC) systems, which can control much more complex systems. This consideration falls beyond the scope of this project, but redesigning the engine and integrating it into a complex PT should be one of the first considerations for the future design. FADEC can act as an interface to other control systems (i.e. Fuel-cell, fuel system) at the same time it maintains the PP within safe operating limits. All relevant information relating the current PP is presented in the Table 4.3.

[2]URL https://www.prattwhitney.com/en/products/general-aviation-engines/pt6a [cited 2 May 2025]

Table 4.3: *Key specifications of the P&W Canada PT6A-67D (Beechcraft 1900D)*

Category	Parameter	Value	Unit	Notes / Equivalent
General	Maximum continuous power	906*	kW	
	Flat-rated Take-off and Go Around (TOGA) power (<300 s)	954*	kW	1 279 Shaft Horse Power (SHP)
	Max. continuous torque	5 084*	Nm	
	Max. take-off torque	5 356*	Nm	
	Max. Gas-gen. shaft speed N_g	39 000*	rpm	20 s transient to 39,530 rpm
	Max Power shaft speed N_p	29 930†	rpm	104 % rated power
	Max. Propeller speed N_{prop}	1 700*	rpm	
	Dry weight	233.5*	kg	534 lb
	Overall length	1888.5*	mm	
	Overall diameter	466.1*	mm	
	Bleed-air extraction (max)	5.25*	% of air mass flow	
	Take-Off/Go-Around (TOGA) limit	48*	°C	Ambient temperature
	Specific Fuel Consumption (SFC)	0.509-0.680†	lb/SHP/h	
	Propeller efficiency	0.85	-	-
Compressor	Stages	5†	-	4 axial IBR + 1 centrifugal
	Max. air mass flow	10.22-11.21†	lb s^{-1}	sea-level SLS
	Max. Pressure ratio	12 :1†	-	β_{max}
	Maximum ITT (continuous)	780*	°C	
	Maximum ITT (take-off, 5 min)	800*	°C	
Combustor	Type	Annular†		reverse-flow†
	Fuel nozzles	14†		radially inward injection
	Spark plugs	2†		1 s^{-1} when in continuous ignition
	Igniter output	8 000†	V	capacitor-discharge
Turbine	Stages	3†	-	1 compressor driver + 2 Power stages
Reduction gearbox	1st-stage ratio	5.78 :1†		
	2nd-stage ratio	3.04 :1†		
	Overall ratio	17.58 :1†		

† Certified operating limit from EASA TCDS PT6A-67 Series, Issue 06 (18 Feb 2022).
* Manufacturer data from PT6A-67D Training Manual and associated P&W Canada publications.

4.3. Budget Breakdown

This section outlines the budget calculations and distribution required to perform a successful retrofit of the Beechcraft 1900D, which includes the time, mass, power, volume, and emissions budgets. The cost budget is not included here, but rather presented more in detail under Chapter 21, to include both the budget breakdown, as well as the expected profits.

Time Budget

The time budget presented in Table 4.4 below contains not only the elements of the propulsion system that are to be designed, but also additional tasks required to complete the design, such as integration with the aircraft. The lower bounds of the times are taken from the estimations made during the project organization phase, which are reported in the Project Plan [19] in the Gantt chart and Work Breakdown Structure (WBS). The upper bounds are then taken to be the lower bounds with an additional 10% margin. The reasoning behind the chosen value of the margin is further expanded upon in Section 4.4.

Total work effort allocated for the design of the elements of the propulsion system is therefore between 1678 and 1845 hours out of the 4000 hours allocated for the completion of the entire design, which is around

between 42% to 46% of the entire DSE allocated time.

Table 4.4: *Development durations budget*

Element	Fraction	Req. Dev. [hrs]
FC	13 %	221 - 243
EPS	5 %	91 - 100
PP	13%	221 - 243
H_2 storage	18%	294 - 323
H_2 conditioning	18%	302 - 332
H_2 distribution	12%	207 - 227
Cooling system	6%	100 - 110
Water Recovery System (WRS)	6%	100 - 110
Control & Data Handling System (CDHS)	5%	80 - 88
Aircraft integration	4%	62 - 68

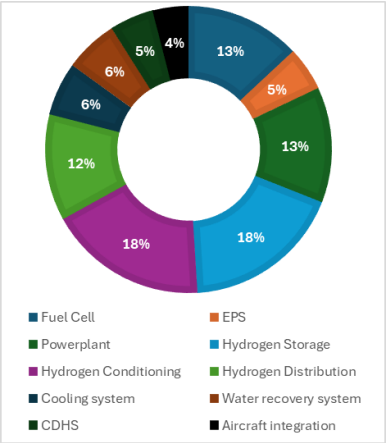

Figure 4.1: *Time fractions*

Mass Budget

By using the requirements, the mass budget of the reconverted Beechcraft can be obtained. REQ-CO-STK-L states that the weight of the PT shall remain within three times that of the original Beechcraft 1900D.

The weight of the original PT was referenced [20], and Table 4.5 outlines the weight and relative fractions of the PP components. Furthermore, the first level estimate of the weight of the PT for the re-converted aircraft can be determined as well.

Table 4.5: *Mass budget of the Beechcraft 1900D*

PP component	Fraction	Weight [kg]
Primary engines	55.5 %	470.4
Engine installation	11.1 %	93.9
Fuel system	12.0 %	101.2
Propulsor	21.5 %	181.9
Total PP weight	**100 %**	**847.3**
SHTARWaRS PP weight	**300 %**	**2542.0**
H2 fuel weight	**-**	**600**
SHTARWaRS MTOW	**-**	**8037.6**

Power Budget

The H_2D_2 operates in accordance with the performance criteria defined by REQ-TE-STK-C and REQ-TE-STK-E. These two requirements served as the basis for determining the necessary power during cruise and take-off. Although REQ-TE-STK-K is also an important factor in determining the required power, it has been set aside for now due to the variability in PAX numbers, with an estimated range of ±3 PAX (approximately ±240 kg), which allows for an adaptable power budget to accommodate fluctuations.

Equation 4.1 computes the ratio of thrust T $[N]$ to the total power input P $[W]$, where η_p $[-]$ is the propeller efficiency and V_∞ $[m/s]$ the cruise velocity[3].

$$T = \frac{P\eta_p}{V_\infty} \tag{4.1}$$

[3] URL https://eaglepubs.erau.edu/introductiontoaerospaceflightvehicles/chapter/propellers/ [Cited 2 May 2025]

Equation 4.2 establish the relationship between thrust and weight, under the assumption that thrust equals drag during cruise [21].

$$D = T = C_{D_0} q_\infty S + \frac{W^2}{q_\infty S \pi e AR} \tag{4.2}$$

the constants needed for Equation 4.1 and Equation 4.2 are defined in Table 4.1, Table 4.3 and Table 4.6.

Table 4.6: *Thrust calculation constants*

Parameter	Value	Unit	Description
C_{D_0}	0.021	–	Estimation of zero-drag coefficient [22]
e	0.736	–	Estimation of Oswald span efficiency for a straight wing [23] $e = 1.78(1 - 0.045AR^{0.68}) - 0.64$
ρ_{cruise}	0.551	kg/m^3	Density at cruise [17]
η_p	0.85	–	Average propeller efficiency within range defined in General Aviation Aircraft Design [24]

Subsequently, the cruise thrust for the re-converted Beechcraft 1900D was calculated based on their respective MTOWs. The corresponding power was then derived, and its fractions relative to the TOGA and maximum continuous power values from Table 4.3 were determined. These fractions served as the basis for estimating the take-off power required for the re-converted aircraft. The resulting values are presented in Table 4.7.

Table 4.7: *Power budget*

Element	Fraction of take-off power	Power [MW]
Power take-off (TOGA)	100%	1.908
SHTARWaRS power take-off	51%	0.973
Element	**Fraction of cruise power**	**Power [MW]**
Power cruise (max. continuous power)	100%	1.65
SHTARWaRS power cruise	51%	0.842

Volumetric Budget

For the sizing and positioning of fuel-tanks, it is essential to have a clear view of the available spaces present in the airframe for the SHTARWaRS PT. For this reason, blueprints of the airframe have been analyzed, and the resulting volumetric budget is given in Table 4.8. The spatial positioning of these cavities is also given by Figure 4.2.

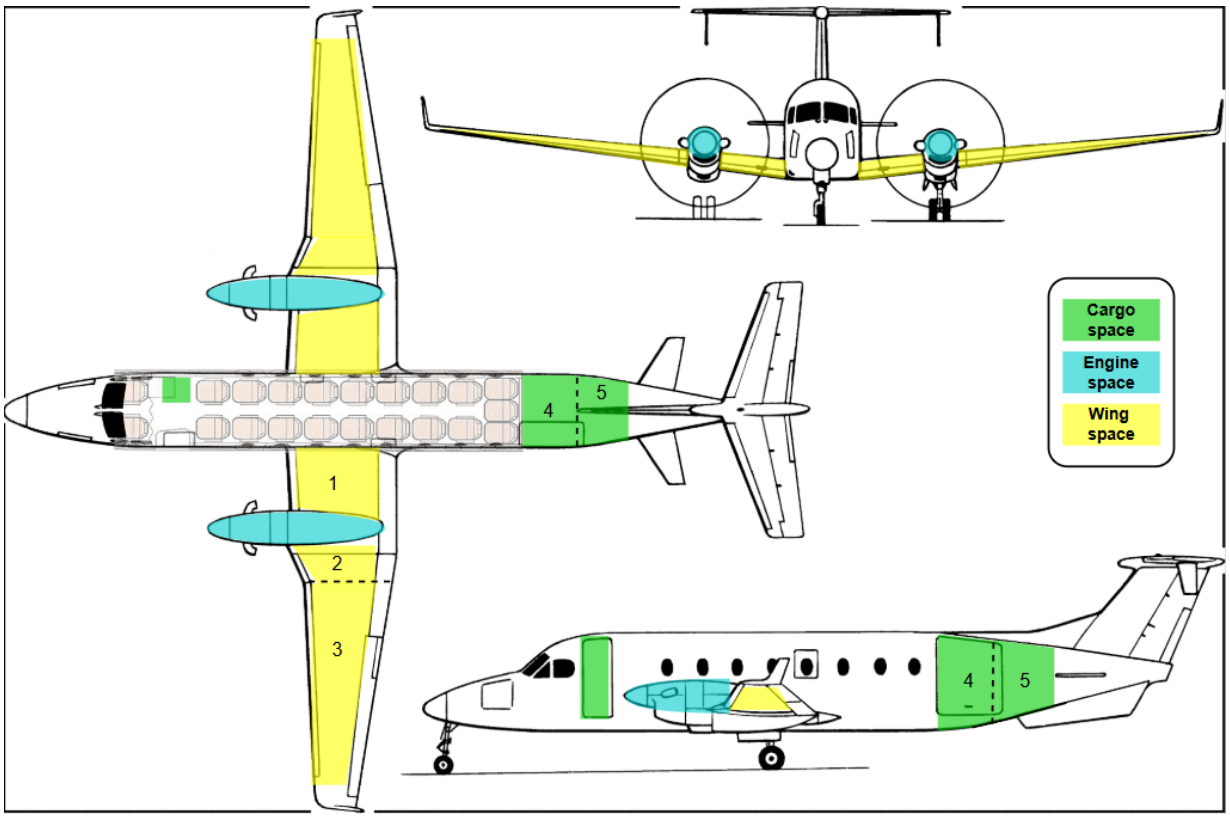

Figure 4.2: *Three-view drawing of the Beechcraft 1900D [25]*

Additionally, a contingency margin has been included for all cavities due to residual uncertainty in the actual configuration. This contingency is set at 10%, as with the time budget, with the rationale behind this values presented in 4.4. Note that the contingency assumes a lower available volume than what has been calculated geometrically. The geometric calculations performed approximate the cavities with sums of simple shapes: the engine pod volume is approximated by an ellipsoid. The wing volume is split into sections 1, 2, 3, which are considered trapezoidal boxes. The aft cargo space was split into sections 4, and 5. The first one is approximated as a volume with constant cross section made up of a semicircle top and rectangular bottom, while the second is a truncated cone. Finally the galley cargo space was considered to be a cuboid.

Table 4.8: *Volumetric budget*

Volume name	Volume	Margin Rationale	Contingent Vol.
Engine pod	2.892	Installation	2.603
Inboard wing (1)	1.144	Structural	1.030
Mid wing (2)	0.500	Structural	0.450
Outboard wing (3)	1.227	Structural	1.104
Aft Storage (4+5)	6.636	Stowage	5.972
Cabin Galley	1.014	Wiring	0.913
Total	**13.413**	**Total**	**12.342**

Based on data in Table 4.8, the volume fractions allocated to contingency can be visualized in Figure 4.3.

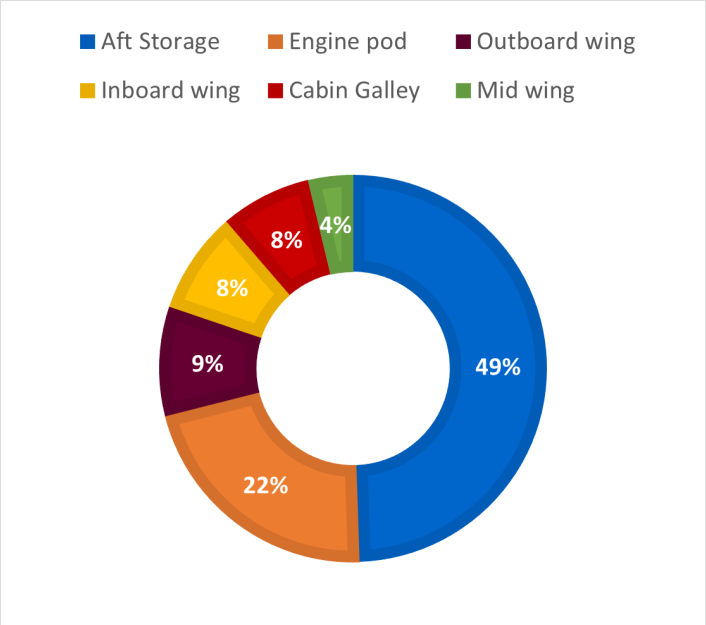

Figure 4.3: *Contingency volume fraction*

Emissions Budget

To be able to assess the impact of the implementations to the PT in later stages, it is pertinent to create a budget that takes into account emissions generated by the aircraft. To do this, due to the limited amount of data, a series of assumptions have to be made:

- The amount of thrust generated by the jet phenomena of the exhaust is negligible. This is a minor assumption since exhaust fumes are expelled at a 45° angle with respect to downstream flow in the current configuration. Thus, for this treaty Equivalent Shaft Horse Power (ESHP) is exactly the same as SHP.
- The minimum thrust produced (at low-idle) is extracted via linear correlation of Thrust generated and Inter Turbine Temperature (ITT). This choice stems from the basis of the quasi-linear [4] relation of the two variables.
- Typical values of emissions per kilogram of kerosene burnt are obtained from EUROCONTROL standard information[5].

A reflection can be made looking at the last row of the table. Having the engine in IDLE position produces less pollutants per kilowatt than having the engine at TOGA power. Thus, it is more efficient to have engine produce little power than high loads. This stems back from the fact that high power settings require high mass flows of propellant in the CC, which in turns increase combustion temperatures (high masses of fuel in the CC can lead to high local concentrations of fuel, which brings mixture ratios closer to stoichiometric values, which produce higher temperatures). High CC temperatures provide energy to initiate chemical pathways that lead to creation of emissions, with higher temperatures typically resulting in higher NO_x emissions.

Engine transient states cannot be explored at this time but are in general, very inefficient in comparison to constant power settings. For example, as the pilot increases thrust from equilibrium, momentarily, more fuel than necessary is injected in an equilibrium CC. This, in turn, increases the mixture ratio, indicating against throttling to TOGA power. This information will be relevant in the future to design the system modes.

[4] URL https://en.wikipedia.org/wiki/Brayton_cycle[Cited 2 May 2025]
[5] URL https://ansperformance.eu/economics/cba/standard-inputs/chapters/amount_of_emissions_released_by_fuel_burn.html[Cited 2 May 2025]

Table 4.9: *Preliminary emissions budget for a Beechcraft 1900D*

Category	Parameter	IDLE	TOGA	Unit	Notes
Specific fuel consumption	SFC	0.509	0.680	$lb\,SHP^{-1}\,h^{-1}$	Raw data.
	Power	797.86	953.75	kW	kW = SHP ×0.7457
Fuel flow (per engine)	$\dot{m}$	226.80	400.98	$kg\,h^{-1}$	
Fuel flow (aircraft)	$\dot{m}_{fuel,total}$	453.59	801.95	$kg\,h^{-1}$	Two engine configuration
Emission Index	CO_2	3.15	3.15	$kg\,kg^{-1}$ fuel	EUROCONTROL 2018
	H_2O	1.237	1.237	$kg\,kg^{-1}$ fuel	EUROCONTROL 2018
	NO_x	0.0016	0.01113	$kg\,kg^{-1}$ fuel	ICAO emissions databank
Emission of aircraft per hour	CO_2	1428.82	2526.15	$kg\,h^{-1}$	Min/Max power per hour.
	H_2O	561.09	992.01	$kg\,h^{-1}$	
	NO_x	0.725744	8.9257	$kg\,h^{-1}$	
Emissions Energetic Intensity	CO_2	1.79	2.649	$kg\,kW^{-1}\,h^{-1}$	Min/Max kilograms of pollutants produced per kilowatt hour.
	H_2O	0.70324	1.040	$kg\,kW^{-1}\,h^{-1}$	
	NO_x	0.0009096	0.01113	$kg\,kW^{-1}\,h^{-1}$	
Emission per km per PAX	CO_2	0.145	0.256	$kg\,km^{-1}\,PAX^{-1}$	Based on 19 pax,
	H_2O	0.057	0.101	$kg\,km^{-1}\,PAX^{-1}$	and design flight speed (144 m/s)
	NO_x	7.36e-05	9.06e-04	$kg\,km^{-1}\,PAX^{-1}$	

The NO_x emissions have been extracted directly from the P&W JT15D engine due to the lack of readily available information on the PT6A-67D. The reason behind this choice of engine is the readily available information of its emissions on the International Civil Aviation Organization (ICAO) Emissions Database[6], being an engine with similar compression ratio, same manufacturer and same time-frame as the one of interest. This engine is however a turbofan for small aircraft, so it serves only as a preliminary analysis.

The rationale behind the use of this source instead of EUROCONTROL[7] is the following: the emission spectra of a CC across power settings ultimately depends on its architecture and the chemistry mechanisms excited. Chemistry mechanisms are presumed to be exactly the same as long as kerosene-air is discussed (and mixture ratio is similar). Thus, the only control variable on the determination of emissions is the architecture. Here is where the chosen engine is a strong candidate. The architecture philosophy and the emissions target of P&W Canada in that time-frame are reflected on the architectures of both chambers. For this reason, the engine is a solid source for data.

4.4. Contingency Management

In this section, the contingencies in each separate budget are determined and managed, and the margins applied are justified.

It is important to state here that the currently applied margins can be large. At such an early design stage, it is challenging to estimate the resource allocation. It is expected that the margins are going to decrease with the increasing maturity of the project as the design steps, tasks and solution used will become increasingly more defined.

Time Budget Margins

The lower time budget value range presented in the Section 4.3 was generated from the work performed in the Project Plan [19]. The upper range value was estimated to be 1.1 times higher than that. Such a margin was chosen for several reasons. First, at such an early stage of the design, it is difficult to confidently assess the time required for the development of a certain element of the system. The scope and exact complexity of each element are continuously being defined. The time allocated per element can shift between the different elements as it becomes more clear how complex is each of the element designs. Additionally, the organization of the design process was already performed, where the time resource was allocated between all design, reporting and presenting tasks. It is not expected that the total time of the technical design phase to change dramatically, however, a margin still must be taken into account.

[6] URL https://www.easa.europa.eu/en/domains/environment/icao-aircraft-engine-emissions-databank [cited on 2/5/2025]

[7] URL https://www.eurocontrol.int/publication/european-aviation-fuel-burn-and-emissions-inventory-system-feis-european-environment [cited 30/4/2025]

Mass Budget Margin

REQ-TE-STK-L dictates the maximum weight the novel PT should have. This means that contingency margins must be defined for the mass budget, since this is limited by one of the key requirements. The European Space Agency has established a set of standard contingency margins for scientific assessment studies [26], and this was considered for the mass analysis of the plane leading to a percentage of 5%. This follows from the document provided above, taking into account that during the process, as far as mass is concerned, only off-the-shelf components may be used. It should be mentioned that no contingency margin was included for the engine weight since this was readily provided by the producer, P&W.

Power Budget Margin

The power was calculated using the estimated MTOW of the re-converted Beechcraft 1900D in Figure 4.3. A range of this value is already justified by the mass budget margin, therefore, the power also falls within a corresponding range. Additionally, an extra margin of 15% was included to ensure a conservative estimate of the power budget [27]. Furthermore, the take-off power listed in Table 4.7 does not include a margin, as it reflects the maximum power (TOGA) specified by the manufacturer.

Volume Budget Margin

The chosen margin of 10% makes for a rather conservative estimate of the volumetric zones present in the aircraft. According to European Space Agency (ESA)'s study [26], the Beechcraft 1900D can be consider as an "off-the-shelf" product requiring some modifications, thus falling under the 10% margin category. At this stage, it is still difficult to asses what, if any, other systems are present in those cavities which might impede the use of that space (structural, wiring, sensors, etc.). This is the rationale behind the large margin.

To get a better estimate and relief the contingency, on a later stage of the design, the airframe on which the PT shall be mounted must be examined to asses the quality of the cavities. Then, the actual volumetric budget, as well as the usability of the spaces can be assessed (perhaps, the aspect ratio of the volume is only fit for some purposes).

5

Aircraft Function Elucidation

The purpose of this chapter is to identify the desired capabilities and functions of the mission and its systems. Before performing the functional analysis, it is necessary to reduce the design scope by defining the mission architecture, its subsystems, the mission concept, and describing their interaction.

Several assumptions can be made, which will affect the design of the Functional Breakdown Structure (FBS) and Functional Flow Block Diagram (FFBD), and later influence the Requirements Discovery. The design is constrained by the provided architecture in the project description. This implies:

- The fuel utilized by the PT shall be hydrogen.
- Electrical power shall be generated by a FC system and the turbine in the PP.
- Thrust shall be generated by the PP and/or the ELMO.
- The FC shall supply electrical power to the ELMO.
- The PP of the aircraft shall comprise of turbopropeller engines.

By fixing certain systems in advance, the functional diagrams can go deeper into mission-specific details and focus mainly on the PT level, trading off concrete subsystems rather than abstract options. It allows defining precise functions and dependencies such as *Achieve H_2 purity* or *Limit NO_x emissions near airports*, and permits us to perform richer subsystem trade-offs aligned with our objectives.

The FBS (figure 5.1) and FFBD (figure 5.2) identify and describe the entire life cycle of the PT, with a major focus on operation. Functions spanning six levels provide a detailed description of the system's desired processes. Each block or function includes the task, the system or subsystem responsible for performing the task, and an identifier to facilitate cross-referencing between diagrams and simplify allocation of tasks in the FBS. Within the operate block, most functions are allocated to PT-related subsystems, further demonstrating the relevance of constraining the scope of the mission; while also ensuring that the PT does not endanger the cabin and PAX, and emissions are limited.

Functions within the *Production* will derive into requirements related to ease of integration, limited effect on stability and controllability, and Life Cycle Assessment (LCA) assessments for a sustainable production. *Decommission* will, once again, touch on sustainability and assembly/disassembly topics, while *Maintenance* will add upon the aforementioned functions, by including requirements related to accessibility and Ground Operations (GO).

While the FBS provides a structured hierarchy of functions, leveraging a quick understanding of the system, the FFBD provides a linear functional analysis, providing a better insight into the mission and operational objectives. The diagram has been divided into a high-level flow, in the red boundary, displaying the four central mission phases, and lower-level functions for production, operation, maintenance and decommission, spanning five different levels. A clear left-to-right flow and outlined boundaries make the diagram more comprehensible. The logical operators used in the FFBD include AND, OR, AND/OR when some different combinations of the following blocks could occur. Lastly, conditional operators, named C*X*. *Boundary markers* organize functional components by hierarchical level and isolate individual loops for an intuitive insight. For example, in Figure 5.2b, within the purple boundary, REF F.2.1.1.1 feeds into the power plant process. This structure makes it straightforward to pinpoint specific functions and to follow iteration loops, like the one governed by C5, a conditional check that determines whether water has been recovered during exhaust treatment. By using reference blocks, these loops merge into higher-level ones, making it possible to trace the flow through to the next mission phase.

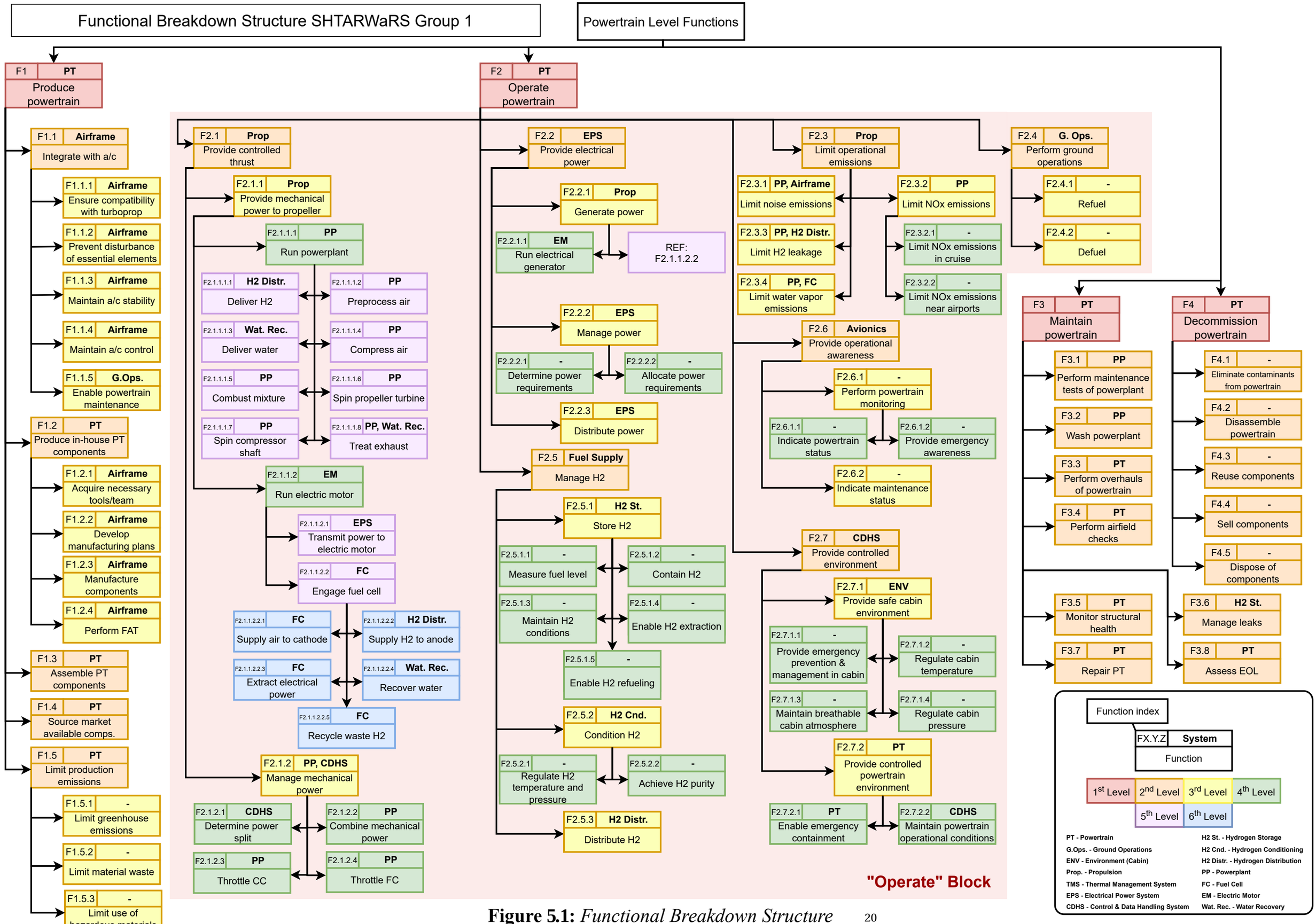

Figure 5.1: *Functional Breakdown Structure*

Functional Flow Block Diagram SHTARWaRS Group 1

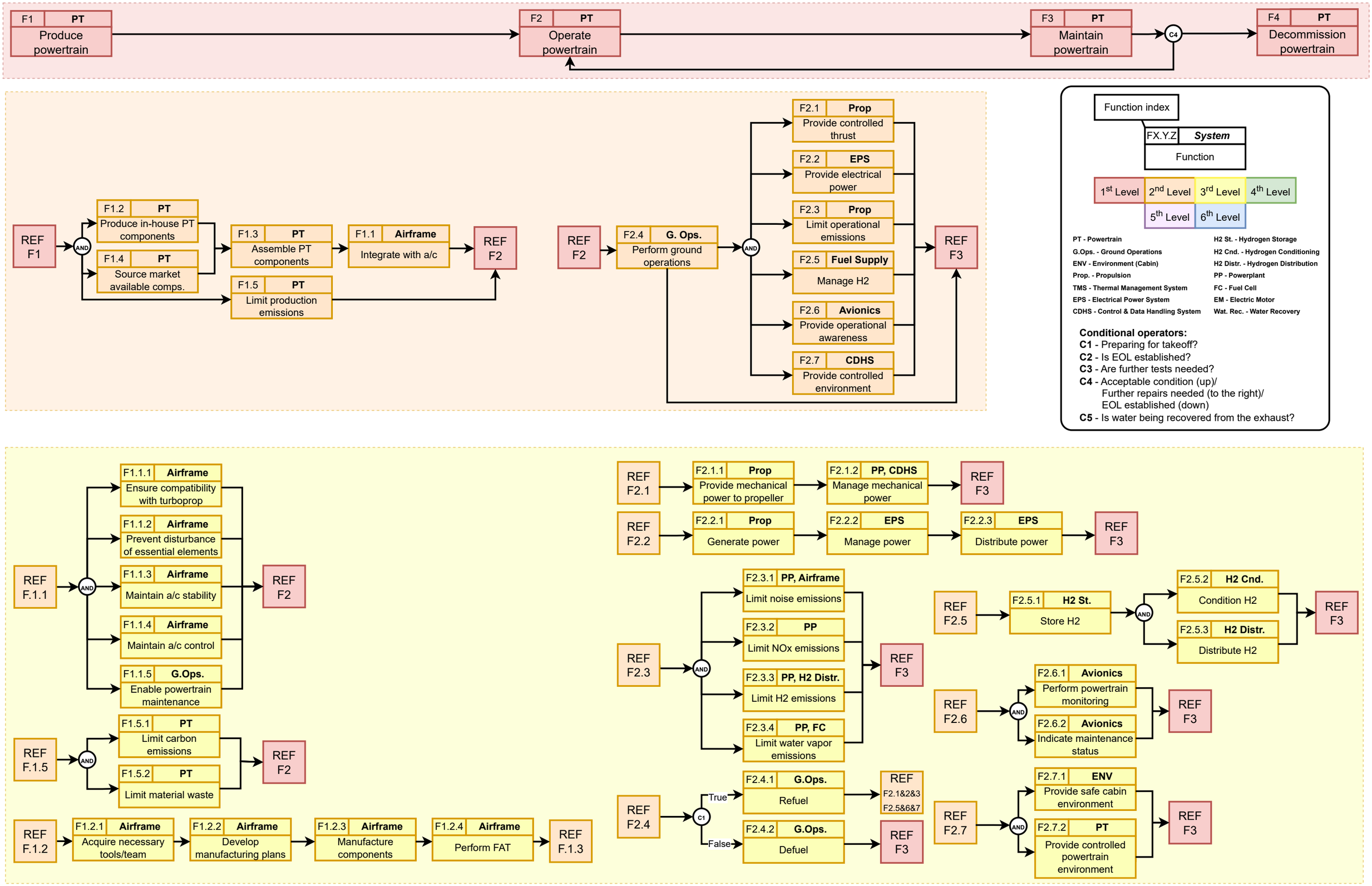

Figure 5.2a: *Functional Flow Block Diagram*

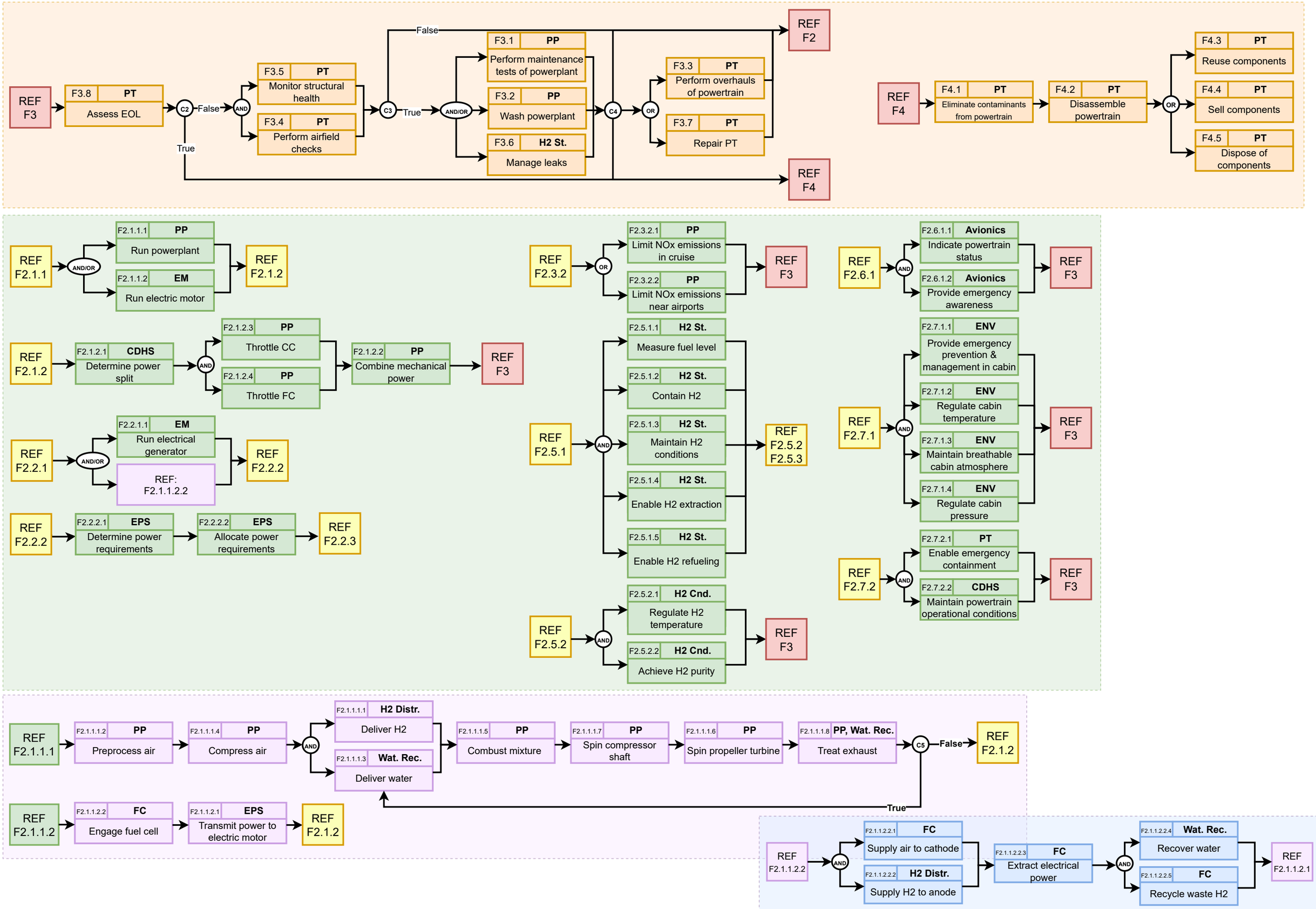

Figure 5.2b: *Functional Flow Block Diagram*

6

Project Development Protocol

This chapter presents the development protocol for SHTARWaRS. Section 6.1 covers the technical risk assessment, identifying risks, rating their likelihood and impact, and specifying mitigation and contingency measures. Section 6.2 details the V&V plan, while Section 6.3 sets out the sustainability strategy through a LCA.

6.1. Technical Risk Assessment

To perform a thorough preliminary technical risk assessment, a clear framework must be set up. This framework consists of risk identification and categorization. Risk identification consists of compilation of all known risks via brainstorming with different technical groups and a revision of the requirement list to determine the requirements that generate the greater risk of failure or damage. Then, the risks are categorized by their likelihood and impact. Finally, a mitigation plan is presented for principal risks, whose risk factor (likelihood×impact) is above the maximum allowed. The Risk Officer is appointed to monitor these risks and appoints a responsible Risk Manager (usually, the System Lead Engineer of the system to which the risk belongs).

Table 6.1 presents the numerical ranges assigned to likelihood and impact. Five ranges have been chosen for each value, as it is a trade-off between accuracy and information density. More resolution would mean more information, but the probability to mis-characterize a risk would be higher. A lower resolution would increment the probability of accurately assessing risks at the cost of overall information conveyed. As the project matures, risk resolution is expected to increase.

Table 6.1: *Quantitative risk mapping*

Likelihood	Impact	Assigned range
Very unlikely	Low	0.1-0.2
Unlikely	Med–Low	0.3-0.4
Possible	Medium	0.5-0.6
Likely	Med–High	0.7-0.8
Very Likely	High	0.9-1.0

It must be noted that it is impossible to accurately quantify all requirements' risk, so mitigation and contingency are key. Hydrogen safety guidelines and new hybrid-electric aircraft certifications were reviewed and used to compile the presented list.

6.1.1. Determining Risks

The risks that will be analyzed can be divided into those that come from regulatory bodies, those that come from the user and those stemming from systems. A comprehensive summary is presented below with the risk and their description.

Table 6.2: *Primary technical risks*

Risk ID	Description
R.CS.TE.1	Hazardous situation arises during nominal and emergency conditions within the operational limitations of the aircraft
RE.ISO.TE.1	The design does not comply with ISO standards
R.USER.TE.1	Range requirement is not met
R.USER.TE.2	The PT is incompatible with the structure
R.USER.TE.3	The aircraft does not fit 15 PAX
R.USER.TE.4	The power mass exceeds the determined maximum of three times the original mass
R.USER.TE.7	Hydrogen cost will exceed 15 €/kg in the EU in 2035
R.USER.TE.8	FC technology will not be available by 2035.
R.H2.TE.1	The hydrogen storage leaks excessively from the storage or piping system
R.H2.TE.3	Fatigue failure of the storage due to cyclical loads
R.H2.TE.4	The storage tank is damaged by an external factor
R.H2.TE.5	The temperature/pressure of the fuel is higher than required
R.H2.TE.6	The temperature/pressure of the fuel is lower than required
R.PT.TE.1	A short circuit occurs within the ELMO
R.PT.TE.3	Foreign object is ingested into the PP
R.PT.TE.4	Flame instabilities will reduce the efficiency of the engine
R.PT.TE.5	Oil leaks into the CC
R.PT.TE.6	Hydrogen leaks into the CC
R.PT.TE.7	Dirtiness in the CC will reduce the efficiency
R.PT.TE.11	Hydrogen pump supplying fuel to CC fails
R.PT.TE.15	Condensation of oxygen and liquid-rich air
R.TM.TE.1	WRS stops working

Each risk is coded with an ID, with the format *R.X.TE.Y*, where *X* determines the type of requirement or system it has been derived from. Here, *CS* and *ISO* refer to CS-23 and ISO regulations; *USER* stems from the stakeholder requirements; *H2* derives from hydrogen systems such as storage, conditioning, or distribution; *PT* denotes PT subsystems, namely the FC and CC; and *TM* stands for the TMS. This allows for tracking risks into specific system functions or stakeholder goals and identify which might be affected.

Table 6.2 above provides a comprehensive overview of the risks. From these, several safety concerns arise both during the design and operations of the hybrid-electric aircraft. These have been considered while generating requirements for the system.

6.1.2. Probability Factor of Risk & Consequences

Due to limited availability of data at this stage of the project, linked to maturity of certain components, it is not feasible to provide specific probabilities for each risk analyzed. The above-mentioned scoring metrics will be used to calculate the overall risk factor, which indicates how much of a concern it is for the system. All the risks and their location in the risk matrix are shown in Figure 6.1. "R." was removed from the risk IDs in the diagram for readability. Colors are used to indicate how influential the risk is for the design. Primary risks can be identified by looking at the ones that have the highest risk factor, which increases more the closer it gets to the top-right of the risk matrix.

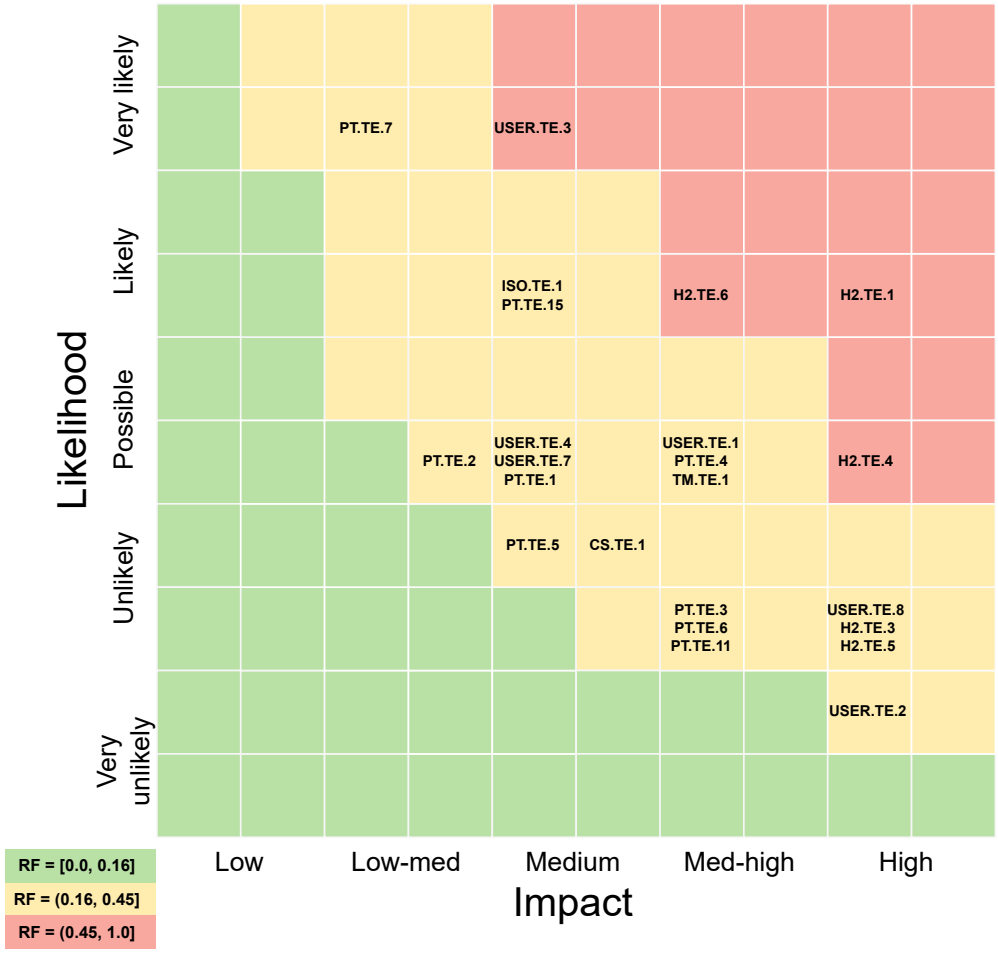

Figure 6.1: *Initial risk matrix*

6.1.3. Risk Mitigation & Contingency

Mitigation are actions that can be taken to lessen the probability of the risk occurring. Contingency are measures taken to lessen the severity of the risk. Following these measures, the likelihood, and severity of the risks were decreased, moving all risks from the High-Impact-High-Likelihood region, as can be seen in the top-right corner in Figure 6.2. During the development of the design, all risks still not within the safe region will have to be taken into consideration, given that they might pose delays in the schedule due to iterations, increments to the budgets or complete failure of a subsystem. Table 6.3 compiles all original (stemming from Table 6.1) and updated risk factors.

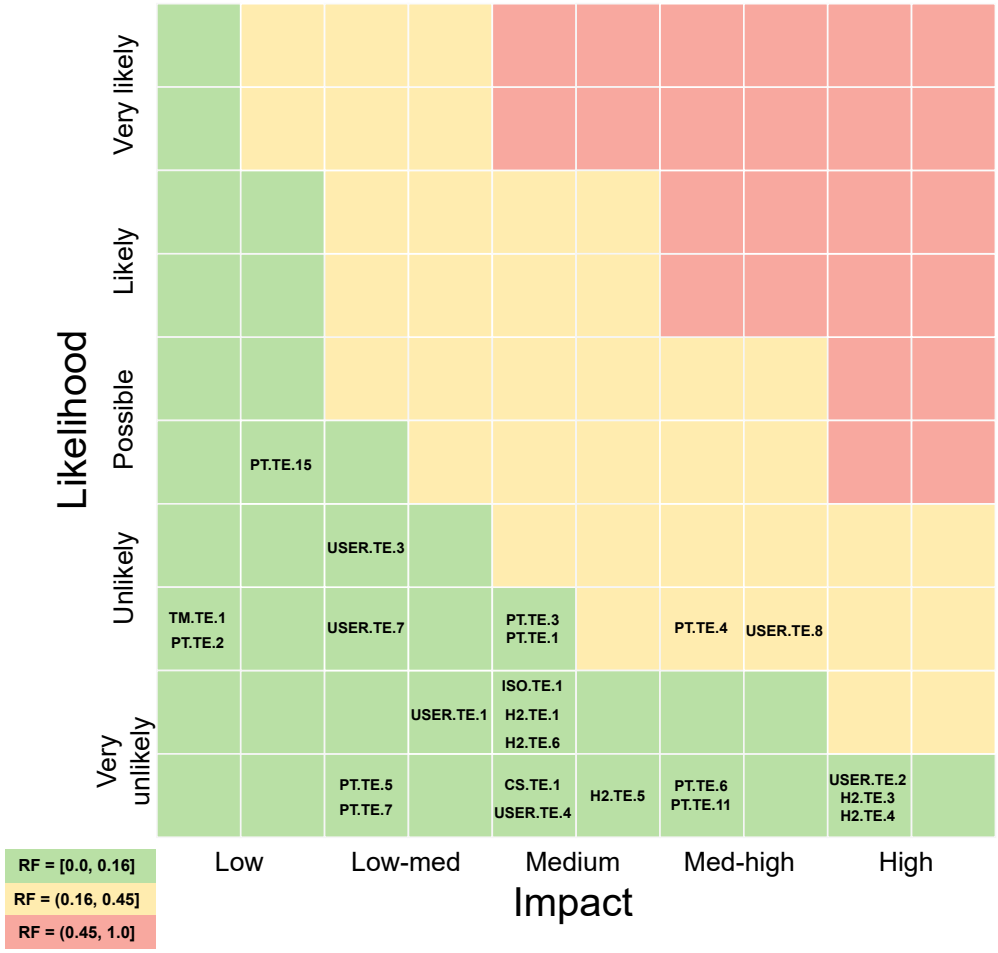

Figure 6.2: *Mitigated risk matrix*

Table 6.3: *Likelihood (L), Impact (I) and Risk Factors (RF) for all identified risks, including Updated (U-) values for the risks exceeding the 0.15 RF maximum.*

Risk ID	L	I	RF	U-L	U-I	U-RF	Risk ID	L	I	RF	U-L	U-I	U-RF
R.CS.TE.1	0.4	0.6	0.24	0.1	0.5	0.05	R.PT.TE.3	0.3	0.7	0.21	0.3	0.5	0.15
R.ISO.TE.1	0.7	0.5	0.35	0.2	0.5	0.1	R.PT.TE.4	0.5	0.7	0.35	0.3	0.7	0.21
R.USER.TE.1	0.5	0.7	0.35	0.2	0.4	0.08	R.PT.TE.5	0.4	0.5	0.2	0.1	0.3	0.03
R.USER.TE.2	0.2	0.9	0.18	0.1	0.9	0.09	R.PT.TE.6	0.3	0.7	0.21	0.1	0.7	0.07
R.USER.TE.3	0.9	0.5	0.45	0.4	0.3	0.12	R.PT.TE.7	0.9	0.3	0.27	0.1	0.3	0.03
R.USER.TE.4	0.5	0.5	0.25	0.1	0.5	0.05	R.PT.TE.11	0.3	0.7	0.21	0.1	0.7	0.07
R.USER.TE.7	0.5	0.5	0.25	0.3	0.3	0.09	R.PT.TE.15	0.7	0.5	0.35	0.5	0.2	0.1
R.USER.TE.8	0.3	0.9	0.27	0.3	0.8	0.24	R.TM.TE.1	0.5	0.7	0.35	0.3	0.1	0.03
R.H2.TE.1	0.7	0.9	0.63	0.2	0.5	0.1	R.PT.TE.2	0.5	0.4	0.20	0.3	0.1	0.03
R.H2.TE.3	0.3	0.9	0.27	0.1	0.9	0.09	R.H2.TE.6	0.7	0.7	0.49	0.2	0.5	0.1
R.H2.TE.4	0.5	0.9	0.45	0.1	0.9	0.09	R.PT.TE.1	0.5	0.5	0.25	0.3	0.5	0.15
R.H2.TE.5	0.3	0.9	0.27	0.1	0.6	0.06							

The primary risks will be lessened by making mitigation and contingencies for them. Below, in Table 6.4 are all the primary risks and their mitigation or contingency, or both. The values above 0.45 RF are critical, and are the first to be considered.

Table 6.4: *Mitigation and contingency strategies with assigned responsible departments*

Risk ID	Mitigation	Contingency	Responsible
R.CS.TE.1	Conduct regular system health checks and implement robust monitoring to detect early precursors	Isolate or disable affected subsystems, and execute predefined emergency procedure	System Engineer
RE.ISO.TE.1	The retrofitted design will be performed with ISO as part of the requirements	N/A	System Engineer
R.USER.TE.1	Add a margin to the fuel tank volume to mitigate higher fuel consumption	The design will be reiterated with a larger range capability to compensate for identified losses	Hydrogen Storage
R.USER.TE.2	Perform gravimetric, volumetric and structural analysis to ensure integration	Iterate design to minimize changes in the original Beechcraft design	Aircraft Integration
R.USER.TE.3	The seating configuration will be calculated to constrain available space	Reconfigure aircraft internal configuration or find new market for design capabilities	Aircraft Integration
R.USER.TE.4	The margins in the mass budget are considered hard, non-negotiable requirements. Include mass in the trade-off criteria	Implement weight-saving measures such as material substitutions or system simplifications	System Engineer
R.USER.TE.7	Integrate projected hydrogen costs into the budgets	Position the aircraft as a sustainability-driven product emphasizing environmental benefits	Hydrogen
R.USER.TE.8	Monitor the development of FC technology and explore other alternatives	Transition to an alternative FC type for the propulsion system, or reevaluate user requirements denoting range and other mission-driven capabilities	FC
R.H2.TE.1	Implement leak detection systems, and design piping and storage with high tolerance to pressure fluctuations	Activate and additional venting system to safely release the hydrogen in a controlled manner	Hydrogen Distribution
R.H2.TE.3	Choose a storage adequate for the cyclical loads it will experience from normal operation. Perform adequate maintenance inspections to be ahead of fatigue	Perform rapid response procedure to isolate and depressurise the storage system, avoiding catastrophic failure	Hydrogen Storage
R.H2.TE.4	Fuel storage is kept in dedicated storage areas with proper insulation and shielding, while also performing regular SHM checks.	Isolate and shutdown to prevent leakage or fire. Activate additional venting if necessary to safely release hydrogen	Hydrogen Storage
R.H2.TE.5	CDHS sensors measure temperature and pressure constantly to avoid fluctuations	TMS is redistributed to recover operating conditions.	CDHS
R.H2.TE.6	CDHS sensors measure temperature and pressure constantly to avoid fluctuations	TMS is redistributed to recover operating conditions. In case of loss of pressure in the storage, divert to nearest suitable airport	CDHS
R.PT.TE.1	Inspect loose or aging wires, and/or add circuit breakers to protect the system from overloading	Shutdown and isolate affected motor to prevent further damage	EPS
R.PT.TE.2	Allow pilot to override fuel flow into the CC	Override fuel flow into the CC	CDHS
R.PT.TE.3	Design nacelle and engine so that they can resist impacts	Power down the engine	Aircraft Integration
R.PT.TE.4	Include geometry modifications, acoustic dampers and/or swirlers in the CC design	Tune fuel-air ratios, pressures, and temperatures	Propulsion
R.PT.TE.5	Oil distribution system regularly checked during maintenance	Shut down CC, fly on FC	Propulsion
R.PT.TE.6	H_2 distribution system regularly checked during maintenance	Shut down CC, fly on FC	Propulsion
R.PT.TE.7	Maintenance checks will keep the PT system clean and healthy	N/A	Aircraft Integration
R.PT.TE.11	Have regular maintenance checks to check wear on the pump	Switch to alternate delivery route, or shutdown engine to maintain integrity of the system	Hydrogen Distribution
R.PT.TE.15	Incorporate temperature and pressure sensors at critical points	Implement venting or purging system to remove any buildup	TMS
R.TM.TE.1	Schedule routine maintenance and inspections to identify wear or failure points	Vent water produced in the FC to avoid a decrease in performance or failure	System Engineer

6.2. Verification & Validation Plan

V&V will be performed to ensure our findings are reliable and that there are no faults in the design methodology. This is done for the wording of the requirements themselves, the tools created, and the requirements will be checked to see if they have been met. These analyses are crucial for the controlled development of the design.

6.2.1. Requirements & Tools Verification & Validation

Some requirements constructed may turn out to be redundant or lacking. It is necessary to perform V&V of the requirements themselves, to insure relevancy and correctness. For this purpose, the "VALID" criteria were used [28]. VALID stands for verifiable, achievable, logical, integral, definitive, and this criterion is used for the V&V of the requirement list.

The system will rely on tools created for designing the PT, all subject to V&V. This section reviews the tools built and sketches V&V plans for those tools. Below are the tools used for the SHTARWaRS project.

- CC Emissions Interpolator
- FC Tool
- Flight Performance Model
- Hydrogen Tank Sizing Tool
- TMS Tool
- GWP & Cost Determination Tool
- EPS Tool

All tools follow a common bottom-up V&V process: unit tests first, then subsystem and system tests, with unit-test lists supplied for each current tool.

Unit Tests

Unit tests are to be performed on tools to ensure that the smallest elements in it are verified. There are several tests listed below that could be used for unit verification.

- **Calculation verification**: Make hand calculations for the result and compare to the output.
- **Inspection of results**: Run the part to be verified and check if the results make sense.
- **Literature verification**: Check the results against known examples in literature.
- **Invalid input test**: Run the code with invalid inputs and check if an error message is returned.

System Tests & Validation of Tools

After all the unit tests have been done, the system that they form is verified and validated. This is done by isolating these larger systems and, in the same way done for the unit tests, verifying the quality of these systems. These verification methods are described after a tool has been described in their respective chapter. As a final step, the tool should be validated to ensure the data it generates is what is needed from it. This is done be analyzing the in-/ output and seeing if it lines up with what is expected from the tool.

6.2.2. Product Verification & Validation

Product V&V is performed in a bottom-up manner according to the V-diagram [29], starting from the subsystem requirements. Verification is to be analyzed first, checking if specifications are met, through testing, analysis, demonstration, or inspection. Most of the verification process will not require a dedicated test facility, but when it is necessary to employ such a facility, it is marked by an asterisk in the table entry, next to the verification method. The subsystem requirements are verified in Table 22.3, and the system requirements are in Table 22.2.

Validation of the product follows from the stakeholder requirements, and aims to determine if the intended use of the product is fulfilled in accordance with the stakeholder needs. The stakeholder requirements related to emissions of Greenhouse Gas (GHG) will be treated together for the purpose of analyzing the sustainability of the finished product. These requirements are validated in Table 3.1.

The stakeholder requirements also provide the basis for the last step of the V&V procedure, the air worthiness certification, which is critical for the marketing of the retrofitted aircraft. Certification is needed before being allowed to sell the plane, but this procedure is out of the scope of this project.

6.3. Sustainable Development Strategy

In order to analyze the sustainable character of this project, a LCA will be performed. The first step in the LCA is the goal and scope definition. This step will provide the structure for the identification of functional unit, and subsequent definition of reference flows.

6.3.1. Sustainable Development Goals

The technical goal of this project is to produce a megawatt-class hydrogen-powered PP which produces as little NO_x emissions as possible. However, this is not the only metric by which this project's sustainability should be measured, as it only gives a notion of emissions during operation. LCA can be used to measure and minimize the environmental impact of the entire life cycle of the aircraft.

Since LCA is an analysis tool, the application of its results must be properly defined to ensure that the design process takes sustainability into account. For this purpose, two uses are identified. During the design phase, it compares alternative design and production options, flagging trade-offs and hot-spots for improvement. Once the final design has been determined, it quantifies the propulsion system's lifetime environmental impact, allowing direct comparison of SHTARWaRS with other aircraft.

Sustainability, especially in material production for hydrogen storage and in the fuel-cell trade-off, is built into the design strategy from the start, not added later. Chapter 7 shows the analysis of sustainability for the hydrogen tank storage and fuel-cell trade-offs. The final design is chosen with the GWP as a KPI, and the sustainability of the final design is analyzed in Chapter 17.

6.3.2. LCA Scope Definition

The scope of the LCA for SHTARWaRS has to include geographical and technological coverages. Analysis of these aspects already implies the introduction of assumptions and limitations, and represents an important stage in the sustainable development strategy.

Hybrid hydrogen/EPSs are a relatively modern technology development, so for the temporal coverage, a reasonable time unit would be 6 months of data collected in the last 3 years. The expected horizon when this technology will be feasible is 2035-2050, and it should be factored in for the time coverage.

Since most research analyzing hydrogen propulsion takes place in the EU, it is safe to consider that preliminary rules and regulations will stem from the EU. This indicates that for the scope of this project, the geographical coverage shall be limited to the EUROCONTROL area.

Finally, the technological scope focuses on a hybrid hydrogen-electric PT. This includes hydrogen combustion within a turboprop, FCs, and an integrated electrical system. The LCA therefore measures the sustainability of short-haul hybrid H_2 aircraft in EU airspace, targeting a 2035-2050 entry-into-service (TRL matched to that horizon) and using data from 2022-25 research projects.

6.3.3. Functional Unit & Reference Flow Determination

The functional unit dictates the metric for an LCA, heavily influencing its results; choosing the right unit is therefore essential. Each design-phase LCA will use a functional unit tailored to the system or component under review, ensuring the impact metric fits the item. These units, and the specific LCAs that need them, will be set when the required trade-off studies are defined.

The final LCA encompassing the entire propulsion system aims to provide a metric for sustainability analysis of the aircraft produced by this design. Because the primary goal of this aircraft is to transport PAX, the functional unit for the entire system will be defined with this in mind.

KPI
1) Available seat kilometers 2) Revenue PAX kilometers

Two KPI are defined for the volume of PAX which can be flown by an airline. The former describes the amount of seats transported times the amount of kilometers flown. The latter is similar, describing the number of paying PAX multiplied by the amount of kilometers flown. Since this project does not aim to describe the airlines' ability to fill seats, the available seat kilometers are the KPI for the use of this aircraft over its lifespan.

LCA Functional Unit
Transport of one available seat for one kilometer.

The functional unit captures how capacity and flight profile affect aircraft performance: fewer PAX or shorter legs change total seat-kilometers delivered over the aircraft's life. Each seat is considered occupied, including the weight of the PAX.

Each LCA must specify a reference flow linking the functional unit to the product that delivers it. For the design and trade-off LCAs, the products are the competing design options; for the final LCA, only the selected propulsion system is assessed across its full life span, accounting for the aircraft's PAX capacity. Hence, the reference flow is transporting one seat-kilometer with the aircraft developed in this project.

6.3.4. Impact Assessment

GHGs are only one part of a product's environmental impact. Selecting relevant impact categories begins with mapping the main damage pathways. This analysis yields the project's most relevant impact categories[1]:

- Climate change - measured as the GWP equivalent of 1 kg of CO_2 over a 100-year time horizon
- Noise pollution - measured in dB
- Water use
- Land use (for production and potential landfill at end of life)
- Acidification potential of the atmosphere (acid rain) - measured as SO_2-equivalence

When designing the hybrid PT, each impact category is weighted by how much design choices can reduce it. Comparing alternative configurations then reveals how each system affects environmental impacts across categories. For the final design analysis of this report, climate change is chosen as the key impact category, as the other impact categories are either too difficult to model with this preliminary design or are difficult to project to 2035. It is recommended to broaden this analysis in further design steps.

6.3.5. Socio-Economic Impact

Beyond the environmental LCA, a hybrid hydrogen-electric PT must be judged on social and economic grounds. Critical fuel-cell materials (e.g., platinum-group metals) come from limited regions, so their supply chains need ethical scrutiny, with any labor-rights issues reported to the client. Public trust hinges on proof-of-concept trials that meet aviation safety standards and clearly explain new procedures. The shift will create jobs and skills in hydrogen handling and logistics, but requires substantial up-front infrastructure investment; payback comes later through lower fuel and operating expenses.

[1] URL `https://ecochain.com/blog/impact-categories-lca/` [Cited 2 May 2025]

7

Trade-off Summary

The decisions made for the trade-offs, and their rationale, will be given in this chapter. First, the methodology will be explained in Section 7.1, then the FC, state, and storage will be chosen in Section 7.2, Section 7.3, and Section 7.4 respectively.

7.1. Trade-off Method, Rationale & Organization

The method for all trade-offs follow a similar procedure. First, system dependencies are determined, and potential general layouts are made. For the remaining options, trade-off criteria are selected and weights are attributed to them. These are condensed into a trade-off table that reveals a design option that is best for the H_2D_2.

3-5 criteria are defined and used for each individual decision. These criteria shall be formed with the aim of determining the optimal design for its application in H_2D_2. Each trade-off criteria shall be given a weight of at least 10%, increasing by increments of 5% where needed. The sum of all weights shall amount to 100%. The range of scores for each option must be from 0 to 1, with 1 amounting to an 'ideal' score for the given criterion and 0 producing an infeasible design. The criteria scoring shall be determined independently of the design options, so that the scores of different design options do not affect each other.

7.2. Fuel Cell Selection

Determining the FC type has a large impact on the design of the rest of the PT, as it determines the requirements for the hydrogen conditioning system, the state at which water is injected into the CC, operational conditions of the aircraft and thermal management requirements. This section aims to determine the FC type so that the other design options may be determined with the correct FC considered.

Three FC types were considered for the SHTARWaRS design: SOFC, LT-PEMFC, and HT-PEMFC. These were judged, in order of importance, on their specific power, ease of aircraft integration, efficiency, sustainability, and cost. When put together in a Trade-off matrix for 2035, as seen in Table 7.1, LT-PEMFC and HT-PEMFC emerge as almost equal victors. That is why the same has been done for 2050 in Table 7.2, which shows the HT-PEMFC to be more dominant. HT-PEMFC has been chosen as the FC for the SHTARWaRS design because while the LT-PEMFC performs similar in 2035, when looking further into the future, HT-PEMFC has more opportunities.

- **Green (△) :** Excellent, exceeding requirements (0.7-1)
- **Blue (○) :** Good, meets requirements (0.5-0.7)
- **Yellow (□) :** Acceptable, despite deficiencies (0.4-0.5)
- **Red (◊) :** Unacceptable (0-0.4)

Table 7.1: *Trade-off matrix 2035*

Criteria	**Specific power**	**Integration**	**Eff.**	**Sus.**	**Cost**	**Score**
Weight	**40%**	**20%**	**15%**	**15%**	**10%**	**100%**
LT-PEMFC	○ 0.68	○ 0.70	○ 0.60	△ 1.00	△ 0.89	**0.74**
HT-PEMFC	○ 0.68	△ 1.00	○ 0.60	△ 1.00	△ 0.71	**0.78**
SOFC	◊ 0.27	◊ 0.30	○ 0.65	□ 0.50	◊ 0.40	**0.38**

Table 7.2: *Trade-off matrix 2050*

Criteria	**Specific power**	**Integration**	**Eff.**	**Sus.**	**Cost**	**Score**
Weights	**40%**	**20%**	**15%**	**15%**	**10%**	**100%**
LT-PEMFC	△ 0.80	∘ 0.70	∘ 0.65	△ 1.00	△ 0.94	**0.82**
HT-PEMFC	△ 1.00	△ 1.00	∘ 0.65	△ 1.00	△ 0.94	**0.94**
SOFC	△ 1.00	◊ 0.30	∘ 0.70	□ 0.50	△ 0.85	**0.73**

As an outcome for the FCs trade-off, for the nearer future, 2035, the HT_PEMFC comes out as a winner, very close to the LT_PEMFC. However, if we project the usage of the FCs to 2050, it is clear that HT_PEMFCs are expected to go over a huge development, when they would clearly be the best option of FCs.

7.3. Hydrogen State Selection

The three states that were evaluated, were GH_2, LH_2, and CcH_2. These were rated on five different criteria. The Mass Efficiency (ME) represents the mass of hydrogen over the storage system mass (not including hydrogen). Specific System Size (SSS) represents the volume of the hydrogen over the volume of the storage system, and was idealized using the density of LH_2 at ambient pressure. The Heat Sink Potential (HSP) is the energy required to change the hydrogen from the storing state to the delivery state, beneficial for the cooling purposes that the hydrogen shall perform within the system. The trade-off also considers safety, grouping the integrated and social risks, which include the severity and frequency of risks, but also the human factor during incidents, the complexity of each system, and the maturity of each state. These were measured to further sum up into the criterion of "Need for Risk Mitigation (NRM)", which uses all of this to provide a qualitative scoring. Lastly, the Operational Flexibility (OF), represented by refueling and logistics, was considered for hydrogen handling depending on its state. The types were scored for each criteria in Table 7.3. Future projections were not performed for the hydrogen state, because it is considered in the OF. It is assumed that the logistics that are the most developed at this point, will be developed further on, in the future.

Table 7.3: *Trade-off matrix hydrogen states*

Criteria	**ME [-]**	**SSS [-]**	**HSP [-]**	**NRM**	**OF**	**Score**
Weights	**25%**	**25%**	**25%**	**10%**	**15%**	**100%**
GH_2	∘ 0.57	◊ 0.314	◊ 0.2509	∘ 0.625	△ 0.8	0.403
LH_2	△ 0.75	∘ 0.642	△ 0.9977	□ 0.5	∘ 0.4	0.737
CcH_2	∘ 0.69	△ 0.898	△ 0.8028	◊ 0.375	◊ 0.2	0.686

LH_2 is victorious in this trade-off and will be used as the state for the storage of the hydrogen.

7.4. Storage Tank Selection

The storage tank will have an inner and outer layer. For the materials of these layers, a trade-off was performed. The combinations of materials are as follows: CF-CF, CF-SG, SG-CF, SG-SG, CF-AL. These pairings were assessed based on their volumetric efficiency, gravimetric efficiency, LCA, and its Maintenance Cost (MC). The result of the trade-off are in Table 7.4, and show that SG-SG, (S-Glass Fiber UD (Prepreg)-S-Glass Fiber UD (Prepreg)), is the best option when all criteria are considered.

Table 7.4: *Trade-off matrix final candidates, including Carbon Fiber UD Prepreg (CF), S-Glass Fiber UD Prepreg (SG), and Al-7075-T6 (Al).*

Criteria	η_v	η_g	LCA	**MC**	**Score**
Weights	**40%**	**35%**	**15%**	**10%**	**100%**
CF–CF	△ 0.8301	∘ 0.5041	♢ 0.338	♢ 0.1	0.605
CF–SG	△ 0.8301	∘ 0.4990	∘ 0.505	♢ 0.1	0.546
SG–CF	△ 0.8297	∘ 0.4948	∘ 0.548	♢ 0.1	0.655
SG–SG	△ 0.8297	∘ 0.4980	△ 0.715	♢ 0.1	**0.698**
CF–Al	△ 0.8301	∘ 0.4866	□ 0.488	♢ 0.3	0.657

As a first sight outcome of this trade-off, it is clear that composite material tanks represent the best suit for the application of H_2D_2s's PT. Among these options, the one that stands out, based on its volumetric efficiency and the sustainability aspects, is the SG-SG variant.

8

Powerplant Design & Emissions Estimation

This chapter presents the PP design and emissions analysis. First, Section 8.1 will discuss the new fuel, its advantages and challenges compared to the current choice (kerosene), in the context of combustion. Once the challenges are well defined, a literature review is presented in Section 8.2 on the current CC architectures used for hydrogen combustion. Section 8.3 then presents the choice of architectural solution, its advantages and drawbacks. After this, the model used to project the engine performance to 2035 is presented in Section 8.4, together with the new engine design parameters. Then, the results from the model used to calculate the performance and emission profile are used to calculate the state of the engine and CC in different flight conditions.

8.1. Hydrogen in Combustion

Hydrogen combustion is at the heart of the redesign process. For this reason, it is necessary to clarify the main challenges and opportunities found in hydrogen combustion. It is also instrumental to understand where these stem from. Clearly understanding the fuel at hand permits to further narrow down the design space and propose conceptual solutions for the CC. For this reason, Figure 8.1 [30–39] has been compiled to visualize the relation of these and get a better understanding on their interrelations.

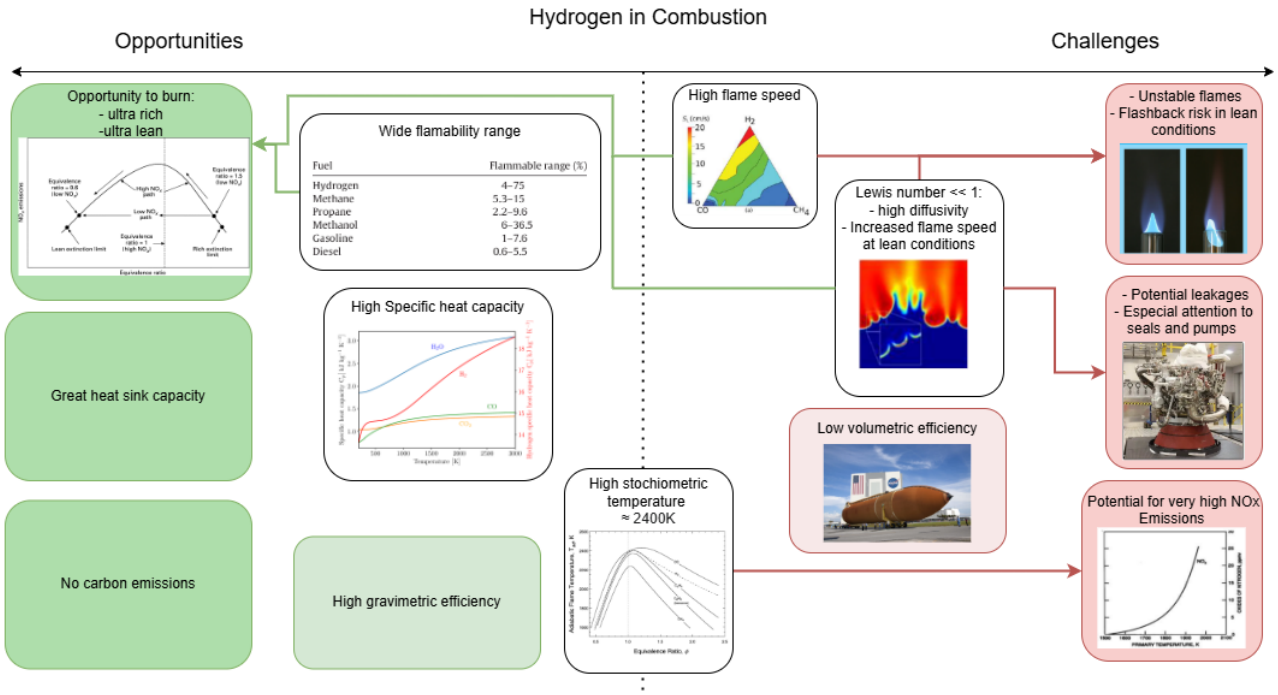

Figure 8.1: *Main opportunities and challenges of hydrogen use*

The main challenges posed by hydrogen use are the instabilities of flames and the flashback risks, especially in lean combustion. Furthermore, due to the high adiabatic temperature of hydrogen, the combustor has the potential to create very high NO_x emissions if burned at stoichiometric conditions. Conversely, hydrogen creates the opportunity to create CCs that burn at ultra-rich or ultra-lean conditions. Hydrogen can act as a great heat sink. It is also preferred in the long term as it does not produce carbon emissions.

8.2. Combustion Type Selection

To minimize the NO_x emission levels, a low Turbine Inlet Temperature (TIT) is desirable. Multiple types of combustion systems are available for hydrogen combustion, either as finished products or as concepts. The choice must also target reducing NO_x emissions, which can be done by combusting at lowered temperatures with low residence times and with an equivalence ratio different from 1. Burning with a low equivalence ratio additionally raises the risk of flashback in the combustion system. The various options [40] researched are:

- RQL
- Lean burn
- Micro-Mix
- Reheat combustion

Of the mentioned types of combustion mechanism, there are multiple that avoid stoichiometric burn (Lean burn, RQL), in the interest of minimizing NO_x. While a lean-burn stage helps in this sense, it is more susceptible to thermo-acoustic instabilities. This prompts the use of a rich-burn stage, which provides a high energy flow as well as relatively low temperatures and low population of oxygen-containing intermediate species, leading to reduced NO_x levels.

For those reasons, the focus turns towards RQL combustion. Here, the quench phase should be fast, to avoid the high-NO_x -emission transition zone related to an near unitary equivalence ratio. The dependence of NO_x emission rate regarding the equivalence ratio is illustrated in Figure 8.2 [41], further accentuating the need to avoid stoichiometric ratios.

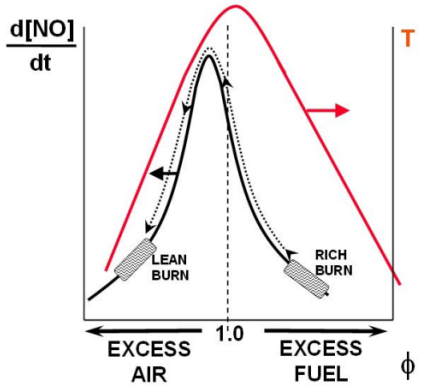

Figure 8.2: *NO_x emission rate depending on equivalence ratio*

8.3. General Combustion Chamber Architecture

The RQL CC consists of three parts. The first section, where all the fuel is injected into a primary zone together with a small amount of high-speed air in the form of one or several jets. This section is then ignited to burn fuel rich, hence the name rich burner. Then, the exhaust gases – at high temperatures and characterized by unburned fuel still in the mixture – leave this first cavity and a crucial process takes place: quick mixing/quenching. In this section, usually with the shape of a duct with inlet ports, new air is blasted onto the exhaust gases. This process should be done as fast as possible, as to quench the mixture, which would inevitably burn closer to stoichiometric conditions. It is crucial to enhance mixing and promote lower temperatures in this zone, so air is usually injected in the form of high-speed air. Blockages and geometric bluff bodies are also usual in this section as to promote turbulence and thus, mixing. Finally, this new mixture is ignited again, creating a lean flame. Thereafter, all remaining air that has not been injected into the CCs is added back to dilute the air and bring the overall temperature down to values acceptable for TIT. The overall structure is shown in Figure 8.3.

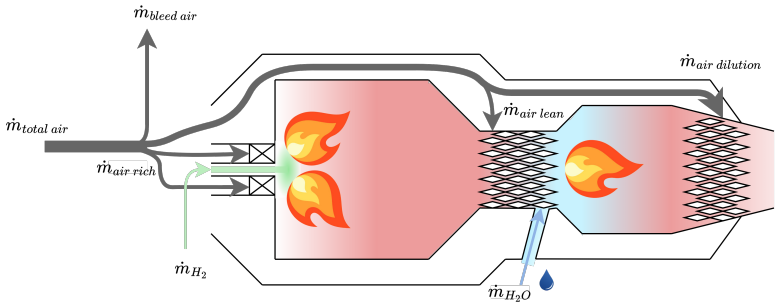

Figure 8.3: *RQL combustor*

As can be seen from Figure 8.2, the lean-burn usually generates higher levels of NO_x than the rich-burn, unless ultra-lean burns are used. Another way to reduce formation of nitrogen oxides is via the injection of third bodies – usually water – that act in a two-fold manner. First, if this third body is injected at low temperature, it will decrease the temperature of the reactants of combustion, hindering chemical reactions by decreasing the amount of molecules with energy greater than the required activation energy. Secondly, third bodies with high specific heats are usually preferred as they absorb part of the heat of the reaction, decreasing the sensible enthalpy of the gases during and after reaction. A possible third way in which third bodies could reduce emissions is by evaporation. If a third body is injected in liquid form – again water is the main contender – a considerable amount of the reaction heat will be used by the latent heat of evaporation of this body. All the strategies discussed work by effectively absorbing heat so that the activation energies of the chemical pathways of formation of nitrogen oxides are delayed or even inhibited. Note that the chemical pathways of the formation of NO_x are activated at around 1600 K and increase to substantial rates by about 1800 K. The optimal efficiency is obtained by directly injecting third bodies into the CC [42]. The most NO_x generating stage of the flight is during TOGA, when power transients bring equivalence ratios close to unity. For this reason, that is when water injection should be at the highest level [43]. It should be mentioned that the thermally "optimal" burn is not the minimal emission burn, quite the opposite indeed. NO_x emissions are a function of burning temperature, and so is efficiency (function of TIT). This immediately points to a trade-off between performance and pollution levels which should be performed.

RQL combustion is the type used for this project. It provides multiple advantages over the other combustor types. Firstly, the lean-burn helps in reducing the NO_x emissions, and by injecting water, the temperature is reduced even more in the lean stage. By using a staged combustion, the release of sensible energy is separated into two sections – rich and lean. This makes it possible to provide substantial power to the gas whilst maintaining moderate temperatures. This is possible due to lowering the gas temperature between burns, in contrast to other models, where all fuel is burned at the same time, reaching very high temperatures.

8.4. Powerplant Redesign

Projecting the performance of the State-of-the-Art (SOA) engine to 2035 is necessary to estimate the characteristics of the new engine, called Entry-in-Service (EIS) engine here-on. To be able to do this, a three step process is presented: first, the SOA engine will be modeled in a cycle analysis tool (GasTurb® 14). After this, statistical analysis is used to extrapolate the main performance parameters to model the EIS engine. Finally, the EIS engine is modeled with the same cycle analysis to get off-design performance.

The use of the cycle analysis needs further clarification. The tool is used as follows: First, a design point is chosen to model (TOGA for all cases, as it has the most readily available information). The geometric, secondary air system and efficiency data necessary is extracted to the best possible accuracy from engine diagrams, figures, and values found in [44]. If none of that data is available, standard values have been approximated – this was only necessary for mechanical efficiency of compressor and turbine, approximated to be 0.98. From this design point, the off-design behavior is obtained with the use of compressor maps. As the current best estimate, one of the standard maps used by GasTurb® 14 for the compressor is used – intermediate pressure ratio, high-pressure Compressor from [45].

8.4.1. State-of-the-art Engine Cycle Analysis

Using the values readily available, the SOA engine cycle can be approximated. Figure 8.4 shows the engine model used and the thermodynamic cycle at TOGA.

Notably, the secondary air system is obtained from [44] requirements of 5% bleed air for cabin pressurization and acclimatization. Furthermore, another 5% is extracted from high-pressure air (station 3) and is injected back into the turbine stator blades. This explains the 43-44-45 phenomena in the T-S diagram, decreasing overall efficiency. The peak thermal efficiency of the engine is computed to be 0.315.

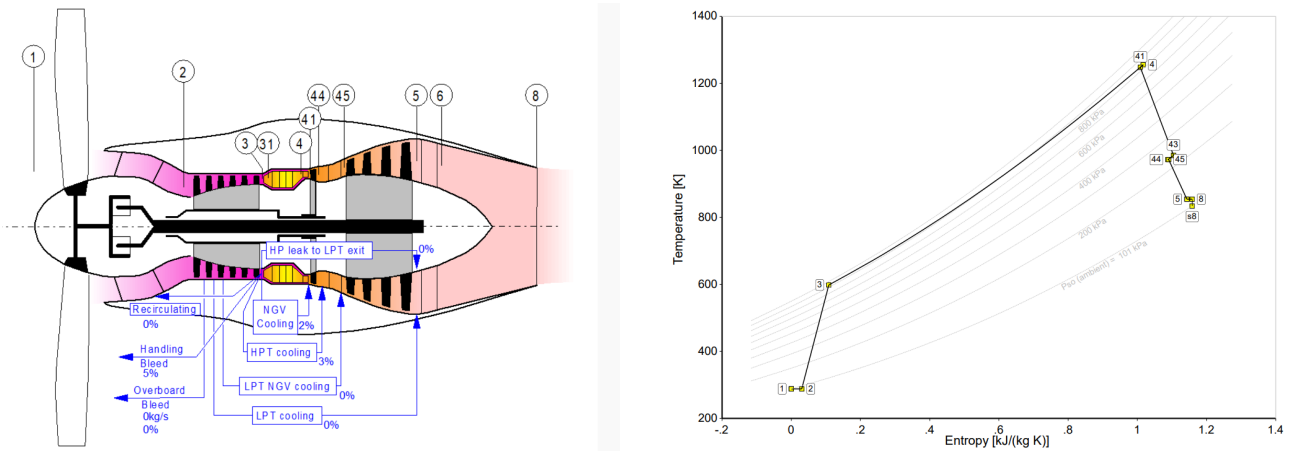

(a) *Schematic of the baseline engine*

(b) *T-S diagram of the brayton cycle in PT6A-67D*

Figure 8.4: *Comparison of the physical layout and its thermodynamic representation.*

From this design point, the off-design parametric analysis can be performed. This is done using GasTurb® 14 tool for off-design analysis, which uses the discussed compressor maps to compute behavior of the engine in non-nominal conditions. This off-design analysis correctly predicts the compressor runs smoothly from around 63% to 105% N1. This is within 1% of the actual minimum and maximum engine speeds, as LOW IDLE, the minimum self-sustaining power setting, is 64% in the PT6A-67D engine [46] and TOGA is 104%.

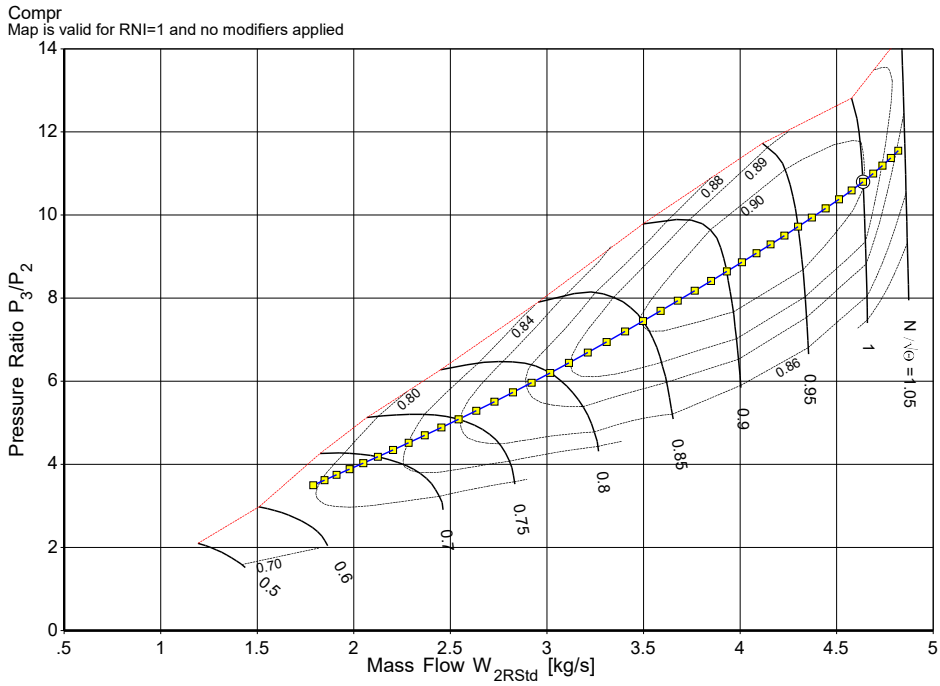

Figure 8.5: *PT6A-67D compressor map with operating line. (W_{2RStd} is the internal name GasTurb 14 used to call air mass flow across engine.)*

The engine compressor map is presented in Figure 8.5 with the operating line marked from 63% to 104%. The use of GasTurb® 14 permits to export several relevant outputs from the analysis, which are presented in Figure 8.8 in comparison to those of the projected EIS engine, but before the discussion of this figure, it is pertinent to present the methodology for projecting engine performance.

8.4.2. Projection of Engine Metrics to 2035 and 2050

Forecasting the performance of an engine entering service in 2035 is, in general, a complex task. This is due to the inherent stochastics of advancements in engine technology. That being said, the engine under consideration is a rather classic design, as it entered service in December 1991, and is highly susceptible to performance increases that have successfully been implemented in newer models of the -60 Series family. These include a redesign of the FADEC to make it fully electronic and implementation of single crystal compressors to increase compressor loading, in models like the newer PT6E-67XP.

With this in mind, the following analysis can be carried out. Two main parameters are extrapolated to 2035 and 2050: Engine thermal efficiency and pressure ratio. With these two parameters, the increase in overall efficiency and performance are both measured.

To compile the information, a single compendium of information has been chosen[44] directly from the manufacturer. This document provides information on all engines of the PT6A-60 Series produced from 1983 until late 2008 when the document was published. A further pruning is performed on the dataset, only engines within 200 HP of the original (1279 HP) are used. This is to ensure engines have the same profile and mission as the one at hand. One more engine is used for the verification of the computed trend-lines: the PT6E-67XP engine, which has been introduced into service in 2020.

Figure 8.6 presents the results of the projections. One thing must be noted. In general, pressure ratio is a discrete target set upon design. For this reason, a discrete behavior can be observed in the dataset, and thus the fitting is worse. Thermal efficiency, on the other hand, shows an excellent fit. The areas in red show the 95% confidence interval.

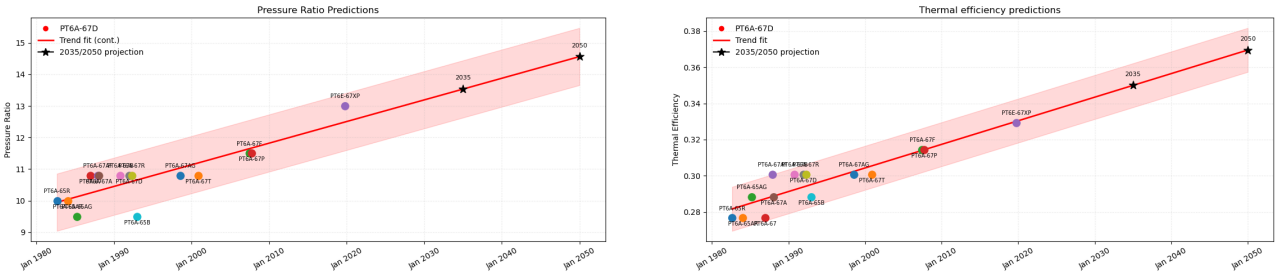

(a) *Pressure-ratio projection*

(b) *Thermal-efficiency projection*

Figure 8.6: *Historic PT6-series data with trend-line (red) and projections for 2035 / 2050 (black stars). Shaded bands show 95 % confidence.*

The final values for the 2035 EIS engine are a pressure ratio of 13.54 and thermal efficiency of 0.35. It must be noted that the increase of the pressure ratio of 25.3% is very similar to the 26.5% increase calculated by SAFRAN[47]. For the 2050 EIS engine, the projected values are a pressure ratio of 14.56 and a thermal efficiency of 0.3695.

The main redesign points have also been identified. These redesigns can, in principle, approach the SOA engine to that projected for the EIS. The main points are:

- Single crystal compressor and turbine blades to increase pressure gradients between cascades.
- Redesign FADEC, stripping the old analogical for a fully electronic system.
- Redesign CC to minimize pressure losses (~ 6% in current design).
- Redesign clearances in HPC, perhaps with the use of shrouded rotating components, and losses due to bleed air.

8.4.3. Projected Performance: Entry-In-Service Engine

With the projections for the 2035 EIS engine, it is possible to revise the model created in GasTurb® 14 inputting these new values. Pressure ratio is simply a design value, so variation of it is straightforward. Thermal efficiency, on the other hand, requires precise tuning of components and efficiencies. Table 8.1 presents the main choices taken by the team. The choices are selected after retrieval of the main redesign points.

Table 8.1: *Baseline vs. 2035 targets for redesigned components*

Component redesigned	State-of-the-art	Entry-in-service 2035	Units
Compressor design efficiency	90	92	%
Turbine design efficiency	93	95	%
Combustor pressure ratio	0.94	0.96	–
Combustion efficiency	99	99.99	%
Rotating component clearances	0.10	0.05	mm
Percentage loss per percentage clearance	2	1.5	%
Mechanical efficiency	98	99	%

With the redesigned components, it is now possible to do that same off-design engine analysis for the 2035 to get the new operating line and engine performance parameters. The new compressor map, presented in Figure 8.7 is presented and demonstrates the increase in pressure ratio and compressor isentropic efficiency in the operating line.

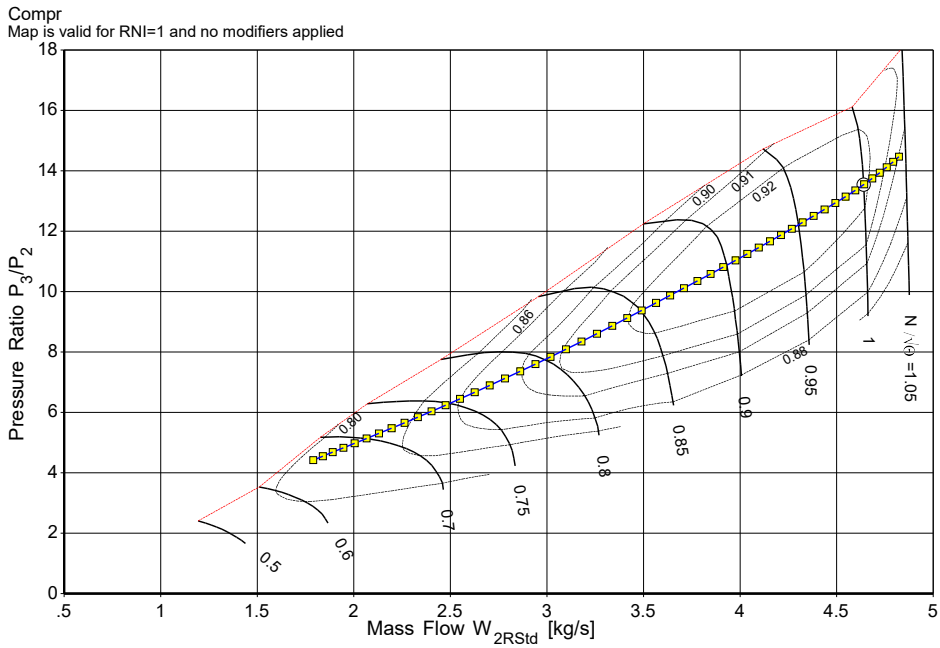

Figure 8.7: *Entry-in-service compressor map*

8.4.4. Performance Comparison

The most relevant results from each design are compiled and presented in Figure 8.8. A discussion is pertinent to unpack all the information present in the figures. plots are discussed left to right, then next row.

- **Shaft power delivered as function of spool speed**: The SOA engine can produce continuous power settings from 46 kW to 963 kW. The maximum power modeled is within 1% of the flat-rated engine (954 kW). The EIS engine has a range of power delivered from 64 to 1223 kW.
- **Isentropic compressor efficiency as function of spool speed**: Compressor efficiencies show the same trend and depict the increase in compressor efficiency as implemented into the model.
- **Pressure ratio as function of spool speed**: Varies almost linearly and demonstrates the expected extreme values.

- **Thermal efficiency as function of shaft power delivered**: demonstrates expected variation and expected peak thermal efficiencies. Note all graphs that depict values against shaft powers have EIS values shifted to the right due to higher power at each setting as depicted in the first graph.
- **Engine air mass flow as function of shaft power delivered**: this information is essential to be able to calculate the effect of throttling in the operating conditions of CC.
- **Fuel mass flow as function of shaft power delivered**: These graphs are very different, as the original engine consumed kerosene, with the highest consumption at 86 gr/s. The EIS engine uses hydrogen, which is much more thermally efficient, thus needing much less flow rate for similar performances.
- **PSFC as function of shaft power delivered**: Again, comparing kerosene burning with hydrogen burning yields very different results.
- **Burner efficiency as function of shaft power delivered**: increased efficiency due to forecasted values and change of fuel.

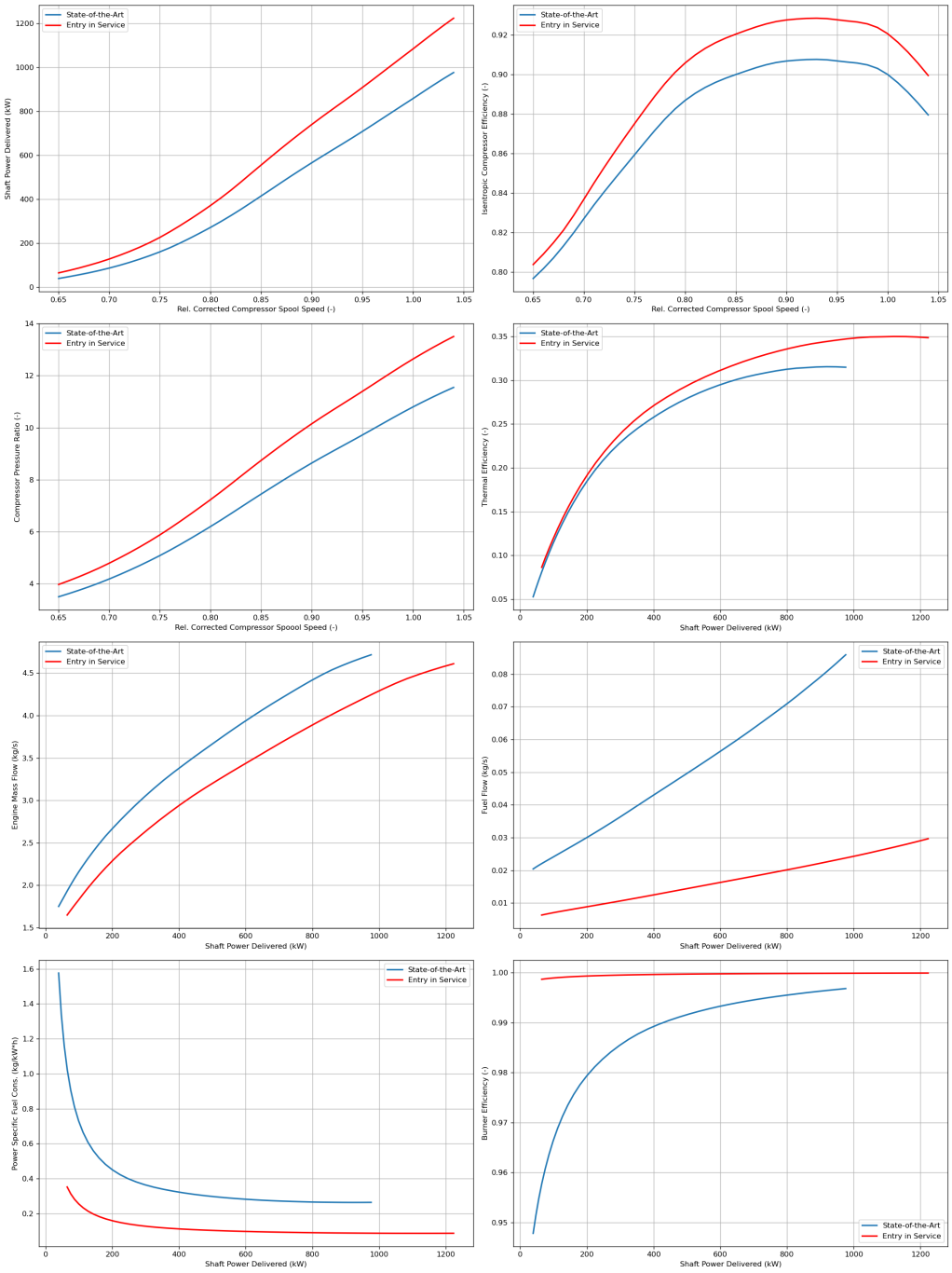

Figure 8.8: *Side-by-side comparison of state-of-the-art and projected EIS 2035 engine performance.*

The values depicted by this graph, resulting from the analysis explained in the previous sections, are very useful to create a simulation of the CC in the EIS at different operating conditions. So from this analysis, having the mass flows, efficiencies, power settings, etc. it is possible to recreate the expected operating conditions in the RQL burner at different stages of the flight. This, in turn, is useful to create a simulation for the NO_x at different power settings and water injection mass flows. This analysis is presented below.

8.5. Water Injection

To have a final selection on the liquid/vapor injection, it is important to quantify the difference of work necessary to compress both states to pressures in the CC. To achieve this, the specific ideal work has been calculated, not considering kinetic or gravitational terms as both are negligible compared to work exchange. The results of compressing are plotted in Figure 8.9.

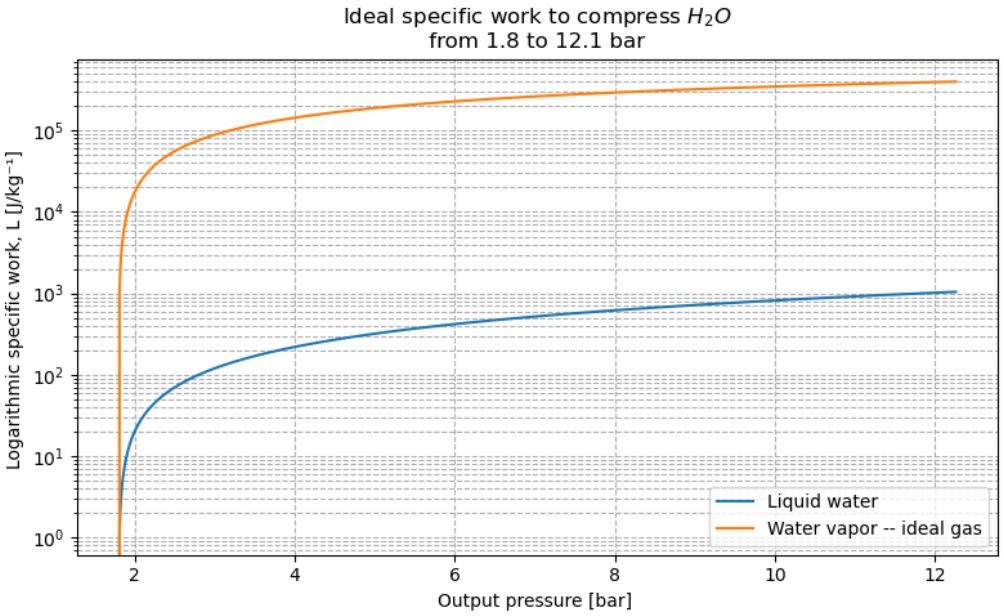

Figure 8.9: *Work to compress liquid and gaseous water for injection*

Injecting water vapor requires two orders of magnitude more specific work. This is conclusive evidence that water will be injected in liquid form into the CC.

8.6. Combustion Chamber Model & Simulation

Now that the architecture and operating conditions are clear, the CC can be modeled to create a preliminary map of its operating conditions. The goal of this simulation is to obtain a correlation between power settings, operating conditions and NO_x produced. This analysis intends to model the CC and obtain NO_x in standard, stable engine conditions: never during transients, stall/surge, choking, flameout or unstable flame conditions.

A key idea to understand the model is that it enforces mass conservation of air by splitting all the air into the air that enters the rich CC, the air that enters in the mixing stage, the bleed air requirement, and the bypass air that only mixes after all combustion has taken place, to cool down the exhaust gases.
With the information in Table 8.2, a simplified CC model can be created. This model will be used to estimate an "order of magnitude" validity of the NO_x created. For this reason, a series of simplifications can be done: the simulation is split into a rich CC, Quick Mix zone, and lean CC, which use a 1D premixed freeflame to model the rich and lean parts and a 0D reactor for the quench zone, respectively. Chemical kinetics are modeled using the Capurso mechanism [39], and the combustion is modeled using Cantera interface for Python [48].

Table 8.2: *Customer requirements concerning the CC*

Condition	Value
$\dot{m}_{\text{kerosene}}$ (g/s)	86.5
$\dot{m}_{H_2,\text{equivalent}}$ (g/s)	29.4
TIT_{max} (K)	1273
Customer requirements	
ϕ_{rich}	5
Bleed air (minimum % total)	5.25
NO_x (ppm) @ 15% O_2	<25

Rich Zone of the Combustion Chamber

The customer requirement for the equivalence ratio effectively fixes the behavior of the rich CC at every operating point of the engine. All the fuel is injected into the rich part of the CC, and since the equivalence ratio is fixed, the air mass flow into the rich CC is also known. This simplifies the analysis of this part to a series of operating lines that can be computed once and then stored to be used in the subsequent parts of the CC. All information is presented in terms of shaft power. This is because shaft power is directly mappable to the power setting imputed in the cockpit, not permitting the pilots to input power settings outside standard operating conditions. The points in the figure are steady-state: attainable static behaviors.

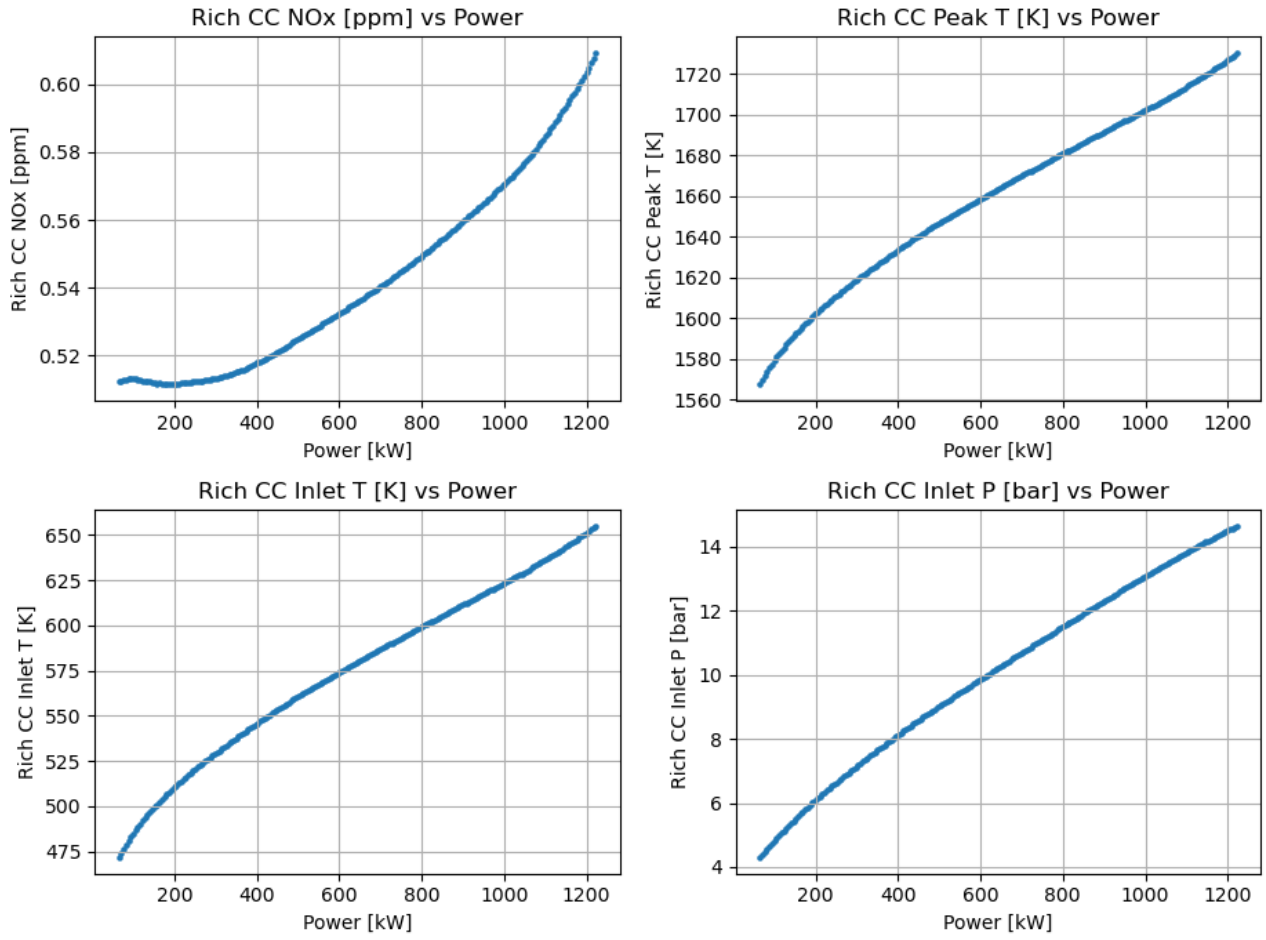

Figure 8.10: *Rich-combustor operating trends across the 64-1,220 kW range.*

This plot demonstrates the characteristics of the inlet and exhaust of the rich CC. From the outputs, the Quick Mix zone can be computed to get an estimation of the NO_x produced.

Quick Mix Zone of the Combustion Chamber

The quick mix zone is designed in the following way: the rich zone exhaust enters the zone, air is injected to lower the equivalence ratio and temperature, and water is injected to further lower the temperature. The mix autoignites after some specified, autoignition, time. That should, however, happen only when the mix reaches the lean zone of the CC, as that increases the temperature dramatically, resulting in a high NO_x production, which is further increased by passing between the equivalence ratio of the rich zone to the lean zone, through 1, for which NO_x formation is the highest. For this reason, the quench zone is designed to avoid autoignition, rapidly mix all the new products and pass them to the lean zone as fast as possible. Additionally, hydrogen has a wider flammability range than Jet-A, making it easier to ignite, further complicating this design.

To manage the design of the quick mix zone for the scope of redesigning the CC of the PT6A-67D engine, several simplifications and assumptions were made. A summary can be seen in Figure 8.3 below. A laminar, 0D reactor simulation was run. Firstly, a rectangular cross-section geometry of specified dimensions was assumed, the equivalence ratio was set to 1.0 and assumed to be constant as that provided the most constraining results. All the products are assumed to mix instantly at the inlet of the quick mix zone, so that the mix can be analyzed as it propagates and its state advances with time.

Table 8.3: *Quick mix zone assumptions*

Parameter	Value
Length	0.1 m
Width	0.02 m
Height	0.15 m
Equivalence ratio	const = 1

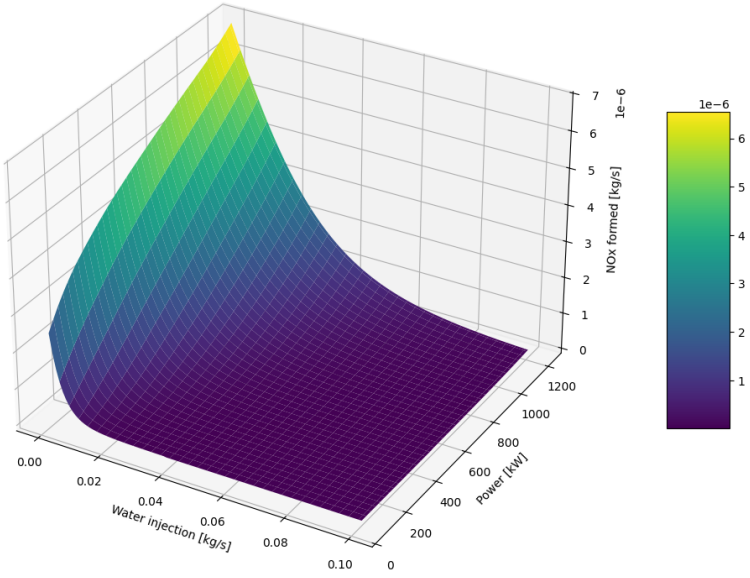

Figure 8.11: *NO_x formation depending on the power and liquid water injection inputs*

The results of this simplified simulation, seen in Figure 8.11, show the conservative estimate of the NO_x produced within this zone normalized to 15% O_2. As expected, most NO_x forms at highest power and no water injection. It can be observed that the maximum value reaches around $7 \cdot 10^{-6} \frac{kg}{s}$; however, this value is decreased downstream, at the RQL exit, as the exhaust gases, containing NO_x, get diluted with bled air. For this reason, this part of the simulation was combined with the lean zone simulation. The NO_x was calculated in kg/s and only later recalculated to ppm units to account for the dilution and compare it to the requirements.

Lean Zone of the Combustion Chamber

Once the upstream conditions have been decided, it is possible to study the lean CC to finalize the full design of the CC. For modeling purposes, it is assumed to be a perfect equilibrium mixture between the exhaust gases and a predetermined amount of air and water. The amount of both mass flows into the mixture is subject to optimization, as air affects the equivalence ratio, and water affects the temperature of the mixture into the lean CC.

Air being directed into the CC changes the equivalence ratio of the lean CC at TOGA. Figure 8.12 presents the change of available bleed air and equivalence ratio as a function of the air injected into the CC. The vertical red line delimits the minimum bleed air that is necessary as per engine requirements, summed with the air already used in the rich CC. The horizontal line delimits the maximum preliminary equivalence ratio of lean CC due to NO_x emissions. In no way will the dry (without temperature moderation) equivalence ratio go higher than 0.8 as that means temperatures well within NO_x creation range. This plot returns the working range of lean CC equivalence ratio $\varphi_{\text{lean}} \simeq [0.234, 0.8]$.

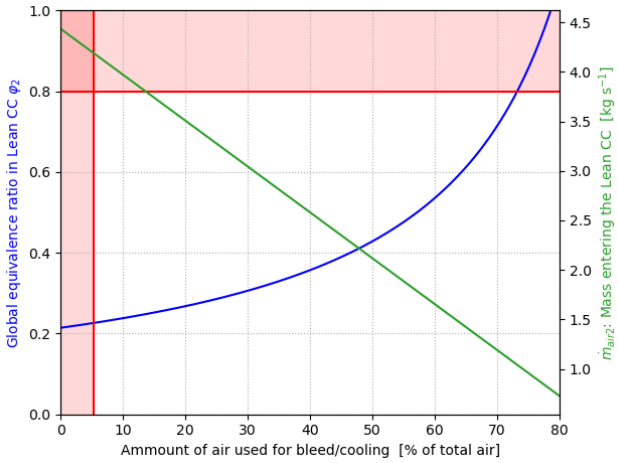

Figure 8.12: *Relation between air mixed, cooling air and bleed air*

Now, compiling all information from previews sections, it is possible to produce operating maps of NO_x as a function of the equivalence ratio and water injection, not only for TOGA, but for the most relevant engine operating conditions. The cases for study are the most normal static engine operating points: LOW idle, cruise and TOGA for the EIS engine, not for the aircraft. These maps are to be used for a series of things:

- Extract NO_x production at every feasible combination of water injection and equivalence ratio.
- Investigate the location and direction of isolines of NO_x produced to observe the effect of water injection on the emissions.
- Observe possible interesting phenomena, such as a quenched flame.
- Check TIT temperatures at all working conditions to locate possible incompatibilities with downstream turbines at high temperatures ($TIT \geq 1273K$).
- Observe gas power produced at the outlet to choose an operating point. This gas power is normalized to the gas power of the original engine.
- Constrain the design space to get a final lean equivalence ratio.

A series of conclusions can be drawn from each graph. These graphs contain the water-injection limit (red line), and a shaded exceedance region. Color scale is common: $\log_{10}$ of wet NO_x in ppm.

The first plot, Figure 8.13, at LOW IDLE, producing 64 shaft kW in the EIS engine:

1. Water available from the FC is the least in this condition. However, since the fuel injected is 6 g/s, the water/fuel ratio is ~ 2.
2. It is the plot with the least NO_x produced and the lowest slope of NO_x isolines. This means it is most efficient to inject water in this zone.
3. Flame quenching is observed in the top of the graph, where it collapses.
4. Gas power observed has minimal variation.
5. For all the discussed, a sensible point to choose the lean equivalence ratio to be is at 0.5. The NO_x emissions at this point are 2.3 ppm.

The second plot, Figure 8.14, at cruise, producing 813 shaft kW in the EIS engine:

1. At cruise, water is at the highest flow rate (it is throttled higher than at TOGA) at 82 g/s. This gives the most flexibility in water injection.
2. NO_x begin to show high production rates near stoichiometric conditions.
3. Gas power begins to demonstrate high variance depending on the zone. It must be noted that 0.74 is the normalized N1 at cruise. Thus, it makes sense to keep gas power close to the expected engine power.
4. A sensible point to locate the design equivalence ratio in this zone is at maximum water injection, on the 0.74 line, for a final equivalence ratio of 0.75. NO_x production is around 3.3 ppm.

The final plot, Figure 8.15, at TOGA, producing 1223 shaft kW in the EIS engine:

1. Water produced is slightly lower than at cruise due to throttle down of the FC.
2. NO_x show high production rates that need to be mitigated with water.
3. Gas power that needs to be produced is located at 1.00.
4. The position of the equivalence ratio to be selected is at most water production along the 1.00 power line. This way, the equivalence ratio is 0.8. The expected NO_x production is around 4.2 ppm.

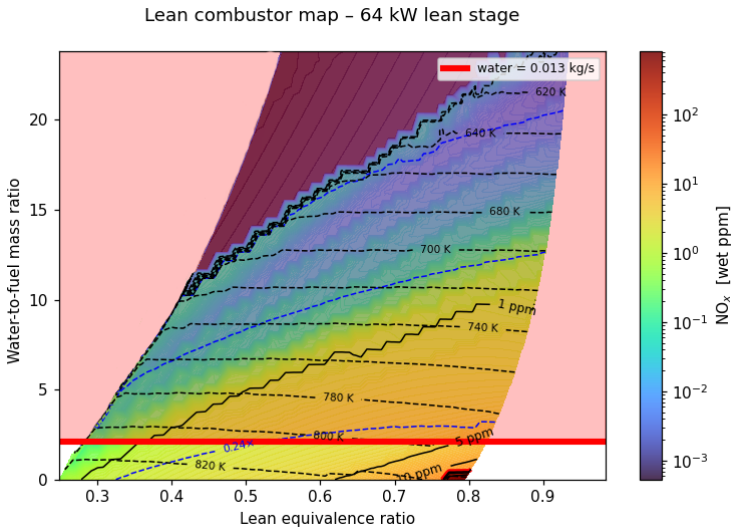

Figure 8.13: *Lean-combustor NO_x background map low idle*

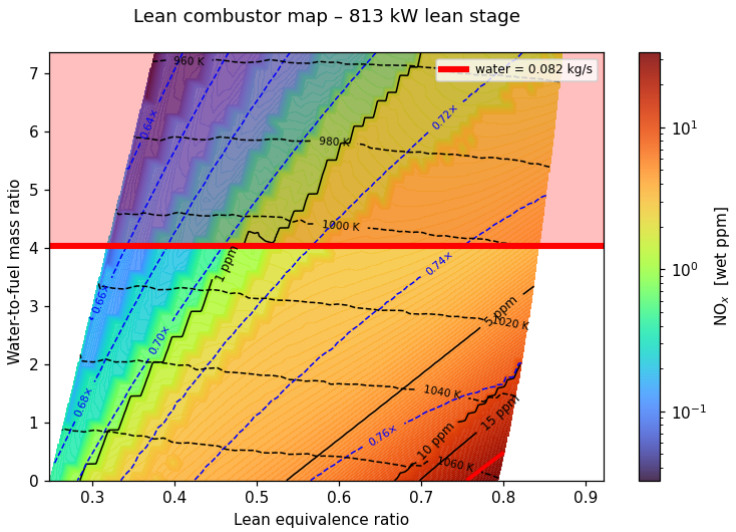

Figure 8.14: *Lean-combustor NO_x background map cruise*

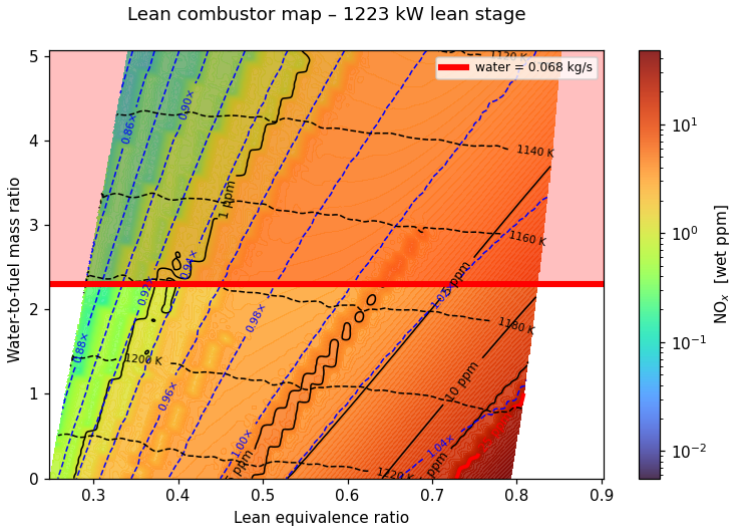

Figure 8.15: *Lean-combustor NO_x background map TOGA*

8.7. Preliminary Emissions Analysis Results

With the values of NO_x produced by the sum of the three stages, it is possible to inform the design of the full aircraft on the emissions at each point. The emissions from all zones are added to obtain more reasonable approximations, even though still far from the real ones. It must be emphasized that this model is only as good as the assumptions taken. For this reason, it must only be taken as an order of magnitude study to obtain insights into trends, interrelations between the variables and best-case scenarios.

To summarize, the CCs in the PT6A-67D engines of the H_2D_2 will be RQL combustors. This will ensure low NO_x emissions, flashback mitigation, and relevantly high-power output. The emissions will be further lowered by water injection in the quench zone of the combustor. The water will be extracted from the FC, condensed to liquid state, compressed and delivered to the CC. NO_x emissions will be minimized while increasing performance by doing a thorough engine redesign and informed RQL design.

Verification & Validation Procedures

The combustion scripts use Cantera, a verified and extensively validated tool. The Capurso Mechanism used for the chemical kinetics is validated to a good extent [39]. The engine cycle analysis GasTurb® 14 is a proprietary software, so it is assumed to be internally verified and validated. Where possible, the predictions have been validated against other predictions.

9

Fuel Cell

This chapter aims to describe the properties of the FC system to be implemented into H_2D_2. As outlined in Section 7.2, HT-PEMFCs will be used. First, the FC performance estimates will be outlined in Section 9.1. Following this, the cost and sustainability of the FC are outlined in Section 9.3 and Section 9.4, respectively.

9.1. Fuel Cell Performance

The FC performance is paramount to the design of H_2D_2. Not only does a change in performance impact the characteristics of the FC, it also has a cascading effect onto the design and complexity of the TMS, the fuel efficiency and the reliance on the CC. Outlining the FC's performance precisely enables all metrics related to the FC to be modeled over the entire flight profile. The most critical performance metrics of the FC are its efficiency and its volumetric and mass power density. Alongside these, the FC operating parameters are defined, enabling the calculation of the mass flows of fuel and air into the FC, as well as the heat it produces.

HT-PEMFCs are a promising technology for the aviation industry, as they are capable of providing high efficiency and power outputs with simpler thermal management than LT-PEMFC's. Despite these benefits, their TRL is not yet mature for aviation, projected to reach a level of 6 by 2030 [49]. Despite this, the performance of HT-PEMFCs can be projected to 2035 in order to create an accurate model for the planned demonstration of H_2D_2.

The FCs' performance is highly dependent on their operating conditions. Optimal operating conditions were compiled by analyzing reports on the optimal performance conditions of HT-PEMFCs in aviation [50] and taking temperature constraints due to TRL into account [51]. These conditions are given in Table 9.1 below.

Table 9.1: *Optimal FC operating conditions*

$\mathbf{p}_C, in$	$\mathbf{p}_A, in$	λ_{O_2}	λ_{H_2}	**T**
1.6 bar	1.66 bar	1.8	1.05	160°C

Increasing anode and cathode pressures, $p_{A,in}$ and $p_{C,in}$, increase FC specific power, but require larger air compressors [50], which increase the FC system mass. This effect is magnified at cruise, where the ambient pressure is lower. At 1.6 bar, a balance between power density and compressor mass is found. Additionally, the anode side is operated at a higher pressure to enable the hydrogen to permeate the FC membrane. The stoichiometric ratios of oxygen and hydrogen, λ_{O_2} and λ_{H_2}, determine how much air and fuel is reacted in the FC. A high stoichiometric ratio signifies more unused input into the FC. The stoichiometric ratio of hydrogen is near 1, as hydrogen waste means more hydrogen must be stored. To remedy this, a hydrogen recirculation loop is introduced, reducing the net stoichiometric ratio to 1. However, this loop must be modeled for accurate FC sizing. This is less critical for air, as it is not stored on the aircraft, hence the larger stoichiometric ratio. Finally, the FC operating temperature is defined as 160°C.

Power Density

The power density of the FC describes amount of power that a FC can produce per unit of mass or volume of the FC at maximum throttle. The mass and volume power densities are both defined for the FC stack for this report. The mass and volume of the BoP are considered separately, and described in Section 9.2.

According to FlyZero's projection on HT-PEMFC technology developments[49], a maximum stack power density of 5 kW/kg can be achieved by 2035. Furthermore, volumetric stack power densities of 3.1 MW/m^3 are possible today. This value is chosen for this report, although an improvement to 4 MW/m^3 is projected for 2040, according to a report from the German Aerospace Center (DLR)[52]. It is of note that these values pertain to the maximum power output of the FC. However, operating below the maximum power setting of a FC increases its efficiency, simplifying the thermal management and reducing the amount of hydrogen burnt. Selecting a design with a larger FC operating at a lower power setting may improve aircraft performance. This will be analyzed further in Chapter 13.

Efficiency

As the FC efficiency changes non-linearly with throttle setting, modeling this and projecting performance to 2035 becomes more complex than estimating the power density. Before delving into the precise modeling of FC efficiency, FlyZero presents an estimate for the peak stack efficiency of 70% by 2035 [49]. This may be used as a simple way to adjust the efficiency curve to 2035 values in case it does not match these projections.

The FC efficiency can be modeled by producing a polarization curve, comparing the voltage and current produced at a certain point of operation. With this, the power and efficiency can be extrapolated to find the efficiency at different operating points. Mutlucan Bayat et al. present a method to estimate the polarization curve of HT-PEMFCs [53]. Utilizing this model and the operating conditions shown in Table 9.1, the estimated polarization curve of the FC can be estimated, as shown in Figure 9.1. By multiplying the current with the voltage, the power is found. By plotting the efficiency from zero to maximum power, Figure 9.2 is found.

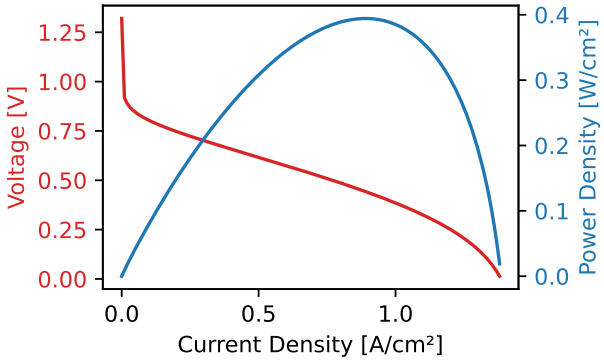

Figure 9.1: *HT-PEMFC polarization curve*

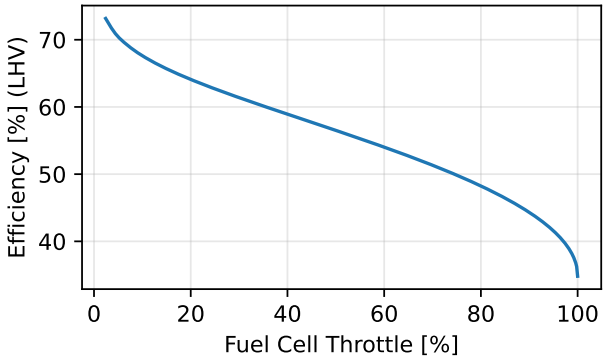

Figure 9.2: *HT-PEMFC power-efficiency curve*

It is evident that the efficiency rapidly falls with increasing throttle. This efficiency drop induces higher amounts of hydrogen used and causes a higher heat production within the FC. As the peak efficiency reaches 0.7, it matches with FlyZero's projections for 2035 [49]. It is of note that the efficiency is taken with respect to the Lower Heating Value (LHV) of hydrogen. An important conclusion which can be drawn from this is that it may be optimal to oversize the FC, operating it at a lower power setting in order to reduce the fuel consumption and heat production.

9.2. Fuel Cell Balance of Plant

The FC BoP maintains the operating condition of the FC. This includes maintaining the temperature of the FC, and ensuring that the correct amounts of hydrogen and air are provided at the correct temperature and pressure. It is important to define the required mass and heat flows for each operating condition in order to design the TMS and BoP for the most constraining condition over the flight profile. This section aims to introduce the FC inputs and outputs, and their conditioning, and describe the main functions of the TMS. More detailed analyses of the hydrogen conditioning and heat management systems are described in Chapter 11 and Chapter 12, respectively.

Fuel Cell Inputs & Outputs

Supplying the FC with the proper amounts of hydrogen and air at the correct conditions is crucial for efficient operation and reliability. The anode and cathode flows are defined in Figure 9.3, describing how the air is conditioned for input into the FC, and how the exhaust is utilized to reduce power loss and recover water. TMS and hydrogen conditioning are not included in this diagram, as they are determined in Chapter 11 and Chapter 12. This chapter shall determine the requirements imposed on those systems.

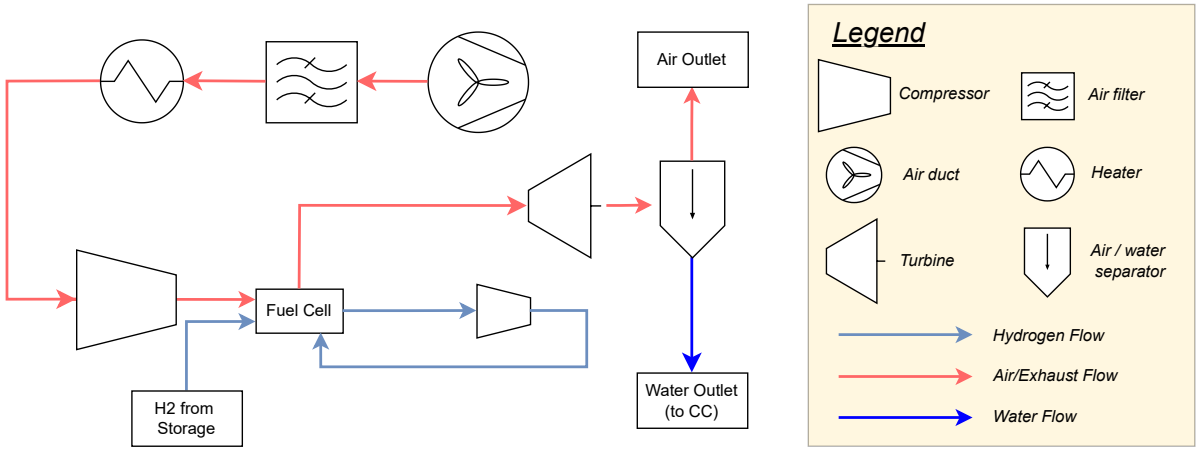

Figure 9.3: *Simplified FC piping and instrumentation diagram*

Two loops are defined for the FC inputs and outputs: the anode flow and the cathode flow. The cathode flow contains all flows of air and exhaust, whereas the anode flow supplies the hydrogen.

The anode flow is supplied by the hydrogen conditioning system, which increases the hydrogen temperature and pressure to 160°C and 1.66 bar, respectively. Since the stoichiometric ratio of the anode loop is 1.05, 5% of hydrogen is not reacted. This hydrogen is recirculated back into the FC via an additional compressor, utilizing nearly all the hydrogen supplied.

The cathode flow takes in ambient air through an air duct, filters it before heating and compressing the air to the FC operating conditions. Upon usage, the pressurized exhaust is fed through a turbine to recover energy and lower the temperature to below the boiling point of water and lower the pressure to equal the ambient condition. This results in minimal electrical power required from the FC, most of which results from the efficiency losses of the compressor and turbine themselves. Immediately following this, the cooler exhaust is fed through a water-air separator, which recovers 85% of the exhausted water, which is pumped into the CC to reduce NO_x emissions. The rest of the exhaust is returned to the atmosphere.

Each mass flow must also be calculated for each power condition of the FC. The mass flow of hydrogen as a function of power and efficiency, and the relative mass flows of each fluid as a proportion of the total mass flow are given in Table 9.2.

Table 9.2: *FC mass flows*

Fluid	Relative mass flow [%]	Equation
$\dot{m}_{H_2,in}$	1.79	$\frac{P_{req}}{LHV_{H_2}\eta_{H_2}}$
$\dot{m}_{H_2,recirc}$	0.09	$(\lambda_A - 1)\dot{m}_{H_2,in}$
$\dot{m}_{O_2,in}$	22.73	$\lambda_C \dot{m}_{H_2,in}\frac{M_{O_2}}{M_{H_2}}$
$\dot{m}_{O_2,out}$	8.52	$\frac{\lambda_C - 1}{\lambda_C}\dot{m}_{O_2,in}$
$\dot{m}_{air_2,in}$	98.21	$\frac{\dot{m}_{O_2,in}}{0.2314}$
$\dot{m}_{H_2O,out}$	15.99	$\dot{m}_{H_2,in}\frac{M_{H_2O}}{M_{H_2}}$

The proportion of mass flows remains constant throughout the flight profile, but their absolute amounts vary with the power required. In Table 9.2, $\dot{m}$ represents the mass flow of a given fluid, and M a molecule's molar mass.

Heat Production

Unlike combustion engines, which dissipate much of their heat through their exhaust, FCs cannot reject much heat through their exhaust, as it is not heated up significantly as it passes through the FC. Nearly all the energy of the reaction in the FC which is not converted to electrical energy becomes heat in the FC which must be removed by the TMS. The heat power produced by the FC is given as:

$$\dot{Q}_{FC} = P_{FC,elec} \frac{1-\eta_{FC}}{\eta_{FC}}, \tag{9.1}$$

where $P_{FC,elec}$ represents the electrical power produced by the FC, and η_{FC} the FC efficiency. Note that the efficiency decreases with power, further increasing the heat production when the power is increased. The heat produced is in the order of magnitude of the power generated, which the TMS must remove while keeping the FC temperature stable. This heat is used to condition the hydrogen for both the FC and CC, but some is rejected to the environment. This process is thoroughly described in Chapter 12.

9.3. Fuel Cell Cost

The cost of the FC can be broken down into four contributors: FC stack production cost, BoP cost, maintenance cost and disposal cost. Each of these can be modeled as a function of the power or the mass of the FC. The stack production cost is projected to be €277.5 per kW of absolute maximum FC power in 2035[49]. As the lifetime of the FC stack is projected to be 15,000 hours by 2035[49], it is necessary to replace the FC once in the aircraft's lifetime (29,800 hours). Since the BoP must only be sized for the maximum power which must actually be produced by the FC — which may be lower than the absolute maximum to increase efficiency — its cost scales with the maximum power required of the FC. The cost of producing the BoP is projected to be €277.5 per kW in 2035[49]. The maintenance costs are estimated as €0.917 per hour per kW of maximum required power,[54] and include regular tasks such as FC purging, inspections and BoP servicing. Finally, the FC disposal cost is €9.35 per kg of FC stack mass[55]. The lifetime cost of the FC system is summarized in Equation 9.2, and will be determined using this equation once the final design is selected.

$$c_{FC} = 277.5 \cdot 2P_{FC,max} + 277.5P_{FC,req,max} + 0.917 \cdot 29,800P_{FC,req,max} + 9.35m_{FC} \tag{9.2}$$

Here, P_{FC} is given in kW, and m_{FC} is the FC stack mass in kg. The terms are in the order they are introduced above.

9.4. Fuel Cell Sustainability

As FCs have hardly been demonstrated in aviation, the sustainability of H_2D_2 FC can be determined by analyzing LCAs of FCs with similar applications, for instance in heavy-duty vehicles. For the purposes of this report, the impact category which will be used to determine the sustainability of the FC will be the GWP over its lifetime. Other factors, such as land use for mining the materials needed and water use during the production/disposal process are also important impact categories to analyze, but are difficult to project to 2035 and compare with the other systems. Additionally, the emissions due to the use of hydrogen as a fuel will be handled in the full sustainability analysis in Chapter 17. The GWP is treated in units of $kgCO_{2,eq}$ over a 100-year time horizon.

The GWP of FCs over their lifetime is largely dominated by emissions which occur during the procurement of platinum and platinum group metals for the catalyst. These emissions currently are responsible for 84.2% of the total GWP of the FC[56]. South Africa hosts 89% of the world's platinum deposits, and produces the most platinum globally [57]. Improving the sustainability of mining techniques in this region of the world, improving the secondary production of platinum and producing more platinum in Europe all reduce the climate forcing of platinum production [57]. Current FC production techniques yields a GWP of 30.5 $kgCO_{2,eq}/kW_{max}$ [58] over a FC lifetime, but improvements of up to 21.94 $kgCO_{2,eq}/kW_{max}$ are realistically attainable by 2035 [56].

10

Electrical Power System

This chapter discusses the design considerations taken for the EPS. First, the selection of ELMO is justified. Thereafter, it is described how ELMO can be cooled, and lastly, the other power components necessary for the functioning of ELMO are looked at.

10.1. Electric Motor Selection

For the choice of ELMO, one option stands above the rest in terms of efficiency, weight and volume, this is the Permanent Magnet Synchronous Motor [59]. It was found that ELMO plus the cooling system has a specific weight of 10 kW/kg. The radius and length of ELMO were shown to be proportional to the cube root of the required power [60]. Using a simple tool that takes the power required as an input, the weight of ELMO and its dimensions were able to be calculated.

Having a very high specific weight means that the heat generated by ELMO is in a very compact space. This requires the utilization of uncommon cooling techniques for ELMOs. Hastecs[59] has found that direct liquid cooling of the windings, and potting on the end windings is required to keep temperatures below 180°C, which is at the limit for continued operation of ELMO. ELMO will have its own cooling loop which operates using a pump powered by the mechanical power of the ELMO. The pressure in this section of the cooling system is high to force the coolant through the windings of ELMO.

10.2. Power System Components

ELMO is not the only component of the power system. To get the electricity to ELMO and have it in the right state, cables, and inverters are required. All the sizing parameters used can be found in Table 10.1. The cables will be aluminum, and carry a voltage of 2000 V. 2000 V is used because this lowers the amperage, which in turn makes the diameter of the cables smaller. The cables also have a thick insulation layer to prevent short circuits from happening or maintenance workers getting electrocuted. Right after the FC system is a DC/DC converter to raise the voltage to 2000 V, and there is one DC/AC three-phase inverter for each ELMO.

To get the total weight of the EPS, the power, and length of all new power cables needs to be mapped. The values for the power that the cables need to carry are given in PU, where 1 PU = FC total power. There will be 4 cables carrying power from the FCs to the DC/AC inverters. They each carry a power of 0.5 PU. Their length is quite short as the FCs are in the wings, close to ELMOs. Their length will thus be 1.5 meters. There will also be two cables between both wings, each with a length of 6 meter, and capable of transferring 0.5 PU. There will be 6 AC cables transferring power from the inverters to the ELMOs.

Table 10.1: *Sizing parameters of EPS*

Motor Specific Power	10 kW/kg [59]
Cable Weight	0.0015 kg/kW/m [61]
Inverter Volume	0.535 l/kW[62]
Inverter Specific Power	20 kW/kg [62]
AP	16.8 kW [63]

The DC/AC inverters work both ways, so that if the FCs fails, electricity can be generated by the combustion motor. It can be seen that a part of the power generated by the FCs is going to auxiliary systems. This has a current of 600 A and a voltage of 28 V [63]. The cabling for this auxiliary system will remain the same as in the original Beechcraft 1900D. That means no weight is added or removed for this.

11

Hydrogen System

The final choice of the state that the hydrogen is stored at is liquid, which, in turn, dictates its conditioning and distribution. This chapter discusses it in terms of the thermal conditioning in Section 11.1 and continues into the pressurization and regulation in Section 11.2.

The hydrogen conditioning and distribution subsystems are heavily linked to each other, as many architecture choices made in one have downstream effects on the other. The subsystems' requirements are derived from the FC and CC, which require different inputs based on the power that is required from them and the operating conditions. The driving requirements are the mass flow, pressure, and temperature required for the FC and CC hydrogen inputs.

Given the high consequence of the hydrogen conditioning and distribution system failing, redundancy is a key aspect of the architecture. Additionally, weight is also a driving constraint, as the system's mass is non-negligible compared to the entire PT.

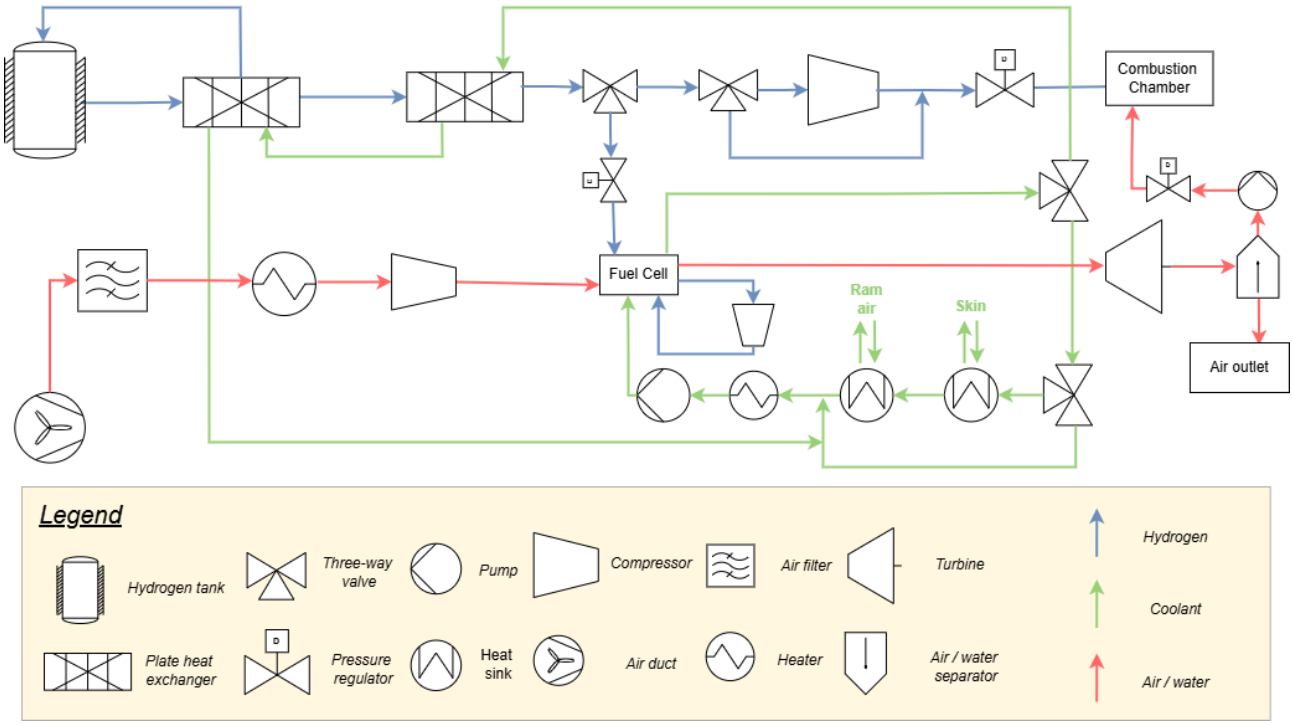

Figure 11.1: *H2-D2 PID*

The main fluid transfer lines and components in the H_2D_2 PT can be seen in Figure 11.1, with the blue lines representing the flow of hydrogen. The components in the loop between the storage and the FC and CC are each there to condition the flow to the appropriate temperature, pressure and mass flow. These components of course all have to be joined using piping, which has different requirements based on the conditions of the flow being transferred. An important note when deciding the hydrogen conditioning system architecture is that the decisions made have cascading effects on other systems, mainly the FC TMS. The effects on this system are explained in Chapter 12.

11.1. Temperature Control

The first key function of the hydrogen conditioning system is achieving the correct temperature at the inlet of the FC and CC. The operational temperature of the FC is nominally 160 °C Table 9.1, which is the target hydrogen inlet temperature. An important design consideration in order to minimize the operational risk is the fact that the FC is much more sensitive to variance in temperature than the CC. Due to this, the system is designed to always achieve a hydrogen temperature equal to the FC temperature. This temperature of 160 °C is warm enough to be injected into the CC, as it is then burned, and making it hotter would require a heavier and more complex conditioning system .

The temperature requirement is the most stringent of the three, as if the flow is too hot or too cold, the efficiency of the FC will be affected, and it could lead to faster degradation, as was explained in Section 9.1. For this reason it is important to have stability and control over the flow temperature. As the hydrogen is stored in liquid form, the temperature control considers the vaporization of the flow as well as the heating to the FC temperature. There are several architecture options to perform this heating, some of which would be electric heaters, heat transfer with the FC TMS, and passive heating using the excess heat from the CC.

The total quantity of energy that needs to be added to the hydrogen flow can be described by Equation 11.1, where the HSP is the specific heat sink potential of the hydrogen. This is the amount of energy that needs to be added to the flow per unit of time and mass flow. It can be defined by the latent heat of vaporization of the hydrogen plus the heat required to heat it to the FC working temperature from its saturation temperature. Due to the large temperature range that the flow will experience, the Specific Heat Capacity (Cp) cannot be considered to be a constant value, thus a more effective way to calculate the HSP of the hydrogen is to calculate its change in specific enthalpy between the end state and the storage state of the hydrogen.

$$HSP = c_p(T_{fc} - T_{sat}) + L = H_{fc} - H_{sto} \tag{11.1}$$

The enthalpy of the fluid at different conditions can easily be calculated with Python libraries such as CoolProp's PropsSI, from which the difference can be determined throughout the temperature range. The change in enthalpy from the storage conditions to the FC inlet conditions can be seen in Figure 11.2, where the first steep line represents the latent heat of vaporization of the hydrogen, in which the fluid absorbs energy without getting hotter, and then it starts to increase in temperature for every additional unit of energy that is added. This curve is not perfectly linear due to the mentioned variability of the Cp.

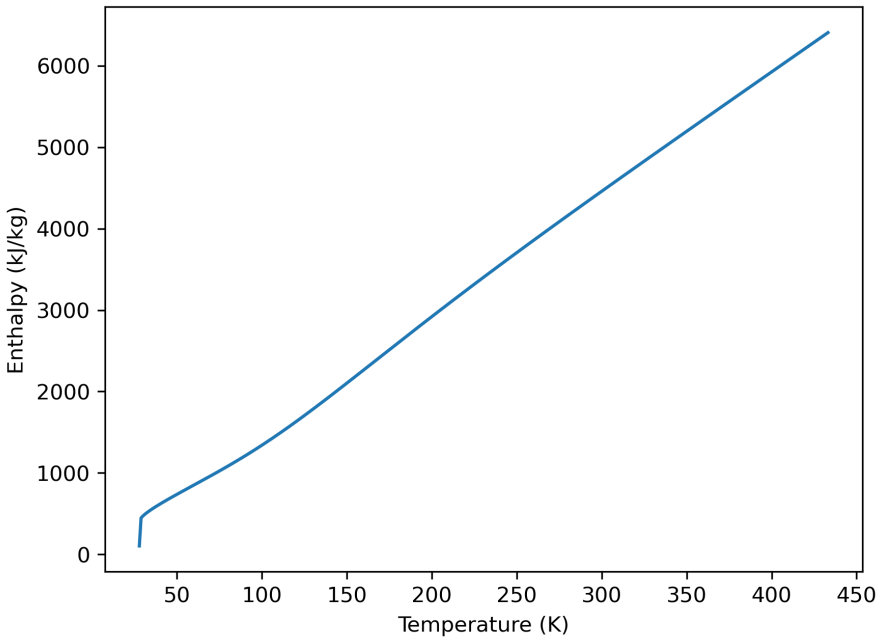

Figure 11.2: *Enthalpy of hydrogen with temperature*

As mentioned previously, the hydrogen flow can be heated electrically, or using the residual heat from the FC or CC. Although electric heating provides exceptional controllability and reactivity of the temperature, it was deemed unfeasible due to the high power required, which would mean the FC would have to provide substantially more power. This would severely impact the design, as more FC power results in higher hydrogen mass flow required, and thus even more power required to heat up said hydrogen. Out of the two remaining options, it was chosen to use the FC rejected heat to heat up the hydrogen, as the cooling requirements for the FC are quite stringent, and if it were not used to heat the hydrogen, larger external heat sinks would be required, leading to a larger system mass and a drag penalty, as is explained in Chapter 12.

Using the rejected heat from the FC to heat up the hydrogen proves to be an efficient and highly reliable way of regulating its temperature. Provided there is enough coolant mass flow, the hydrogen will always reach a temperature very close to the FC working temperature. This is ideal for FC efficiency, and due to the coolant changing in temperature with different FC temperatures, no additional control is required to make sure this requirement is met. This simplicity aids in the integration of the system, and reduces the risk of introducing hydrogen into the FC at a sub-optimal temperature. The design and sizing of the Heat Exchanger (HEX) required for this heat transfer is treated in Chapter 12.

11.2. Pressurization & Pressure Regulation

The hydrogen conditioning system must guarantee the pressure of the hydrogen is as required by the FC and CC. The two systems require different pressures, so this pressure control must be done separately for each. For the FC, the pressure is nearly constant throughout the flight profile at at 1.8 bar. This is low enough that no components are required to increase the pressure from the storage to the FC, and thus a simple pressure regulator is enough to step down the pressure to the required for the FC. For the CC however, the pressure required varies greatly depending on the ambient pressure. Assuming that the turboprop compression ratio is 13.54, as elaborated in Subsection 8.4.2, the pressure required for the hydrogen inlet will vary from 13.7 bar at sea level to 5.09 bar at the cruise altitude of 25000 ft (assuming International Standard Atmosphere (ISA) conditions).

Shown in Figure 11.3 is the phase diagram for hydrogen with the saturation line in blue. This line represents a continuum of options for the hydrogen storage pressure and temperature. Given that the required pressure for the CC at cruise conditions, which is most of the flight time, is 5.09 bar, it is possible to set the storage pressure to higher than this pressure, and thus remove the need to pressurize the hydrogen further during cruise. A margin is necessary to allow for ramping up and proper control of the pressure, assuming there will also be pressure drops in the pipes.

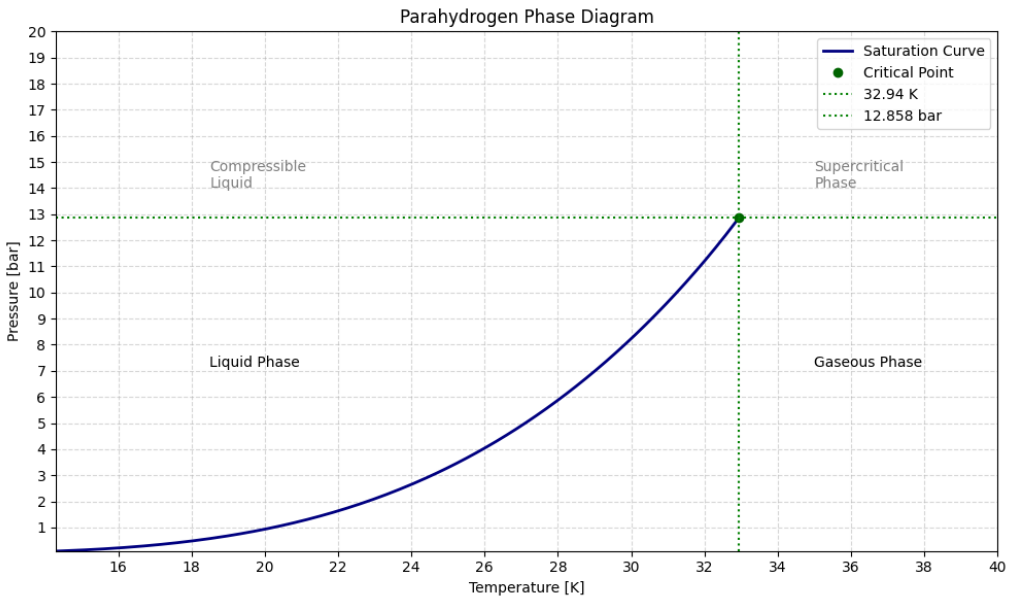

Figure 11.3: *Hydrogen phase diagram*

As can be seen in the phase diagram, the highest pressure that can be achieved in the storage vessel without the hydrogen becoming supercritical is 12.858 bar. The working pressure in the tank should be minimized in order to limit its volume [64], so a margin of 2 bar has been set, resulting in a storage pressure of 7 bar.

In all flight phases except for cruise, the hydrogen will need to be pressurized to higher than the CC working pressure. There are two options for this, mainly being a cryogenic pump to pressurize the hydrogen while it is in liquid state, or a hydrogen compressor that compresses the GH_2 after it has been vaporized. A GH_2 compressor was chosen for this architecture. The main reason for this was that the cryopumps available off-the-shelf are over-engineered for the purposes of this project. The smallest and lightest range of cryopumps provide mass flows of hydrogen of one order of magnitude higher [65] than the maximum overall required by SHTARWaRS, of around 60 g/s. Further considerations include volumetric and gravimetric constraints, since using a cryopump requires heavier and more voluminous piping than hydrogen gas, as well as financial cost of such a solution. Due to the fact that only the final hydrogen entering the CC pressure is a requirement for the architecture, it is equally feasible to use both technologies, but clearly the smaller sized compressor is the more cost efficient solution [66].

11.3. Hydrogen Storage

After defining the fuel as LH_2, the actual fuel tank can be sized around the amount of LH2 needed. Moreover, the calculations may be applied to the S-glass fiber material, as it was also chosen during the trade-off. This section describes the rationale for the tank sizing process, as well as the materials and configuration trade-offs for the tank. For this analysis, the tank's wall structure of dual-vessel, with a vacuum gap-Multilayer Insulation (MLI) insulation was considered, as decided upon in the midterm report.[64] The tank was sized based on the hydrogen mass required to be stored, using a structural analysis for the storage pressure, and a thermal analysis for the heat influx thorough the wall.

The first step is to size the inner volume of the tank by using the *CoolProp* Python library. Based on the inputted pressure and temperature, the LH_2 and GH_2 densities are found. Subsequently, using these densities and the fill ratio, the total volume of hydrogen to be stored is computed. For simplifying the volume calculation, the domes of the tank are assumed to be hemispherical. Having the radius of the inner tank, the inner length of the cylindrical part can be computed.

Secondly, using the computed volume, hydrogen gas and liquid data and the venting pressure, the maximum allowable heat allowed to influx the tank during the dormancy period, is computed. Equation 11.2 [67] presents the time derivative calculation of the heat influx applied to the set dormancy.

$$Q_{\text{leak}} = \frac{dT}{dt}\left[m_l\left(\frac{\partial h_l}{\partial T}\right)_P + m_g\left(\frac{\partial h_g}{\partial T}\right)_P + \left(m_l\left(\frac{\partial h_l}{\partial P}\right)_T + m_g\left(\frac{\partial h_g}{\partial T}\right) - V\right)\frac{dP_s}{dT}\right] - (h_l - h_g)\frac{dm_g}{dt} \tag{11.2}$$

Now having the structural constraints, Maximum Allowable Working Pressure (MAWP) and venting pressure, as well as the insulation constraint of the maximum allowable heat influx, the actual sizing may be performed. This process is divided in the two stages mentioned before, the structural and the heat stage.

The structural analysis is driven by the MAWP inside of the tank. For simplification, the inner layer of the tank is assumed to carry the pressured load due to internal pressure. Using the pressure and the material's maximum allowable strength, the thickness of the inner wall can be computed.

For the reason of choosing S-glass fiber, netting analysis is being performed, which assumes that 100% of the loads are taken by the fibers. This is done by taking into account the winding angle of the composite layers. Since optimization parameters for any aviation fuel tank are volume and weight, a minimum thickness optimization was incorporated into the netting analysis. Filament winding is the technique used to layer continuous fibers composite matrix. It is widely used to manufacture hollow and circular shapes like pipes and tanks in the aerospace industry. Guidelines from [68] were taken for the netting analysis. The layers are winded in two directions. However, as usually approached when manufacturing cylindrical tanks, one of the angles is set to 90°, namely in the hoop direction[68]. The two thicknesses, in the two directions, are computed using Equation 11.3 and Equation 11.4, respectively.

$$t_{\alpha_1 f} = \frac{N_\theta \cos^2 \alpha_2 - N_\phi \sin^2 \alpha_2}{\sigma_{\alpha_1} \left(\cos^2 \alpha_2 \sin^2 \alpha_1 - \sin^2 \alpha_2 \cos^2 \alpha_1\right)} \tag{11.3}$$

$$t_{\alpha_2 f} = \frac{N_\theta \cos^2 \alpha_1 - N_\phi \sin^2 \alpha_1}{\sigma_{\alpha_2} \left(\cos^2 \alpha_1 \sin^2 \alpha_2 - \sin^2 \alpha_1 \cos^2 \alpha_2\right)} \tag{11.4}$$

In Equation 11.3 and Equation 11.4, N_θ and N_ϕ are the loads in the hoop and axial directions, whereas α_1 is the angle being iterated on for minimizing the thickness, and $\alpha_2 = 90°$. As an assumption for this method, α_1 does not iterate beyond 54° to avoid computing unrealistic negative thicknesses. By summing these two values, and dividing by the fiber volume fraction FVF given by the materials' datasheets, Equation 11.5 is to be minimized with respect to the orientation angle.

$$t_{final} = \frac{t_{\alpha_1 f} + t_{\alpha_2 f}}{FVF} \tag{11.5}$$

Considering the heat influx, a simplified model was developed, taking into account conduction presented in Equation 11.6 [69] and radiation as in Equation 11.7 [67] through vacuum and MLI. The heat influx due to radiation was calculated using the Gebhart method, as being done in [67], where B_{21} is the Gebhart factor between the two walls as Equation 11.8 and σ is the Stefan-Boltzmann constant for radiation. The purpose of this phase is to optimize the vacuum gap and the outer layer thickness. The process of doing the heat analysis is supposed to be iterative, with the thickness of the outer wall initially being the same as of the inner wall. However, since the influence of the outer wall thickness on the insulation is relatively small, the vacuum gap and outer thickness values converge after one iteration.

$$Q_{\text{cond}} = \frac{T_{\text{amb}} - T_{\text{tank}}}{\frac{\ln\left(\frac{r_{\text{in}}+t_1}{r_{\text{in}}}\right)}{2\pi L k_1} + \frac{\ln\left(\frac{r_{\text{in}}+t_1+t_{\text{MLI}}}{r_{\text{in}}+t_1}\right)}{2\pi L k_{\text{MLI}}} + \frac{\ln\left(\frac{r_{\text{in}}+t_1+t_{\text{MLI}}+d_v}{r_{\text{in}}+t_1+t_{\text{MLI}}}\right)}{2\pi L k_{\text{vac}}} + \frac{\ln\left(\frac{r_{\text{in}}+t_1+t_{\text{MLI}}+d_v+t_2}{r_{\text{in}}+t_1+t_{\text{MLI}}+d_v}\right)}{2\pi L k_2}} \tag{11.6}$$

$$Q_{\text{rad}} = \sigma \cdot \varepsilon_2 \cdot B_{21} \cdot \left(T_{\text{amb}}^4 - T_{\text{tank}}^4\right) \tag{11.7}$$

$$B_{21} = \frac{(A_1/A_2) \cdot \varepsilon_{\text{MLI}}}{1 - (1-\varepsilon_{\text{MLI}})(1-\varepsilon_2)(A_1/A_2) - (1-\varepsilon_2)(1-(A_1/A_2))} \tag{11.8}$$

For a better visualization, Figure 11.4 shows how the wall of the tank is layered. The figure also explains which heat transfer is analyzed through each of the layers. For calculation simplification, but also for a more conservative approach, the temperature of the outer wall in contact with vacuum is considered to be at ambient temperature, and the temperature where the vacuum ends and MLI starts is considered the hydrogen storage temperature.

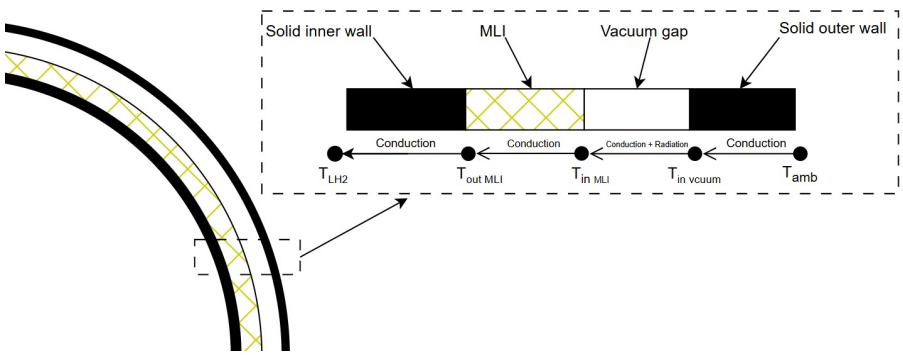

Figure 11.4: *Tank wall layering*

Within the equation above, the vacuum gap is represented as dv, t_{MLI} is the mli thickness based on inputted number of layers, r_{in} is the internal radius of the tank, t_1 is the thickness of the inner wall and t_2 is the outer

tank thickness. Moreover, the thermal conductivity k and emissivity ϵ contain the name of the layer they refer to in the subscript.

Furthermore, the last parameter to size is the thickness of the outer wall with respect to the load it has to withstand. A similar structural approach is performed as for the inner tank, with the pressure difference being the one between ambient and vacuum. In the end, the thickness is chosen based on the constraining case, namely the maximum thickness coming from the structural side or the thermal side of the process.

12

Thermal Management System

The TMS is required to ensure the proper work of the PT, mainly by keeping the FC within its operating temperature range and conditioning the hydrogen. The TMS contains 3 fluid loops: hydrogen, coolant liquid, and air. Each of them are constructed separately, but intertwine with each other several times. This chapter outlines the sizing methodology, while the corresponding sizing results and masses of the TMS are presented in the final system design description in Section 14.3.

12.1. Coolant Loop

The choice for the coolant liquid is a solution of Ethylene Glycol (EG) and water, thanks to its multiple aerospace applications. EG is usually used as antifreeze in the automotive industry, and as de-icing agent in aerospace. The freezing point of this solution is independent of the pressure of the liquid, and is only influenced by the concentration. On the other hand, the boiling point is highly dependent on pressurization, as well as the proportion of EG.

The plateau of useful properties for the EG, especially its freezing point, is bounded between 60% and 75% of EG in the mixture [70]. Since the upper bound for the concentration of solution that can be modeled using the PropSI library in Python is 60%, this is the number chosen for the coolant liquid within TMS. Considering the maximum operating temperature of the FC, and adding a safety margin, it was decided to pressurize the coolant as to raise its boiling point at 180°C.

To determine the required pressure for the solution, first, the Antoine equation given in Equation 12.1 [71].

$$log_{10}(p) = A - \frac{B}{C+T} \tag{12.1}$$

was applied for pure EG and pure water separately. Then, using the rule of mixtures and the given concentration of 60%, the overall pressure was calculated. Temperature T is known, at 180°C, and should be expressed in kelvin as 453 K, while the parameters A, B, C are taken from literature [71]. For EG, it is known that

$$A = 4.97012, \qquad B = 1914.951, \qquad C = -84.996,$$

leading to a pressure of $p = 0.584$ bar for the EG to boil at the selected temperature. Applying the same considerations for the pure water, the pressure at which water's boiling point is at 180°C, is 10 bar, as taken from tabulated data [72]. Now, applying the rule of mixtures, we get to

$$p_{mix} = 0.6 \cdot 0.584 + 0.4 \cdot 10 = 4.35\ bar \tag{12.2}$$

and this is the required pressure within the coolant loop in order to make sure that the coolant maintains its liquid phase, with the least limiting conditions as possible.

12.2. Piping

When the fluids are moving through the pipes, pressure losses occur due to friction, and temperature losses due to conduction. These losses need to be calculated for every pipe section to know the temperature, and pressure at the end of a section because that will be used as input for the next TMS component. There will be two different kinds of pipes used: for LH_2, and for the other fluids. LH_2 needs a vacuum gap in the insulation due to the temperature difference being large with the ambient air around it. Not having this would incur a significant loss of heat. The rest of the piping is not as affected by this big temperature difference; thus they only require one layer of insulation around the pipe.

The pressure drop will be calculated using Equation 12.3, otherwise known as the Darcy-Weisbach equation[1].

$$P_{drop} = \frac{\lambda_f}{d_{in}} \frac{\rho_f V_f^2}{2} L \qquad (12.3) \qquad \lambda_f = \frac{64}{Re} \qquad (12.4) \qquad \lambda_f = 8\left[\left(\frac{8}{Re}\right)^{12} + (X+Y)^{-1.5}\right]^{\frac{1}{12}} \qquad (12.5)$$

- λ_f : Darcy-Weisbach friction coefficient
- P_{drop} : Pressure drop experience at the end of the pipe
- ρ_f : Density of the fluid
- V_f : Velocity of the fluid
- d_{in} : Inner diameter of the pipe
- L : Length of the pipe

The Darcy-Weisbach friction coefficient can be calculated with Equation 12.4 for laminar flow, and using Equation 12.5 for turbulent flow. Re is the Reynolds number. For the friction coefficient of the turbulent flow, X and Y are needed. These can be obtained by using Equation 12.6, and Equation 12.7 respectively.

$$X = \left\{-2.457 \ln\left[\left(\frac{7}{Re}\right)^{0.9} + \frac{0.27k}{D}\right]\right\}^{16} \qquad (12.6) \qquad Y = \left(\frac{37530}{Re}\right)^{16} \qquad (12.7)$$

The thermal losses can be analyzed by calculating the energy transfer by dividing the temperature difference by the sum of the thermal resistance. There are three thermal resistances experienced by a pipe section: From the flowing liquid to the inner pipe(Equation 12.8), rough the pipe wall for each layer of pipe(Equation 12.9), and from the outside of the outermost layer to the surrounding medium(Equation 12.10)[2].

$$R_L = \frac{1}{\dot{m}c_p\left(1 - \exp\left(\frac{-h_L S_L}{\dot{m}c_p}\right)\right)} \qquad (12.8) \qquad R_W = \frac{\ln(d_{out}/d_{in})}{2\pi k L} \qquad (12.9) \qquad R_A = \frac{1}{h_A S_A} \qquad (12.10)$$

Having the energy transfer, Equation 12.11 is utilized to determine the change in temperature in a section of pipe.

$$\Delta T = \frac{Q}{m * c_p} \qquad (12.11)$$

With all these equations, the pressure and temperature drop throughout a pipe can be analyzed. This will be done for every section of pipe the TMS contains.

[1] URL https://ocw.tudelft.nl/wp-content/uploads/B._oe4625_Chapter01.pdf [Cited 12 June 2025]
[2] URL https://www.mathworks.com/help/hydro/ug/HeatTransferinTLPipeExample.html [Cited 12 June 2025]

12.3. Heat Exchangers

This section discusses the design and integration of the HEXs of the TMS. This includes three types of HEXs: ram air ducts, skin HEXs and plate HEXs.

12.3.1. Ram Air Duct with Radiator

Radiator with a ram air duct are implemented to dissipate heat of the FC. Since they cause additional drag due to the pressure drop across the HEX, the design aims to mitigate this effect by leveraging the Meredith effect. As the air heats up while passing through the radiator, it expands and accelerates through the nozzle, generating a small amount of thrust that partially offsets the drag [73]. Beltrame et al. concluded that minimal drag and maximum thrust are achieved when the full available duct length is used and the maximum diffuser area ratio is utilized [73]. Figure 12.1 illustrates the architecture of the ram air duct, where the HEX is placed after the diffuser and followed by the nozzle. The internal structure of the radiator is illustrated in Figure 12.2, where the cold fluid consists of the air entering through the ram air duct and the hot fluid is the circulating coolant. Although Beltrame et al. [73] propose positioning the radiator at a 70-degree angle to improve FC heat dissipation while reducing drag and increasing thrust, this analysis was not carried out due to time constraints.

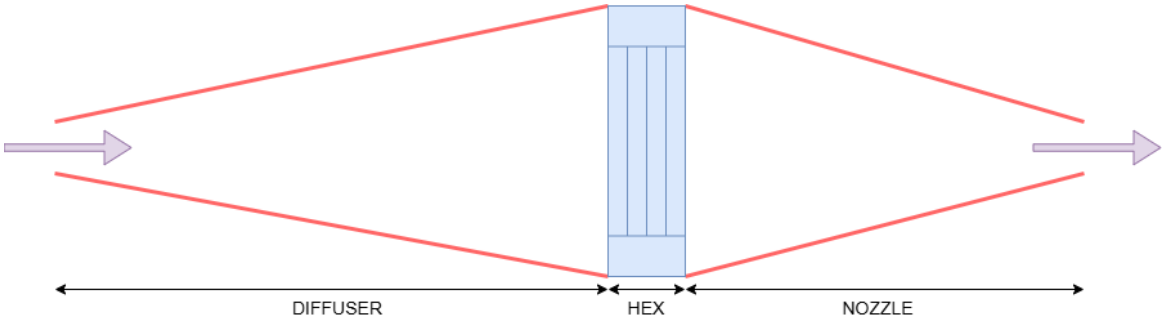

Figure 12.1: *Ram air duct*

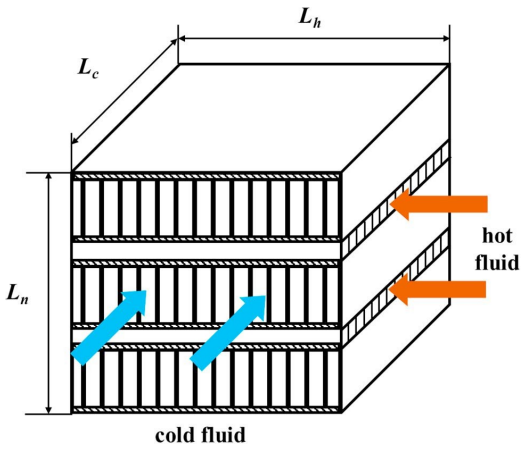

Figure 12.2: *Internal architecture of a radiator [74]*

Figure 12.3 illustrates how each turboprop is equipped with one ram air duct positioned at the right of the engine. This architecture and integration is reproduced from Rietdijk and Selier, who performed a feasibility study for a retrofit of a widely used regional aircraft, a DHC-8 Q300, with a LH2FCE propulsion system [75].

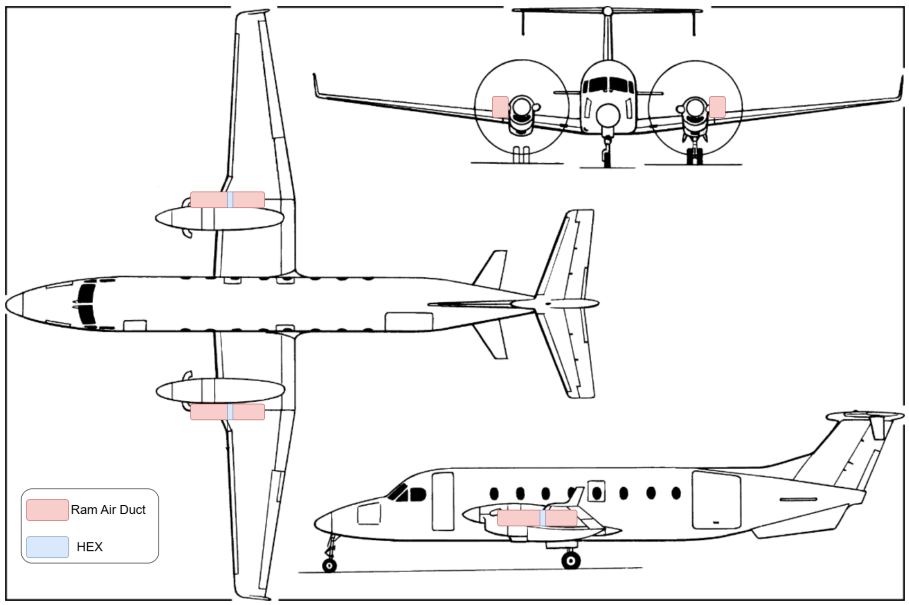

Figure 12.3: *Ram air duct integration [25]*

The radiator, a plate-fin HEX was sized using a method proposed by Shah et al. [76]. Equation 12.12 describes the heat Q that needs to be dissipated by the radiator, U the overall heat transfer coefficient, A the total heat exchange area and ΔT_{lm} is the log-mean temperature difference between the coolant and the air.

$$Q = U \cdot A \cdot \Delta T_{lm} \tag{12.12}$$

The log-mean temperature difference is calculated using Equation 12.13, with the subscripts in and out denoting the temperatures of the incoming and outgoing flows, respectively.

$$\Delta T_{lm} = \frac{(T_{coolant,in} - T_{air,out}) - (T_{coolant,out} - T_{air,in})}{ln(\frac{T_{coolant,in} - T_{air,in}}{T_{coolant,out} - T_{air,out}})} \tag{12.13}$$

The overall heat transfer coefficient represents the total resistance to heat transfer across the radiator, computed by Equation 12.14.

$$U = (\frac{1}{h_{air}} + \frac{1}{h_{coolant}})^{-1} \tag{12.14}$$

Where h_{air} and $h_{coolant}$ are the individual heat transfer coefficients of the air and coolant, they quantify the rate of heat transfer between a surface and the corresponding fluid due to convection, computed with Equation 12.15.

$$h = \frac{Nu \cdot k}{D_h} \tag{12.15}$$

Pr is the Prandtl number and Nu is the Nusselt number of the coolant, given by Equation 12.16. The Prandtl number is a dimensionless number that characterizes the relative effectiveness of momentum and heat transport within the fluid. The Nusselt number is a dimensionless parameter that represents the ratio of pure convection to pure conduction heat transfer at the solid surface. D_h is the hydraulic diameter given by Equation 12.17, where A_0 is the minimum free flow area of the HEX and P is its perimeter.

$$Nu = 0.023 \cdot Re^{4/5} \cdot Pr^{0.3} \tag{12.16}$$

$$D_h = \frac{4 \cdot A_0}{P} \tag{12.17}$$

The Meredith effect functions as an open Brayton cycle, but it only becomes effective when the incoming airflow has a sufficiently high velocity [77]. The expected Thrust Ratio (TR) of the ram air duct is estimated with Equation 12.18, derived by expert Fabio Beltrame, where TR is dependent on the flight Mach number M_0, altitude, the total pressure ratio $\eta_{p,07}$ of the total exit pressure divided by total freestream pressure of the airflow and the temperature difference in the radiator ΔT^0_{HEX}.

$$TR \approx \frac{\sqrt{\frac{2\gamma}{\gamma-1}R\left(1-\frac{1}{(1+0.5(\gamma-1)M_0^2)(\eta_{p07})^{\frac{\gamma-1}{\gamma}}}\right)\left(T_0\left(1+0.5(\gamma-1)M_0^2\right)+\Delta T^0_{\mathrm{HEX}}\right)}}{M_0\sqrt{\gamma R T_0}\left(1+\frac{C_{d,d}+C_{D,\mathrm{sp}}}{2}\right)} - 1 \tag{12.18}$$

Where $C_{D,d} + C_{D,sp}$ is assumed to be 0.11. TR is the ratio of thrust produced by the duct (F_n), divided by the total ram air duct gross drag (D_g) minus one as shown in Equation 12.19. Moreover, the total gross drag can be estimated from general TMS operating conditions, as seen in Equation 12.20, where the exit velocity of the nozzle is estimated using Bernoulli's equation with Equation 12.21 [76].

$$TR = \frac{F_n}{D_g} - 1 \tag{12.19}$$

$$D_g = \dot{m}_{air} \cdot (V_\infty - V_{exit}) \tag{12.20}$$

$$V_{exit} = \sqrt{V_\infty^2 - \frac{2 \cdot \Delta p}{\rho_\infty}} \tag{12.21}$$

The total pressure ratio $\eta_{p,07}$ is calculated with the pressure drop Δp, which indicates the pressure drop across the entire length of the radiator, which is the summation of the pressure drop in the duct (Equation 12.22) [73] and HEX (Equation 12.23) [76].

$$\Delta p_{\text{diffuser}} = \frac{1}{2}\rho_\infty V_\infty^2 \epsilon_{\text{diffuser}}\left(1-\frac{1}{AR^2}\right) \tag{12.22}$$

$$\Delta p_{HEX} = \frac{\mu_{\text{air}}}{2\rho}\left(\frac{4L}{D_h^2}\right)\left(\frac{\dot{m}_{\text{air}}}{A_0}\right)(f \cdot Re) \tag{12.23}$$

Where $\epsilon_{\text{diffuser}}$ is the effectiveness of the diffuser and f is the Fanning friction factor (Equation 12.24). This factor is utilized in Equation 12.25 and Equation 12.26 to calculate the Reynolds number Re and core mass velocity G of the flow, respectively.

$$f = 0.046 \cdot Re^{-0.2} \tag{12.24}$$

$$Re = \frac{G \cdot D_h}{\mu_{air}} \tag{12.25}$$

$$G = \frac{\dot{m}_{air}}{A_0} \tag{12.26}$$

12.3.2. Plate Heat Exchangers

The TMS incorporates two plate HEXs: the first acts as an vaporizer to vaporize the hydrogen, while the second functions as a superheater, further raising the hydrogen's temperature to reach the desired level before entering the CC. Figure 12.4 depicts the internal configuration of a cross-flow plate HEX, where the blue stream represents the cold hydrogen and the red stream indicates the hot coolant. Cross-flow is selected for its enhanced heat transfer efficiency.

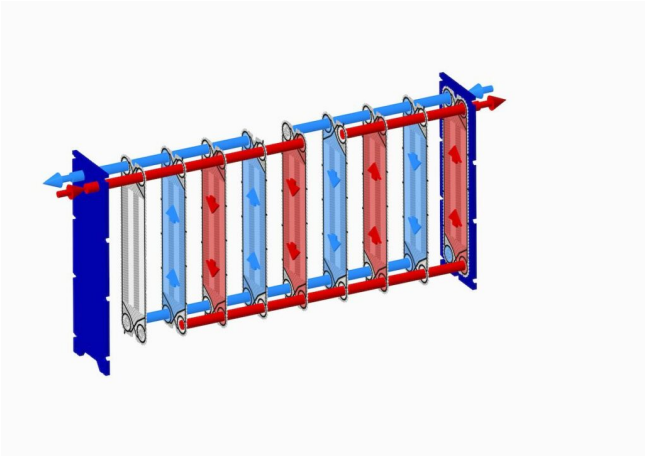

Figure 12.4: *Internal architecture of a plate HEX*[3]

The heat dissipated by the plate HEX can be estimated using Equation 12.27, with the overall heat transfer coefficient calculated via Equation 12.28. ΔT_{lm} is obtained from Equation 12.13, and N_{plates} and N_{passes} represent the number of plates and flow passes, respectively [76].

$$Q_{plate} = U_{plate} \cdot A \cdot \Delta T_{lm} \cdot N_{plates} \cdot N_{passes} \tag{12.27}$$

$$U_{plate} = (\frac{1}{h_{hydrogen}} + \frac{1}{h_{coolant}} + R_{f,hydrogen} + R_{f,coolant} + \frac{t_{plate}}{k_{plate}})^{-1} \tag{12.28}$$

The last term accounts for the resistance to conductivity between fluids and material, where t_{plate} is the plate thickness and k_{plate} the thermal conductivity of its material. $R_{f,hydrogen}$ and $R_{f,coolant}$ are the fouling resistance from vapor hydrogen and the coolant [4], respectively. Fouling resistances account for the performance degradation caused by deposits on heat transfer surfaces.

Subsequently, the Nusselt number of the coolant is required to compute its individual heat transfer coefficient, computed by Equation 12.29 [78].

$$Nu_{coolant} = C_{h,coolant} \cdot Re^{y}_{coolant} \cdot Pr^{0.33}_{coolant} \cdot (\frac{\mu}{\mu_w})^{0.17} \tag{12.29}$$

Where $\frac{\mu}{\mu_w}$ is assumed to be equal to 1, because of the narrow tubes of the plate HEX. $C_{h,coolant}$ and y are constants derived from the Chevron angle of the plate, which is taken to be 30 degrees, as suggested by Nilpueng et al. [79]. The chevron-type plate HEX was chosen, since its design improves the fluid mixing inside the channel and enhancing the heat transfer rate by 20 - 30% [79].

The pressure drop across the plate HEX is the summation of the pressure drop of the channel (Equation 12.30) and collector of the plate (Equation 12.31) [76].

$$\Delta p_{channel} = 2f \cdot \rho_{fluid} (\frac{\dot{v}_{fluid}}{A_{pipe}})^2 \cdot L_{plate} \cdot D_h \tag{12.30}$$

$$\Delta p_{collector} = 1.4 N_{passes} \cdot (\frac{\dot{m}_{fluid}}{\pi \cdot \frac{D_{collector}}{4}})^2 \cdot \frac{1}{2\rho_{fluid}} \tag{12.31}$$

Where $\dot{v}_{fluid}$ is the volumetric flow rate of the corresponding fluid.

[4] URL https://powderprocess.net/Tools_html/Data_Diagrams/Heat_Exchanger_Fouling_Factor.html#google_vignette [Cited 17 June 2025]

12.3.3. Skin Heat Exchanger

The TMS features a single Skin Heat Exchanger (SHX) on each wing, and the heat transfer through these components is calculated in the same manner as for the HEX. The sizing of the SHX was performed using a predefined method by Coutinho et al. [80]. Specifically, the total heat transferred by each SHX is determined using Equation 12.12. The global heat transfer coefficient of the SHX must be obtained with Equation 12.32, neglecting the wall thermal resistance, radiation effects or fouling factors.

$$U = (\frac{1}{h_{ext}} + \frac{1}{h_{int}})^{-1} \tag{12.32}$$

The area of the SHX, is given as the available skin area of the aircraft. The design positions the SHX on the wings, thus the A_{SHX} is 2.3 m^2 for each of the wings. Such value is obtained from the surface area between the engine and fuselage, only on the top side of the wing. This assumption minimizes the effect on the aircraft skin, and reduces the risk of altering the original airframe.

The convective heat transfer coefficients of the internal and external flow are required, where the internal is defined by Equation 12.15. The calculation of the Nusselt number of the coolant flow considers a turbulent flow in circular tubes, using Equation 12.33.

$$Nu = \frac{(\frac{f}{8}) \cdot (Re - 1000) \cdot Pr}{1 + 12.7 \cdot (\frac{f}{8})^{\frac{1}{2}} \cdot (Pr^{\frac{2}{3}} - 1)} \tag{12.33}$$

Where f is the friction factor calculated using Equation 12.34.

$$f = (0.79 \cdot ln(Re) - 1.64)^{-2} \tag{12.34}$$

Furthermore, the external flow convective heat transfer coefficient is calculated with the flight conditions, the Reynolds and Prandtl numbers using Equation 12.35.

$$h_{ext} = \rho_\infty \cdot c_p \cdot v_\infty \cdot 0.185 \cdot (log10(Re))^{-2.584} \cdot Pr^{-\frac{2}{3}} \tag{12.35}$$

During flight the ambient air adjacent to the outer surface of the wing increases temperature through ram effects, decreasing the efficiency of the SHX. The effective wall adiabatic temperature follows from Equation 12.36.

$$T_{aw} = T_\infty \cdot (1 + r \cdot \frac{\gamma - 1}{2} \cdot M_\infty^2) \tag{12.36}$$

Where r represents the recovery factor for the turbulent boundary layer, and equals $Pr^{1/3}$.

12.3.4. Compressors, Pumps, Turbines, Valves

Apart from the compressors and turbines present on the FC loops, there is still one other compressor used for hydrogen gas pressurization after passing it through the HEX. It is a crucial component to make sure that the pressure requirements of hydrogen entering the FCs is successfully met. Additionally, all fluid loops include a series of valves for flow control, which must be sized accordingly, and need to be factored in toward the overall weight of the TMS.

The mass of all mentioned components can be estimated using statistical formulas[81] devised for the same range of use as within the SHTARWaRS project:

$$m_{comp} = 0.0400683 \cdot P_{comp} + 5.17242, \tag{12.37}$$

$$m_{turb} = 0.0400683 \cdot P_{turb} + 5.17242, \tag{12.38}$$

$$m_{valve} = 0.568 \cdot \dot{m}_{cool}^{0.5541}. \tag{12.39}$$

It should be mentioned that for the turbine mass estimation, the same formula is used as for the compressor. The power required by compressor / provided by turbine is estimated using the same formula,

$$P = \frac{\dot{m} \cdot c_p \cdot \Delta T}{\eta}, \tag{12.40}$$

except that the flow passing through each component has different properties.

There is also a need to use several pumps throughout the fluid loops: one pump is pressurizing the coolant for each of the FC, while another pump pressurizes water after it passes through the separator. The mass of each pump is also given by a statistical formula [81]

$$m_{pump} = 0.0138289 \cdot P_{pump} - 0.366129, \tag{12.41}$$

based on the power definition for each of them:

$$P_{pump} = \frac{\dot{m}\, d_p}{\rho\, \eta_{pump}}, \tag{12.42}$$

where d_p is the pressure drop across the pump.

12.4. Sustainability of TMS

Sustainability of the TMS shall be separately analyzed from multiple points of view. The aspects in question are material properties and production, and actual coolant liquid considerations. It is important to consider both the long lasting impact on the environment, as well as immediate health concerns for humans.

12.4.1. Material Choice

The pipes used in the TMS are made up of mainly stainless steel, with some sections being aluminum [82]. The 3-way valves are comprised of stainless steel and brass, and the sealing is done using PTFE (Teflon) and PEEK [83]. Additionally, the pressure regulators are also constructed out of stainless steel varieties and brass [84]. Considering that the other components of the TMS are also produced from various combinations of the aforementioned materials, it is safe to consider all relevant materials are considered.

The metals used do not pose major sustainability concerns, but the plastics used may be more closely monitored. While PTFE itself is not harmful to life, the PFOA/PFOS involved in its production is carcinogenic. The alternative for this substances, called GenX, has proved to be even more questionable, with the possibility to generate long-lasting neuro-degenerative effects [85]. The other plastic used, PEEK, is considerably safer, being used in aerospace applications, as well as medical implants, thanks to its properties, including ultra-high vacuum compatibility. PEEK is also a thermoplastic making it easier to melt down and recycle [86]. Unfortunately, Teflon cannot be substituted for the scope of this project, so its production's counter effects need to be monitored and documented. The performance of this plastic overrides the possible harming effects it has.

12.4.2. Liquid Coolant

The actual liquid used for the heat transfers within the TMS may also have an impact on the sustainability analysis for the overall system. The choice was made for a solution of 70% EG with water. The EG breaks down in around 10 days in air, and in several weeks in water and soil [87]. Furthermore, considering the reduced volume of EG used for the cooling system, compared to de-icing operations -which is the main activity involving this compound-, the environmental impact of the cooling liquid may be classified as minimal.

13

Synthesis of Design

This chapter explains the approach taken to select a final design. First, it is described how the design space was constructed in Section 13.1, followed by a summary of constraints applied in Section 13.2. Lastly, the final trade-off is presented in Section 13.3.

13.1. Concurrent Design Tool

This section presents the simulation framework used to generate the complete design of the whole PT. In this context, the term 'system' specifically refers to the PT, which is comprised of the subsystems of: hydrogen storage, TMS, EPS, FC and combustor. This system integration model manages the interconnections between all of the models from different subsystems. The main purpose of this tool is to facilitate compatibility between the subsystems – constructing the PT in a unified fashion. By centralizing the PT design and effectively creating its digital twin using this Concurrent Design Tool (CDT), interoperability of subsystem interfaces is ensured.

13.1.1. High-Level Concurrent Design Tool Logic

The first step to enable the compatibility between each subsystem and within the aircraft is to define a design space. The first independent variable of the design space was chosen to be the power split between the combustor and the FC. This choice primarily considers the NO_x emissions, which are proportional to the power output from the combustor. On the other hand, the size of the FC is highly dependent on the power it has to output. As the FC is one of the two energy generators of the system, alongside the combustor, the other subsystems are heavily reliant on the size of the FC. For this reason, the other two independent variables used for the system's modeling are the TOGA throttle percentage and the cruise throttle percentage. They are also crucial for the sizing of the FC because they drive the maximum and the continuous power that the FC is expected to deliver.

In the case of each percentage, split, TOGA or cruise, a higher percentage means more FC - less combustor used. Therefore, for each combination of the power split, TOGA throttle and cruise throttle, a design will be output. After a design is constructed, a constraints analysis will be performed to ensure its feasibility. Subsequently, the design will be stored and utilized in a trade-off analysis incorporating all of the still viable options.

The diagram in Figure: Main script flow diagram shows the top-layer rationale of the code. The main characteristics for each subsystem are their mass and volume, for further analysis into integration. For this reason, each subsystem model outputs its respective mass and volume. However, because of the interdependencies within the system, some models also output other values that help with the modeling continuity. As may be seen in Figure: Main script flow diagram, each output-input relationship is color-coded, for easier visualization of the interactions.

Five models have been developed for the detailed design of different subsystems, and further integrated together within this stage of the design. The computation's sequence for sizing the components adheres to the list below:

- The EPS module takes the power split as an input, and based on this, it sizes the ELMOs, inverters, and cables. It also outputs the heat dissipated by the subsystem, that would be taken into account for the thermal management subsystem.
- The flight performance and the FC models were combined into one, and it outputs all of the rest parameters needed for the TMS, but also the size of the FC and the mass of hydrogen needed for the completion of the mission.
- Having all the necessary data, the TMS could be sized. It also outputs the drag penalty because of the radiators and the increment of power needed to run the cooling system.
- The design will iterate over these two variables until the MTOW converges for each power split and throttle combination.
- The storage tank can be sized based on the hydrogen mass, and the cargo space may be calculated based on the tank's volume.

As said before, the model's MTOW has to converge towards a stable value for the model to be feasible. The change in MTOW happens due to the change in drag and change in AP needed for the TMS to run, as well as the updated masses of subsystems. Convergence is encouraged using an under-relaxation term of $\alpha = 0.5$ is used to prevent per-step oscillation, with sign flips in the MTOW increase being used to apply and modulate the under-relaxation factor. This iteration procedure may be visualized as a pseudo-code in 1.

Algorithm 1 MTOW convergence iteration using under-relaxation term $\alpha = 0.5$

Initialize $MTOW_{\text{prev}} \leftarrow 0.0$, $\alpha(under-relaxationfactor) \leftarrow 0.5$, $\delta_{\text{prev}} \leftarrow 0$, $TOLERANCE \leftarrow 0.001$
for $i = 0$ to $i_{\max}$ **do**
  $MTOW_{\text{cand}} \leftarrow Calculate\_MTOW\_from\_subsystems\_masses$
  $\delta \leftarrow MTOW_{\text{cand}} - MTOW_{\text{prev}}$
  if $i > 0$ **and** $\delta \cdot \delta_{\text{prev}} < 0$ **then**
    $\alpha \leftarrow \alpha/2$ ▷ Dampen update on oscillation
  end if
  if $i == 0$ **then**
    $MTOW \leftarrow MTOW_{\text{cand}}$
  else
    $MTOW \leftarrow MTOW_{\text{prev}} + \alpha \cdot \delta$
  end if
  if $|\delta|/MTOW_{\text{prev}} <$ tolerance **then**
    break ▷ Convergence achieved
  end if
  $\delta_{\text{prev}} \leftarrow \delta$
  $MTOW_{\text{prev}} \leftarrow MTOW$
end for

The model needs to be initialized for the first run. The MTOW is initialized as the sum of the preliminary masses estimated earlier during the project, and the OEW of the original Beechcraft 1900D. Moreover, since this was not taken into account so far, the drag due to the radiators and the AP are initialized to zero. As the c_D and the AP are outputs of the TMS, after the MTOW recalculation, the whole sequence of Flight Performance & Propulsion (FPP)+FC, storage, cargo, and TMS are being iterated until convergence. After a design is converged w.r.t. the MTOW, the design data are stored in tensor for further constraint analysis and trade-off.

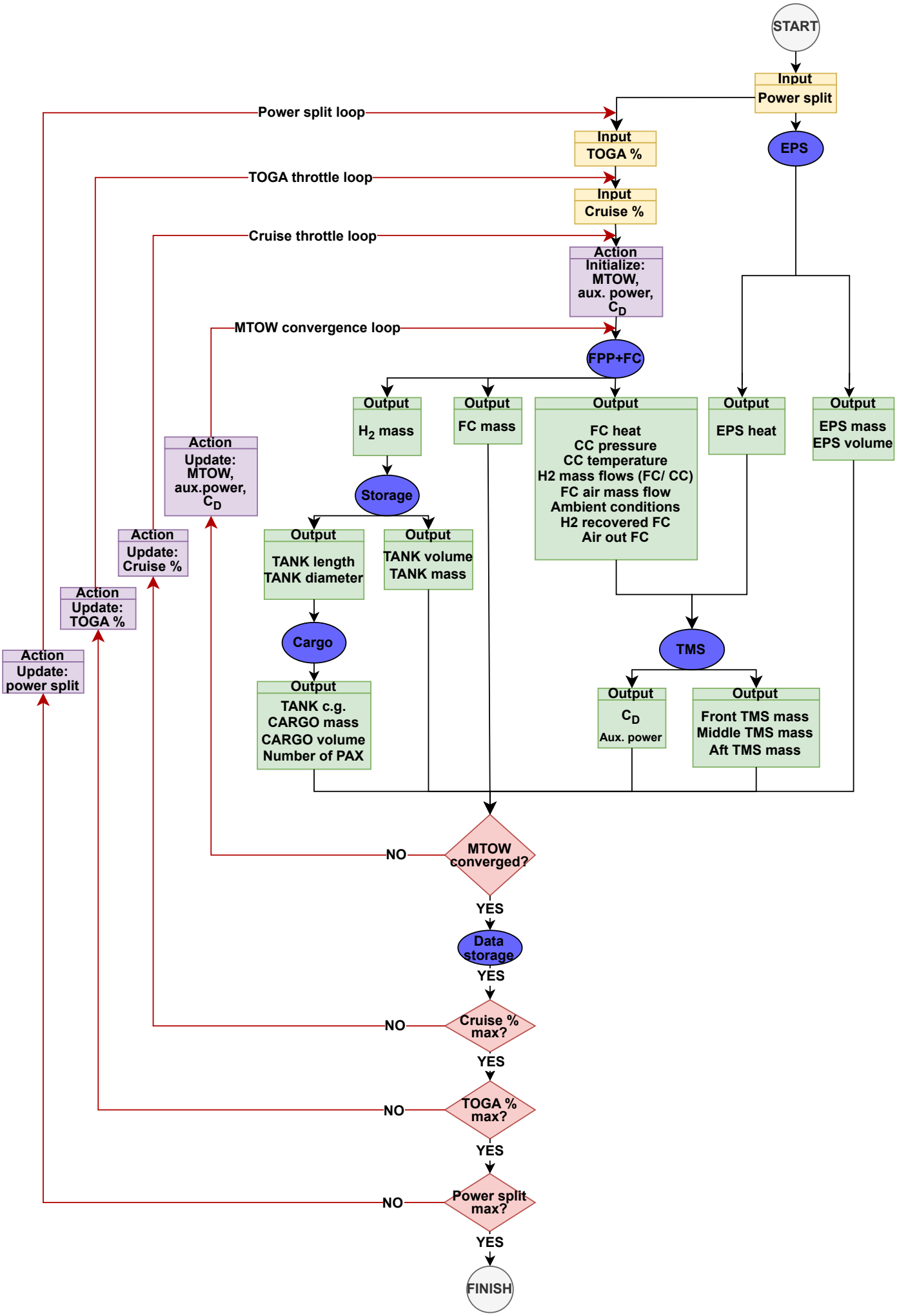

Fig. Main script flow diagram

13.1.2. Flight Performance & Propulsion Model

An integral aspect of the CDT is the flight model developed to simulate the performance of both the FC and turboprop across an assumed flight profile. Aside from the fuel mass, the FPP model also serves to determine the NO_x across the simulated flight profile, ensuring the fuel mass adheres both to the reduced maximum range of 707 km (instead of its maximum 2315 km range [88]), all in accordance with REQ-TE-STK-C. By modulating the shaft power by a proposed power split between CC and FC for each phase or leg of the flight profile, the required H_2 mass can be narrowed down and fed back into storage and TMS models, while the NO_x emissions are stored for further design elimination and sustainability evaluations.

The model subsumes the FC and turboprop tools and maps into its runtime, allowing for the FC and turboprop conditions and outputs to be recorded at every timestep across the simulated flight profile. Algorithm 2 serves as a high-level pseudocode description of the calls to the engine maps displayed in Figure 8.8 as well as the thermodynamics used in order to return accurate turboprop data. Note that here, R_{LHV} refers to the J-A1 to H_2 ratio in LHV, P_r references the required power, and P_a the shaft power. These engine maps were used in order to interpolate the mass flow rates of air and fuel through the engine corresponding to a particular shaft power delivered by the turboprop. Even with these interpolated relations, several assumptions had to be made at this stage of design due to insufficiency of publicly available information. While some values could be inferred from PT6A-65 engine specifications found in P&W's Pilot Familiarization Manual [44], and subsequently projected to 2035, others had to be assumed. Table 13.1 details all values used for the PT6A-67D turboprop model, along with their provenance. Note that for this preliminary design, the inlet efficiency, η_{in} is taken to be 1.0 by assuming isentropic conditions through the inlet. The low flight speeds ($M \leq 0.4$) lends itself well to this initial estimation. In parallel, the FC model is implemented to be later used in the TMS tool of the overall CDT.

Table 13.1: *PT6A-67D turboprop parameters used in the cycle analysis*

Engine Parameter	Chosen Value
Air mass flow range[1], $\Delta\dot{m}$ [kg/s]	0.454
Min. air mass flow[1], $\dot{m}_{\text{min}}$ [kg/s]	4.536
Inlet efficiency[2], η_{in}	1.00
Compressor pressure ratio[1], Π_{comp}	12.0
Compressor efficiency[2], η_{comp}	0.85
Combustor pressure ratio[1], Π_{cc}	0.973
Combustor efficiency[2], η_{cc}	0.97
TIT[1], T_{04} [K]	1274
Turbine efficiency[2], η_{turb}	0.85
Mechanical efficiency[2], η_{mech}	0.95

The model's second step builds the flight profile and cruise range from published Rate of Climb (ROC), Rate of Descent (ROD), and manufacturing reserve-hold data. Table 13.2 lists each Beechcraft 1900D segment's altitude, mean speed, ROC [25], and Skybrary standards of ROD for descent and approach [89]. The reference airspeeds are, however, interpolated between estimated values found online, as Beechcraft 1900D operations manuals were not publicly available [90]. Taxi-out and taxi-in are fixed at 10 minutes each, with a 45 minutes manufacturing reserve hold [25].

Table 13.2: *Mission and operating conditions*

Flight Phase	Pressure altitude, h [m]	Mean Speed, V [m s^{-1}]	ROC / ROD [m s^{-1}]
Taxi-out	0	8.23	0
Take-off	0 - 2438	54.02	13.28
Climb 1st stage	2438 - 4877	61.73	13.28
Climb 2nd stage	4877 - 7620	61.73	13.28
Cruise	7620	142.50	0
Descent 1st stage	7620 - 1525	142.50	−7.62
Reserve-hold required	1525	102.89	0
Descent 2nd stage	1525 - 305	102.89	−7.62
Approach	305 - 0	60.20	−3.15
Taxi-in	0	8.23	0

[1] Values estimated from P&W's Pilot Familiarization Manual [44]
[2] Values estimated with no available literature

As can be seen from Algorithm 2, the entry point for the engine computations rests on isolating flight conditions obtained from the simulated flight profile. A full thermodynamics analysis beginning at the engine inlet (station 0), through to the turbine exhaust (station 5), is used to estimate the thermal efficiencies of both the J-A1 and H_2 dependent turboprops, while the fuel mass flow rate is interpolated from the aforementioned PT6A-67D engine maps.

The flight profile linearly interpolates velocities between known waypoints and combines these velocities with the ROC/ROD values to determine the cruise and hold phases of flight. This – along with the so-called 'powerpoint' definitions – works in tandem to create a full flight profile with time-dependent shaft and required powers. These in turn feed the turboprop model simplified by Algorithm 2, to perform a time-march of the fuel consumption and thermal efficiencies. Numerical integration of the fuel mass flow rate leads to the total fuel mass estimate for both the retrofitted and original Beechcraft 1900D.

As a sanity check, the unmodified Beechcraft 1900D fuel mass is also estimated for its maximum range (2315 km). The resulting fuel burn of 1,929.0 kg is obtained resulting in a 7.84% underestimation of the actual fuel mass. While not a perfect result, an error < 8% is definitely an encouraging result that reinforces confidence in the tool.
An example of the shaft power as a fraction of the maximum continuous power is given in Figure 13.1b, representing a slight increase in the required cruise shaft power due to the higher mass at cruise. This is largely caused by the far lower fuel mass flow rate (Figure 13.1d) of hydrogen, leading to a lower fuel burn by the start of cruise.

Algorithm 2 PT6A-67D engine performance algorithm

procedure ENGINE($T_0, P_0, \rho_0, V_0, R_{LHV}, P_r, P_a, \dot{m}_{H_2O}$)
▷ **0: Pre-Processing**
  $M_0 \leftarrow \dfrac{V_0}{\sqrt{k_{air}\, R_{air}\, T_0}}$
  $\eta_{prop} \leftarrow$ PROPEFF(M_0)
  if $P_a = \emptyset$ **then**
    $P_a \leftarrow \dfrac{P_r}{\eta_{prop}}$
  end if
  $\dot{m}_{air} \leftarrow$ INLETFLOW(P_a) ▷ interpolated from engine map
▷ **1: Brayton Cycle Calculations**
  $(T_{02}, P_{02}) \leftarrow$ STATION02(T_0, P_0, M_0)
  $(T_{03}, P_{03}) \leftarrow$ STATION03(T_{02}, P_{02})
  $(T_{04}, P_{04}) \leftarrow$ STATION04(P_{03})
  $\dot{m}_{fuel} \leftarrow (\dot{m}_{H_2O}, P_a)$ ▷ interpolated from engine map
  $(T_{05}, P_{05}) \leftarrow$ STATION05($\dot{m}_{air}, \dot{m}_{fuel}, T_{02}, T_{03}, T_{04}, P_{04}$)
  $\eta_{th} \leftarrow$ THERMALEFF($\dot{m}_{air}, \dot{m}_{fuel}, T_{03}, T_{04}, T_{05}, P_0, P_{05}, V_0$)
  return $(\dot{m}_{fuel}, \eta_{th}, \eta_{prop}, \dot{m}_{air})$
end procedure
▷ **2: Helper Functions**
function PROPEFF(M_0)
  return piecewise curve with $\eta_{prop,max} = 0.85$ ▷ Mattingly et al., pp. 601 [91]
end function
function INLETFLOW(P_a)
  return INTERPOLATE(P_a) ▷ interpolated from engine map
end function
function STATION02(T_0, P_0, M_0)
  return $T_{02} = T_0(1 + \frac{k_{air}-1}{2} M_0^2)$, $P_{02} = P_0(1 + \eta_{in} \frac{k_{air}-1}{2} M_0^2)^{k_{air}/(k_{air}-1)}$
end function
function STATION03(T_{02}, P_{02})
  return $T_{03} = T_{02}\left(1 + \frac{1}{\eta_{comp}}\left(\Pi_c^{(k_{air}-1)/k_{air}} - 1\right)\right)$, $P_{03} = P_{02}\Pi_c$
end function
function STATION04(P_{03})
  return $T_{04} = T_{04,set}$, $P_{04} = P_{03}\Pi_{cc}$
end function
function STATION05($\dot{m}_{air}, \dot{m}_{fuel}, T_{02}, T_{03}, T_{04}, P_{04}$)
  power balance **return** (T_{05}, P_{05})
end function
function THERMALEFF($\dot{m}_{air}, \dot{m}_{fuel}, T_{03}, T_{04}, T_{05}, P_0, P_{05}, V_0$)
  return η_{th} ▷ from gas-generator work balance
end function

The thermal efficiency is significant as shown in Figure 13.1c – especially during cruise – representing a roughly 7% increase on the unmodified turboprop's performance at cruise. Note that these results should solely be taken as demonstrations of the simulated flight profile, as determining the actual use of the CC versus the FC (and subsequent design variables) is naturally the CDT's primary aim.

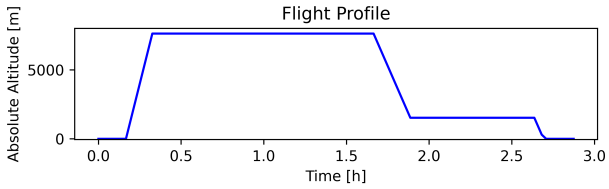

(a) *Altitude vs time*

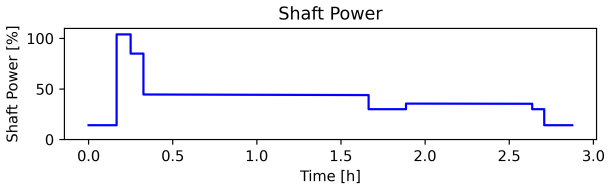

(b) *Shaft power (fraction of max. continuous) vs time*

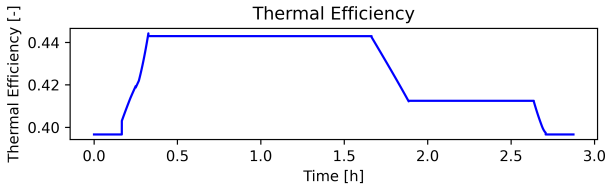

(c) *Thermal efficiency vs time*

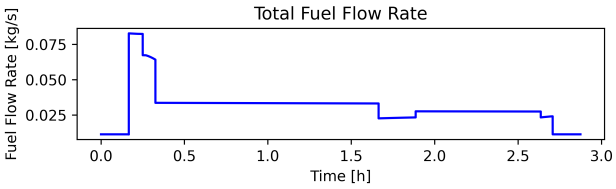

(d) *Fuel flow rate vs time*

Figure 13.1: *H_2D_2 flight and power profiles alongside associated engine thermal efficiency and total fuel flow rate*

13.1.3. Design Space Description

The CDT generates potential PT designs across three axes, namely the proportion of FC power at takeoff (power split), FC throttle at take-off (TOGA throttle), and maximum FC throttle at cruise (cruise throttle). These three axes in combination with the ensuing stored design variables create a four-dimensional design space tensor upon which constraints and objective functions can be applied in order to arrive at the optimal PT design. The stored PT variables are as follows:

- Mass of EPS
- Mass of FC
- Maximum mass of hydrogen for a flight
- Mass of storage
- Volume of FC
- Volume of storage
- Volume of the ELMO
- MTOW
- Length of the storage
- Diameter of the storage
- Mass of cargo
- Mass of TMS (including its division between TMS stored near the wings, hydrogen storage, and piping)
- Maximum mass of NO_x produced over a flight
- Take-off and cruise maximum NO_x mass flow rates
- FC cost
- Nominal mass of hydrogen (without reserves)
- ELMO power
- CO_2 equivalent of FC
- CO_2 equivalent of storage
- CO_2 equivalent of EPS

While this vector naturally does not contain all PT design parameters and consequent impacts on flight performance, such as the increase in drag count due to the addition of radiators, these elements provide enough data for the application of constraints and objective functions. Any additional variables generated by the CDT but not stored in the design space tensor can be subsequently obtained upon selection of the optimal design.

13.2. Design Space Restriction

Choosing an optimal design from the design space is not a straightforward task. Therefore, it is crucial to eliminate clearly infeasible designs prior to any design trade-off. Several constraints, described in this section, were identified from requirements, cumulatively contributing to a 67.08% reduction in the design space.

13.2.1. Integration Constraint

Aspects of design impacting the PT's integration into the Beechcraft 1900D were grouped as a single set of 'integration' constraints. This included: the PAX requirements stemming from the storage tank sizing, control and stability requirements, and volumetric considerations from the limited available volume. This amalgamation of requirement enforcements led to a design space pruning of 30.01%.

Minimum Number of Passengers Constraint

As for REQ-CO-STK-G, H_2D_2 shall transport at least 15 PAX, therefore any design considering a lower number of PAX is unfeasible.

The method for calculating the number of PAX is based on the sizing of components and is closely related to the component integration into the aircraft. The working logic of the tool developed for this purpose is presented in the pseudo-code on the right.

Several geometry simplifications were made, which can be seen in the tool implementation. The back of the fuselage starts tapering off at some point and additionally, the fuselage has a rectangular cross-section with rounded edges, which allows for simplifying it to an elliptical shape. A circular cross-section was not assumed in order to have a more accurate output, and also for maximizing the volume within the fuselage. For the purpose of this analysis the back of the fuselage is considered to have two sections: a cylinder with an elliptical cross-section and a truncated cone from the point where the fuselage start tapering-off.

The output of this tool is not only the number of PAX, but also the positioning of the storage tank and, therefore, fuel, part of TMS and aft cargo, which are later used in the Centre of Gravity (CG) range determination. Again, there is a minimum limit for the number of PAX, by REQ-CO-STK-G. However, since the tank and the aft cargo space are being sized as well, certain design options might result in extra space, for including more rows of seats. For this reason, the PAX number was kept a variable.

Algorithm 3 Aft Configuration Algorithm

procedure AFTCONFIG(L_{tank}, d_{tank}, FuselageDims, Layout)
▷ **0: Initial Tank Placement**
$X_{back} \leftarrow$ PLACEINCONE(L_{tank}, d_{tank})
$X_{front} \leftarrow X_{back} - L_{tank}$
▷ **1: Seat Interference Check**
$\Delta \leftarrow X_{last,seat} - X_{front}$
if $\Delta > 0$ **then**
$N_{removed} \leftarrow \lceil \Delta / \text{seat\_pitch} \rceil$
$N_{PAX} \leftarrow N_{PAX,0} - 2 \cdot N_{removed}$
$X_{last,seat} \leftarrow X_{last.seat} - N_{removed} \cdot \text{seat\_pitch}$
else
$N_{PAX} \leftarrow N_{PAX,0}$
end if
▷ **2: Forward Shift if Space Exists**
if $X_{front} > X_{last,seat}$ **then**
$X_{front} \leftarrow X_{last,seat}$
$X_{back} \leftarrow X_{front} + L_{tank}$
end if
▷ **3: Tank and TMS Specs**
$L_{cyl} \leftarrow \max(L_{cyl}, L_{tank})$
$L_{cone} \leftarrow L_{tank} - L_{cyl}$
$V_{cyl} \leftarrow$ CYLVOLUME(L_{cyl})
$X_{cyl} \leftarrow X_{cyl,start} + L_{cyl}/2$
$V_{cone} \leftarrow$ CONEVOLUME(L_{cone}, d_{tank})
$X_{cone} \leftarrow$ CONECG(L_{cone}, d_{tank})
$V_{tank} \leftarrow V_{cyl} + V_{cone}$
$X_{tank} \leftarrow \dfrac{V_{cyl} \cdot X_{cyl} + V_{cone} \cdot X_{cone}}{V_{tank}}$
▷ **4: Aft Cargo Specs**
$L_{cargo} \leftarrow l_{cone} - L_{cone}$
$V_{cargo} \leftarrow$ CONEVOLUME(L_{cargo}, d_{tank}, d_{end})
$M_{cargo} \leftarrow \rho_{cargo} \cdot V_{cargo}$
$X_{cargo} \leftarrow$ CONECG(L_{cargo}, d_{tank}, d_{end})
return $(X_{front}, X_{back}, X_{tank}, V_{tank}, X_{cargo}, M_{cargo}, V_{cargo}, N_{PAX})$
end procedure

Controllability & Stability Constraint

It is necessary to recompute the CG range for the retrofitted aircraft to ensure that is is within Beechcraft 1900D CG range (6.79-7.51 m w.r.t. the nose) which would ensure stability and controllability of H_2D_2, as for REQ-CO-SYS-J.2. Here, the method for this calculation is described.

The following process is used to calculate the CG range of H_2D_2: first, the original Beechcraft data was compiled and/or calculated, the OEW of the Beechcraft was estimated as it was not readily available, the additional components were fitted in the available space, a loading diagram was generated and, finally, the CG range was extracted. The original Beechcraft 1900D data, relevant masses and CG locations with respect to the nose, is provided in the Table 13.3 below. The calculated values are shown in gray, the rest were extracted from the Beechcraft 1900D documentation or were determined using the scaled diagram of the plane. For the purpose of calculating the OEW, two configurations were assumed as two critical CG locations were reported.

- Configuration 1 - maximum fuel loaded, resulting in the most forward CG position
- Configuration 2 - maximum payload loaded, resulting in the most aft CG position

That assumption is valid as for MTOW the loading configuration is not specified and the aircraft cannot carry maximum fuel and maximum payload at the same time, which indeed can result in a range of MTOW CG positions. Additionally, the fuel CG position can be assumed to be constant with its varying mass as it is housed in the wings and the weight spreads uniformly in the available volume, thus on the longitudinal axis of the wing. However, the payload CG location does not follow the same logic. PAX and cargo are simulated as discreet point masses and they have specified positions along the fuselage. For that reason, the OEW was first calculated from Configuration 2, as all the data was readily available and the payload position could be analyzed from the data on the aircraft inner layout [25]. Then, the necessary Configuration 1 payload CG position was calculated to result in the same OEW CG and the validity of that position was verified. This analysis resulted in an Beechcraft 1900D OEW CG position of 6.76 m w.r.t. the nose.

Table 13.3: *Beechcraft 1900D CG data [25]*

	Configuration 1		**Configuration 2**	
	Mass [kg]	**CG location [m]**	**Mass [kg]**	**CG location [m]**
MTOW	7765	6.79	7765	7.51
Fuel	2022	7.29	300	7.29
Payload	812	5.71	2534	8.99
OEW	4932	6.76	4932	6.76

The additional components necessary for the retrofit were added at this point. The positioning of components was constrained by the CG range and available volume, which was already observed in the Midterm Report [64], and additional simplifications were introduced to allow for a preliminary estimation when iterating through designs. The component placement, with the PAX and cargo, can be seen in Figure 14.2. The components were grouped with respect to their systems and then placed in discreet locations based on their geometry or the geometry of the space available if the exact shape of the component was still unknown. Then, their impact on the OEW CG could be accounted for.

The one system that stands out is the TMS as its components are located in multiple different spaces of the aircraft and the coolant weight in the piping is non-negligible. For that reason, the TMS was divided into two parts, in the wing and at the back of the fuselage, under the storage tank. Therefore, the coolant is distributed between those two spaces. The specific component division and placement was described more in-depth in Chapter 12.

The next step is loading the aircraft with cargo first, then PAX and, lastly, fuel. The PAX weight is estimated based on an individual weight with hand luggage of 84 kg[1] was assumed, in accordance with EASA standards, and the cargo weight is estimated based on the available cargo volume and an average cargo density of 161 kg/m^3 [2] in accordance with ICAO standards. The resulting loading diagram in Figure 16.1 identifies the most forward and aft CG locations of H_2D_2.

[1] URL https://www.easa.europa.eu/en/light/topics/passenger-weight-and-why-it-matters-safe-and-efficient-air-operations [Cited 17 June 2025]

[2] URL https://www.icao.int/MID/Documents/2024/Aviation%20Statistics%20Workshop/PPT-Session%203.pdf [Cited 17 June 2025]

The described method is used to determine the updated CG range of the retrofitted aircraft and used as a constraint, therefore all designs resulting in a non-compatible CG range are eliminated at this point.

Volumetric Constraint

Each design iteration sizes the individual components and calculates their volume. Along other constraints, the volumetric fit must be checked for to ensure integration into the aircraft.

The available space in the Beechcraft 1900D was estimated through aircraft technical sketches and the number of PAX of individual designs. Then, with the component positioning as stated in the Midterm Report [64], visualized later in Section 14.2 in Figure 14.2, that space was compared to the volume of individual components. At this stage of the analysis, the shape of the spaces and components are not yet taken into account, however, it was preliminarily estimated and confirmed that the integration is possible as the component shape can generally be adjusted to the available space if needed.

13.2.2. Wing & Power Loading Constraint

An aircraft wing and power loading constraint analysis is crucial for selecting an appropriate PT while ensuring all performance goals are satisfied. Since the project involves retrofitting an existing airframe rather than developing a new one, the analysis shows how the fuel selection limits the design space rather than to determine sizing.

REQ-CO-SYS-J.1 and REQ-CO-SYS-J.3 confirm that the original and modified Beechcraft 1900D should share identical performance characteristics, the hybrid-electric version must not substantially increase the H_2D_2 MTOW in order to comply with REQ-CO-SYS-J.5, as well as the MTOW budget of 8037.6 kg defined in Chapter 4. The aircraft constraint analysis begins by casting the pertinent performance parameters into mathematical form. These relationships are then rearranged into the standard expression P/W=f(W/S), where W/S is wing loading and P/W is the power loading. In doing so, a region of feasibility is identified which can in turn be used to apply a design space-pruning constraint, thus ensuring that the take-off power and wing loading remains within the original Beechcraft's envelope.

The method for determining this region of feasibility is given by Gudmundsson and assumes a simplified drag model [92]. Table 13.4 represents the performance characteristics of the unmodified Beechcraft 1900D and Equation 13.1 presents the equations used to calculate the specific coefficients of the aircraft. The chosen constraints together with their governing expressions are summarized in Table 13.5. These equations are derived from the balance of forces, acting on the aircraft, at each flight stage analyzed.

Table 13.4: *Performance characteristics used in the Beechcraft 1900D constraint analysis [25]*

Parameter (symbol)	Value / units	Parameter (symbol)	Value / units
Gravitational acceleration, g	$9.806\,\mathrm{m\,s^{-2}}$	Take-off speed, V_{TO}	$54.0\,\mathrm{m\,s^{-1}}$
Sea-level air density, ρ_{SL}	$1.225\,\mathrm{kg\,m^{-3}}$	Approach speed, V_L	$54.0\,\mathrm{m\,s^{-1}}$
Cruise density, ρ_{cruise}	$0.550\,\mathrm{kg\,m^{-3}}$	Stall speed (TO flaps), $V_{\mathrm{stall,f}}$	$46.3\,\mathrm{m\,s^{-1}}$
Zero-lift drag coefficient, C_{D_0} [93]	0.023 (-)	Stall speed (clean, MTOW), $V_{\mathrm{stall,c}}$	$52.0\,\mathrm{m\,s^{-1}}$
Aspect ratio, AR	10.81 (-)	Cruise speed, V_{cruise}	$144\,\mathrm{m\,s^{-1}}$
Oswald efficiency factor, e	0.736 (-)	Required rate of climb, ROC	$10.2\,\mathrm{m\,s^{-1}}$
Wing area, S	$28.8\,\mathrm{m^2}$	Average climb speed, V_y	$73.4\,\mathrm{m\,s^{-1}}$
Maximum take-off mass, m_{TO}	8037.6 kg	Maximum landing mass, $m_{L,\mathrm{max}}$	8037.6 kg
Take-off power (TOGA), P_{TOGA}	1.908×10^6 W	Runway-friction coefficient, μ_{TO} [92]	0.04 (-)
Take-off ground run, S_g	1163 m	Landing-distance requirement, S_{land}	851 m
Propulsive efficiency, η_{prop}	0.85 (-)		

$$
\begin{aligned}
C_{L_{\max,\mathrm{TO}}} &= \frac{m_{TO}\, g}{0.5\, \rho_{SL}\, V_{\mathrm{stall},f}^2\, S}, \quad C_{L_{\max,L}} = \frac{m_{L,\max}\, g}{0.5\, \rho_{SL}\, V_{\mathrm{stall},f}^2\, S}, \\
C_{L_{\mathrm{TO}}} &= \frac{m_{TO}\, g}{0.5\, \rho_{SL}\, V_{\mathrm{TO}}^2\, S}, \qquad C_{D_{\mathrm{TO}}} = C_{D_0} + k\, C_{L_{\mathrm{TO}}}^2
\end{aligned}
\tag{13.1}
$$

Table 13.5: *Constraint analysis of the unmodified Beechcraft 1900D*

Constraint	**Expression used in sizing**
Take-off ground run	$\frac{P}{W} = \left[\frac{1.21}{g\, \rho_{SL}\, C_{L_{\max,\mathrm{TO}}}\, S_g} \left(\frac{W}{S}\right) + \frac{0.605}{C_{L_{\max,\mathrm{TO}}}} \left(C_{D,\mathrm{TO}} - \mu\, C_{L,\mathrm{TO}}\right) + \mu \right] \frac{V_{\mathrm{TO}}}{\eta_{\mathrm{prop}}}$
Stall limit	$\left(\frac{W}{S}\right)_{\mathrm{stall}} = \frac{1}{2}\, \rho_{SL}\, V_{\mathrm{stall,\,f}}^2\, C_{L_{\max}}$
Landing limit	$\left(\frac{W}{S}\right)_{\mathrm{land}} = \frac{1}{2}\, \rho_{SL}\, V_L^2\, C_{L_{\max,L}}$
Cruise (steady level flight)	$\frac{P}{W} = \left(\frac{q\, C_{D_0}}{W/S} + \frac{k\, W/S}{q} \right) \frac{V_{\mathrm{cruise}}}{\eta_{\mathrm{prop}}}, \qquad q = \frac{1}{2}\, \rho_{\mathrm{cruise}}\, V_{\mathrm{cruise}}^2$
Rate-of-climb (initial)	$\frac{P}{W} = \left[\frac{\mathrm{ROC}}{V_y} + \frac{q\, C_{D_0}}{W/S} + \frac{k\, W/S}{q} \right] \frac{V_y}{\eta_{\mathrm{prop}}}, \qquad q = \frac{1}{2}\, \rho_{SL}\, V_y^2$

Figure 13.2 shows the constraint analysis of the original Beechcraft 1900D. This feasible region is used as an eliminating factor for generated designs, with 61.66% of the design space eliminated due to either incompatible wing or power loading at take-off, ensuring that the remaining designs would not necessitate an airframe redesign. Note that this matches almost perfectly with the overall design space reduction as integration was the leading factor in the elimination of infeasible designs.

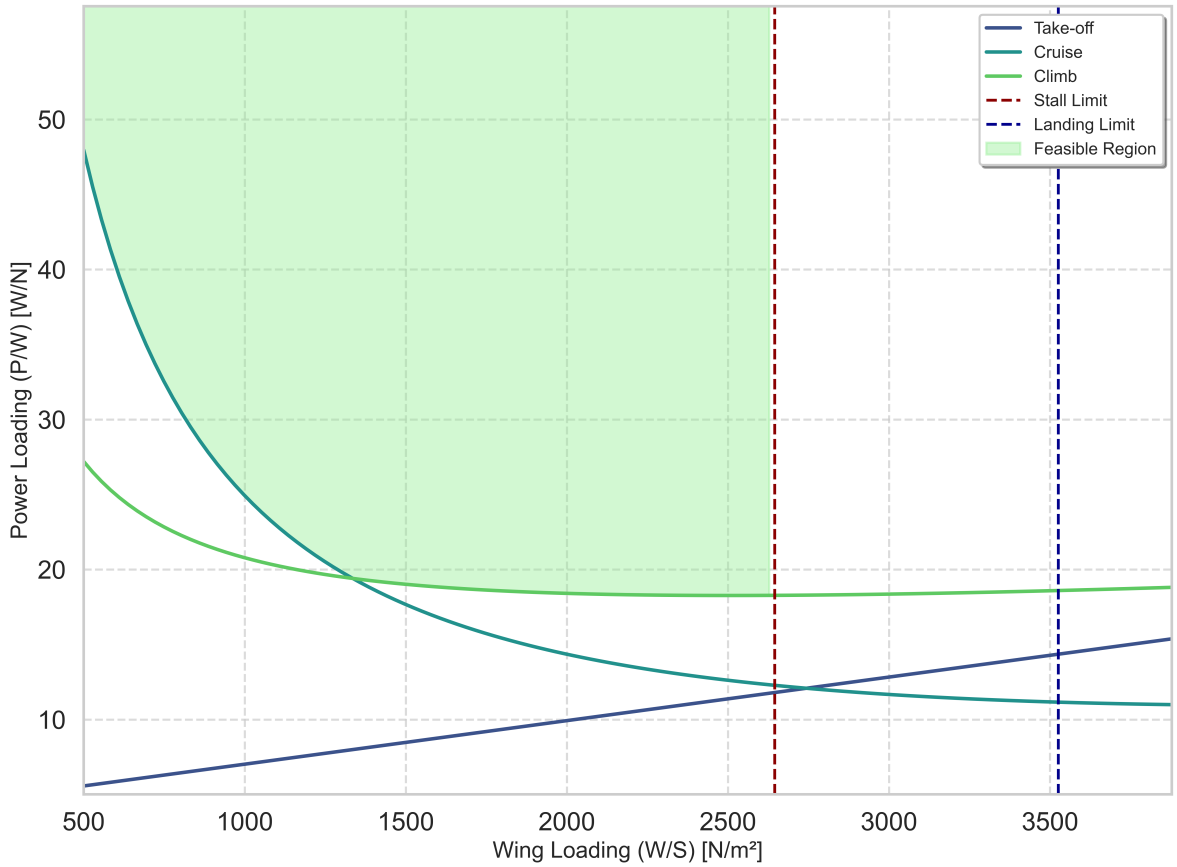

Figure 13.2: *Constraint analysis of the original and modified Beechcraft 1900D*

13.2.3. NO_x Emissions Constraint

The design space can be further narrowed down by applying an NO_x emissions constraint. REQ-TE-SUB-B.4.1 states that the aircraft shall produce maximum of 25 ppm of NO_x at 15% O_2. For convenience of comparison, this constrained is analyzed separately for take-off and cruise conditions as the mass flow rates through the engine change greatly between these two conditions. The maximum allowable value was recalculated to a mass flow rate in $\frac{g}{s}$, using the mass flow rates of air and fuel at the specified flight conditions. This resulted in a constraining NO_x production of 0.243 $\frac{g}{s}$ at TOGA and 0.177 $\frac{g}{s}$ at cruise. However, this constraint did not eliminate any designs as the all proposed options generated considerably less NO_x than the maximum tolerable value.

13.2.4. Effect of Constraints

As previously stated, the overall reduction in the design space due to the constraints described above represents 67.08% of all generated designs. The Kernel Density Estimate (KDE) plots shown side-by-side in Figure 13.3 clearly demonstrate this reduction. Indeed from Figure 13.3a, designs originally exhibit extraordinarily poor sustainability and cost performance, likely due to unphysical sub-system sizes. These form sporadic clusters far away from the valid (constrained) design space shown in Figure 13.3b where a much more centralized cluster of designs can be observed. Note that the significance of the GWP and lifetime cost is expanded upon in the following section. Each plot in Figure 13.3 has auxiliary histograms for both cost and GWP. The purpose of these histograms is to facilitate a better visualization of the designs' densities in the respective regions along the plot.

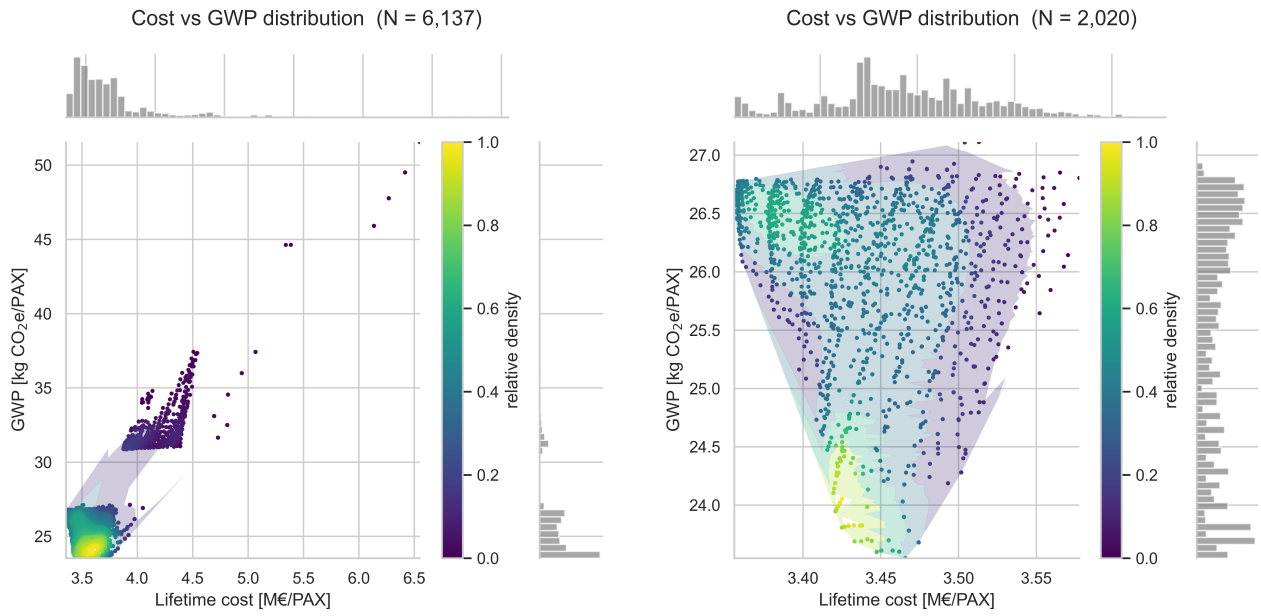

(a) *Unconstrained design space (N = 6,137)*

(b) *Constrained design space (N = 2,020)*

Figure 13.3: *KDE plots of constrained versus unconstrained s and lifetime costs across the design space*

13.3. Final Design Trade-off

Selecting a final PT configuration from the 2,965 valid designs post-constraint application involves an automated trade-off between two key metrics: GWP per PAX and lifetime cost per PAX. Given the stated mission objective that "the aviation sector needs to demonstrate a hydrogen-electric PT in short-to-medium haul aircraft by 2035, as part of the EU Clean Aviation program", demonstrating cost-effective sustainability was determined to be the driving factors for design selection. Indeed, a PT design leveraging both GWP and cost of its design, integration, operation and disposal in a Beechcraft 1900D would form a compelling product that may also benefit from EU subsidies further incentivizing its wider adoption for short-to-medium haul flights.

Prior to a description of the design space, the KDE plots shown in Figure 13.3 can be expanded upon having underlined the importance of their two constituent axes. We can observed staggered columns of valid designs with a region of high design point density in the upper left of Figure 13.3b plot, and second, more pronounced region of design density in the lower left. We equally see from the relative density plots parallel to the constrained KDE plot axes, that lifetime cost takes a more central form of distribution, whereas the GWP distribution skews to the more unsustainable design points. These observations come together to indicate a small region of 'optimal' designs that effectively minimize both GWP and lifetime cost per PAX.

In order to even further reduce the number of individual designs under direct consideration and highlight the section of minimized GWP and lifetime cost per PAX, a Pareto front was employed as depicted in Figure 13.4. The red boundary shows the convex Pareto front obtained from the constrained design space whereby GWP and lifetime cost per PAX are both minimized. The functions and calculations used to determine said performance metrics can be found in Chapter 17 and Chapter 21 respectively. Any design lying on this boundary can be considered 'Pareto-optimal', and is therefore taken into the final trade-off for the selected design. Going along this boundary from top to bottom and left to right represents a decrease in GWP for an increase in lifetime cost per PAX. The steep initial section indicates that large gains can be obtained for minimal cost increases while the plateau region corresponds to large increases in cost for minimal decreases in GWP.

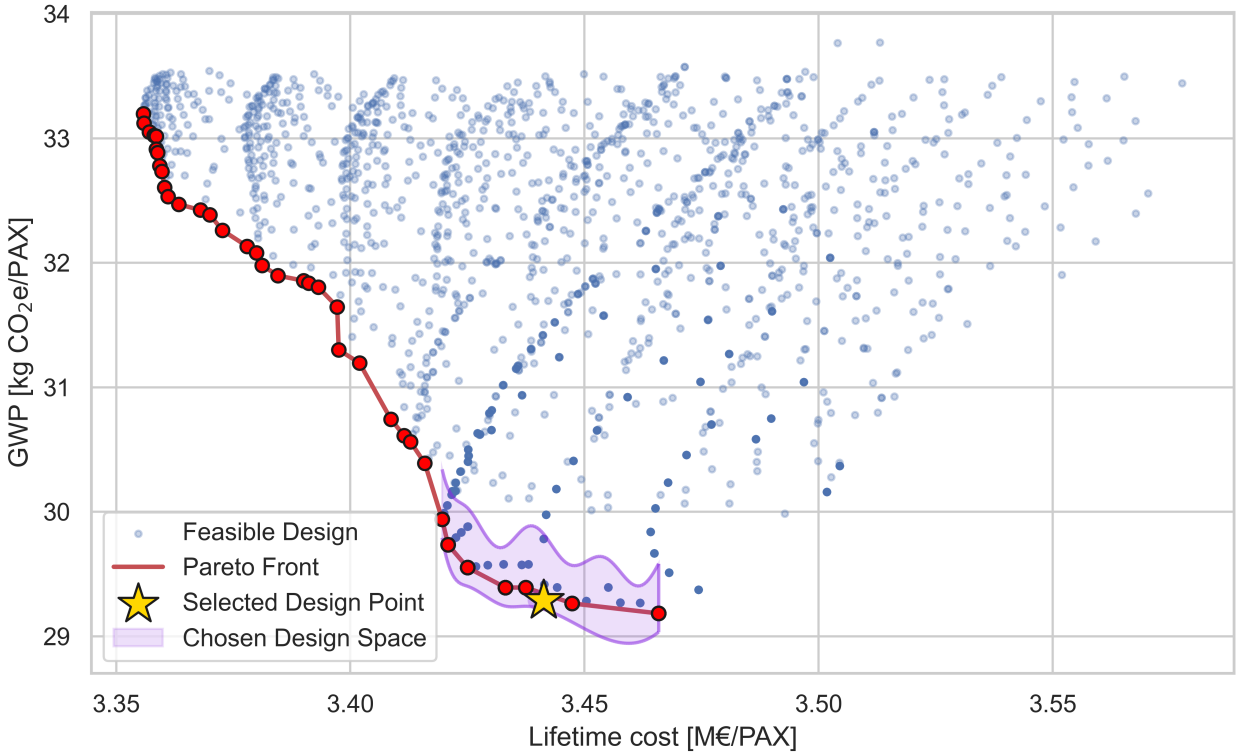

Figure 13.4: *Pareto front overlaid on design space*

While not provided a direct cost target or emissions goal other than the NO_x emissions across a flight, it remains true that an express objective of the SHTARWaRS project is to provide a cost-competitive and low-emissions hydrogen PT for commercial use in short-to-medium haul aviation. As such, the percentage change in GWP versus the percentage change in lifetime cost is evaluated for each of the Pareto-optimal designs to determine at which point gain in one metric is exactly counterbalanced by the loss in another. This design point is thus determined to be optimal due to the lack of external stakeholder pressures, although it should be noted that a more stringent financial budget requirement or increased clarity on potential EU subsidies could shift this needle for the PT design selection. Similarly, a variation in stakeholder-mandated GWP per PAX may again point at a different optimal design.

Firstly, the chosen design space was determined, as seen in Figure 13.4. Then, the design region was further analyzed for a higher granularity, and the final design point was selected. This design point was chosen for the most feasible balance it yields, namely a lifetime cost of around 3.44 M€/PAX and a GWP of approximately 29.3 $kgCO2_{eg}/PAX$.

14

Description of Final Design

This chapter describes the configuration, layout and capabilities of the final design for H_2D_2. It starts from a broad overview of the entire aircraft's layout and operational capabilities in Section 14.1. Moreover, Section 14.2 describes how the different systems are interconnected with each other, and presents how they fit within the whole aircraft. Further on, Section 14.3 zooms-in towards the different systems and describes their individual characteristics and impact on the entire design.

14.1. Aircraft-Level Characteristics

The aircraft, H_2D_2 itself, is a Beechcraft 1900D with a modified propulsion system. This new PT uses LH_2 as the energy carrier, instead of the original kerosene. In addition, H_2D_2 uses a hybrid approach to power generation comprising of both CC and FC, working in tandem to exploit the high energy capacity of hydrogen. For the implementation of this hybrid hydrogen-electric PT, many subsystems have undergone significant updates to design or have been created specifically for the SHTARWaRS PT. The main subsystems experiencing these updates were the hydrogen storage system, TMS, the FC, and EPS.

With these changes taken into account, the aircraft reached an MTOW of 7948 kg and a maximum power of 1908 kW, characteristics that keep H_2D_2 within the original class of the original Beechcraft 1900D. For this reason, the new aircraft is able to operate on the same class of airfields as the unmodified Beechcraft 1900D. On the other hand, the main operational deviations from the baseline that came in with the new PT are the range, which decreased to 707 km, and the PAX capacity, which dropped to 15 seats.

Taking into account the sustainability of the new PT, the operational CO_2 emissions are nonexistent, while the NO_x emissions are 0.00196 g/s at TOGA and none at cruise as the aircraft is powered entirely by the FC during that phase of the flight as seen in Figure 14.1. The total NO_x produced during one flight came up to a value of 1.11 g. The NO_x emissions were the main driver for the trade-off between hydrogen combustion or FC usage. For this analysis, a complete flight profile was considered, and the power split between the two was defined as observed in Figure 14.1.

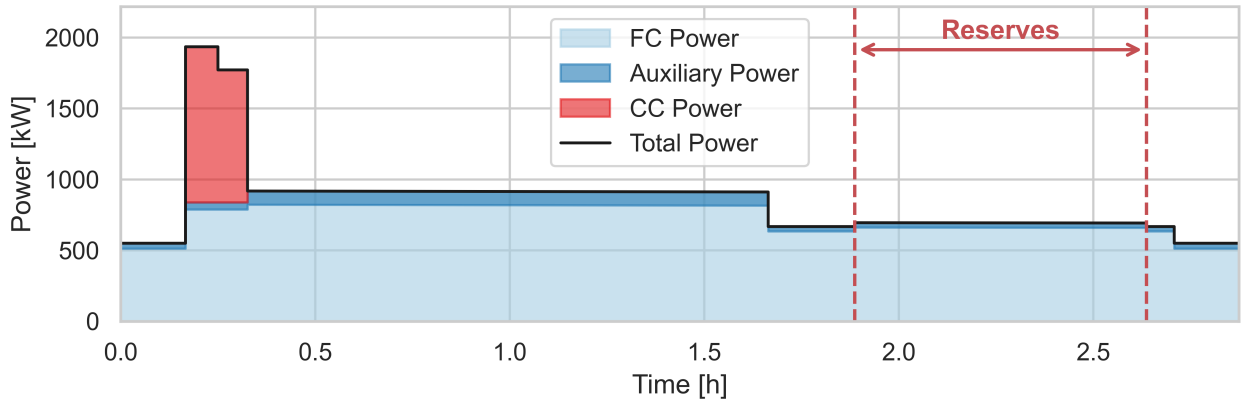

Figure 14.1: *Power profile of the final design*

This plot is generated separating the entire flight profile into two conditions: TOGA and cruise. This is due to the fact that TOGA is a constraining condition for TMS sizing and all the other phases of the mission profile are treated together to minimize the throttling changes between the CC and FC. Note also the stepwise increases in total power represent a limitation of the FPP model – specifically its inability to model transients in provided power. On the scale of a 707 km flight, however, these transients can be assumed to be negligible. For TOGA, **the final design proposes a TOGA power split of 0.32, which means that the FC provides 32% of the total power required at this flight phase, and power split of 100% during cruise**, which comes from sustainability considerations. Additionally, another parameter that is optimized for is the throttle level of the FC. The FC can be throttled from the minimum value to 100%, where that throttle level is inversely proportional to its efficiency as at higher throttle levels the FC produces more heat, which in turn influences the TMS design and fuel burn. For that reason, different throttle levels were considered during different phases of flight. **The final design proposes the TOGA throttle level of 28% and cruise throttle level of 30%.**

14.2. Configuration & Layout

The inner layout of H_2D_2 follows from the engineering decisions and constraints described in Section 13.2. ELMO is integrated into the existing engine, the wing space is occupied by the FC and most of the TMS components, whereas the aft of the fuselage is fitting the storage tank, rest of the TMS, together with the cargo space. Due both to MTOW limitations and the need to constrain the CG, it was decided to forgo the front cargo space given the already sufficient aft cargo mass. A two-dimensional view of the subsystem positions and volumes within the existing Beechcraft 1900D airframe and body is provided below in Figure 14.2.

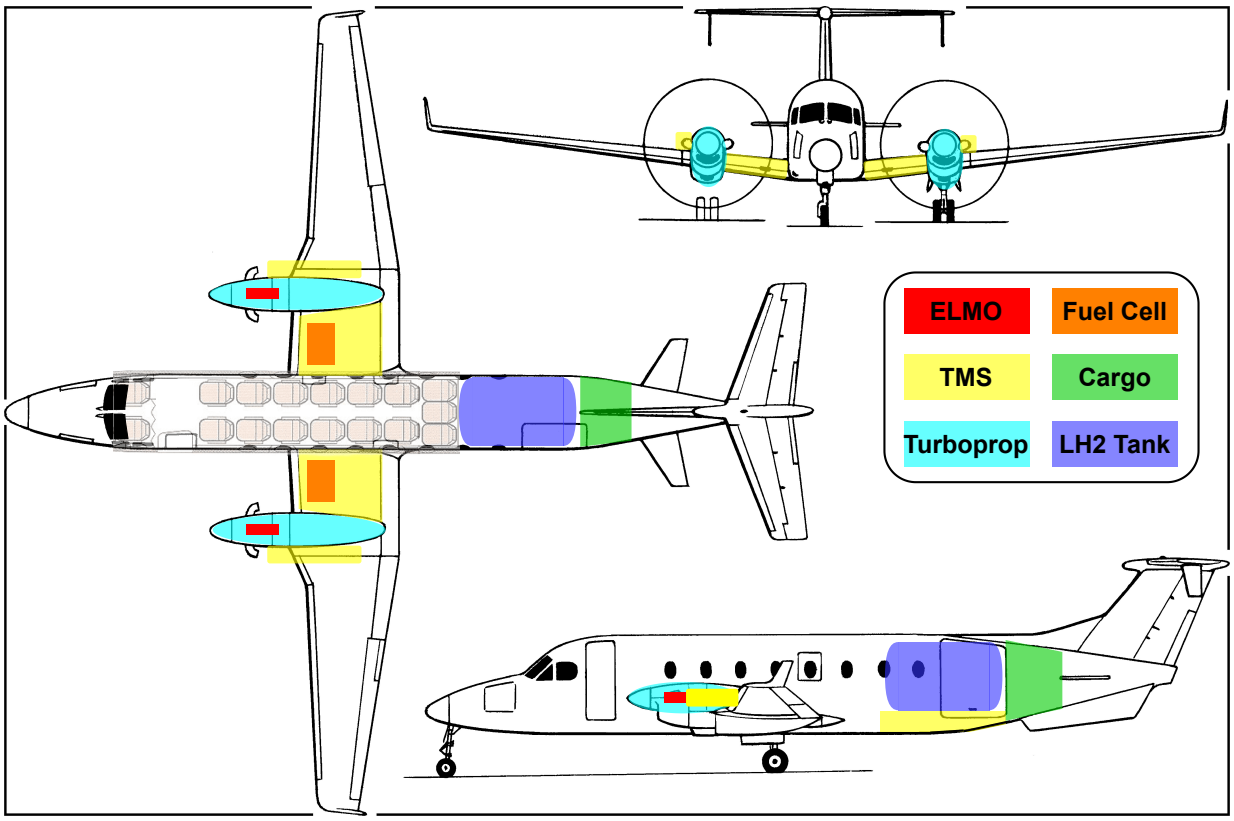

Figure 14.2: *H_2D_2 simplified inner layout [25]*

In addition to the annotated three-view drawing provided above, a CAD model of the H_2D_2 aircraft with the hydrogen PT is provided below in Figure 14.3. Note the reduced number of PAX, down from the Beechcraft 1900D original 19-PAX maximum, now replaced with 15 in order to accommodate the presence of the hydrogen storage tank. The FC stack can also seen in the empty volume at the interface between wing and fuselage in its cuboidal form-factor.

Figure 14.3: *H_2D_2 model [CAD software used: CATIA v5©, NX© and Blender©]*

14.3. System-Level Characteristics

This section examines each individual system in detail, describing its characteristics and its influence on the overall design. Each subsection focuses on one of the following systems: FC, TMS, storage, or EPS. Table 14.1 provides a summary of the masses and corresponding volumes of the systems.

Table 14.1: *System masses and volumes summary*

System	Parameter	Value	Unit
EPS	EPS mass	101.66	kg
	ELMO volume	0.00432	m^3
FC	FC mass	597.91	kg
	FC volume	0.96437	m^3
Hydrogen	Hydrogen mass	215.72	kg
	Nominal hydrogen usage	153.99	kg
Storage System	Storage system mass	243.23	kg
	Storage system volume	4.294	m^3
	Storage system length	2.509	m
	Storage system diameter	1.542	m
TMS	Air compressor mass	12.12	kg
	Air turbine mass	13.26	kg
	FC H_2 recirculation compressor mass	5.17	kg
	CC H_2 compressor mass	6.25	kg
	Coolant pump mass	44.52	kg
	Air-water separator mass	3.76	kg
	Radiator mass (total)	28.11	kg
	Vaporizer HEX mass	1.42	kg
	Superheater HEX mass	32.71	kg
	Total valve mass	4.80	kg
	Total pipe mass (incl. fluid)	76.80	kg
	Total TMS mass	275.99	kg
Cargo	Aft cargo mass	321.20	kg
Aircraft	MTOW	7947.74	kg

14.3.1. Fuel Cell Final Design Characteristics

As stated above, the FC is one of the two power generators. The final FC was design as a HT-PEMFC. It consists of a stack which performs at 62% efficiency during the TOGA regime and 60.75% efficiency during the cruise phase. The efficiency is changing due to the different throttle settings of the two phases.

From an operational point of view, the power density of the FC stack is 5 kW/kg, and it can deliver 4 MW/m^3. Moreover, considering the consumption of hydrogen, during take off 0.009 kg of hydrogen are consumed per second, while the cruise requires a hydrogen mass flow of 0.0108 kg/s. On top of these performance characteristics, the actual sizing data for the FCs are presented in Table 14.1.

14.3.2. Thermal Management System Final Design Characteristics

Table 14.2 provides the sizing of each subsystem of the TMS. The integration of these components in the aircraft is leading in terms of their viability, as some of them need to fit inside the wings, and others in the back. It was chosen to perform the vaporization and heating of the hydrogen in the rear of the aircraft, close to the storage. The alternative would be to transfer LH_2 from the rear to the wings, where it would be vaporized and heated. The overall mass of the system was lower for the option of conditioning the hydrogen in the rear, which is why it was chosen. The additional HEXs (ram air and SHX) are place in the wings, in proximity of the FC.

Table 14.2: *TMS sizing*

Subsystem of TMS	Parameter	Value	Unit
Radiator	Area (each)	0.09	m^2
	Thickness (each)	19	mm
	Diffuser aspect ratio	3.6	–
	Compactness (provided by expert Fabio Beltrame)	1100	m^2/m^3
	Length Ram Air Duct	2.44	m
Plate HEX: Vaporizer	Plate size	0.05	m^2
	Thickness	0.5	mm
	Number of plates	1.0	–
	Number of passes	1	–
Plate HEX: Superheater	Plate size	0.05	m^2
	Thickness	0.5	mm
	Number of plates	10.0	–
	Number of passes	1	–
SHX	Area per wing	2.3	m^2

Furthermore, the drag penalty caused by the radiator within the ram air duct is shown in Figure 14.4, with the maximum in-flight value calculated around 0.0006.

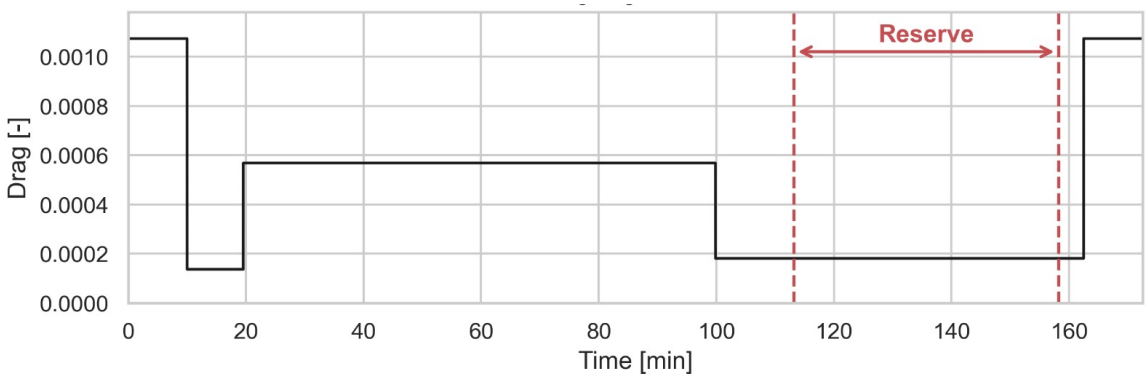

Figure 14.4: *C_D penalty flight profile caused by the ram air duct*

Moreover, Figure 14.5 presents the heat profile of the TMS, showing the amount of heat dissipated by each HEX during flight.

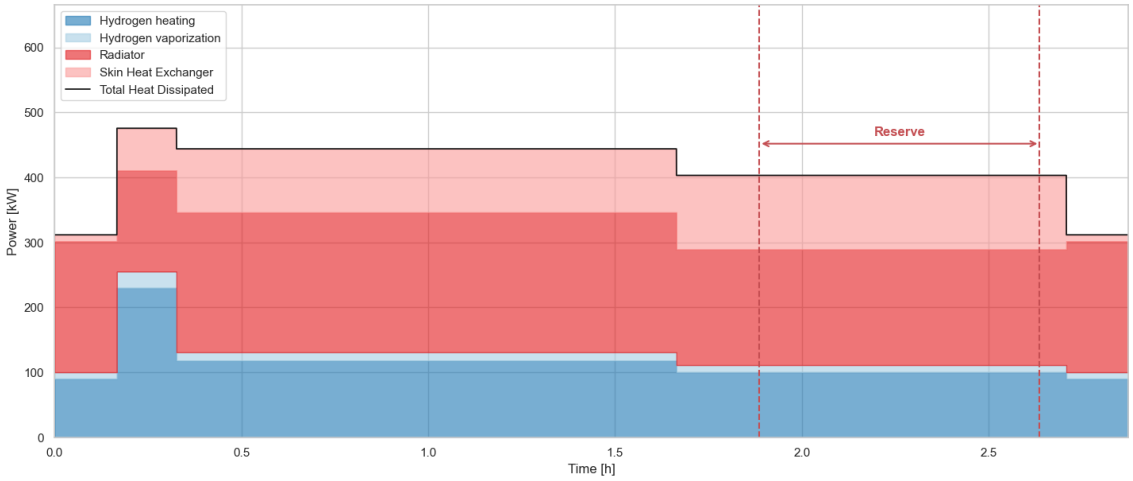

Figure 14.5: *Heat profile from TMS*

14.3.3. Storage Tank Final Design Characteristics

The storage tank is the component of the PT that facilitates the optimal condition of the hydrogen to be stored in the liquid state, at the desired temperature and pressure. For this reason, the tank has a multi-layer wall. It consists of an inner was, designed to sustain the inside pressure of the hydrogen, an insulation layer of MLI and vacuum, and an outer wall that acts as a protective layer against the environment. The inner and outer walls are made of S-glass fiber, while the MLI layer is made of stainless steel sheets with vacuum spacing.

Since the inner wall is the most loaded structurally, its thickness is 2 mm, while the outer wall has a thickness of 1 mm. Considering the heat influx through the wall of the tank, the vacuum gap has a thickness of 3 cm. The MLI has thickness of $3e-3$ cm.

Taking into account the spacing constraints of the fuselage, the tank is a cylinder with torispherical caps with the outer diameter of 1.542 m, and length of 2.52 m. This facilitates the transportation of 15 PAX. The total mass and volume of the storage tank may be seen in Table 14.1.

Lastly, the support structure used for the thermal analysis and the mass estimation of this tank is a scaled-up version of an existing design, with tapered members called 'flexures' connecting the inner and outer vessel around the circumference.

14.3.4. Electrical Power System Final Design Characteristics

The EPS consists of three main components, namely the actual ELMO, the current converter and the cabling. ELMO performs at a specific weight of 10 kW/kg and a temperature of 180°C. This performance translates into an efficiency of 97% projected to 2035.

Taking into account the converter, it has a specific power of 20 kW/kg and a volumetric power of 18700 kW/m^3, at a 99% efficiency estimate for 2035. On the other hand, the cables weight 0.0015 kg/kW/m. As a note, the cable system was doubled for redundancy. The total EPS sizing characteristics may be seen in Table 14.1.

15

System Interfaces & Interdependencies

This section defines the main SHTARWaRS component interfaces by means of a resource flow and Communication Flow Diagram (CommFD). These are accompanied by supplemental descriptions to identify and describe the anticipated interplay between components.

15.1. Resource Flow Diagram

It is pertinent to study the physical interfaces between the components. These interfaces guide the design possibilities and demonstrate the inputs and outputs of each component. A small discussion on every type of resource and its flow is now presented. The full resource flow diagram is provided in Figure 15.1 for a better visualization of the information presented below.

- Hot bleed air is taken directly from the compressor bleed air system in the PP and is treated with external cold air HEX to provide acclimatized, pressurized air for the cabin.
- If the propeller is feathered, the SHP provided by the PP is directed by the gearbox back to the ELMO. This converts it to electric energy to be stored in batteries. This process can be reversed to feed the ELMO and produce SHP.
- SHP are produced by the PP and the ELMO in normal operating conditions and are combined in the gearbox to provide power to the propeller.
- Coolant (warm & cold) exchanges between the FC, radiator, and HEX.
- Electric Power (EP) is produced by the FC and fed to the converter to change it to alternate current to feed the ELMO. Possibly EP could be directed directly to the batteries if the power is not needed. Additional EP could be stored in batteries to provide EP for the PP startup motor.
- Water is produced by both the PP and the FC and can be injected back into them if needed. Possibly, some of the water from the FC can be directed to the CC to decrease NO_x emissions.
- Air is taken from the environment by the PP and the FC compressor, in parallel. The compressed air is directed into the air HEX the then be delivered either to the cabin for cooling or to the FC to react.
- Hydrogen is delivered from the tanks, part of it acts as heat sink in the air HEX. Then the hydrogen is fed into hydrogen HEX, giving conditioned hydrogen for the FC and CC.

It is important to note here that not all components and connections are finalized. The next design considerations are going to shed light on the details of EPS and TMS. The diagram depicts a simplified, preliminary set-up of the resource flow and shows a limited level of detail.

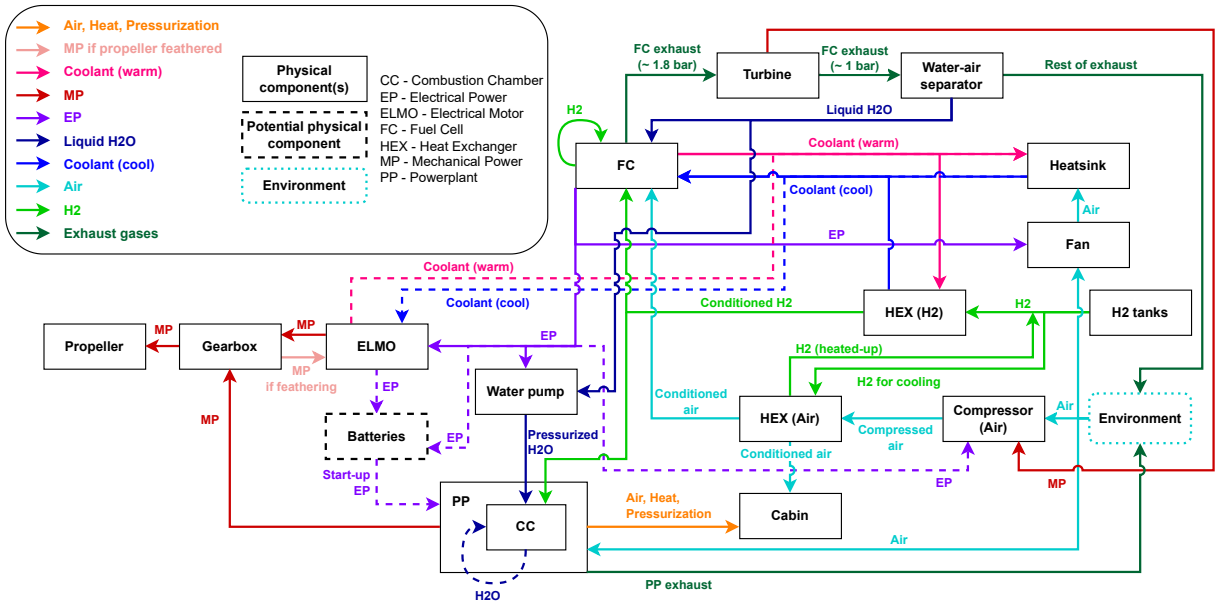

Figure 15.1: *Resource flow diagram*

15.2. Communication Flow

The SHTARWaRS PT is a complex system which includes multiple components in direct communication and providing feedback. The data flow between various interfaces of the aircraft can be visualized by means of a CommFD as demonstrated by Figure 15.2. The operational center is represented by the CDHS, which gathers feedback from the FC, PP, cooling system and hydrogen system, as well as manual input from the pilot. Commands are then provided to the propeller, ELMO, FC, PP, hydrogen system, as well as the fire prevention system as required.

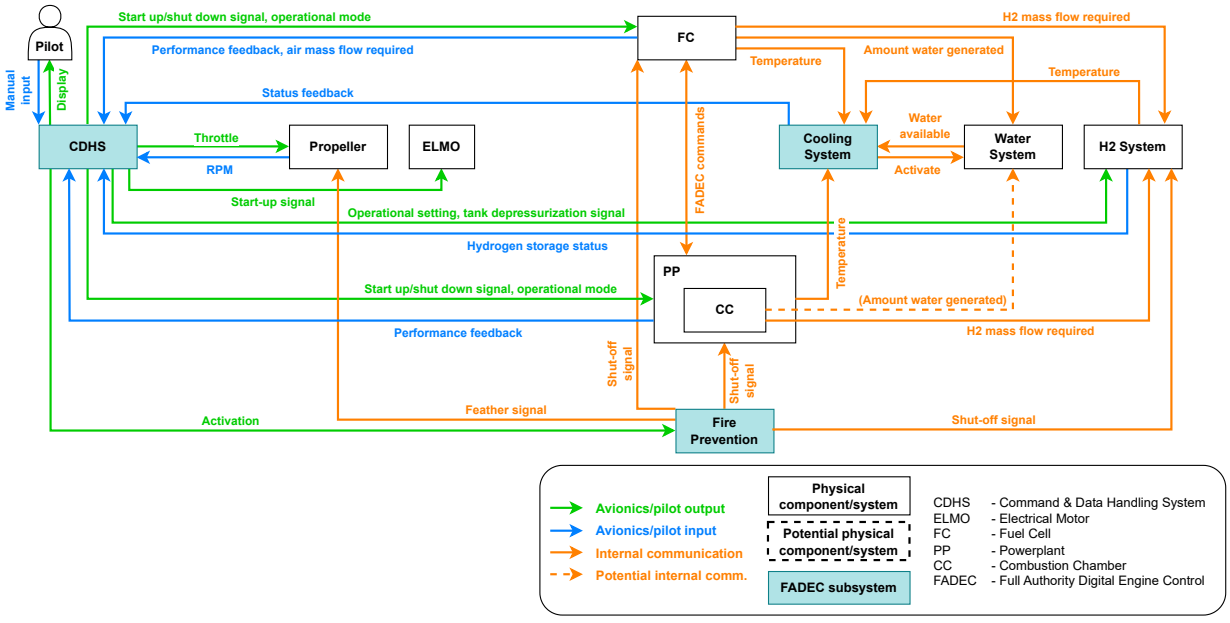

Figure 15.2: *Communication flow diagram*

FADEC is a system integrated in the PP and as such, it connects to the CC and FC as well as the CDHS. A subsequent triggering of the fire prevention system should feather the propeller, cut off the hydrogen supply, and shut down the affected CC or FC. The hydrogen system receives control signals from the FC and the CC as well as operational settings from the CDHS, while providing temperature readings to the TMS, and storage status back to CDHS. Similarly, the WRS registers how much water is generated by the CC and FC, and transmits the water level to the cooling system. The latter is also activating the WRS when more H_2O is required.

The FCs are started up or shut down by the CDHS, to which they provide performance feedback. Various data flows from the FC to other subsystems, like the required hydrogen mass flow, the amount of water generated, and the temperature. On the other side of the spectrum, the PP, including the CC, communicates with the FCs through FADEC commands, and feeds the temperature readings to the cooling system. The CC specifically provides a hydrogen requirement to the H_2 system, and an amount of water generated level to the WRS.

15.3. Electrical Block Diagram

The electrical block diagram in Figure 15.3 shows the connections between the different components of the EPS. There are two FCs that both go through a DC/DC boost converter to get to 2000 Volt. A small amount of power get siphoned away to the auxiliary systems. The remaining electricity is split over the two DC/AC inverters that provide 3-phase AC to the ELMO. If the FC system is unable to provide electricity for the aircraft, the ELMO can work as a generator, providing power to the auxiliary systems.

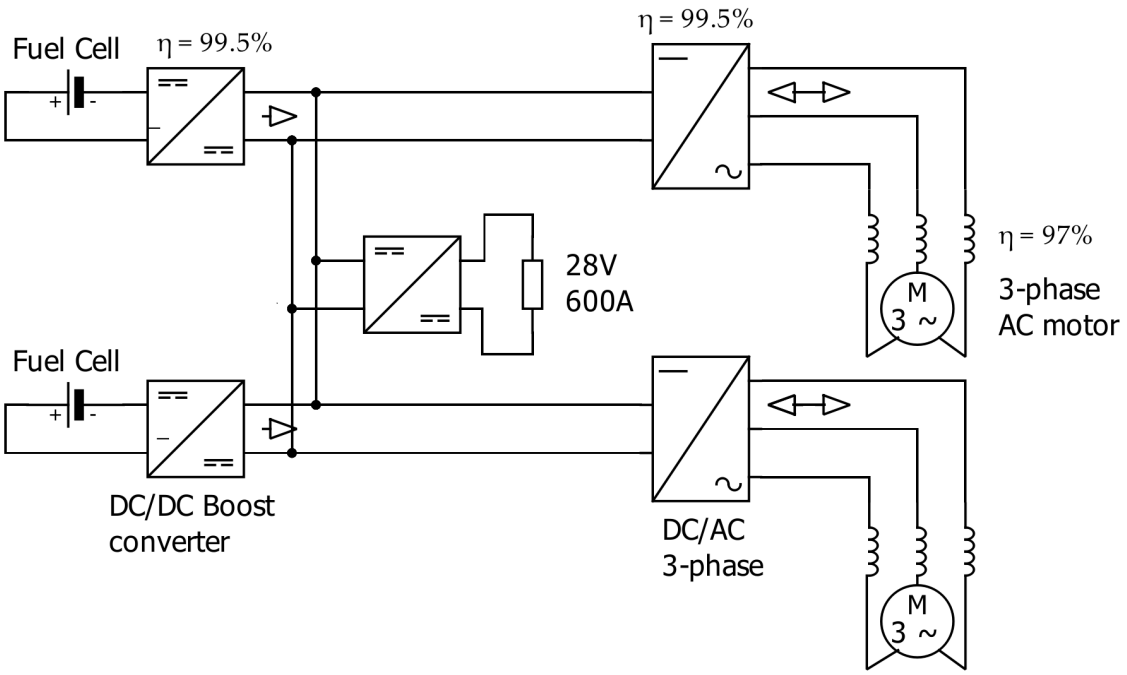

Figure 15.3: *Electrical diagram*

15.4. Data Handling

To get a general idea of the data flow between the different systems, a Data Handling Block Diagram was made and can be seen in Figure 15.4. It has the CDHS at its center because it receives all information and processes it to give every system the right commands. There is information received and transmitted to external parties. These are the Air traffic control and the ADS-B for traffic information.

Sensors in the aircraft also gather information that is used by the CDHS. These are displayed in the environment group. On the right of the picture are the systems. These provide monitoring data of themselves, which gets used by the CDHS to operate these systems. The Pilot gets information from the flight instruments, which in turn receives it from the CDHS. Some data flows also include an amount. The data transferred to and received from external sources is around 10kbit/s[94] for general aircraft. The Flight Data Recorder receives 3 kbit/s, and can save this for two hours, making the total storage 21.6Gbit[1]. For the other systems, no reference could be found, or the data flow is negligible. It is also not of paramount importance to get the exact data flow, as they do not influence the constraint of the SHTARWaRS PT design.

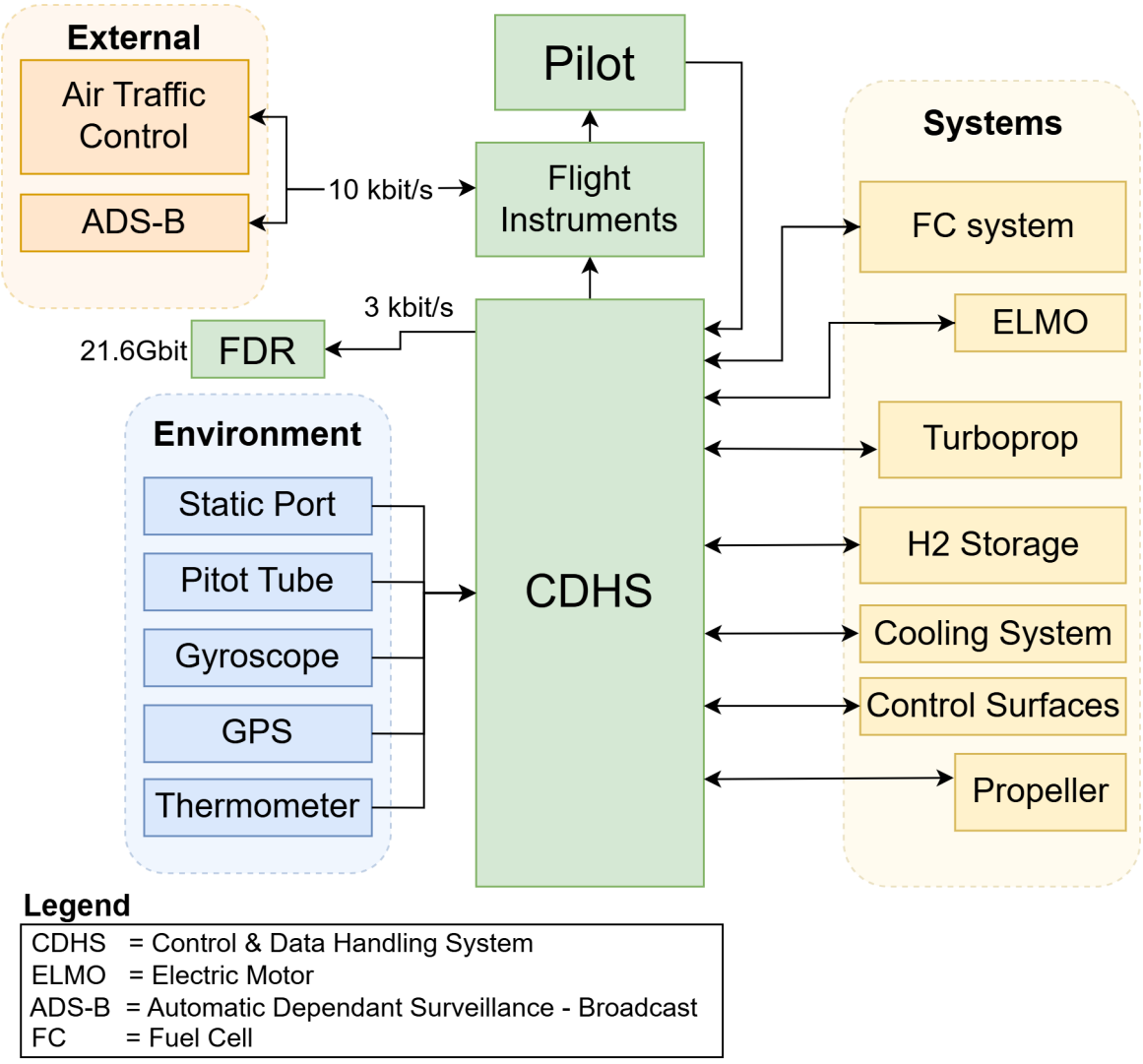

Figure 15.4: *Data handling block diagram*

[1] URL https://skybrary.aero/articles/flight-data-recorder-fdr [Cited 17 June 2025]

16

Impact of Retrofit on Aircraft Characteristics

This chapter describes how the entire retrofit influenced the characteristics of the aircraft. First, the aircraft systems are discussed in Section 16.1. The aerodynamic, structural and stability and controllability considerations are described in Section 16.2, Section 16.3 and Section 16.4, respectively.

16.1. Aircraft Systems Redesign

Every aircraft needs a multitude of systems to function. Here, selected aircraft systems are addressed in the context of the retrofit. The redesign of those system was out of scope for the SHTARWaRS project, however, the necessary changes are identified here.

Secondary Air System
The secondary air system has not changed considerably, as all the engine redesign has considered the 5% handling bleed needed to compress air to for the cabin. When the engine is not in use, air can be extracted from the FC feed line to be used for cabin air conditioning. If needed, further conditioning can be considered in the future by passing air through HEX.

Hydraulic System
Hydraulic system is significantly affected by the engine redesign. The hydraulic pump connected to the gas generator could be connected instead to the gearbox of the power turbine, that is, the same as the propellor, such that the ELMOs could power the system in the case the engines are off. This would indeed be necessary for all flight and ground conditions with only the FC working.

Oil System
Engine oil system would not be significantly affected as long as the connection to the gas generator shaft is maintained.

Auxiliary Power System
Although the Beechcraft 1900D does not have an AP unit by itself, electric system system is sustained by batteries, that are capable of powering the ELMO for the engine starter. A full redesign of the electric system is necessary.

16.2. Aerodynamic Considerations

The aerodynamic considerations of the aircraft were not considered during the design of the PT. However, the effect of the integration of the new TMS system on the performance of the aircraft was investigated. Here, the Ram Air HEX integration, displayed in Figure 12.1, leads to an increase in drag. As explained in Chapter 13, the CDT feeds this updated value into a new iteration of the model, until the MTOW converges. The mitigation of this adaption is, however, not limited to an iteration of the design, but also to the minimization of radiator area in the TMS tool. Here, the conditioning of the FC and H_2 is performed with every other component first and, if necessary, the radiator is added to the system. This design philosophy minimizes the radiator area, and thus, mitigates the effect of the Ram Air HEX on the aircraft performance.

16.3. Structural Considerations

The integration of the PT on the aircraft and the design of the systems themselves poses several structural challenges. The converged H_2 storage design defined in Chapter 11 is able to withstand the operating conditions of LH_2 which pose both thermal and structural loads on the wall of the tank. The analysis of the tank is, however, not limited to analytical methods, and was also investigated through a simplified Finite Elements Method (FEM) case to test both the pressurization and hydrostatic loads in Chapter 20. Further analysis is recommended to test permeation, and crash scenarios for certification.

The integration of the FC, piping system and redesigned turboprop would force adaptations to the wing. However, given that only the CC was replaced, and the wing loading does not substantially increase, a redesign is not required. A more detailed explanation is given in Chapter 13.

Lastly, the inclusion of the tank in the rear of the plane would cause safety issues to the PAX on the cabin. Thus, the support structure presented in Chapter 11, and a firewall separating the cabin and the H_2 storage bay are included. The support structure, as explained before, has been analyzed previously so no further analysis is required [67].

16.4. Stability & Controllability Considerations

The CG range of H_2D_2 is determined using the method described in Figure 13.2 using the data provided in Chapter 14. A loading diagram is generated as seen in Figure 16.1 - it visualizes the shift of the CG as the aircraft is loaded with cargo, PAX and fuel, consecutively. As there is only one cargo compartment in the aircraft and one fuel tank, the diagram only contains two different CG locations - before and after loading. The PAX, however, are loaded row-by-row and can either be loaded started from the front of the airplane or from the back. That is why the diagram shows two separate lines of CG shift, to take that into account. The resultant CG range varies from 7.03 to 7.32 m w.r.t. the nose of the aircraft.

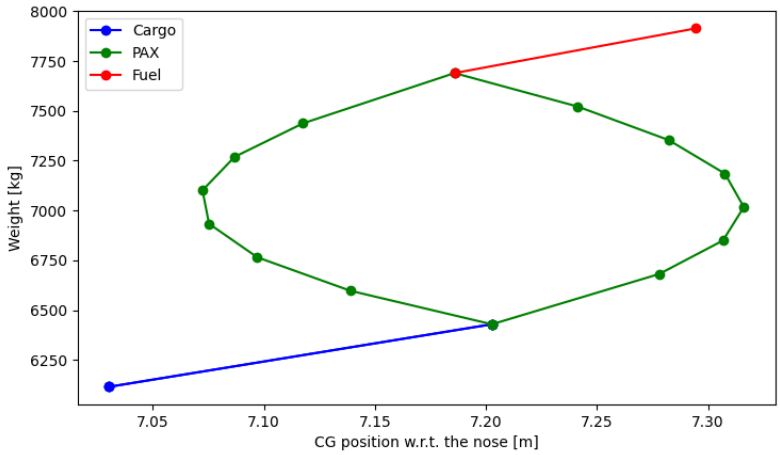

Figure 16.1: *H_2D_2 loading diagram*

16.5. Material Considerations

The scope of SHTARWaRS is limited to the design of the PT. Given the technology projection of most of the components, the only system were materials were considered was the H_2 storage. Here, several materials were traded-off in Section 7.4, where the final material and its properties are presented.

All those considerations were analyzed in order to ensure feasibility of the retrofit. It can be inferred from this that the changes made to the PT of the Beechcraft 1900D will impact the operation of the aircraft in a controlled way which can be adjusted for.

17

Sustainability of Final Design

As outlined in the sustainability development strategy in Section 6.3, the sustainability of the final design will be determined to ensure it meets its requirements and compared to competing aircraft. The sustainability is simplified to only consider the climate forcing of the aircraft, measured in the GWP of the lifetime of the aircraft over a 100-year time horizon. First, a breakdown of the different contributions to the climate forcing by different systems are described. Subsequently, the sustainability is compared to a preliminary estimate of the GWP of the Beechcraft 1900D today, and in future with the use of SAF.

The GWP of H_2D_2 can be examined by splitting the aircraft lifetime into two segments: use and production/disposal. This split was chosen to ease analysis, as previously performed LCAs of systems could be analyzed, ignoring their use. Separately, the climate impact of H_2D_2 during use could be determined by the necessary fuels and emissions it produces during its lifetime. The GWP of the aircraft during use is analyzed by determining the exhausts of the aircraft over all of its flight missions, as well as determining the GWP of the production of its fuel. The rest of the aircraft's lifetime, including production, disposal and maintenance are all determined separately by researching previously performed LCAs of the aircraft's systems.

The emissions during aircraft use stem from three mechanisms: the production and emission of NO_x and water during flight, and the impact of the production of hydrogen. The forcing of each of these is determined by multiplying the masses of each fluid produced or used over a flight by their GWP over a 100-year time horizon and finally adjusting for the functional unit, Available Seat Kilometer (ASK). The masses are determined by analyzing an example flight profile, as determined in Subsection 13.1.2. Table 17.1 outlines for each fluid the mass produced over a flight profile, its GWP and its contribution to the aircraft's climate forcing.

Table 17.1: *Climate forcing analysis of H_2D_2 use*

Fluid	**Mass [kg/flight]**	**GWP [kg$CO_{2,eq}$/kg]**	**Climate Forcing [g$CO_{2,eq}$/ASK]**
Hydrogen Production	154	2 [95]	29.33
Water Emissions	1376	0.06 [1]	0.0655
NO_x Emissions	0.00111	59 [96]	0.00106

The production of hydrogen is evidently the largest contributor to global warming for H_2D_2's use. This is due to the high use of hydrogen and it's non-negligible GWP. The GWP of hydrogen is calculated as an optimistic estimate for the emissions from the production, storage and transport of green hydrogen. For this, large-scale electrolysis fueled by wind power was assumed. Although the emissions of water are large, its climate impact is small due to its short lifetime in the atmosphere. As NO_x emissions are small, its climate forcing is also negligible. Contrails are assumed negligible, as although FCs produce contrails in more flight regimes than traditional aircraft, their climate impact is far smaller than traditional aircraft, as they are thinner and less persistent [97]. The low cruising altitude of H_2D_2 also minimizes the production of contrails[98]. Additionally, the NO_x emissions fall far below the 25 ppm limit at all stages of flight.

The production and disposal of the aircraft is determined by analyzing climate impact of the unmodified Beechcraft 1900D and each of the systems it will be retrofitted with. Table 17.2 highlights these effects. The total CO_2-equivalent emissions are determined and displayed per functional unit for an aircraft lifespan of 20 years with 920 flights per year.

Table 17.2: *Climate forcing analysis of H_2D_2 production and disposal*

System	Climate Forcing [$gCO_{2,eq}$/lifetime]	Climate Forcing [$gCO_{2,eq}$/ASK]
Beechcraft 1900D	528947 [99]	2.738
FC & TMS	91181 [58]	0.472
EPS	2738 [1] [2]	0.0142
Storage	1594 [100]	0.00825

Here, the production of the airframe and the FCs dominate the climate impact. This is due to the large amounts of metal in the airframe and the use of platinum in the FCs. The total climate forcing is **41.9 $gCO_{2,eq}$/ASK**. The breakdown of the different contributions is shown in Figure 17.1.

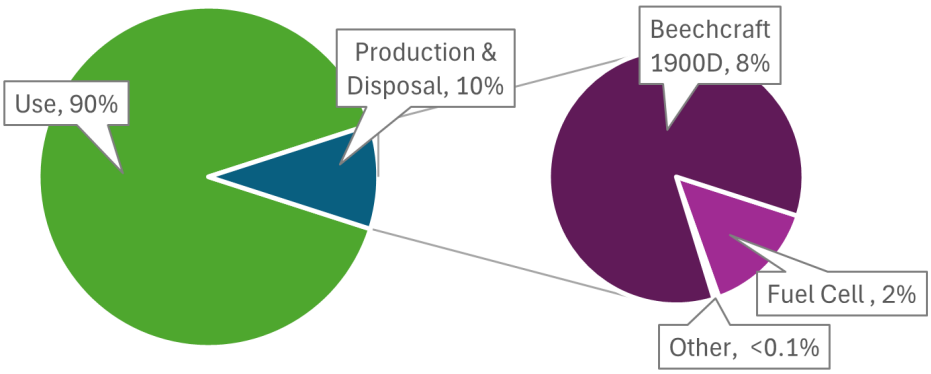

Figure 17.1: *Proportion of contribution to climate forcing of each system*

The climate effect of H_2D_2 can now be compared with the original Beechcraft 1900D, using both traditionally sourced kerosene and SAF. A first-order estimate of the climate forcing of the Beechcraft 1900D was performed by analyzing its estimated carbon dioxide emissions over its lifetime and adding the estimated climate forcing due to production. The fuel used by the Beechcraft 1900D emits 155 $gCO_{2,eq}$/ASK over its lifetime [101]. Thus, **H_2D_2 is four times more sustainable than the current Beechcraft 1900D**. However, utilizing optimistic projections for SAF emissions improves the Beechcraft 1900D's sustainability to 57 $gCO_{2,eq}$/ASK when using SAF [2, 102], which is still worse than the climate forcing of H_2D_2. Other environmental factors of SAF also reveal high land use for production, worsening the case for this decision. A quick economic analysis of utilizing SAF also reveals a fuel cost of €42 per PAX per flight[102], as opposed to the €41 per PAX per flight of H_2D_2. However, taking the development costs into account, the cost of operation per ASK is 29% lower per PAX than H_2D_2's, which is mainly influenced by the difference in seat capacity of the aircraft. With all this taken into consideration, H_2D_2 is more sustainable than it's immediate fossil-fueled counterpart, while operating at a higher cost which may be counteracted via carbon taxes.

18

Sensitivity Analysis

The design and performance of H_2D_2 may vary greatly as hydrogen technology develops over the next decade. The development of FCs and the cost and sustainability of hydrogen are critical in the choice of a design point and the performance of the aircraft. For the purposes of this sensitivity analysis, the sustainability of hydrogen production and the sensitivity to the development progress of HT-PEMFCs will be considered. For the former, its projections are highly varying, and improvements in this may shift the design space greatly. The latter analysis will examine the effects of not reaching development projections of HT-PEMFCs by 2035, analyzing both specific power and efficiency. This analysis does not impact the final design of H_2D_2, but serves instead as a tool to see how changes in the development of hydrogen technologies could impact the design.

18.1. Hydrogen Global Warmin Potential Sensitivity Analysis

The production of green or pink hydrogen through electrolysis significantly improves the effect of hydrogen production on the climate. In some cases, the production may even result in a negative GWP according to Patel et al. [103]. With storage and distribution considered, it is reasonable to estimate that the GWP of hydrogen production may drastically reduce by 2035 [103]. For this sensitivity analysis, the GWP of hydrogen production was set to 0.2 $kgCO_{2,eq}$/kg, ten times lower than the initial estimate. Since most emissions of each design point stem from hydrogen production, this change significantly changes the design space, which is shown in Figure 18.1.

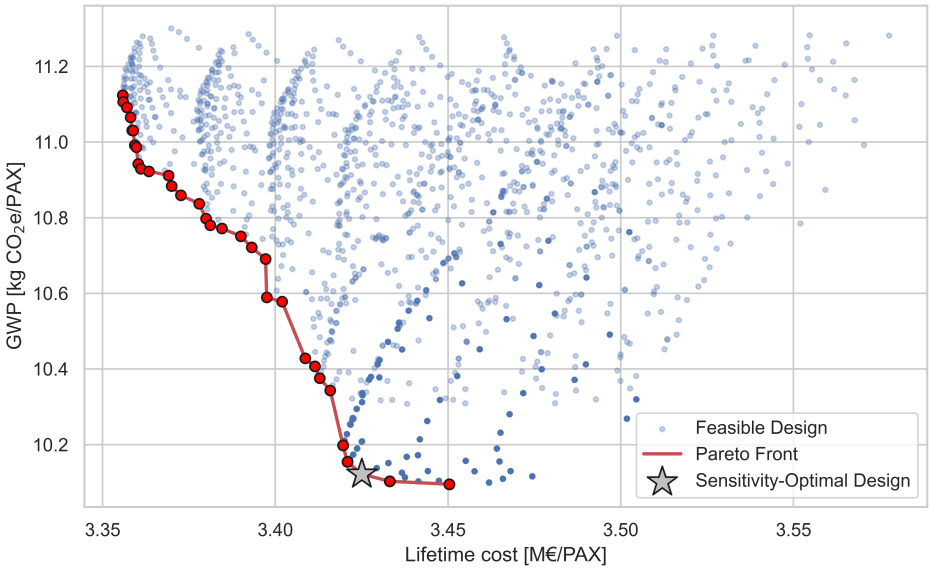

Figure 18.1: *H_2-sensitivity adjusted design space with Pareto front*

As expected, the cost for each design point remains the same, but the sustainability drastically reduces to the order of 14.3 $gCO_{2,eq}$/ASK, which is over five times better than before the change. Additionally, the shape of the pareto front is drastically different, and a clear optimal region in the bottom right is defined, with a lifetime cost of €3.42 million per PAX and a GWP of 10.1 $kgCO_{2,eq}$ per PAX per flight. For comparison, the chosen design for H_2D_2 costs €3.44 million per PAX and emits 29.29 $kgCO_{2,eq}$ per PAX per flight

This point of analysis is quite similar to the real design point, with 30% of take-off power supplied, with the FC TOGA throttle set to 35%. The design parameters are presented in Table 18.1. At cruise, the FC still provides all of the aircraft's maximum continuous power. This design has a slightly smaller FC, operating at a slightly lower efficiency at cruise.

Table 18.1: *Comparison of H_2D_2 and concept with very sustainable hydrogen production*

Design Point	MTOW	FC Mass	Hydrogen Mass	TMS Mass	Storage Mass	Storage Volume
H_2D_2	7911 kg	563 kg	160 kg + 64 kg reserve	275 kg	252 kg	4.49 m^3
H_2-sensitive design	7791 kg	431 kg	162 kg + 65 kg reserve	285 kg	254 kg	4.55 m^3

With this change, the design has a ≈1% cheaper lifetime cost than H_2D_2 and has three times smaller climate impact than H_2D_2. Figure 18.2 displays the contributors to the GWP of the H_2-sensitive design. As expected, the contribution of hydrogen production to the optimal design shrinks significantly. As the design remains largely unchanged, the other contributors to the aircraft's climate forcing remain the same, but form a larger proportion of the design's total.

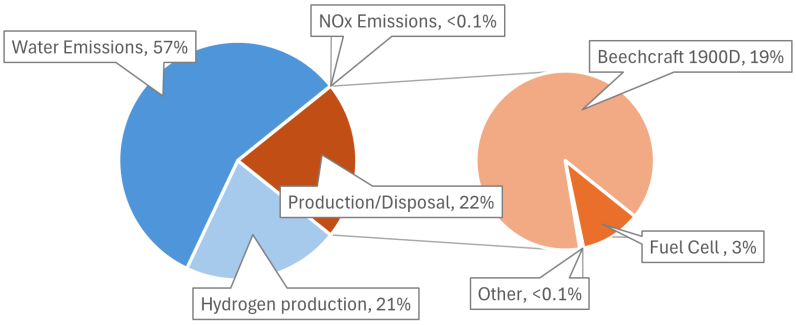

Figure 18.2: *Sustainability pie chart of design result from sensitivity analysis*

18.2. Fuel Cell Specific Power Sensitivity Analysis

One major assumption made throughout the report was the projection of technological development to 2035. This included the development of HT-PEMFCs, which are currently not mature enough for use in aviation. In this section, the design will be analyzed in the case which the power density of HT-PEMFCs does not develop as expected. Section 18.3 describes the impact of lower efficiency. Both sections do not change the final design, but aim to describe scenarios in which FC technologies do not develop as quickly as expected.

Between 2030 and 2035 the power density of HT-PEMFCs is expected to rise from 3 kW/kg to 5 kW/kg[49]. This is a significant improvement in a very short time period. For this analysis, the design space will be compiled assuming that this rise does not occur, and the power density of HT-PEMFCs is 3 kW/kg in 2035. This will not impact the FC efficiency, but is expected to drastically increase the FC size and volume, which may lead to a more restricted design space and larger hydrogen use due to the greater mass. Figure 18.3 displays the adjusted design space.

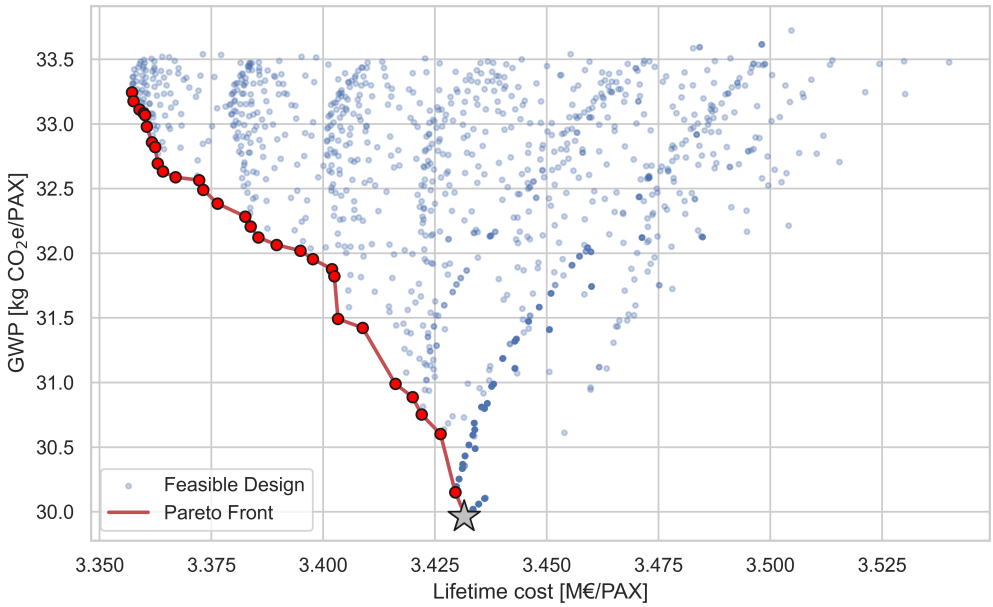

Figure 18.3: *FC power density sensitivity adjusted design space with Pareto front*

As expected, the many more design options were pruned as 79.84% of the design space was deemed infeasible (as opposed to the 67.66% originally. Included in this pruning is the original design point, as its FC mass is too large. The optimal design in the conceptual design space nonetheless operates similarly to the chosen design. The FC still provides the entire power during cruise, and the gas turbine only assists during take-off and climb. The take-off power split is very similar to the chosen design, at 0.3, but the FC throttles are increased to 0.4 at TOGA and 0.45 at cruise to limit the FC size increase. This decreases the operational efficiency, increasing the hydrogen use and GWP. The changes in system masses are shown in Table 18.2.

Table 18.2: *Comparison of H_2D_2 and concept with low FC power density*

Design Point	MTOW	FC Mass	Hydrogen Mass	TMS Mass	Storage Mass	Storage Volume
H_2D_2	7911 kg	563 kg	160 kg + 64 kg reserve	275 kg	252 kg	4.49 m^3
FC power density sensitive design	8010 kg	634 kg	165 kg + 65 kg reserve	296 kg	256 kg	4.64 m^3

The decrease in FC efficiency increases the heat produced by the FC and the hydrogen required for the same power. This change increases the size of the storage and TMS systems. However, the cost and sustainability of the sensitivity design point are similar to the chosen design, being less than 1% cheaper but emits slightly more than 2% more $CO_{2,eq}$ than the chosen design. Thus, the design is not significantly sensitive to the power density of the FC for the change assumed. This is somewhat surprising, as the FC power density was chosen as the most important tradeoff criterion for the FC tradeoff in Chapter 7. As the FC power density does not largely affect other systems, this parameter does not largely effect the entire design when remaining within reasonable values. It is estimated that if the power density is lowered far below what is expected of its technological development, implementing them as the main power source during cruise may not be viable. For the scope of this sensitivity analysis, however, this was not the case.

18.3. Fuel Cell Efficiency Sensitivity Analysis

The FC efficiency has a large impact on the systems surrounding it. Lower efficiency means more heat production and more hydrogen required, increasing TMS and hydrogen storage mass, respectively. In this analysis, the projected peak stack efficiency of 0.7 is reduced to 0.6, by reducing the power-efficiency curve by 14%. This results in the design space shown in Figure 18.4.

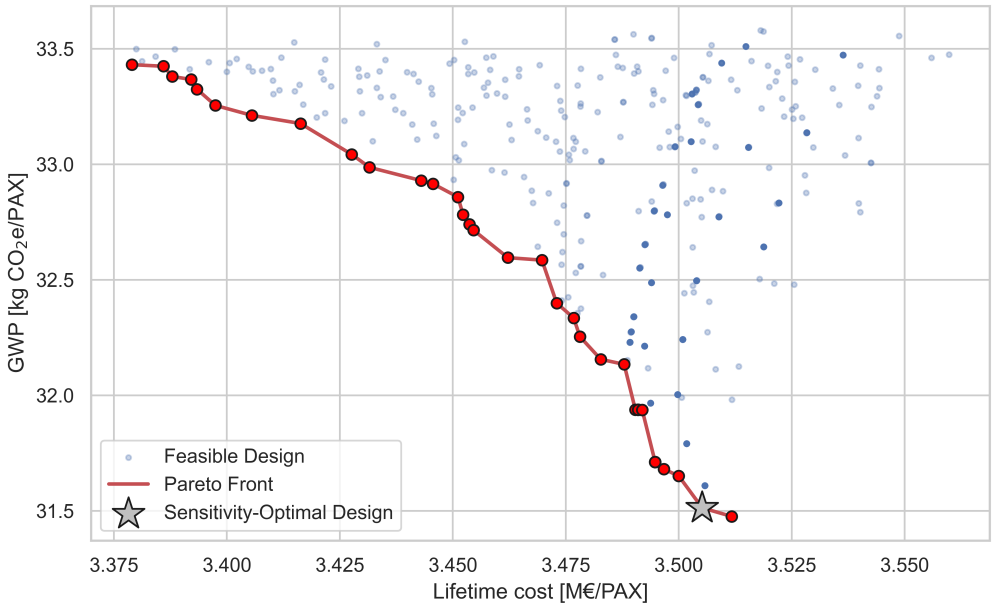

Figure 18.4: *Comparison of H_2D_2 and concept with low FC efficiency*

Out of the entire design space, 89.54% were deemed infeasible, due to the increased demand from the storage and TMS. The remaining points are more expensive and less sustainable than the chosen design. If FC efficiencies would not develop as projected, the design point would thus accordingly change. In this scenario, the optimal FC power split is 25%, with TOGA and cruise throttle set to 25% and 30%, respectively. This is also sufficient to provide the entire power during cruise with the FC. To compensate for the lower overall efficiency, the throttle is lowered compared to the chosen design in order to retrieve some lost efficiency. With this scenario in place. the design is 2% more expensive over its lifetime and is responsible for 7.5% more climate forcing than H_2D_2. The system sizes for this scenario are compared to H_2D_2 in Table 18.3.

Table 18.3: *Comparison of h2d2 and concept with low FC efficiency*

Design Point	MTOW	Fuel Cell Mass	Hydrogen Mass	TMS Mass	Storage Mass	Storage Volume
H_2D_2	7911 kg	563 kg	160 kg + 64 kg reserve	275 kg	252 kg	4.49 m^3
FC efficiency sensitive design	7988 kg	549 kg	170 kg + 70 kg reserve	350 kg	270 kg	4.92 m^3

The design is more sensitive to changes in FC efficiency than power density, but within the range of projections, either change does not massively change the flight profile, though individual systems (such as TMS) do see significant changes. In each scenario changing the FC parameters, the conclusion for selecting a final design where the FC provides the entire aircraft power during cruise remains the same.

18.4. Sensitivity Analysis Conclusions & Recommendations

The various sensitivity analyses provided different designs with different characteristics, but all shared one major conclusion: it is optimal to provide the entire aircraft power by the FC during cruise. This was the case when analyzing a positive change in the GWP of hydrogen production and negative changes in FC developments. Thus, although the design is sensitive to changing various parameters, the overall flight profile and design philosophy remains the same. This sensitivity analysis only analyzes three cases where parameters change. It is recommended to expand this analysis to other systems which have technological development projections to 2035, such as the hydrogen storage, and complex systems whose design may vary greatly when the detail is increased, such as the TMS. Additionally, it is recommended to analyze the effect of changing multiple parameters at once, such as FC efficiency and power density at the same time. This was not done in this report due to the computational requirements to run such an analysis and the limited time in this project between compiling the final design and the submission of this report.

19

Operations & Logistics Concept

The integration of hydrogen-based propulsion systems introduces a significant transformation in the way aircraft are operated, maintained, and supported throughout their life cycle. This chapter presents the operational and logistic concept description in Section 19.1 and the Reliability, Availability, Maintainability & Safety (RAMS) considerations in Section 19.2.

19.1. Operational & Logistic Concept Description

The operations and logistics for the SHTARWaRS aircraft are similar in some areas compared to a conventional aircraft, but having hydrogen technologies onboard causes some substantial changes.

The operational changes concerning the pilot depend on the flight phase and concern mostly the activation of FC and the gas generator at relevant times. At TOGA, the FCs will be at maximum power and the PP will provide the extra power needed for TOGA. This is done to reduce NO_x emissions near airports. Then, the pilot will need to know how to switch to FC power during landing, and maneuvers leading up to landing. The rest of the flight profile will not change significantly relative to the original Beechcraft 1900D, as the stability and performance characteristics stay similar.

During GO, a few specific alterations have to be made to the operation of the aircraft. After taxiing, the power can be shut off by stopping the hydrogen flow. The HT-PEMFC have a start-up time of less than a minute. Hydrogen flow subsequently only needs to be turned on just before power is required from the FC. Between the flights, the time that the tank stays dormant must be tracked to ensure timely venting. Due to the state that the hydrogen is in, special trucks are needed that can transport the LH_2 to the aircraft. Specially trained personnel is required for the handling of the hydrogen while refueling. As LH_2 is stored at temperatures around 20 K, it can be dangerous to work with, without the proper knowledge. Mechanics trained in hydrogen FC and storage are required as well. Proper maintenance is vital for the safety of all aircraft systems, especially for those which deal with hydrogen.

Another aspect that ought to be looked at for logistics, is the sourcing of hydrogen. There are many ways of producing hydrogen, but for this project only green or pink hydrogen will be permitted. As the other options produce carbon emissions, which would go against the goal of SHTARWaRS being carbon-neutral. Green hydrogen is obtained using renewable energy produced by solar panels or wind turbines for water hydrolysis. It represents a way to create fuel for hydrogen vehicles, and to take the load off an overloaded power network. Pink hydrogen is alternatively obtained using nuclear energy for water hydrolysis, thus also representing a carbon-free method of hydrogen production.

The projected lifetime of an airplane of this category is around 20 years. After reaching its End Of Life (EOL), the aircraft will be scrapped, since it has reached the limit of its certification.

19.2. Reliability, Availability, Maintainability, & Safety

The RAMS are key aspects of the H_2D_2. Their characteristics will be described to get a better idea of how dependable the aircraft is. Reliability influences the other aspects the most, and will be studied first. The components of the PT will be looked at here, as that is what will be altered from the original Beechcraft. These components are shown in Figure 19.1 for one side of the aircraft (duplicated for the other side), and the failure rate of each of these components can be seen in Figure 19.1.

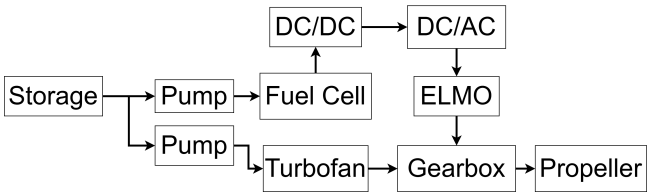

Figure 19.1: *Reliability block diagram for one side of the aircraft*

Component	Failure Rate/h	Reliability
Storage	8.65×10^{-8}	0.99999991
Pump	1.49×10^{-6}	0.999998
FC	8.43×10^{-6}	0.999992
Turbofan	3.00×10^{-6}	0.999997
Inverter	7.06×10^{-6}	0.999993
ELMO	4.53×10^{-6}	0.999995
Gearbox	5.26×10^{-7}	0.9999995

Table 19.1: *Component failure rates and reliabilities [104]*

Reliability

The reliability of the turbofan comes from the fact that only three engines have failed in 1,000,000 flight hours, and the FC has a failure rate of 8.43×10^{-6} per hour [105]. From the Reliability Block Diagram, seen in Figure 19.1, the total reliability of the whole system can be analyzed with the information provided in Figure 19.1. If one of the visualized systems fails, the propeller will not receive all its power anymore. That is why all their reliabilities, from the pump and onward, are multiplied to get a total reliability of one half of the PT. This equals 0.999966, or one failure in $\approx 30,000$ hours. As the aircraft can fly with only one engine operational, the reliability increases by using Equation 19.1 to determine reliabilities in parallel.

$$R_{tot} = 1 - (1 - R_1) \cdot (1 - R_2) \tag{19.1}$$

This gives a reliability of 0.9999999988. It additionally needs to be multiplied with the reliability of the storage tank, as this one is in series with both sides of the PT. This results in a reliability of 0.999999901 and a failure rate of 9.1×10^{-8} per hour for the H_2D_2 PT. This failure rate means that dual engine failure would only occur 1 in 11 million flight hours, which is enough to certify the aircraft [106].

Maintainability

From the reliability, we move on to the maintainability. Preventive maintenance will be mostly performed. Any system failure is extremely undesirable, also when not resulting in a crash. That is why periodic maintenance and inspection will be performed on the PT. The PT6A engine family requires inspection every 100 flight hours. At 1,800 flight hours a detailed inspection of the hot end needs to be performed and at 3,600, the engine gets overhauled[1]. Every flight also has basic checks before take-off. The FC has a lifetime of 15,000 hours. Like the other parts, it still requires maintenance, which mostly consists of changing out filters. Considerably less maintenance is required than for the turbine. As the failure of the hydrogen storage can have extreme consequences, it is essential to perform structural health monitoring on the tank through regular inspection and non-destructive testing. Some examples of those techniques include acoustic emission monitoring, ultrasonic testing and vibration-based monitoring.

Availability

The availability depends on both the reliability, and maintainability, as it describes the probability of the system being operational. Operational availability is the specific term that will be looked at, as it describes the time the H_2D_2 will function satisfactory in an actual operational environment. The effect of the reliability is apparent, as if a component fails, the aircraft will be out of commission until it is fixed. The scheduled maintenance and inspection also takes time to perform, and will keep the H_2D_2 grounded. Delays are also counted in the operational availability.

Safety

That brings us to the last letter of RAMS, safety. Safety can be defined as the freedom from hazards to humans and equipment. The concept of safety has already mostly been handled in Section 6.1, as the risks

[1] URL `https://bfgaero.com/2024/10/07/comprehensive-maintenance-checklist-for-pt6a-engines/` [Cited 17 June 2025]

are a hazard, and the contingencies and mitigation increase the safety of the H_2D_2. The most important risks to safety have been listed below.

- **R.H2.TE.1**: The hydrogen storage leaks excessively.
- **R.H2.TE.4**: The storage is damaged by an external factor.
- **R.H2.TE.6**: The temperature/pressure is not regulated in the storage tank.
- **R.PT.TE.3**: Foreign object ingested into the PP.

It is evident from these risks that the main concern for safety comes from the hydrogen storage. This is because failures in this component themselves can already cause significant damage to the aircraft, as hydrogen is very volatile. And as discussed in the reliability part, there is only one storage system, and when it fails, everything that requires hydrogen also stops working. To ensure safety, a Technical Risk Assessment (TRA) was performed and the risks were mitigated, all described earlier in Subsection 6.1.2 and Subsection 6.1.3.

20

Project Design and Development Logic

20.1. Future Project Design & Development Logic

The design determined in this report represents the final design of H_2D_2 during the DSE. This section aims to describe the limitations of the project, as well as the next steps necessary for the refinement and production of the H_2D_2 system for the completion of the SHTARWaRS project. The limitations encountered during the design are introduced to clarify the sources of remaining uncertainties. A schematic of the project design and development plan is presented in this section as well, detailing the major life cycle phases as well as a detailed manufacturing plan.

20.1.1. Design Development Past the DSE

Nearing the end of this 10-week study, the PT architecture has been designed, and many details about the design have been defined. However, SHTARWaRS is not ready to be implemented in an aircraft immediately. This section aims to describe the process which would be required after the DSE to fulfill the ultimate aim of SHTARWaRS and produce a marketable, sustainable aircraft.

There are two main areas that this project has not treated: the design of components whose performance was projected to 2035, and the design of components and systems which are not related to the PT. Components whose performance is currently not good enough to be used in aviation and whose expected performance in 2035 was used for design will have major developmental changes as time progresses. To ensure that the SHTARWaRS design remains relevant, these changes should be tracked, and the design updated accordingly. Once technological advances meet the expectations outlined here, the design of each affected (sub)system can be explored in much more detail.

FC technology and hydrogen storage technologies are projected to develop rapidly through the next decade, so special attention should be given to these systems. Both of these, together with the TMS will require transient analysis, as compared to the simplified models in this report, so that behaviors such as FC ramp-up or tank pressurization during refueling can be investigated.

In addition, the design of the turboprop was not precisely examined in this report. Further research should go into the design of an efficient and reliable hydrogen-fueled turboprop. Namely, an analysis of the CC, in a higher order, where turbulence is considered, would produce more accurate results for the exhaust composition. Once the updated tools are verified, a final design is deemed feasible, and the company is built, the team will be able to move towards the development of the individual components.

Designing the full integration of the PT into the aircraft is also outside the scope of this project, as changes to the aircraft structure, landing gear and other systems will likely be required, but not treated here. These systems should be analyzed and adapted to meet certification standards. Components or subassemblies developed in-house will also have to be validated by an external party, and a production quality assurance must be set up. Once these adaptations have been adopted, further development can be made to ensure that the entire assembly complies with CS-23 regulations so that an airworthy model can be built, and large-scale production can be planned and then ultimately conducted.

After this, the team will ensure the supply chain of spare parts, and certify MRO providers, with the purpose of ensuring an ongoing maintenance service during operation. Lastly, the condition of the aircraft will be tracked, and evaluations of maintenance costs, or the operational needs of the company will be completed to assess on the retirement timing. Once decommissioning takes place, the removal, and disposal of parts and systems will be driven by the reduce of waste and reuse of usable parts. Once decommission is complete, a full report will document all relevant information for the authorities, investors, and other stakeholders.

These steps are detailed in the *P*&*DD* diagram below, where several conditional statements determine possible outcomes, such as technology developing, unfeasible designs, or the unavailability of components, to mitigate risk and provide alternative routes. (Sub)tasks are positioned chronologically from top to down, with parallel/series tasks stemming from prior ones. The main life cycle phases (Design, Manufacturing, Assembly, Integration & Testing (AIT), Operations, and EOL) are explicitly defined and encompass the main tasks allocated on the left side of the diagram. Operational tasks are also present, to ensure smooth transitions between the *R*&*D*, manufacturing and AIT phases among others. To ensure a satisfactory decommission and deregistration of H_2D_2, the team will provide all required documentation in a timely manner, to minimize the effect on the company and the affected stakeholders.

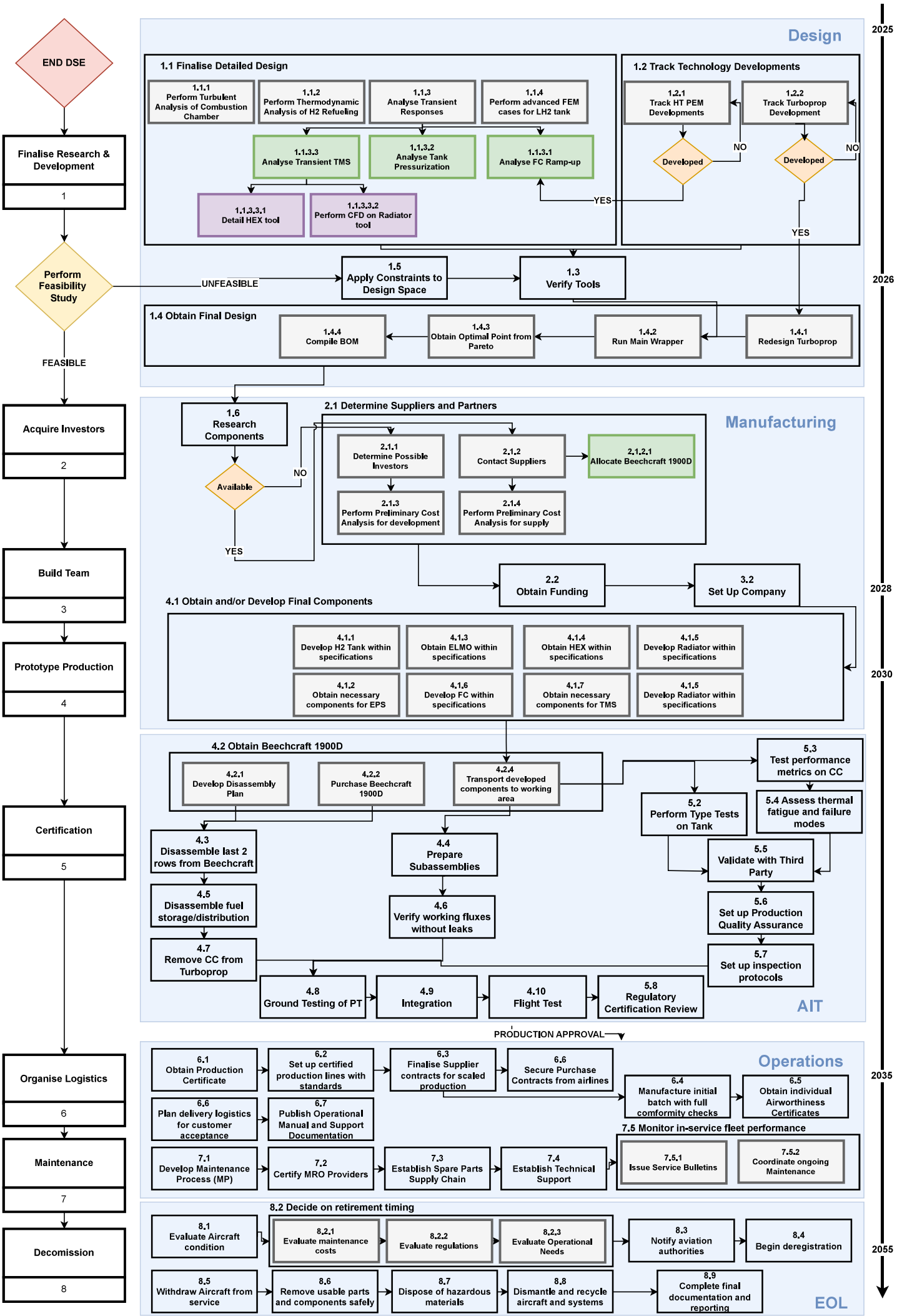
END DSE
Finalise Research & Development
1
Perform Feasibility Study
UNFEASIBLE
FEASIBLE
Acquire Investors
2
Build Team
3
Prototype Production
4
Certification
5
Organise Logistics
6
Maintenance
7
Decomission
8
2025
2026
2028
2030
2035
2055
Design
1.1 Finalise Detailed Design
1.1.1 Perform Turbulent Analysis of Combustion Chamber
1.1.2 Perform Thermodynamic Analysis of H2 Refueling
1.1.3 Analyse Transient Responses
1.1.4 Perform advanced FEM cases for LH2 tank
1.1.3.3 Analyse Transient TMS
1.1.3.2 Analyse Tank Pressurization
1.1.3.1 Analyse FC Ramp-up
1.1.3.3.1 Detail HEX tool
1.1.3.3.2 Perform CFD on Radiator tool
YES
1.2 Track Technology Developments
1.2.1 Track HT PEM Developments
1.2.2 Track Turboprop Development
Developed
NO
Developed
NO
YES
1.5 Apply Constraints to Design Space
1.3 Verify Tools
1.4 Obtain Final Design
1.4.4 Compile BOM
1.4.3 Obtain Optimal Point from Pareto
1.4.2 Run Main Wrapper
1.4.1 Redesign Turboprop
Manufacturing
1.6 Research Components
Available
NO
YES
2.1 Determine Suppliers and Partners
2.1.1 Determine Possible Investors
2.1.2 Contact Suppliers
2.1.2.1 Allocate Beechcraft 1900D
2.1.3 Perform Preliminary Cost Analysis for development
2.1.4 Perform Preliminary Cost Analysis for supply
2.2 Obtain Funding
3.2 Set Up Company
4.1 Obtain and/or Develop Final Components
4.1.1 Develop H2 Tank within specifications
4.1.3 Obtain ELMO within specifications
4.1.4 Obtain HEX within specifications
4.1.5 Develop Radiator within specifications
4.1.2 Obtain necessary components for EPS
4.1.6 Develop FC within specifications
4.1.7 Obtain necessary components for TMS
4.1.5 Develop Radiator within specifications
AIT
4.2 Obtain Beechcraft 1900D
4.2.1 Develop Disassembly Plan
4.2.2 Purchase Beechcraft 1900D
4.2.4 Transport developed components to working area
4.3 Disassemble last 2 rows from Beechcraft
4.4 Prepare Subassemblies
4.5 Disassemble fuel storage/distribution
4.6 Verify working fluxes without leaks
4.7 Remove CC from Turboprop
4.8 Ground Testing of PT
4.9 Integration
4.10 Flight Test
5.8 Regulatory Certification Review
5.3 Test performance metrics on CC
5.4 Assess thermal fatigue and failure modes
5.2 Perform Type Tests on Tank
5.5 Validate with Third Party
5.6 Set up Production Quality Assurance
5.7 Set up inspection protocols
PRODUCTION APPROVAL
Operations
6.1 Obtain Production Certificate
6.2 Set up certified production lines with standards
6.3 Finalise Supplier contracts for scaled production
6.6 Secure Purchase Contracts from airlines
6.4 Manufacture initial batch with full comformity checks
6.5 Obtain individual Airworthiness Certificates
6.6 Plan delivery logistics for customer acceptance
6.7 Publish Operational Manual and Support Documentation
7.5 Monitor in-service fleet performance
7.1 Develop Maintenance Process (MP)
7.2 Certify MRO Providers
7.3 Establish Spare Parts Supply Chain
7.4 Establish Technical Support
7.5.1 Issue Service Bulletins
7.5.2 Coordinate ongoing Maintenance
EOL
8.2 Decide on retirement timing
8.1 Evaluate Aircraft condition
8.2.1 Evaluate maintenance costs
8.2.2 Evaluate regulations
8.2.3 Evaluate Operational Needs
8.3 Notify aviation authorities
8.4 Begin deregistration
8.5 Withdraw Aircraft from service
8.6 Remove usable parts and components safely
8.7 Dispose of hazardous materials
8.8 Dismantle and recycle aircraft and systems
8.9 Complete final documentation and reporting

20.1.2. Limitations

Having set out the final design for SHTARWaRS, it is equally important to recognize the project's limitations. Firstly, the PT6A-67D engine comes from the 1980s, resulting in an older technology. While historically proven, its architecture predates modern efficiency, compliance, and integration standards. This results in a fuel-efficiency penalty and longer maintenance windows due to scarce parts. Collectively, these factors constrain the performance of H_2D_2.

Secondly, the compressed schedule of the DSE requires a rapid workflow, which in turn means relying on simplified calculations. Furthermore, the design depends on assumptions about future technological maturity that cannot yet be verified. Some key areas of interest suffer from either lack of data or restricted data access, further constraining the project.

As we look to the detailed design of the PT, the assumptions and limitations incorporated here are anticipated to play a lesser role, either as certain models and tools are improved, or as additional tools begin to take form, such as the HEX tool. While limitations were identified at this stage, we remain confident in the final design as a full V&V was performed to reinforce confidence therein.

20.2. Production Plan

The following section outlines a more detailed production plan for the manufacturing, assembly and integration of all components and (sub)assemblies. Regardless of whether the items are developed in-house or not, the manufacturing and/or testing of such items is mentioned here. When designing for production, several factors are of key importance. Quality must be ensured for fitness of design, not for first-rate components, ensuring the project is developed within the scheduled time and the effect of the cost budget is minimized. Adhering to local airworthiness regulations is essential to move forward towards an optimized production process. Despite regulations being more limited for hydrogen-powered aircraft, it is expected to see an increased focus on such aircraft, and a development of these regulations by the time the first prototype is built.

However, given the novelty of this design, it is crucial to ensure a final product that is reliable, maintainable and safe. This will ease the transition to public hydrogen-powered aircraft projects. Lastly, as mentioned before, during the operational life of H_2D_2, the company must provide support to airlines, and track costs so that the SHTARWaRS project does not come to an end. These considerations were taken into account while developing the following production plan. Then, the main objectives of this plan are to:

- Retrofit the Beechcraft 1900D with the H_2D_2 design
- Ensure airworthiness compliance
- Achieve performance, safety and maintainability targets.

For that, the section will be divided into the disassembly of the original aircraft systems in Subsection 20.2.1, the development of the *hydrogen system* in Subsection 20.2.2, the EPS and FC in Subsection 20.2.3, the PP in Subsection 20.2.4. These steps will essentially be carried out in parallel, followed by the final integration, assembly and certification in Subsection 20.2.5 which happen sequentially, after the aforementioned are completed.

20.2.1. Disassembly

The objective of this phase is to safely remove the existing propulsion system, the associated subsystems, and several auxiliary components; while preserving the structural and system integrity of the airframe. By the end of this phase, the aircraft shall be ready for inspection and any modification deemed necessary.

Parallel to the acquisition of the aircraft, the team shall prepare a *Job Hazard Analysis*, ensure all staff are qualified and safety equipment is operational, and prepare a risk assessment. Following this, the electrical and control systems will be disconnected. Then, auxiliary systems such as cooling, sensors or the exhaust can be removed. The primary propulsion unit displayed in Figure 20.1 can now be disassembled.

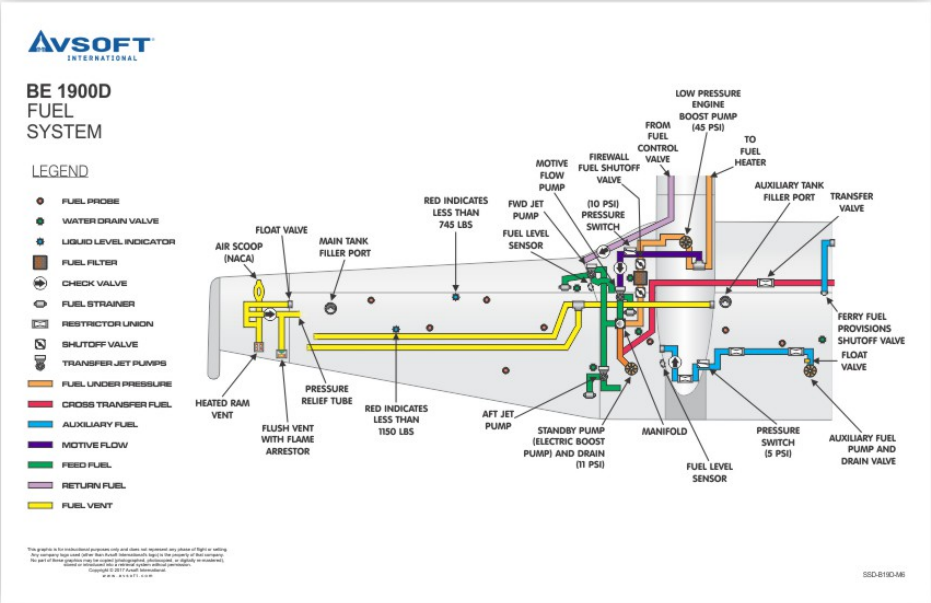

Figure 20.1: *Beechcraft 1900D engine wiring and piping [107]*

Before commencement, the team must verify whether all fluid systems have been depressurized. Then, the (cross, under pressure, feed, return and auxiliary) fuel supply system can be removed after ensuring no leaks are detected, and the fuel supply has been disconnected and no fuel is present. Similarly, the pneumatic pipes that ensure the venting of the fuel and the fuel storage compartments can be removed, aiming to minimize the effect on the airframe. Following this, the engine mounts and brackets can be removed, and the airframe and engine can be inspected and cleaned. A log status will ensure that pieces to be scrapped or refurbished are tracked, and an Non-Destructive Testing (NDT) can be performed to the attachment points.

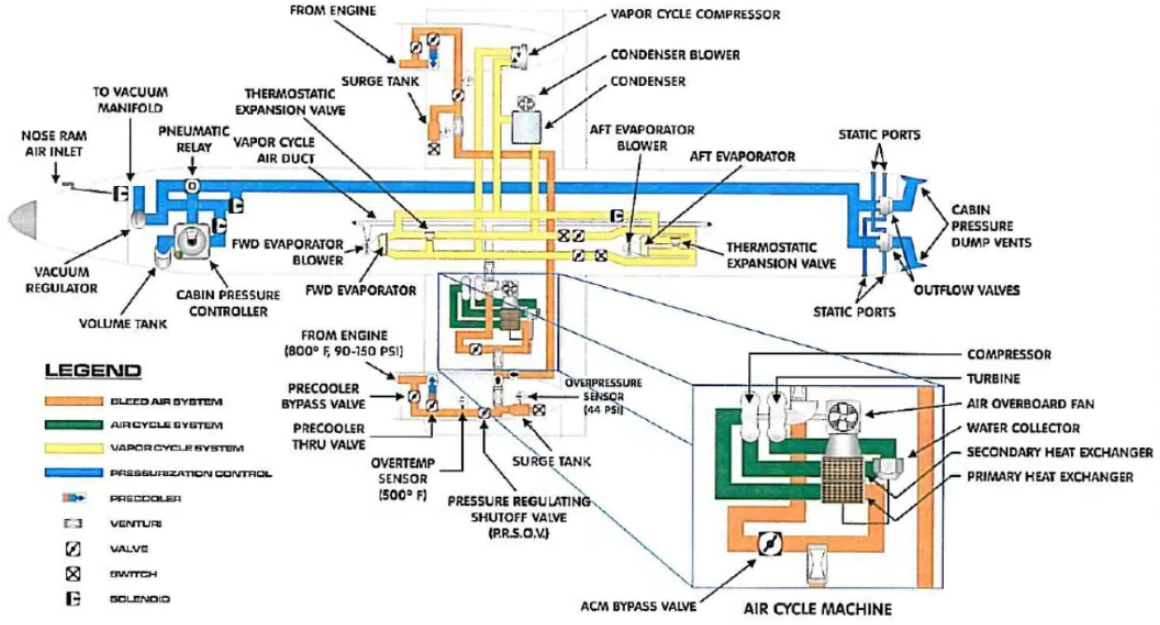

Figure 20.2: *Beechcraft 1900D pressurization and air conditioning distribution [107]*

However, not all systems must be removed. Some such as the oxygen flow in case of depressurization, or the pressurization and air conditioning distribution displayed in Figure 20.2 will only require some alterations. In this case, the bleed air system must be disconnected upon removal of the engine, to prevent damage on the system. The remaining components can, however, remain in the aircraft, since the redesigned engine will have the same function as the original one. Similarly, despite some changes in the CDHS system and EPS, the main components will remain in the aircraft, to reduce the effect and cost of disassembly. After inspection, the aircraft is now ready for integration of the H_2D_2 systems.

20.2.2. Hydrogen System

Parallel to the disassembly of the Beechcraft 1900D, the development of different systems can be commenced. The hydrogen system is composed by the hydrogen storage tank, and the conditioning and distribution, namely the piping system, which includes several HEX and compressors, among other components already described in Chapter 12 and Chapter 11.

The development of the tank will follow after the convergence to a final design. Following the analysis displayed in Chapter 11, the tank will first have to undergo extensive FEA (*Task 1.1.4)*, including the addition of transient responses for the (de)pressurization, and thermal analysis to investigate the conditioning of hydrogen, and ensure the fuel stays within operational conditions. A simplified analysis is presented in Figure 20.3, where the pressurization and hydrostatic pressure for the final tank designed are investigated. It is important to note that this analysis does not validate the designed tank, as it incorporates several assumptions. The material used considers orthotropic properties for composite plies, as opposed to the fiber winding that was explained during the design. Additionally, the properties considered do not take into account the full effect of temperature variations.

For now, the FEM results allow us to shift from spherical caps to the standardized DIN 28011, given that the resulting stresses are within the allowable range. However, in the future, it is recommended to analyze the tank design in accordance with both the manufacturing technique and the conditions under which the tank will be exposed. However, this is out of the scope of this project.

Following this analysis, the outer and inner vessels, as well as the support structure can be manufactured. For that, the material selected is *S-Glass Fiber*.

To ensure a high-strength fiber-reinforced product, the fabrication will follow the filament winding process, where bands of resin-impregnated fiber are wound over a cylindrical spindle using a controlled fiber placement machine. Following the winding, the part is placed in an autoclave for curing. The chosen design for the tank will use 2 winding angles to ensure the inclusion of the hoop and helical fibers. The alternation between these two layers, is very effective in enhancing the strength of the vessel.

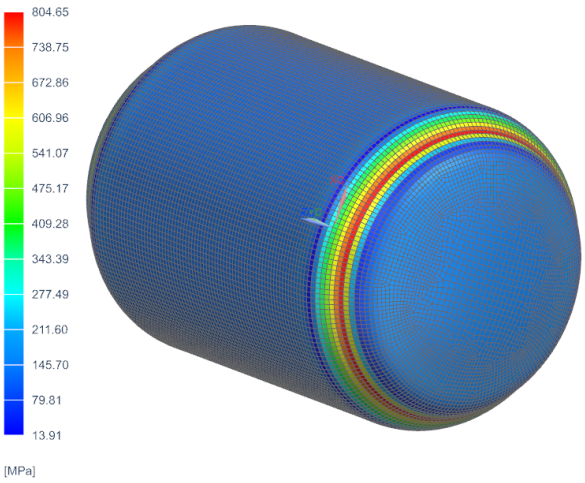

Figure 20.3: *Simplified pressurization and hydrostatic FEA of the H_2 storage inner vessel*

Following the integration of ports, the inner vessel can be extensively tested for burst, leak, permeation, drop, and bonfire among others. The support structure will also be tested according to the expected vibrations during a simulated flight. Once, the storage assembly is complete, the tank can be validated and later integrated to the fuel supply system.ed and later integrated to the fuel supply system.

The fuel supply system is made up of standardized components that do not need isolated testing. The piping selected for the design is item *E19B* from *Mouldpro* [108], and other components such as the compressors or the HEX will have to be selected or manufactured based on the final design. For that, suppliers will be contacted once the design is finalized. Once all components are gathered, the fuel supply system can essentially be assembled, and the conditioning and distribution of the hydrogen tested. Here, leaks under- or over-pressurization and temperatures outside the working region of the fluids must be investigated and mitigated.

20.2.3. Electrical Power System

Once the electrical schematics have been reviewed and the power cables, wiring and sensors have been disconnected; the new EPS can be installed. For that, new (primary and secondary) power cables will be integrated, routing them through designated cable ducts and secured per aircraft standards (AC43.13), revisiting the design presented in Figure 15.3. Then, new sensors, control switches, circuit breakers, and relays can be installed.

The integration of the FC will depend on the development of HT-PEMFC technologies. Once technology meets the expectations of this design, development can commence. For that, the following must be followed:

- Install FC modules in dedicated compartments, ensuring ventilation
- Integrate stack frame mounts and structural reinforcements
- Connect fuel lines, coolant loops and power cables
- Install gas leak sensors in FC bays
- Coordinate thermal sensors and fuel flow monitoring

Lastly, the installation of the ELMO and gearbox in the engine is necessary to test the correct functioning of the hybrid system. For that, the gearbox mounting, alignment and coupling must be integrated. Then, the electrical power connection to ELMO can be checked, and the torques and alignments can be thus verified. Given the high accuracy required for this subassembly, ensure ground testing prior to full integration into the aircraft.

20.2.4. Partial Powerplant Redesign

The removal of the engine from the nacelle will allow for access to the CC module. After disassembly of the engine, the legacy combustor liner and components can be removed (after disconnecting fuel lines, pressure sensing lines and sensor wiring). Then, the cleaning and inspection of the combustor housing can be carried out.

The RQL with generic geometry can then be obtained from the supplier, after testing, and installed into the housing. Here, verification of alignment with the compressor and turbine is essential. The following adaptations must be made:

- Install new fuel injectors
- Connect quench air ports
- Install flame detection sensors
- Reassemble engine on test cell
- Verify flame stability, sensor feedback, prevention of leaks, and emissions
- Integrate to aircraft

Here, safety and quality assurance are crucial along the entire process, given the effect of this system on the overall performance of the completed H_2D_2.

20.2.5. Assembly, Integration & Test

Once all subsystems have been tested and assembled, it is time to integrate all components and full testing of the aircraft.

For the final assembly, the fuel and cooling system, the EPS, and PP assembly are installed. After verifying

all mechanical fasteners, routing and securing wiring harnesses to standard is required. Then fuel, cooling and electrical interfaces can be connected, safety systems integrated, and avionics and software updated. Before certification, however, some final checks must be performed.

A full structural inspection of the retrofitted areas is required. The following tests must be performed:

- Continuity tests on electrical systems
- Pressure and leak tests on hydrogen and cooling systems
- Clearance and alignment checks on moving components
- Verification of sensors, wiring and monitoring equipment

Then, ground operational tests can be performed on the PP; for idle. partial and max power runs; while monitoring temperatures, pressures, RPM, and sensor feedback. After testing the shutdown system and the correct operation of avionics and flight displays, H_2D_2 can move forward to the flight test. Here, taxi, take-off, climb, cruise and landing performance will be analyzed and compiled. Following the validation by a third-party, with any necessary updates, H_2D_2 will obtain airworthiness. After which the production line can be set up. A schematic of the production line is presented below in Figure 20.4.

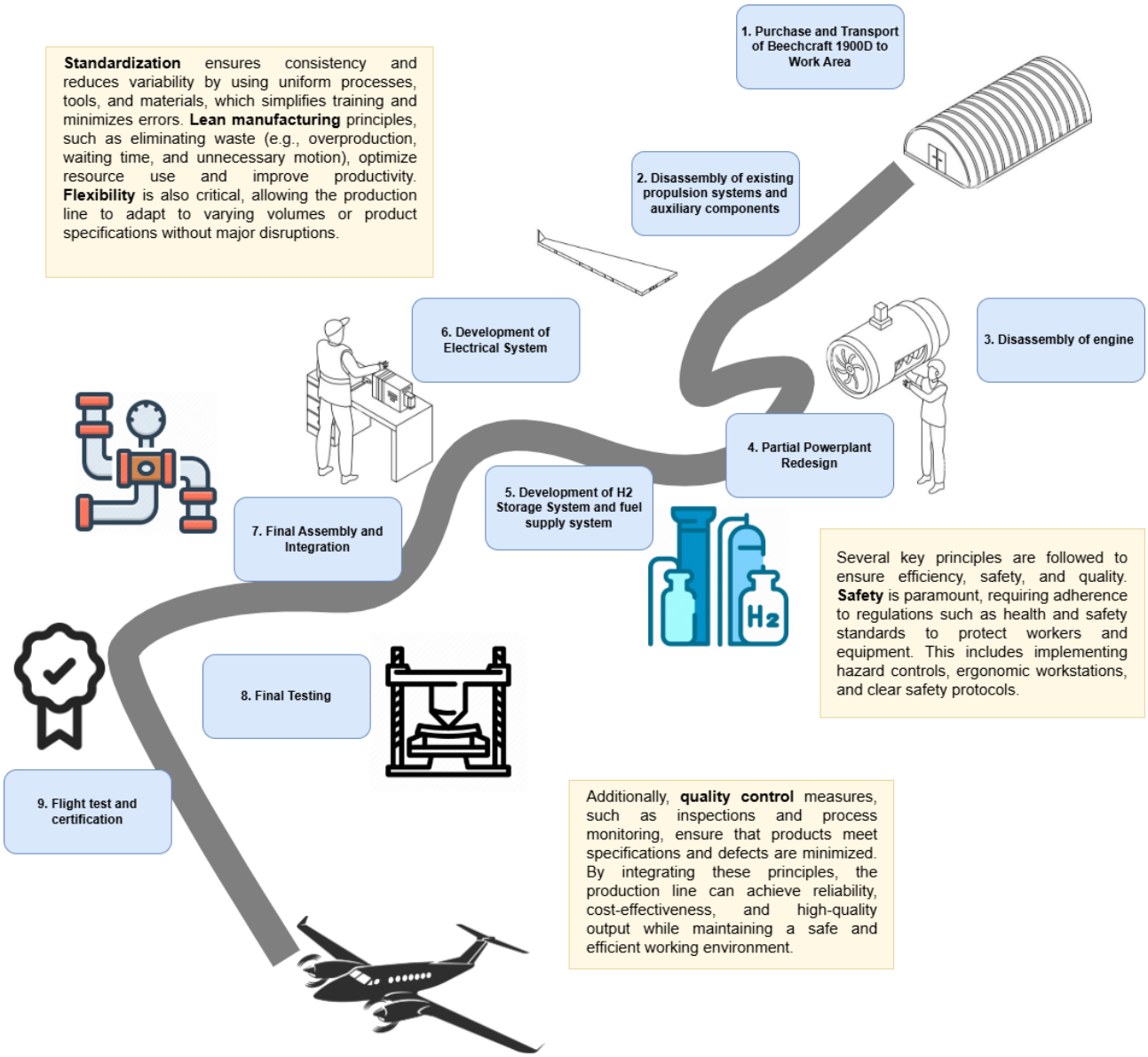

Figure 20.4: *Production line for H_2D_2*

20.3. Project Gantt Chart

The Project Gantt Chart, seen in Figure 20.5 shows the same tasks as in the Development flow diagram. They are displayed in a Gantt Chart to show the amount of time each task would roughly take and when they would be finished. The CC has been left out of the Gantt Chart, for visibility reasons. It can be seen that the production and certification takes up the most of the time.

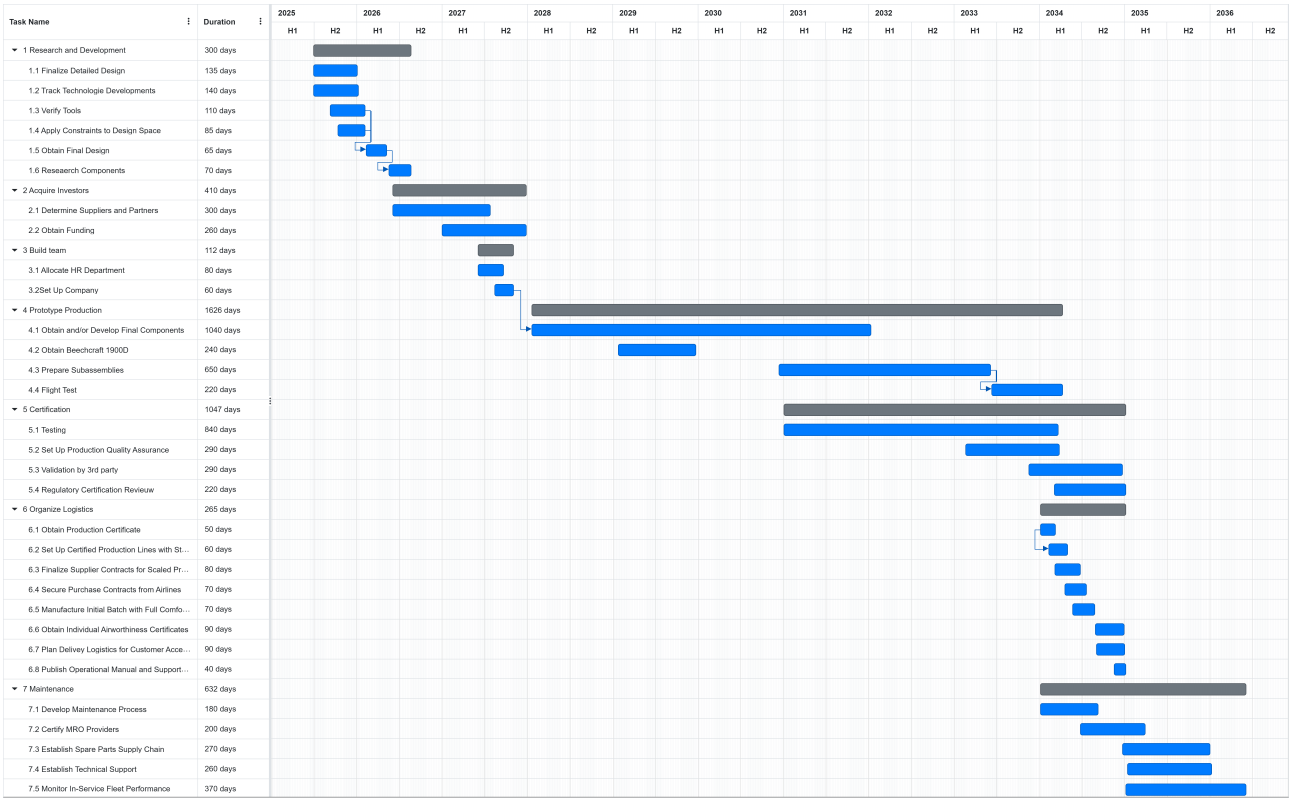

Figure 20.5: *Project Gantt Chart*

21

Economic Feasability

21.1. Cost Breakdown Structure

The Cost Breakdown Structure (CBS) is crucial to understand the partial financial contributions to the development cost as well as the purchase price of the H_2D_2. The CBS is also an important instrument for determining the ROI of the project. For constructing the CBS, multiple aspects should be taken into account: detailed design and development, manufacturing and acquisition, operations and support, and disposal. It should be mentioned that some of the reference prices were sourced in (USD) $, and they have been converted to (EUR) € using a rate of 0.87 (ECB rate 18.06.2025), for the sake of consistency. The overall cost breakdown is visible in Figure 21.1, with the total costs calculated on the basis of specific costs and the system characteristics.

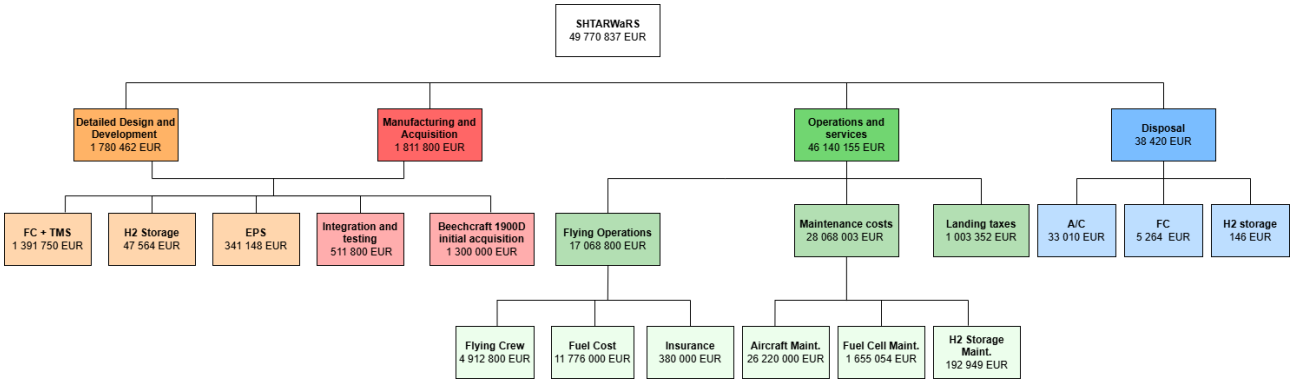

Figure 21.1: *Cost breakdown structure*

Detailed Design & Development

This first section of the overall cost identifies the specific cost for the FC and TMS together, as well as the specific costs of the hydrogen storage and the EPS. The FC design and development cost is estimated as 555 €/kW [109], including TMS, while the hydrogen storage development specific cost is set at 212 €/kg of hydrogen stored [110]. Additionally, the EPS cost is 267 €/kW [111] of ELMO power,

Manufacturing & Acquisition

The M&A is closely related to DD&D, this being the reason why they are presented as linked in the CBS. For the subsystems like FC, TMS, EPS, and hydrogen storage, the manufacturing cost is included in the specific cost of design. The distinct acquisition costs are for the initial acquisition of a Beechcraft 1900D, and for its certification and testing. The plane price tag is set at 1.3 million €[112], while the testing and certification cost is a one-time expenditure of 255 millions €[113]. The cost of certification and testing needs to be divided by the expected total number of planes in the fleet, which in this case is estimated at 500, for a 10% market share [5]. This leads to an estimated cost of 511 800 €per unit sold.

Operations & Support

The O&S costs may be divided into flying operational costs, maintenance, and landing taxes. The landing taxes are expressed in reference to taxes at the Rotterdam The Hague Airport, for a plane in the 6000-20000 kg range, and the cost is 54.53 €/landing [114]. The flying operations spending splits between crew's pay of 89 €/hr[115], the fuel cost for hydrogen (4 €/kg)[116], and the yearly insurance for the plane of 18 000 €[117]. The maintenance section includes the stock aircraft maintenance cost of 1.31 million €[117], to which the costs for the FC and the hydrogen storage need to be added. The FC takes 127 €/kW [54] to maintain, while for the storage, 43 €/kg [118] are required.

Disposal

The disposal costs are split between the stock Beechcraft 1900D specific value of 6693 €/ton [119], the cost of FC recycling, and the cost of disposing of the hydrogen storage tank. The FCs have a specific price of recycling of 9.35 €/kW [55], while the storage tank, being made of S-glassfiber, takes only 0.6 €/kg [120] to dispose of.

21.2. Return on Investment

The ROI is the metric that evaluates the profitability of an investment. Moreover, in the context of the aviation industry, it is a suitable driver for fleet sizing and flight scheduling along the lifetime of the aircraft. The ROI represents the ratio between the net profit and the total costs (including initial investment and lifetime costs) over the lifetime of the aircraft.

The profitability analysis is being done from the perspective of an airline company, willing to invest in a fleet of H_2D_2 aircraft. For a generalization of the ROI, this analysis sets the net profit to zero, determining the average ticket price, per flight, over the lifetime of the aircraft for achieving a break-even outcome. On the other hand, this analysis assumes a conservative 20-year aircraft lifetime [121]. On top of that, a typical aircraft of this class performs about 1380 flight hours per year [5]. Moreover, researching into various airlines (Wasaya Airways, Gum Air) that operate the Beechcraft 1900D, the flight time averages 1.5 hours for this model, also matching REQ-TE-STK-C considering cruising at Mach 0.4. This results in 920 flights per year. These data will be used further for the ROI analysis, considering the production and acquisition of a fleet comprising 500 aircraft. Based on this data, Equation 21.1 calculates the average ticket price, for a break-even outcome in 20 years of aircraft operation.

$$\text{ticket price} = \frac{\text{init. price} + \text{no. of years} * \text{operational cost} + \text{disposal cost}}{\text{no. of years} * \text{flights per year} * PAX} \tag{21.1}$$

Considering the break-even situation with the parameters presented above, the average ticket price is €187, per PAX, per flight. This result comes from the one-time cost of the aircraft of €2.04 million, and the recurrent average costs of maintenance and depreciation, with a value of €2.4 million and €63,568, respectively, per year. As a result, the annual income translates into €2.57 million per year. Figure 21.2 visualizes the constant income and the constant average operational costs. It is worth to mention this scenario, is an intermediate scenario, taken for the ease of analysis. This is not a feasible, realistic one. The cumulative profit is also being plotted to show that indeed, the break-even occurs after 20 years of operations at €187 per ticket. The cost drops from the second operational year, because the first year adds up the acquisition costs as well as the operational costs, while after that, only operational costs are taken into account.

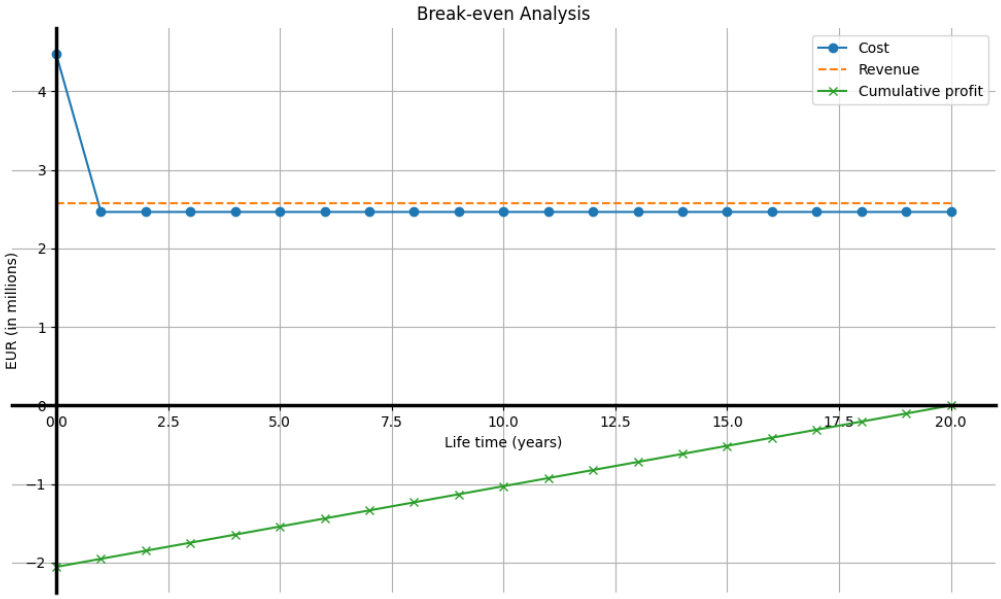

Figure 21.2: *Break-even scenario after 20 years at €187 per ticket*

Considering the profits, it is to be mentioned that the initial cost of the aircraft does not contain the profit margin of the design and production team. However, the lifetime of an aircraft is in most cases limited by its profitability, rather than the engineering constraints. This happens because the maintenance costs increase by an average of 3.24% as the aircraft ages [122], with more often and more complex procedures being needed for older aircraft. For that reason, the maintenance cost of the aircraft was adjusted for a more realistic scenario, as may be observed in Figure 21.3.

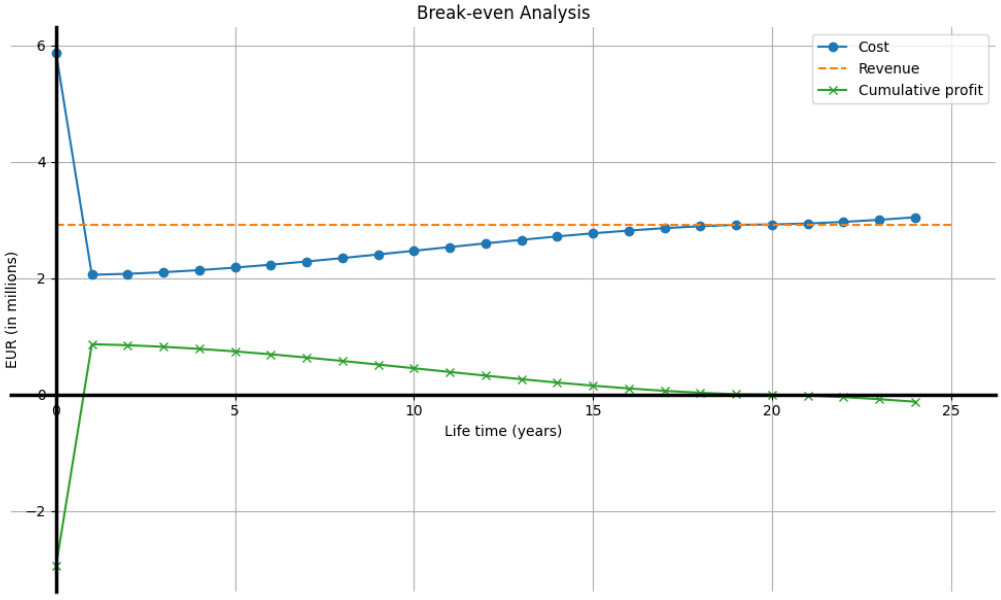

Figure 21.3: *Profitability over H_2D_2 lifetime, at €221 per ticket*

Again, in Figure 21.3 the revenue is set to a constant, but the profit is the actual profit of each year, rather than cumulative profit. In order to make the aircraft profitable for the entire life cycle, the ticket prices were increased by 18%, reaching €221 per seat. The sudden decrease in costs is represented by the initial acquisition of the aircraft in the first year of operations. With this pricing, the client may break even after 2 years of operations, accumulating profit for the rest of the 18 years. The total profit made by one aircraft sums up to €7.225 million, averaging €361,256 per year, along the decreasing profit trend over the life cy-

cle. Considering the actual ROI of investing in one H_2D_2 aircraft, it is represented by the ratio of net profit over investment. For simplicity, the total expenditures along the life cycle of the aircraft is considered as investment. Therefore, the actual ROI = 14%, considering the net profit of €7.225 million and the total costs of €49.77 million. Although this analysis is a generalization because of the constant ticket price, it may be adjusted by the airline in order to align with the desired strategy, including a fluctuation in the ticket price, to offset the increasing cost in maintenance.

22

Compliance with Requirements

All requirements are shown below in Table 22.1, Table 22.2, and Table 22.3. The tables also contain the V&V procedures, whether the design complies with such requirement, and a brief description with the reason for compliance or the necessary steps to meet the requirement. The first table shows the stakeholder requirements, the second the system requirements, and the last table presents the subsystem requirements. In the table below, ✓ indicates the requirement has been met, and ✓* indicates the requirement has been verified through analysis, but further testing is required for validation. Then, χ indicates the requirement has not been met or checked during the design, for which further analysis will be required as explained during the production plan. The table contains the V&V procedures to be followed, where I stands for inspection, A for analysis, D for demonstration, and T for test. These will be explored in more detail in Section 6.2.

Table 22.1: *Stakeholder requirements*

ID	Requirement	M	Verification Method	✓	Compliance and future tasks
REQ-TE-STK-A	The a/c shall contain a hybrid-electric PT	I	Check if the PT is hybrid-electric	✓	FC and PP have been included in the design
REQ-TE-STK-B	Limiting emissions shall be a performance metric	A	Confirm this performance metric was taken into account for the design of the system	✓	Sustainability was considered for the objective function during the final design selection and NO_x emissions were considered for the constraint analysis
REQ-TE-STK-C	The a/c shall have a minimum range of 700 km	D	The a/c shall be flown under nominal conditions and operations to determine the maximum range	✓*	The simulated range of H_2D_2 is 707km, but a demonstration is required
REQ-TE-STK-D	The PT shall include a TMS	I	Check if there is a TMS in the design	✓	TMS was integrated into the design
REQ-TE-STK-E	The a/c shall be able to provide 0.94 [MW] propulsive power during cruise	A	Compute if the PT is able to provide 0.94 MW of power	✓	The systems were designed according to this condition, but additional testing is required
REQ-CO-STK-F	The a/c shall produce fewer emissions than the original a/c.	T*	The emissions will be measured of the PT and compared to similar a/c	✓*	The emissions from the PT were analyzed and included in the constraint analysis, but further testing might be required
REQ-CO-STK-G	The a/c shall be able to transport at least 15 people	I	Check if there are 15 usable seats for PAX on the a/c	✓	Number of PAX equals 15
REQ-CO-STK-H	The a/c shall be financially desirable for consumers	A	Determine the total cost per available seat kilometer (CASK) to compare against competitors'	χ	The CASK for H_2D_2 is 0.2644 EUR, compared to 0.1877 EUR for the original aircraft. To assess whether the aircraft is financially viable, the team must monitor developments in regulations, such as the potential introduction of taxes to conventional aircraft. In addition, the price of the tickets falls within the typical range for aircraft of similar capacity and range.

Continued on next page

Table 22.1 – continued from previous page

ID	Requirement	M	Verification Method	✓	Compliance and future tasks
REQ-CO-STK-L	The PT shall not exceed a weight of 2541 [kg] (3 times the original PT)	I	weigh the PT and compare to 3x the original	✓*	The estimated mass of the PT does not exceed such value, but further inspection will be required when the system is manufactured and assembled
REQ-CO-STK-M	The system shall be completed and feasible by 2035	A	Make a schedule of when each stage of the design is achieved	✓	Design was completed in time, and technology projected to required year
REQ-CO-STK-N	The PT shall comply with CS-23	A	The retrofitted Beechcraft 1900D design shall be checked against relevant CS-23 regulations	✓*	TRA was performed, but certification is required
REQ-CO-STK-O	The a/c shall comply with H_2 safety ISO standards	A	The hydrogen storage, conditioning, and distribution shall be checked against the relevant ISO standards	✓*	TRA was performed, but certification is required

Table 22.2: *System requirements*

ID	Requirement	M	Verification Method	✓	Compliance and future tasks
REQ-TE-SYS-A.1	The PT shall provide at least 1.9 of propulsive power during the most demanding phase	T*	The PT will be mounted on a test bed and the propulsive power will be measured	✓*	The system was designed for such value, but testing of the finished aircraft is required
REQ-TE-SYS-A.2	The PT shall provide controlled thrust	T*	Thrust input shall be varied along its range and measured to conclude if it changes accordingly	✓*	Thrust was modeled as a variable during the flight profile, and the control system is developed in Chapter 15
REQ-TE-SYS-A.3	The PT shall have a transient response equal or superior to a normal turboprop	T*	An input will be given to the PT and the transient response will be measured	✓*	The original turboprop has not been replaced, so the response is equal to the original, but the addition of ELMO must be considered
REQ-TE-SYS-B.1	Limiting hydrogen emissions shall be a performance metric	A	Confirm this performance metric was taken into account for the design of the system	✓*	It was considered for refueling losses during nominal operations. Mitigations were considered to reduce leakage
REQ-TE-SYS-B.2	Limiting noise near airports shall be a performance metric	A	Confirm this performance metric was taken into account for the design of the system	✓	The implementation of the FC will inherently reduce the noise as compared to the original model during taxiing and approach
REQ-TE-SYS-B.3	Limiting water emissions shall be a performance metric	A	Confirm this performance metric was taken into account for the design of the system	✓	It was included in the emissions metric for the constraint analysis
REQ-TE-SYS-B.4	Limiting NO_x emissions regarding air quality shall be a performance metric during operations near airports	A	Confirm this performance metric was taken into account for the design of the system	✓	NO_x production was implemented in the constraint analysis
REQ-TE-SYS-B.5	Limiting NO_x emissions regarding climate shall be a performance metric during cruise	A	Confirm this performance metric was taken into account for the design of the system	✓	NO_x production was implemented in the constraint analysis
REQ-TE-SYS-C.1	The PT shall use hydrogen as a fuel	I	Check if hydrogen was used	✓	LH_2 was selected as the stored fuel
REQ-TE-SYS-C.2	The PT shall be able to store at least 224 [kg] of hydrogen	T	Measure how much hydrogen is needed to fill the hydrogen tank	✓*	The tank and hydrogen system were designed for such conditions, but testing of fueling is required
REQ-TE-SYS-C.3	GO shall be performed between flights	I*	Perform GO and assess the accessibility of tasks	✓	As determined in the FFD and *Development Plant*, ground operations are indeed fulfilled between flights
REQ-TE-SYS-D.1	The heat sink potential of hydrogen shall be exploited	A	Confirm the heat sink potential has been used in the final design	✓	The heat sink potential was exploited in TMS to maintain the operating conditions of the FC

Continued on next page

Table 22.2 – continued from previous page

ID	Requirement	M	Verification Method	✓	Compliance and future tasks
REQ-TE-SYS-D.2	The PT shall contain a WRS	I	Check if the design contains a WRS	✓	The WRS treats the exhaust of FC and feeds into the PP
REQ-CO-SYS-F.1	The a/c shall produce no carbon emissions	T	Test the exhaust gases of the a/c for traces of carbon emissions	✓*	Analysis demonstrates no traces of carbon emissions, but testing is required
REQ-CO-SYS-F.2	The a/c shall meet NO_x emissions sustainability goals	A	Estimate the GHG emissions of the a/c and compare with sustainability goal	✓	NO_x emissions remain below the subsystem requirements below this
REQ-CO-SYS-H.1	The fuel cost per PAX [2035] shall be less than the original Beechcraft 1900D design	A	Estimate the fuel cost per PAX of the a/c and compare with original	✓	The projected cost of hydrogen for 2035 is 4€/kg, as explained in Chapter 2
REQ-CO-SYS-I.1	CDHS shall provide operational awareness	D	Read the displays in the cockpit	✓	The original CDHS is updated based on the updated CommFD
REQ-CO-SYS-J.1	The PT shall be compatible with the original turbopropeller	I	Check the compatibility of the components	✓	Standard components were implemented, with the specifications of the original engine in mind
REQ-CO-SYS-J.2	The a/c stability margin shall not be compromised w.r.t the original Beechcraft 1900D	A	Compute the updated margin for the center of gravity	✓	Component integration and stability analysis was implemented in the constraint analysis
REQ-CO-SYS-J.3	The a/c shall be able to land within the specifications mentioned for the Beechcraft 1900D	D	Perform a D landing with specified maximum runway (rwy) length, landing speed etc.	χ	A demonstration will be performed during certification
REQ-CO-SYS-J.5	The airframe shall be compatible with the redesigned turboprop	I	Check if the integration of redesigned turboprop within the airframe is successful	✓	Mass loading in the wing was taken into account during the constraint analysis, and a volumetric analysis was performed as well
REQ-CO-SYS-M.1	The design shall be finished in 10 weeks	D	Check at end of week 10 if design is finished	✓	Design was completed prior to the deadline
REQ-CO-SYS-M.2	The design shall be feasible by 2035	A	Estimate the feasibility of technology in 10 years' time based on previous studies	✓*	The technology was projected to 2035, and feasibility will be revisited during the production
REQ-CO-SYS-N.1	Fuel tank shall be isolated from the personnel compartments.	I	Check if fuel tank compartment is divided from the civilian compartment	✓	A firewall was implemented between the tank and cabin
REQ-CO-SYS-N.3	PP and FC fuel supply systems shall be independent of each other	I	Verify if the hydrogen flow to each of the 2 is independent of the other	χ	The system is not independent during conditioning, but redundancies were considered to mitigate the risks
REQ-CO-SYS-N.4	The system shall provide a mean of discharging the stored fuel	D	Perform a test run to demonstrate successful defueling in case of emergency	✓*	Accessibility to the tank is provided, but the test is still pending
REQ-CO-SYS-N.5	The system shall provide energy for at least 30 min at maximum power/ thrust condition.	T*	Put the PT on a testbed and set it to maximum thrust for 30 mins, check for any failures	χ	Testing is required
REQ-CO-SYS-N.6	The fuel tank shall withstand, without failure, the vibration, inertia, fluid and structural loads that it may be subjected to in operation.	T	Vibrational testing on the fuel tank	χ	Despite a simplified FEM analysis, the tank must be subjected to dynamic loads under the correct operating conditions
REQ-CO-SYS-N.7	Fuel system components in an engine nacelle or in the fuselage shall be protected from damage which could result in spillage of enough fuel to constitute a fire hazard as a result of a wheels-up landing on a paved rwy	T	Exert a force upon the fuel system components in their protective structure similar to what would be experienced by a wheels up landing and check for failure	χ	To be performed during certification

Continued on next page

Table 22.2 – continued from previous page

ID	Requirement	M	Verification Method	✓	Compliance and future tasks
REQ-CO-SYS-N.8	The cooling system shall maintain the designated temperature of the PT components for any atmospheric conditions, during operation and after shutdown	A	Make a model that checks if the designated temperatures can be maintained for all atmospheric conditions and operational modes	✓*	The temperature of crucial components was analyzed through the TMS tool and flight performance tool, for operating conditions. Additional tests might be required
REQ-CO-SYS-N.9	The exhaust system shall ensure the exhaust gases do not generate a fire hazard	I	Check that no objects are in the path of the exhaust gasses that could be a fire hazard	χ	Inspection to be performed after integration of the engine
REQ-CO-SYS-N.10	The exhaust system shall ensure the personnel compartments are not contaminated with carbon monoxide	T*	Run PT in a completed a/c and check for carbon monoxide leaks into the cabin	χ	Test to be performed after integration
REQ-CO-SYS-N.11	Any combustion system components shall be isolated by firewalls from the rest of the a/c	I	Inspect that the CC components are separated from the rest of the a/c by firewalls	✓	The combustion system is isolated and protection is provided by a firewall

Table 22.3: *Subsystem requirements*

ID	Requirement	M	Verfication Method	✓	Compliance and future tasks
REQ-TE-SUB-A.1.1	The FC shall provide a minimum of 0.94 [kW] electrical power to the ELMO	T	Connect the fuel stack system to a hydrogen supply and measure the electrical output	✓*	The FC was designed for such conditions but testing is required
REQ-TE-SUB-A.1.1.1	Fuel supply system shall supply hydrogen to the FC anode with a mass flow of 0.0085 [kg/s]	T	Connect the fuel supply system to a hydrogen supply and measure the mass flow out	✓*	The fuel supply system was designed for such conditions but testing is required
REQ-TE-SUB-A.1.1.2	Fuel supply system shall supply air to the FC cathode with a mass flow of 0.46 [kg/s]	T	Place the fuel supply system in open environment and measure the mass flow out	✓*	The fuel supply system was designed for such conditions but testing is required
REQ-TE-SUB-A.1.1.3	The FC system shall provide access for water recovery	I	Inspect the water recovery access port(s) in the FC system	✓	The system includes a WRS that feeds into the PP
REQ-TE-SUB-A.1.1.5	The FC system shall recirculate at least 0.00042 $[kg/s]$ of H_2	T	Connect the FC to fuel supply and measure waste H_2 levels/reintroduction effectiveness	✓*	The FC was designed for such conditions but testing is required
REQ-TE-SUB-A.1.1.6	Fuel supply system shall supply hydrogen to the FC anode with a pressure of 1.66 bar	T	Connect the FC to fuel supply and measure the anode inlet H_2 pressure	✓*	The fuel supply system was designed for such conditions but testing is required
REQ-TE-SUB-A.1.1.7	Fuel supply system shall supply air to the FC cathode with a pressure of 1.6 bar	T	Connect the FC to fuel supply and measure the cathode inlet air pressure	✓*	The fuel supply system was designed for such conditions but testing is required
REQ-TE-SUB-A.1.1.8	Fuel supply system shall supply hydrogen to the FC anode with a temperature of 433 [K]	T	Connect the FC to fuel supply and measure the anode inlet H_2 temperature	✓*	The fuel supply system was designed for such conditions but testing is required
REQ-TE-SUB-A.1.1.9	Fuel supply system shall supply air to the FC cathode with a temperature of 433 [K]	T	Connect the FC to fuel supply and measure the cathode inlet air temperature	✓*	The fuel supply system was designed for such conditions but testing is required
REQ-TE-SUB-A.1.2	The EPS system shall distribute electrical power	T	Activate EPS and measure electrical power at relevant components	✓*	The EPS is designed to distribute power, as displayed in the Electrical Block Diagram, but testing is required
REQ-TE-SUB-A.1.2.1	The EPS system shall deliver 0.94 [kW] of electrical power to the ELMO	T	Connect EPS to a power source, power ELMO and measure the power delivered	✓*	The EPS is designed to deliver such power, as displayed in the Electrical Block Diagram, but testing is required
REQ-TE-SUB-A.1.2.2	The EPS shall provide fault-tolerant insulation in case of a short-circuit	T	Short-circuit a simplified EPS model and inspect the insulation	✓*	The designed EPS follows standards, for human safety, but testing is required

Continued on next page

Table 22.3 – continued from previous page

ID	Requirement	M	Verification Method	✓	Compliance and future tasks
REQ-TE-SUB-A.1.2.3	The EPS shall provide automatic isolation in case of a short-circuit	T	Short-circuit a simplified EPS model and verify that the appropriate part was automatically isolated	✓*	The designed EPS follows standards, for human safety, but testing is required
REQ-TE-SUB-A.1.3	The ELMO shall be able to transform mechanical power to electrical power with at least 95 [%] efficiency	T	Connect ELMO to a rotating shaft and measure the electrical power output	✓*	Such efficiency was considered for the design, but testing is required
REQ-TE-SUB-A.2.1	The PT shall provide at least 35300 [kN] at maximum thrust	T*	Run PT on the highest thrust setting and measure the generated thrust	✓*	The system was designed for such value, but testing is required
REQ-TE-SUB-A.2.2	The PT shall use turboprop engines	I	Visually inspect turboprop engines	✓	The turboprop engines from the original aircraft were not replaced
REQ-TE-SUB-A.2.2.1	The fuel supply system shall supply hydrogen to the CC with a mass flow of 0.0096 [kg/s]	T	Connect the fuel supply system to hydrogen supply, activate and measure the mass flow of hydrogen output	✓*	The fuel supply sustem was designed for such conditions but testing is required
REQ-TE-SUB-A.2.2.2	The WRS shall be able to supply water to the CC with a mass flow of 0.082 [kg/s]	T	Connect the WRS to a water supply, activate and measure the mass flow of water output	✓*	The WRS was designed to deliver such flow properties, but testing is required
REQ-TE-SUB-A.2.3	The FC and PP shall be able to provide a maximum thrust equal to the original Beechcraft 1900D in case of one PP failure (engine-out)	T*	Run PT, disengaging one PP, at highest thrust setting and measure the generated thrust	✓*	Analysis shows that the new PT provides higher power than the original one. However, a test is required to meet this requirement
REQ-TE-SUB-A.2.4	The PP shall be able to provide a maximum thrust equal to the original Beechcraft 1900D in case of FC failure	T*	Run PP or PT, disengaging FC, at highest thrust setting and measure the generated thrust	✓*	Analysis shows that the new PT provides higher power than the original one. However, a test is required to meet this requirement
REQ-TE-SUB-A.2.5	The ELMO shall be able to transform electrical power to mechanical power with at least 95 [%] efficiency	T	Connect ELMO to an electrical power source and measure the mechanical power output	✓*	The ELMO was designed according to such value, but testing is required
REQ-TE-SUB-A.2.6	The PT shall convert rotational mechanical power to thrust	D	Run PT and inspect that propellers are being engaged	✓*	The original turboprop design was not altered, and a demonstration will display that the requirement is met
REQ-TE-SUB-A.2.7	The CDHS shall manage the required power split between PP and FC	T	Command the CDHS to provide and maintain various combinations of power from 100% PP to 100% FC successfully	✓*	The design will comply with this requirement, as displayed in the CommFD, but testing is required
REQ-TE-SUB-A.2.7.1	The CDHS shall be able to throttle the FC	T	command the CDHS to run through various levels of throttle for the FC power	✓*	The design will comply with this requirement, as displayed in the CommFD, but testing is required
REQ-TE-SUB-A.2.7.2	The CDHS shall be able to throttle the PP	T	command the CDHS to run through various levels of throttle for the PP power	✓*	The design will comply with this requirement, as displayed in the CommFD, but testing is required
REQ-TE-SUB-A.2.8	The PT shall be able to combine the mechanical power from PP and ELMO	T	test if during operation, both PP and ELMO are inputting power	✓	The integration of the ELMO allows for this, but testing is required
REQ-TE-SUB-B.4.1	The NO_x emissions shall not exceed 25 ppm at 15% Oxygen	T	measure NO_x emissions levels during the range of operating modes of the engine	✓*	The analysis states that NO_x emissions will max at 1.1 gr/flight, which is below the requirement. However, testing or a higher-order analysis is required
REQ-TE-SUB-C.2.1	The storage recirculation loop shall maintain the H_2 storage conditions (temperature, pressure and phase distribution) within safe margins	I	Check if conditions stay within operational range	✓*	The fuel supply system accounts for tank pressurization, for maintaining conditions. However, testing is required
REQ-TE-SUB-C.2.2	The storage shall enable H_2 refueling	I*	perform GO and check if refueling is successful	✓	The tank design allows for refueling during GO, or for conditioning
REQ-TE-SUB-C.2.3	The storage shall enable H_2 extraction	I*	perform GO and check if defueling is successful	✓	The tank design allows for H_2 extraction

Continued on next page

Table 22.3 – continued from previous page

ID	Requirement	M	Verification Method	✓	Compliance and future tasks
REQ-TE-SUB-C.2.4	Equipment bays shall include fire detection and automatic suppression	I*	Check the existence of fire detection and mitigation systems	✓	As displayed in the CommFD, the *Fire Prevention* unit, will detect and mitigate fires
REQ-TE-SUB-C.2.5	The minimum dormancy time shall be 24 hours	T*	Test the behavior of the hydrogen within the tank under nominal operating conditions	✓*	The dormancy time was analyzed during the design of the tank, but further testing and analysis is required.
REQ-TE-SUB-C.3.1	The integration of the PT into the a/c shall enable maintenance	I*	Perform GO and asses the accessibility of tasks	✓	The integration of the PT components does not prevent access for maintenance neither in the fuselage, wing, or PP
REQ-TE-SUB-C.3.1.1	The integration shall enable access for disassembly	I*	Perform GO and asses the accessibility of task	✓	The integration of the PT components does not prevent access for disassembly neither in the fuselage, wing, or PP
REQ-TE-SUB-C.3.1.2	The integration shall enable access to refuel	I*	Perform GO and asses the accessibility of task	✓	The integration of the PT components does not prevent access for refueling in the fuselage, where access is allowed through the rear hatch
REQ-TE-SUB-C.3.1.3	The integration shall enable access to defuel	I*	Perform GO and asses the accessibility of task	✓	The integration of the PT components does not prevent access for defueling in the fuselage, where access is allowed through the rear hatch
REQ-TE-SUB-D.1.1	TMS shall maintain the FC between operational limits	T	Measure FC temperature during operation	✓*	The TMS was designed for such conditions, but testing is required
REQ-TE-SUB-D.1.1.1	TMS shall maintain the FC temperature below 170 [K]	T	Measure FC temperature during max power being generated	✓*	The TMS was designed for such conditions, but testing is required
REQ-TE-SUB-D.1.1.2	TMS shall maintain the FC temperature above 150 [K]	T	Measure FC temperature when its not providing electricity	✓*	The TMS was designed for such conditions, but testing is required
REQ-TE-SUB-D.2.1	TMS shall deliver 0.082 kg/s water to the PP	T	Perform measurement on the water being supplied to the PP	✓*	The TMS was designed for such conditions, but testing of the *air loop* is required
REQ-TE-SUB-D.2.2	TMS shall recover all water vapor exhausted from the FC	T	The water vapor exhausted from the FC will be measured and compared to the water vapor it should create due to the inserted hydrogen	✓*	The TMS was designed for such conditions, but testing of the *air loop* is required
REQ-TE-SUB-E.1.1	The a/c shall provide a minimum 0.94 [MW] propulsive power during cruise	T*	The PT will be tested for thrust that can be maintained for the duration of cruise flight	✓*	The entire a/c was designed for such conditions, but testing of the complete, integrated system is required
REQ-CO-SUB-F.2.1	The system shall be designed with the available seat kilometers as sustainability metric.	A	Confirm this sustainability metric was taken into account for the design of the system	✓	This metric is included in Chapter 17
REQ-CO-SUB-I.1.1	CDHS shall indicate PT status	I	Check the CDHS if it displays PT status	✓	The requirement is met as displayed in the CommFD
REQ-CO-SUB-I.1.2	CDHS shall provide emergency awareness	D	Input data that would indicate an emergency into the CDHS and see how it reacts	✓*	The requirement is met as displayed in the CommFD, but demonstration is required
REQ-CO-SUB-I.1.3	CDHS shall indicate the maintenance status	I	Look at CDHS to verify it contains a maintenance status	✓	The requirement is met as displayed in the CommFD
REQ-CO-SUB-I.2.1	The PT shall provide emergency prevention & management in the cabin	I	Check if the PT is able to provide emergency prevention and management in the cabin	✓	The requirement is met as displayed in the CommFD
REQ-CO-SUB-I.2.2	The PT shall regulate the cabin temperature	T	Check if the cabin pressure is regulated during operation	✓	The temperature is regulated as in the original Beechcraft 1900D
REQ-CO-SUB-I.2.3	The PT shall provide a breathable cabin atmosphere	T	Check cabin atmosphere during operation	✓	The temperature is regulated as in the original Beechcraft 1900D
REQ-CO-SUB-I.2.4	The PT shall regulate cabin pressure	T	Check cabin pressure during operation	✓	The temperature is regulated as in the original Beechcraft 1900D

Continued on next page

Table 22.3 – continued from previous page

ID	Requirement	M	Verification Method	✓	Compliance and future tasks
REQ-CO-SUB-I.2.5	The PT shall enable emergency containment	D	Cause controlled failure of PT and check if containment system activates and performs	✓*	The requirement is met as displayed in the CommFD, but demonstration is required
REQ-CO-SUB-J.2.2	The integration of the PT shall not make the a/c uncontrollable during any flight phase according to the X-plot	A	The X-plot will be made for the designed a/c and stability for any flight phase will be gathered from it	✓	The updated cg range remains within the original one, so the controllability of the aircraft remains unaltered. Then, an X-plot is not required to meet this requirement
REQ-CO-SUB-J.3.1	The modified a/c shall be able to land within the specifications of the original aircraft	D*	The a/c shall perform a landing and the time taken will be measured.	χ	A demonstration is required to assess whether the retrofitted aircraft is capable of delivering the desired result
REQ-CO-SUB-J.4.1	The PP shall not interfere with essential elements such as the FC or TMS stored in the wings	I	Check essential elements for any interference caused by the PT	✓	The PP redesign and integration of the CC does not affect the distribution or structure within the fuselage
REQ-CO-SUB-J.4.2	The PP shall not interfere with the fuselage	I	Check the fuselage for any interference caused by the PT	✓	The integration of the components was taken into account during the constraint analysis, and also checked through a 3D model. Elements interfering with the PT were removed or reallocated to safe areas, when applicable
REQ-CO-SUB-J.4.3	The PP shall not interfere with the wing	I	Check the wing for any interference caused by the PT	✓	The integration of the components was taken into account during the constraint analysis, and also checked through a 3D model. Elements interfering with the PT were removed or reallocated to safe areas, when applicable
REQ-CO-SUB-J.4.4	The PP shall not interfere during GO	D*	Check that during GO, no interference is caused by the PT	✓*	The integration of the components was taken into account during the constraint analysis, and also checked through a 3D model to allow access to crucial components
REQ-CO-SUB-J.4.5	The PT shall not interfere with the cabin	I	Check the cabin for any interference caused by the PT	✓	The integration of the components was taken into account during the constraint analysis, and also checked through a 3D model to allow access to crucial components
REQ-CO-SUB-N.8.1	The a/c shall not operate out of the altitude range determined for the Beechcraft 1900D	A	Cross-reference flight envelope of original Beechcraft 1900D and set operational limits of retrofitted a/c accordingly	✓	The flight envelope was determined in the flight performance tool
REQ-CO-SUB-N.8.2	The a/c shall not operate out of the temperature range determined for the Beechcraft 1900D	A	cross-reference flight envelope of original Beechcraft 1900D and set operational limits of retrofitted a/c accordingly	✓	The flight envelope was determined in the flight performance tool

23

Conclusion

The aim of this report is to present the design of a robust, low-maintenance, low NO_x emission hybrid hydrogen-electric powered aircraft PT for the retrofit of the Beechcraft 1900D. The purpose of the newly designed PT - combining FCs with CC - is to increase the aircraft's sustainability s while complying with the legal and operational requirements, and keeping the original aircraft's airframe unchanged. Figure 23.1 displays the final design, which is capable of transporting 15 PAX a distance of 707 km at a ticket price of €212 while contributing 4 times less to anthropogenic climate forcing than the current Beechcraft 1900D.

Figure 23.1: *H_2D_2 model [CAD software used: CATIA v5©, NX© and Blender©]*

The H_2D_2 PT design balances the use of FCs and the CCs for the majority of flight conditions. FCs increase efficiency and reduce NO_x at the cost of added mass and complexity, whereas the CCs provide power without adding weight to the design.

The document begins by analyzing the market for the H_2D_2. From this, it became apparent that a hybrid-electric hydrogen-powered aircraft has many strengths that can make it a viable product. The available budgets were determined for time, mass, power, and volume. To determine the needed functions and properties, a functional flow and block diagram were constructed, providing a better insight into the hierarchy and linearity between functions.

Subsequently, the requirements were defined and V&V methods were listed, to keep track of the comprehension of all required performances that must be met. As a follow-up, the technical risks were assessed and presented in risk matrices, together with the mitigation and contingency plans.

Besides, the V&V plan was presented, divided in the requirements and tools V&V, and product validation. The sustainability development plan was defined, by performing an LCA, together with a socio-economical impact assessment.

Trade-offs were performed for two of the main sub-systems of the PT, namely the fuel storage and FC modules. The HT-PEMFC cell was chosen to be used within the PT, and LH_2 was determined to be the state of the hydrogen. A MLI-vacuum insulated, with G10 inner and outer walls tank was selected for further detailed design.

Focusing on the power plant redesign, the original combustor was adapted to hydrogen, and optimized for lowering NO_x emissions. For this reason, an RQL combustion was chosen, together with the WRS for lowering the emissions even further. The performance of the combustion engine was extended into the future, to get a better idea of the emissions in 2035.

The properties and design consideration for the subsystems were determined. Starting with the FC, the efficiency varies with the power output, having a higher efficiency at the cost of less power produced, The necessary mass flows, and the heat it produces were analyzed, and cost and sustainability factors were mapped. A Permanent Magnet Synchronous motor was selected due to its superior power density and efficiency compared to other ELMOs. The architecture of distribution, and conditioning of hydrogen has been created, and their associated parameters, like pressure, or temperature were established. A steady state model of the TMS was developed to map all the temperatures, mass flows, and pressures of coolant and hydrogen throughout the whole system.

With the definitions of all subsystems described, the Design was synthesized. The different models and tools made for the subsystems were combined to look at different design points and optimize for low cost, and low GWP. With a final design point selected, all the different characteristics of the H_2D_2 were described, and the layout of the systems could be established. These were compared with the original characteristics of the Beechcraft 1900D to check if they have been kept similar.

The operations & logistics concept was described together with the RAMS aspects, and steps have been taken for further development past the DSE of the H_2D_2 aircraft. Following that, the expenses and return of investment have been estimated. Finally, all the requirements have been checked to see if they have been met. H_2D_2 is four times more sustainable than competing aircraft at a similar price.

Bibliography

[1] D.S. Lee et al. "The contribution of global aviation to anthropogenic climate forcing for 2000 to 2018". In: *Atmospheric Environment* 244 (Jan. 2021). ISSN: 13522310. DOI: 10.1016/j.atmosenv.2020.117834.

[2] *Policy Net Zero CO2 Emissions Roadmap*. Tech. rep. IATA Sustainability and Economics, Sept. 2024.

[3] IATA. *Aviation Net-Zero CO2 Transition Pathways*. 2024.

[4] Thijmen Boter. "Bio-SAF vs. e-SAF: land-use efficiency of conversion routes for sustainable aviation fuel production in the EU". PhD thesis. Utrecht University, May 2023.

[5] Maximilian Spangenberg. "Air s.Pace ELectric Innovative Commuter Aircraft D2.1 Economic Feasibility Study for a 19 PAX Hybrid-Electric Commuter Aircraft". In: (2020).

[6] Xiaoqian Sun, Yu Zhang, and Sebastian Wandelt. "Air Transport versus High-Speed Rail: An Overview and Research Agenda". In: *Journal of Advanced Transportation* 2017 (2017), pp. 1–18. ISSN: 0197-6729. DOI: 10.1155/2017/8426926.

[7] Moshe Givoni and Piet Rietveld. "Choice of Aircraft Size - Explanations and Implications". In: *Tinbergen Institute* 113 (3 2006).

[8] Jon Hemmerdinger. "Airframers Textron delivers first Cessna SkyCourier, to FedEx". In: *FlightGlobal* (May 2022).

[9] Frederick Larkin. "How Textron Aviation's SkyCourier Utility Turboprop is Positioning in the Market". In: *Skies* (Jan. 2024).

[10] "Airbus showcases hydrogen aircraft technologies during its 2025 Airbus Summit". In: (2025).

[11] ZeroAvia. *Complete Flight Testing Campaign of Dornier 228 Hydrogen-Electric Aircraft Retrofit*. Accessed: 2025-04-29. 2024. URL: https://zeroavia.com/complete-flight-test/.

[12] Jack Daleo. "ZeroAvia, FlightSafety International to Train Pilots on Hydrogen-Electric Aircraft". In: *FLYING Magazine* (Mar. 2025). Accessed: 2025-04-29. URL: https://www.flyingmag.com/zeroavia-flightsafety-international-to-train-pilots-on-hydrogen-electric-aircraft/.

[13] Mordor Intelligence. *Turboprop Planes Market - Size, Forecast, and Outlook*. 2025. URL: https://www.mordorintelligence.com/industry-reports/turboprop-aircraft-market.

[14] TU Delft. "AE3-S01 Systems Engineering Lecture Notes". In: (Sept. 2006).

[15] EASA. *Certification Specifications for Normal, Utility, Aerobatic, and Commuter Category Aeroplanes CS-23*. Tech. rep. Nov. 2003. URL: https://www.easa.europa.eu/en/document-library/certification-specifications/cs-23-initial-issue.

[16] *ISO 19887-1:2024 - Gaseous Hydrogen - Fuel system components for hydrogen-fuelled vehicles*. Version 1. Oct. 2024.

[17] Raytheon Aircraft. "Raytheon Beechcraft 1900D Limitations". In: (Dec. 2001).

[18] *Type-certificate data sheet*. Tech. rep. EASA, Jan. 2022.

[19] Matei Albu et al. *SHTARWaRS - Project Plan - DSE 1*. Tech. rep. Delft University of Technology, Apr. 2025.

[20] Dahlia Pham et al. "Advanced Turboprop Transport Aircraft Modeling for the Electrified Powertrain Flight Demonstration Project". In: June 2023. DOI: 10.2514/6.2023-3870.

[21] J.M. Hoekstra. *AE1110-I Introduction to Aerospace Engineering*. Lecture 3: Forces: Lift, Drag, Slide 53. 2022.

[22] Egbert Torenbeek. *Synthesis of Subsonic Airplane Design*. Kluwer Academic Publishers, 1982.

[23] Mohammad Sadraey. "Wing design". In: *Wing Design*. Daniel Webster College.

[24] Snorri Gudmundsson. "The Anatomy of the Propeller". In: *General Aviation Aircraft Design*. Elsevier, 2014, pp. 581–659. DOI: 10.1016/B978-0-12-397308-5.00014-3.

[25] Janes. *Beechcraft 1900D*. Feb. 2021. URL: https://customer.janes.com/display/JAU_9418-JAU_.

[26] European Space Agency, SRE-PA, and D-TEC staff. "Margin philosophy for science assessment studies". In: (June 2012). URL: www.esa.int.

[27] Daniel P. Thunnissen. "Method for Determining Margins in Conceptual Design". In: *Journal of spacecraft and rockets* 41 (1 Jan. 2004).

[28] Prof. Dr. Eberhard Gill. *AE3211-I-L04-VV-AOCS-V18 - AE3211-I Systems Engineering & Aerospace Design (2024/25 Q3)*. 2025. URL: https://brightspace.tudelft.nl/d2l/le/content/684925/viewContent/3902488/View.

[29] Prof. Dr. Eberhard Gill. *AE3211-I-L02-Methods-V19 - AE3211-I Systems Engineering & Aerospace Design (2024/25 Q3)*. 2025. URL: https://brightspace.tudelft.nl/d2l/le/content/684925/viewContent/3902483/View.

[30] Mokrane Chaabane, Belkacem Adouane, and Ahmed Benzaoui. "Composition and Stoichiometry Effects of Biogas as Fuel in Spark Ignition Engine". In: *International Journal of Automotive and Mechanical Engineering* 15.1 (2018). Fig. 5a reproduces the *NO_x vs. equivalence-ratio "U-curve"* used in the slide, pp. 5036–5052. DOI: 10.15282/ijame.15.1.2018.11.0390.

[31] Michael G. Zabetakis. *Flammability Characteristics of Combustible Gases and Vapors*. Table 1 lists the *4–75% vol. flammability window for H2* and companion fuels. Washington, D.C.: U.S. Bureau of Mines, Bulletin 627, 1965.

[32] M. W. Chase Jr. (ed.) *NIST Chemistry WebBook: Thermodynamic Data for Hydrogen*. https://webbook.nist.gov/cgi/cbook.cgi?ID=C1333740&Plot=on&Type=JANAFG. JANAF curve used for the *specific-heat (C_p) comparison plot*. 1998.

[33] Jayaprakash Natarajan, Tim Lieuwen, and J. Seitzman. "Laminar Flame Speeds of H2/CO Mixtures: Effect of CO2 Dilution, Preheat Temperature, and Pressure". In: *Combustion and Flame* 151.1–2 (2007). Triangular flame-speed map reproduced in the "High flame speed" box, pp. 104–119. DOI: 10.1016/j.combustflame.2007.05.003.

[34] Mehdi Jadidi, Sara Moghtadernejad, and Ali Dolatabadi. "A Comprehensive Review on Fluid Dynamics and Transport of Suspension/Liquid Droplets and Particles in High-Velocity Oxygen-Fuel Thermal Spray". In: *Progress in Materials Science* 79 (2015). Fig. 2 gives the *approx. 2400 K adiabatic-temperature vs. ϕ curve*, pp. 1–52. DOI: 10.1016/j.pmatsci.2015.07.002.

[35] T. L. Howarth, E. F. Hunt, and A. Aspden. "Thermodiffusively-Unstable Lean Premixed Hydrogen Flames: Phenomenology, Empirical Modelling, and Thermal Leading Points". In: *Combustion and Flame* 253 (2023). DNS image used in the "Lewis number «1 / high diffusivity" inset, p. 112811. DOI: 10.1016/j.combustflame.2023.112811.

[36] Robin Schultheis and Andreas Dreizler. "Development of a Flashback Correlation for Burner-Stabilised Hydrogen-Enriched Flames". In: *Combustion and Flame* 240 (2022). Bunsen photos in "Unstable flames / flashback risk" drawn from this work, p. 112043. DOI: 10.1016/j.combustflame.2022.112043.

[37] NASA Stennis Space Center. *RS-25 Certification Engine Hot-Fire Test (Oct. 17 2023)*. https://www.nasa.gov/centers-and-facilities/stennis/nasa-conducts-1st-hot-fire-of-new-rs-25-certification-test-series/. Photo shown under "Potential leakages—attention to seals & pumps". 2023.

[38] NASA. *Barges Fill NASA Rocket Stage with Liquid Propellant*. https://www.nasa.gov/image-article/barges-fill-nasa-rocket-stage-with-liquid-propellant-2/. Image of oversized LH2 tank illustrating "Low volumetric efficiency". 2021.

[39] Tommaso Capurso et al. "NOx pathways in lean partially premixed swirling H_2–air turbulent flame". In: *Combustion and Flame* 248 (2023), p. 112581. ISSN: 0010-2180. DOI: 10.1016/j.combustflame.2022.112581. URL: https://doi.org/10.1016/j.combustflame.2022.112581.

[40] M. Khosravy el_Hossaini. “Review of the New Combustion Technologies in Modern Gas Turbines”. In: *Progress in Gas Turbine Performance*. Ed. by Ernesto Benini. Rijeka: IntechOpen, 2013. Chap. 6. DOI: 10.5772/54403. URL: https://doi.org/10.5772/54403.

[41] Scott Samuelsen. “3.2.1.3 Rich Burn, Quick-Mix, Lean Burn (RQL) Combustor 3.2.1.3-1 Introduction”. In: *Unpublished or Unknown Source* (n.d.).

[42] J. Serrano et al. “Experimental analysis of NOx reduction through water addition and comparison with exhaust gas recycling”. In: *Energy* 168 (Feb. 2019), pp. 737–752. ISSN: 0360-5442. DOI: 10.1016/J.ENERGY.2018.11.136. URL: https://www.sciencedirect.com/science/article/pii/S0360544218323478.

[43] David L. Daggett et al. “Water Injection on Commercial Aircraft to Reduce Airport Nitrogen Oxides”. In: *40th Joint Propulsion Conference and Exhibit cosponsored by the AIAA, ASME, SAE, and ASEE*. Mar. 2010. URL: https://ntrs.nasa.gov/api/citations/20100015629/downloads/20100015629.pdf.

[44] *PT6A Pilot Familiarization*. Tech. rep. Pratt & Whitney Canada, Aug. 2003.

[45] I. Halliwell. *Preliminary Engine Design – A Practical Overview for the NASA John H. Glenn Research Center*. Technical Report. Internal publication. Cleveland, OH: NASA Glenn Research Center, 2000.

[46] FlightSafety International. *Beech 1900 Airliner Pilot Training Manual*.
Volume 2: Aircraft Systems. For training purposes only. FlightSafety International, Inc. Marine Air Terminal, LaGuardia Airport, Flushing, NY, 2000.

[47] Yann Fefermann et al. “Hybrid-Electric Motive Power Systems for Commuter Transport Applications”. In: *30th Congress of the International Council of the Aeronautical Sciences (ICAS 2016)*. Paper 2016_0438. International Council of the Aeronautical Sciences. Daejeon, Republic of Korea: ICAS, 2016.

[48] David G. Goodwin et al. *Cantera: An Object-oriented Software Toolkit for Chemical Kinetics, Thermodynamics, and Transport Processes*. https://www.cantera.org. Version 3.1.0. 2024. DOI: 10.5281/zenodo.14455267.

[49] Wasim Bhatti et al. *Fuel Cells - Roadmap Report FZO-PPN-COM-0033*. Tech. rep. Aerospace Technology Institute - FlyZero, 2022.

[50] M. Schroder et al. “Optimal operating conditions of PEM fuel cells in commercial aircraft”. In: *International Journal of Hydrogen Energy* 46 (66 Sept. 2021), pp. 33218–33240. ISSN: 03603199. DOI: 10.1016/j.ijhydene.2021.07.099.

[51] Caizhi Zhang et al. “Determination of the optimal operating temperature range for high temperature PEM fuel cell considering its performance, CO tolerance and degradation”. In: *Energy Conversion and Management* 105 (Nov. 2015), pp. 433–441. ISSN: 01968904. DOI: 10.1016/j.enconman.2015.08.011.

[52] Marc Schmelcher and Jannik Haby. “Hydrogen fuel cells for aviation? A potential analysis comparing different thrust categories”. In: *German Aerospace Center (DLR) Institute of Propulsion Technology* (2022).

[53] Mutlucan Bayat, Mehmet Ozalp, and Huseyin Gurbuz. “Comprehensive performance analysis of a high-temperature PEM fuel cell under different operating and design conditions”. In: *Sustainable Energy Technologies and Assessments* 52 (Aug. 2022), p. 102232. ISSN: 22131388. DOI: 10.1016/j.seta.2022.102232.

[54] Todd Ramsden. *An Evaluation of the Total Cost of Ownership of Fuel CellPowered Material Handling Equipment*. Tech. rep. National Renewable Energy Laboratory, 2013. URL: https://docs.nrel.gov/docs/fy13osti/56408.pdf.

[55] Tim Kemperdick et al. “Techno-economic analysis of proton exchange membrane fuel cell recycling through pyro- and hydrometallurgy”. In: *Journal of Cleaner Production* 508 (May 2025), p. 145432. ISSN: 0959-6526. DOI: 10.1016/J.JCLEPRO.2025.145432. URL: https://www.sciencedirect.com/science/article/pii/S0959652625007826.

[56] Christian Spreafico and Nils Thonemann. “Prospective life cycle assessment of proton exchange membrane fuel cell. Comparing data from patents and papers”. In: *International Journal of Hydrogen Energy* 99 (Jan. 2025), pp. 45–52. ISSN: 03603199. DOI: 10.1016/j.ijhydene.2024.12.211.

[57] Maria-Pilar Martinez-Hernando et al. “Life cycle sustainability assessment of the platinum supply chain in the European Union”. In: *Sustainable Production and Consumption* 46 (May 2024), pp. 679–689. ISSN: 23525509. DOI: 10.1016/j.spc.2024.03.017.

[58] Gaia Gentilucci, Antonella Accardo, and Ezio Spessa. “Life Cycle Analysis of a PEM Fuel Cell System for Long-Haul Heavy-Duty Trucks”. In: (Sept. 2024). DOI: 10.4271/2024-24-0020.

[59] Xavier Roboam et al. *Hastecs : Hybrid aircraft : research on thermal and electric components and systems*. Oct. 2021.

[60] THE Miller J. R. Hendershot Jr. *Design of Brushless Permanent-Magnet Motors*. Magna Physics and oxford science publications, 1994.

[61] Eric Hendricks hapman Eliot D. Aretskin-ariton Sydney Schnulo. “Electrical Cable Design for Urban Air Mobility Aircraft”. In: ().

[62] zeroavia. *600kW Electric Propulsion System for Aviation*. Brochure. 2025. URL: https://zeroavia.com/wp-content/uploads/2025/05/V2-of-EPS-Brochure-Draft.pdf.

[63] Michael D. Hayes. *Airline Transport Pilot Oral Exam Guide-BE-1900 Systems*. 2020.

[64] M. Albu et al. *SHTARWaRS - DSE Midterm Report*. Tech. rep. Tutors: Dr. Ivan Langella, Prof. Dr. Arvind Gangoli Rao; Coaches: Jakob Smretschnig, Dante Raso. Delft, The Netherlands: Faculty of Aerospace Engineering, Delft University of Technology, May 2025.

[65] Inc. Provac Sales. *CTI Cryo-Torr 8F Cryo Pump, Rebuilt*. 2025. URL: https://www.provac.com/products/cti-cryo-torr-8f-cryo-pump-rebuilt.

[66] Austin Scientific. *Cryopump Equipment Price List*. Tech. rep. 2006. URL: www.oxford-instruments.com.

[67] N. Renauld. “Design and Analysis of Inner Support Structures for Double-Walled Liquid Hydrogen Storage Vessels”. Supervised by Julien M.J.F. van Campen, Saullo Giovani Giovani Pereira Castro, Otto Bergsma, Maurice Hoogreef, A Chadwick, and L Brandt. Master’s thesis. Aerospace Engineering: Delft University of Technology, 2024.

[68] B. W. Tew. “Preliminary design of tubular composite structures using netting theory and composite degradation factors”. In: *Journal of Pressure Vessel Technology, Transactions of the ASME* 117 (4 1995), pp. 390–394. ISSN: 15288978. DOI: 10.1115/1.2842141.

[69] Filippo Mazzoni et al. “Design space exploration through liquid H2 tank preliminary sizing and design of experiments analysis”. In: *International Journal of Hydrogen Energy* 95 (Dec. 2024), pp. 1252–1260. ISSN: 0360-3199. DOI: 10.1016/J.IJHYDENE.2024.08.017.

[70] CORECHEM Inc. *GlycoChill+ Ethylene Glycol Heat Transfer Fluid - CORECHEM*. 2025. URL: https://corecheminc.com/product/glycochill-e200-inhibited-ethylene-glycol-heat-transfer-fluid/.

[71] W.S. Jones and W.S. Tamplin. *Glycols*. Reinhold Publishing Corporation, 1952, pp. 27–62.

[72] *Water Boiling Point at Higher Pressures -Data & Calculator*. 2005. URL: https://www.engineeringtoolbox.com/boiling-point-water-d_926.html (visited on 06/11/2025).

[73] Fabio Beltrame et al. “OPTIMAL DESIGN OF A RAM AIR COOLING DUCT HOUSING THE CONDENSER OF AN AIRBORNE ORC WHR UNIT”. 2024.

[74] Jun-Hong Hao et al. “An experimental study on the offset-strip fin geometry optimization of a plate-fin heat exchanger based on the heat current model”. In: *Applied Thermal Engineering* 154 (May 2019), pp. 111–119. ISSN: 13594311. DOI: 10.1016/j.applthermaleng.2019.03.072.

[75] B. Rietdijk and M. Selier. *ARCHITECTURE DESIGN FOR A COMMERCIALLY VIABLE HYDROGEN-ELECTRIC POWERED RETROFITTED REGIONAL AIRCRAFT*. Tech. rep. Conscious Aerospace.

[76] Ramesh K. Shah and Dusan P. Sekulic. “FUNDAMENTALS OF HEAT EXCHANGER DESIGN”. In: JOHN WILEY & SONS, INC, 2003.

[77] Martijn Vroom. “Preliminary Sizing of Balance-of-Plant Systems for Liquid Hydrogen Fuel Cell-Electric Propulsion in Regional Retrofitted Aircraft”. PhD thesis. Delft University of Technology, 2025.

[78] Sylwia Wcislik. “The Influence of Nusselt Correlation on Exergy Efficiency of a Plate Heat Exchanger Operating with TiO2:SiO2/EG:DI Hybrid Nanofluid”. In: *Inventions* 9 (1 Jan. 2024), p. 11. ISSN: 2411-5134. DOI: 10.3390/inventions9010011.

[79] Kitti Nilpueng et al. “Effect of chevron angle and surface roughness on thermal performance of single-phase water flow inside a plate heat exchanger”. In: *International Communications in Heat and Mass Transfer* 91 (Feb. 2018), pp. 201–209. ISSN: 07351933. DOI: 10.1016/j.icheatmasstransfer.2017.12.009.

[80] “A Study on Thermal Management Systems for Hybrid-Electric Aircraft”. In: *Aerospace* 10 (9 Sept. 2023). ISSN: 22264310.

[81] Valentine Habrard et al. “Liquid Cooling Thermal Management System Modeling for Preliminary Design of Hybrid Fuel Cell Aircraft”. In: *AIAA Aviation and Aeronautics Forum and Exposition, AIAA AVIATION Forum 2023* (2023). DOI: 10.2514/6.2023-4303. URL: /doi/pdf/10.2514/6.2023-4303.

[82] Demaco Cryogenics. *PRODUCT SHEETS*. 2025. URL: www.demaco-cryogenics.com.

[83] GSR Ventiltechnik GmbH & Co. KG. *Engineering Valves Solutions*. 2025. URL: www.ventiltechnik.de.

[84] Emerson Electric Co. *TESCOM 26-2700 Series Backpressure Control Regulator Emerson NO*. URL: https://www.emerson.com/no-no/catalog/automation/industrial-factory-automation/hydrogen-valves-regulators/tescom-26-2700-en-gb.

[85] Ola Wasel et al. “Differential Developmental Neurotoxicity and Tissue Uptake of the Per- and Polyfluoroalkyl Substance Alternatives, GenX and PFBS”. In: *Environmental Science and Technology* 57 (48 Dec. 2023), pp. 19274–19284. ISSN: 15205851. DOI: 10.1021/ACS.EST.3C05023/SUPPL_FILE/ES3C05023_SI_001.PDF. URL: https://pmc.ncbi.nlm.nih.gov/articles/PMC11299994/.

[86] Laurence W. McKeen. “High-Temperature Polymers”. In: *The Effect of Creep and Other Time Related Factors on Plastics and Elastomers* (Jan. 2009), pp. 337–372. DOI: 10.1016/B978-0-8155-1585-2.50012-1. URL: https://linkinghub.elsevier.com/retrieve/pii/B9780815515852500121.

[87] Agency for Toxic Substances and Disease Registry. *Ethylene Glycol | ToxFAQ | ATSDR*. 2015. URL: https://wwwn.cdc.gov/TSP/ToxFAQs/ToxFAQsDetails.aspx?faqid=85&toxid=21.

[88] Luxaviation. *Beechcraft 1900D*. 2025. URL: https://www.luxaviation.com/wa/spec/111.

[89] *SKYbrary, Rules of Thumb*.

[90] PeeWeeSweden. *Beech 1900D Reference Speeds - Carenado - Alabeo Support - X-Plane.Org Forum*. Sept. 2016. URL: https://forums.x-plane.org/forums/topic/107190-beech-1900d-reference-speeds/.

[91] Jack D.. Mattingly, William H.. Heiser, and David T.. Pratt. *Aircraft Engine Design*. 2nd ed. American Institute of Aeronautics and Astronautics, 2002. ISBN: 1563475383.

[92] Snorri Gudmundsson. “Initial Sizing”. In: *General Aviation Aircraft Design*. Elsevier, 2022, pp. 57–91. DOI: 10.1016/B978-0-12-818465-3.00027-6.

[93] Dr. Jan Roskam. *Preliminary Sizing of Airplanes*. DARcorporation. Vol. part I. 1997.

[94] Greg Pisanich and Fritz Renema. *Bandwidth Enabled Flight Operations: Examining the Possibilities*. Technical Report. Retrieved from NASA Ames Research Center. Moffett Field, CA: QSS Group Inc., NASA Ames Research Center, 2003.

[95] Amela Ajanovic, Marlene Sayer, and Reinhard Haas. “On the future relevance of green hydrogen in Europe”. In: *Applied Energy* 358 (Mar. 2024), p. 122586. ISSN: 03062619. DOI: 10.1016/j.apenergy.2023.122586.

[96] Agnieszka Skowron, David S. Lee, and Ruben R. De Leon. “Variation of radiative forcings and global warming potentials from regional aviation NO x emissions”. In: *Atmospheric Environment* 104 (Mar. 2015), pp. 69–78. ISSN: 13522310. DOI: 10.1016/j.atmosenv.2014.12.043.

[97] Klaus Gierens. “Theory of Contrail Formation for Fuel Cells”. In: *Aerospace* 8 (6 June 2021), p. 164. ISSN: 2226-4310. DOI: 10.3390/aerospace8060164.

[98] U. Schumann. “On conditions for contrail formation from aircraft exhausts”. In: *Meteorol. Zeitschrift,* 5 (Feb. 1996).

[99] Magnus Andersson and Emil Inberg. “Life cycle assessment of a regional hybridelectric aeroplane”. PhD thesis. Chalmers University of Technology, 2024.

[100] A World Of Energy. *Life Cycle Analysis of hydrogen storage tanks*. Accessed: 2025-05-21. 2022. URL: https://www.awoe.net/Hydrogen-Storage-LCA.html.

[101] Christopher Koroneos et al. “Life Cycle Assessment of Kerosene Used in Aviation (8 pp)”. In: *The International Journal of Life Cycle Assessment* 10 (6 Nov. 2005), pp. 417–424. ISSN: 0948-3349. DOI: 10.1065/lca2004.12.191.

[102] Magda Kopczynska and Florian Guillermet. *EUROPEAN AVIATION ENVIRONMENTAL REPORT*. Tech. rep. European Union Aviation Safety Agency, 2025.

[103] Gulam Husain Patel et al. “Climate change performance of hydrogen production based on life cycle assessment”. In: *Green Chemistry* 26 (2 2024), pp. 992–1006. ISSN: 1463-9262. DOI: 10.1039/D3GC02410E.

[104] Leonardo Checcucci. “RAMS Estimation of Hybrid-Electric Aircraft Propulsion Architectures”. Relatore: Marco Fioriti. Laurea Magistrale Thesis. Corso di Laurea Magistrale in Ingegneria Aerospaziale: Politecnico di Torino, 2023.

[105] *D1.1: Concept of Modular Architecture for Hybrid Electric Propulsion of Aircraft*. Tech. rep. MAHEPA Project, Dec. 2017.

[106] FAA. *AC 25.1309-1B - System Design and Analysis*. 2024. URL: https://www.faa.gov/regulations_policies/advisory_circulars/index.cfm/go/document.information/documentID/1043037.

[107] *Beech 1900D: Quick Study Guide*. Tech. rep. AVSOFT, Aug. 2004.

[108] *Datasheet Hoses EPDM*. Tech. rep. Mouldpro.

[109] *FUEL CELLS Roadmap Report Aerospace Technology Institute-FlyZero-Fuel Cells-Roadmap Report 2*. 2022.

[110] *Advanced materials for hydrogen storage tanks | Horizon-europe.gouv.fr*. URL: https://www.horizon-europe.gouv.fr/advanced-materials-hydrogen-storage-tanks-34822.

[111] D.Felix Finger et al. “Cost Estimation Methods for Hybrid-Electric General Aviation Aircraft”. In: Dec. 2019. URL: https://www.researchgate.net/publication/337757069_Cost_Estimation_Methods_for_Hybrid-Electric_General_Aviation_Aircraft.

[112] *Beechcraft 1900D Charter - Rental Cost and Hourly Rate*. URL: https://www.paramountbusinessjets.com/private-jet-charter/aircraft/beechcraft-1900d.

[113] Pierluigi Della Vecchia et al. “Retrofitting Cost Modeling in Aircraft Design”. In: *Aerospace 2022, Vol. 9, Page 349* 9 (7 June 2022), p. 349. ISSN: 2226-4310. DOI: 10.3390/AEROSPACE9070349. URL: https://www.mdpi.com/2226-4310/9/7/349/htm%20https://www.mdpi.com/2226-4310/9/7/349.

[114] *Charges in euros*. URL: http://www.vliegclubrotterdam.nl/.

[115] *Pilot Pay Endeavor Air*. URL: https://www.endeavorair.com/content/endeavor-air/en_us/careers/pilots/Pilot_Compensation.html.

[116] Hussein Basma, Yuanrong Zhou, and Felipe Rodriguez. “FUEL-CELL HYDROGEN LONG-HAUL TRUCKS IN EUROPE: A TOTAL COST OF OWNERSHIP ANALYSIS”. In: (Sept. 2022).

[117] *Beech 1900D brochure, performance, market, operating costs.* URL: https://www.guardianjet.com/jet-aircraft-online-tools/aircraft-brochure.cfm?m=Beech-1900D-198.

[118] *Cost Comparison: Liquid vs. Gaseous Hydrogen for Heavy-Duty Applications | FASTECH.* URL: https://www.fastechus.com/blog/cost-comparison-liquid-vs-gaseous-hydrogen.

[119] Janina Scheelhaase et al. "Economic and Environmental Aspects of Aircraft Recycling". In: *Transportation Research Procedia* 65 (C Jan. 2022), pp. 3–12. ISSN: 2352-1465. DOI: 10.1016/J.TRPRO.2022.11.002. URL: https://www.sciencedirect.com/science/article/pii/S235214652200669X.

[120] Essam Shehab et al. "Cost Modelling for Recycling Fiber-Reinforced Composites: State-of-the-Art and Future Research". In: *Polymers* 15 (1 Jan. 2022), p. 150. ISSN: 20734360. DOI: 10.3390/POLYM15010150. URL: https://pmc.ncbi.nlm.nih.gov/articles/PMC9823720/.

[121] Gabriel Leigh. *Nothing but a number? Aircraft age explained | Flightradar24 Blog.* URL: https://www.flightradar24.com/blog/aviation-explainer-series/nothing-but-a-number-aircraft-age-explained/?utm_source=chatgpt.com.

[122] Iata. "Maintenance Costs for Aging Aircraft 2018 1st Edition". In: (2018).